

*Report on the Hydrocarbon Exploration and Seismicity in
Emilia Region*

INTERNATIONAL COMMISSION ON HYDROCARBON EXPLORATION AND
SEISMICITY IN THE EMILIA REGION

Members of the Commission

Peter Styles, Chief of the Commission

Professor of Applied Geophysics, Keele University, Keele, Staffordshire, United Kingdom.

Paolo Gasparini, Secretary of the Commission

Professor Emeritus of Geophysics, University of Napoli “Federico II”, Napoli, Italy

Chief Executive Officer of AMRA Scrl (Analisi e Monitoraggio del Rischio Ambientale).

Ernst Huenges

Head of Section Reservoir Technologies at GFZ (Deutsches GeoForschungsZentrum), Potsdam, Germany.

Paolo Scandone

Retired Professor of Structural Geology, University of Pisa, Pisa, Italy.

Stanislaw Lasocki

Professor of Earth Sciences, Head of Department of Seismology and Physics of the Earth's Interior, Institute of Geophysics, Polish Academy of Sciences, Warsaw, Poland.

Franco Terlizzese

Petroleum engineer, General Director for Mineral and Energetic Resource, Ministry of Economic Development, Rome, Italy.

Index

Main Report	4
I. Mission of ICHESE	4
A. Introduction	4
B. Charge to the Commission	5
C. Conduct of the Study	5
D. Organization of the Report	6
II. Review of state of knowledge of antropogenically influenced seismicity	8
A. Introduction	8
B. Anthropogenically Influenced Seismicity	8
C. Mechanisms of Fluid Injection and Abstraction Related Seismicity	34
D. Conclusions	47
III. Emilia Seismic Activity and Seismotectonic context	48
A. The Emilia Seismic Activity	48
B. Seismotectonic context	59
IV. List of available information	65
A. Well locations and historical development	65
B. Stratigraphy and standard logging data	69
C. Seismic profiles	78
D. Seismological data	84
E. Production and injection data	92
F. Reservoir	102
G. Other	110
V. Answer to the first question	113
A. The “RIVARA-STORAGE” project	113
B. Review of the available documentation	114
VI. How the Commission addressed question two	115
A. Methodology	117
VII. Processing of seismic and production data	121
A. Velocity model and identification of significant faults	121
B. Relocation focal mechanism and tectonic stress transfer	134
C. Reservoir model	145
D. Statistical analysis of seismic series and production data	152
E. Geothermal activity analysis	177
VIII. Conclusions	179
IX. Conclusioni	188
Acknowledgment	198
References	199

Main Report

I. Mission of ICHESE

A. Introduction

The Technical-Scientific Commission for evaluating the possible relationships between hydrocarbon exploration and a marked increase of seismicity in the Emilia Romagna area hit by the May 2012 earthquakes (ICHESE) was appointed in the aftermath of the magnitude (M) major than 5.0 seismic events which occurred in Emilia-Romagna in the period May 20-May29 2012, producing significant damages and fatalities.

It was appointed by Dr. Franco Gabrielli, Head of the Department of Civil Protection of the Presidency of Council of Ministers with the decree No. 5930 of December 11, 2012 following the request of the President of Emilia-Romagna Region (Ordinances no. 76 of November 16, 2012 and no. 81 of November 23, 2012).

The composition of ICHESE was subsequently modified by the Head of Civil Protection through the decree of March 25, 2013 (following the ordinance No. 30 of March 15, 2013 of the President of the Emilia Romagna Region) and the decree of May, 8, 2013 (following the ordinance No. 54 of May 8, 2013 of the President of Emilia Romagna Region).

The Commission is composed of the following experts in seismicity, induced seismicity and hydrocarbon exploration:

Peter Styles, Chief of the Commission

Professor of Applied Geophysics, Keele University, Keele, Staffordshire, United Kingdom.

Paolo Gasparini, Secretary of the Commission

Professor Emeritus of Geophysics, University of Napoli "Federico II", Napoli, Italy
Chief Executive Officer of AMRA Scarl (Analisi e Monitoraggio del Rischio Ambientale), Napoli, Italy.

Ernst Huenges

Head of Section Reservoir Technologies at GFZ (Deutsches GeoForschungsZentrum), Potsdam, Germany.

Paolo Scandone

Retired Professor of Structural Geology, University of Pisa, Pisa, Italy.

Stanislaw Lasocki

Professor of Earth Sciences, Head of Department of Seismology and Physics of the Earth's Interior, Institute of Geophysics, Polish Academy of Sciences, Warsaw, Poland

Franco Terlizzese

Petroleum engineer, General Director for Mineral and Energetic Resource, Ministry of Economic Development, Rome, Italy.

A biographical sketch of all the members is contained in Appendix A.

B. Charge to the Commission

The Commission was appointed with the following statement of charge (Decree of the Chief of Civil Protection No.5930 of December 11, 2012):

“The International Committee shall produce a report answering the following questions, on the basis of the technical-scientific knowledge available at the moment:

1) Is it possible that the seismic crisis in Emilia has been triggered by the recent researches at the Rivara site, particularly in the case of invasive research activities, such as deep drilling, fluids injections, etc.;

2) Is it possible that the Emilia seismic crisis has been triggered by activities for the exploitation and utilization of reservoirs carried out in recent times in the close neighbourhood of the seismic sequence of 2012?”.

The Technical-Scientific committee activity has a duration of six months from the date of takeover. The results and evaluations of the Committee will be delivered to the Technical Secretary enforced at the “Servizio geologico, sismico e dei suoli” of Regione Emilia Romagna in accordance with the ordinance n.81 of November 23, 2012 in order to **provide** useful information for the rebuilding and urban planning of the area.

C. Conduct of the Study

The ICHESE Commission, on the base of seismo-tectonic considerations, defined the area of interest for the study as reported in **Figure I.1**. The area covers a surface of about 4000 Km².

Three exploitation licences are included in the area (Mirandola, Spilamberto e Recovato), The Minerbio reservoir, located at the south-eastern margin of the defined area, was also included as part of due diligence and to ensure a cautious approach. Additionally, because of the short distance between the first mainshock and the geothermal field of Casaglia (Ferrara), the Commission decided to consider Casaglia in the study.

The Commission decided that as far as possible the specific data on which interpretations and conclusions are based must be declared and made public, with due respect to possible requests of confidentiality by companies.

The Commission decided to ask for all the available data on seismic activity, ground deformation, geology, reflection seismology, hydrocarbon exploration, exploitation, gas storage and geothermal activities. For this reason, the Commission conducted interviews with the representatives of INGV (*Istituto Nazionale di Geofisica e Vulcanologia*), OGS (*Istituto Nazionale di Ocenografia e di Geofisica Sperimentale*), Seismological Service of Regione Emilia-Romagna, and the companies performing hydrocarbon exploitation and exploration and natural gas storage activities in the study area and asked for the available data. The Commission also interviewed *Independent Gas Management*, a company which studied the geological setting of the area in order to prepare a gas storage project in deep aquifers.

The collected information is reported in Chapter 4.

Besides a thoughtful study of the scientific literature and reports available on this issue, the Commission decided:

- to perform a re-evaluation of the main available reflection seismology and well logging data to check the tectonic model of the area and to build a 3D velocity model to be used for the re-location of seismic activity (see Section 7.A);
- To recalculate the classical parameters (geographical coordinates, depth, focal mechanism) of the seismic activity with epicentres in the considered area recorded by the INGV seismic network starting from 2005 and to estimate the Coulomb stress transfer due to the May 20 major events (see Section 7.B);
- to perform statistical analysis of seismic, injection and extraction of hydrocarbons data in the study area starting from 2005, including May 2012 (see Section 7.D);
- To check the physical model of the reservoirs (see Section 7.C);
- to analyze the operational and recorded seismic data related to geothermal fields of Casaglia (Ferrara) (see Section 7.E).

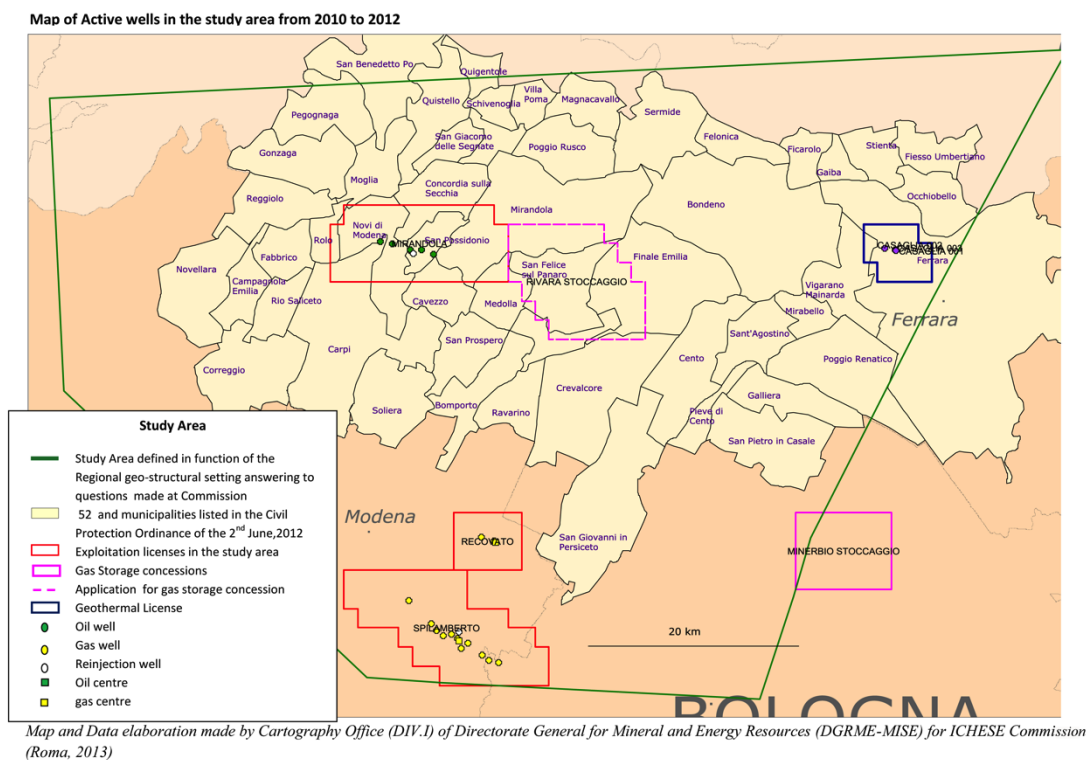


Figure I.1 Study areas defined by the Commission.

D. Organization of the Report

The report comprises nine main sections:

- §I. *Mission of ICHESE:*
- §II. *Review of state of knowledge of relevant induced seismicity*

- §III. *Emilia 2012 Seismic Activity and Seismotectonic context*
- §IV. *List of available information*
- §V. *Answer to the first question*
- §VI. *How we addressed question two*
- §VII. *Processing of seismic and production data*
- §VIII. *Conclusions (in English)*
- §IX. *Conclusioni (in Italian)*

Five appendices are included with the report:

- A. *Biographies of Commissioners*
- B. *Induced and triggered seismicity*
- C. *List of available data*
- D. *Available data (CD)*
- E. *Earthquake location and focal parameters*

II. Review of state of knowledge of antropogenically influenced seismicity

A. Introduction

Earthquakes almost always occur when the forces acting to generate movement (shear stress) along a pre-existing fracture exceed the frictional forces (normal stress) acting to resist that movement. When that fracture/fault moves it radiates energy into the surrounding rock in a complex way as a combination of wave types depending on where the fracture is located with respect to a free surface and other geological discontinuities. The radiated energy is transported away by a sequence of wave trains of which the first but not the largest is a compressional wave (P-Wave) where the direction of cyclic deformation is parallel to the direction of transport, followed by waves which produce shear deformations perpendicular to the direction of propagation, called not surprisingly shear waves (S-Wave). If a free surface is relatively close to the failure then strong deformations can occur and propagate at and below that surface as Rayleigh (vertically polarised) and Love (horizontally polarised) wave trains. The S, Rayleigh and Love waves are slower than the P waves and the two latter have frequency dependent velocities (dispersion). These seismic waves transport energy and can be detected on sensitive instruments. If the earthquake magnitude is in excess of 1.5-2.0 local magnitude (M_L), the waves may be felt; and if magnitudes are higher (probably in excess of 4.0 M_L) the waves can cause significant damage and possible loss of life.

B. Anthropogenically Influenced Seismicity

In areas, which are geologically active, such as zones of active rifting or active thrusting in the forelands of mountain belts, it is very likely that the crustal and cover rocks are in a critically stressed state. In such areas minor perturbations to an already precariously balanced stress system can initiate fault movements with associated, sometimes large, earthquakes. The important distinction made by [1] and [2] is between induced and triggered events. For induced seismicity human activity accounts for either most of the stress change or most of the energy associated with the earthquakes. In triggered seismicity human activity accounts for only a small fraction of the stress change and of the energy associated with the earthquakes, whereas tectonic loading plays the primary role. It is conceptually possible to divide earthquakes into a number of different categories but it should be appreciated that the boundaries between these are diffuse:

- **Tectonic Earthquakes**, due to naturally existing stress systems, where the tectonic stress has already exceeded the resisting frictional stress and the region was seismogenically 'ripe'.
- **Anthropogenic Earthquakes, where human activity has played some part in bringing the stress system to failure:**
 - a. **Induced Earthquakes**, where external anthropogenic activities produce stress changes, which are sufficiently large as to produce a seismic event. The rock-mass may not necessarily have been in a

stress-state, which would have led to an earthquake in the reasonably foreseeable future (in a geological sense). Earthquakes produced by procedures such as thermal or hydraulic stimulation of a rock, such as Hydraulic Fracturing and Enhanced Geothermal Systems, fall into this category.

- b. **Triggered Earthquakes** where a small perturbation generated by human activity has been sufficient to move the system from a quasi-critical state to an unstable state. The event would have eventually occurred anyway although probably at some unknown, later time. That is, these activities have advanced the earthquake clock. In this case the additional perturbing stress is often very small in comparison with the pre-existing stress system. The necessary condition for the occurrence of seismicity is a tectonically pre-stressed fault near the human operations altering the stress field, where ‘near’ can be even tens of km away depending on the duration and type of the stimulus. Under certain circumstances, such stress changes can eventually cause the loaded fault to fail. Importantly, since technological operations act only to activate the tectonic stress release process, the magnitudes of such earthquakes can be high, and within the same range as those of natural earthquakes, depending on the amount of elastic strain accumulated on the fault due to tectonic loading.

1. How do we tell the difference between natural and triggered/induced seismicity?

It is clear that there are many, many possible mechanisms which can bring about the minor stress changes which are necessary to generate seismic events during anthropogenic activities, The magnitude of these man-made events can be large and is controlled by the ambient stress field, the magnitude and the duration of the perturbation and the dimensions of the faults which are available to be stimulated. Some of the physical mechanisms are illustrated in **Figure II.1**. Dahm et al [3] sums up the situation very well:

“Human operations, such as mining, hydrocarbon production, fluid withdrawal or injection, drilling, hydro-fracturing and reservoir impoundments, can positively and negatively impact tectonic stresses, pore pressure, fluid migration and strain in the sub-surface. Earthquakes occurring in spatial and temporal proximity to such operations are immediately under suspicion to be triggered or induced. The discrimination between natural, triggered, and induced earthquakes is a difficult task, and clear rules and scientific methods are not well established or commonly accepted”.

Although at present it is not possible to discriminate unequivocally between man-made and natural tectonic earthquakes, some characteristics of seismic processes have already been identified, which can speak for or against possible connections between seismicity and human technological activity.

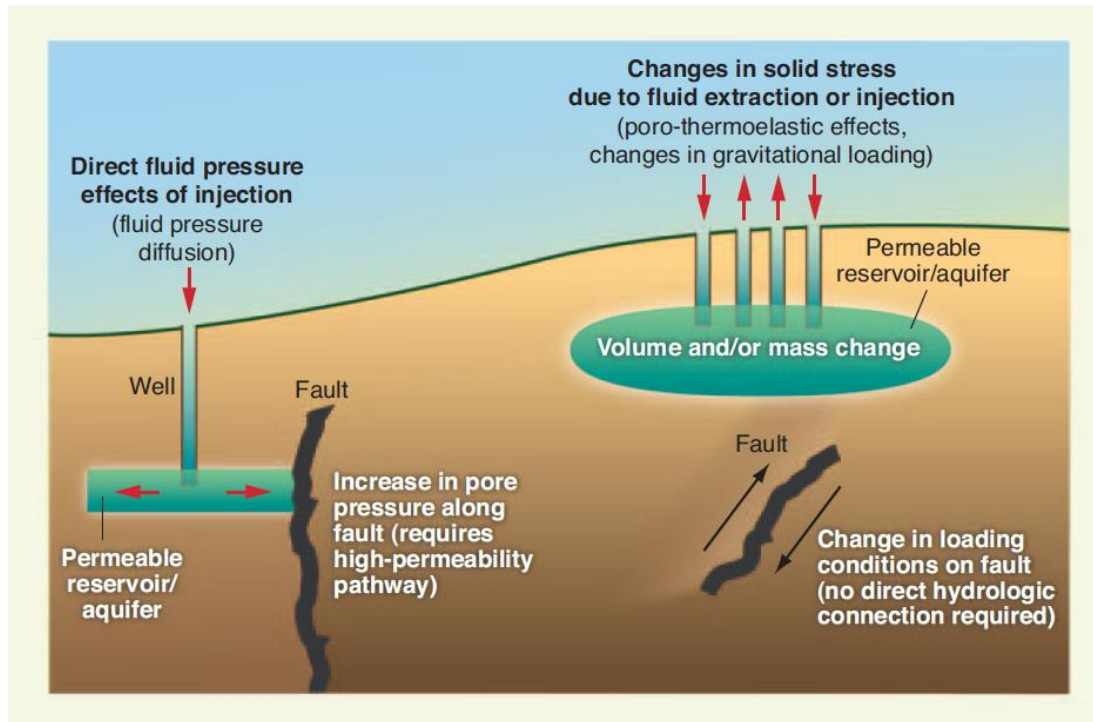


Figure II.1 Potential causative mechanisms for triggered/induced seismicity from [4].

There are seven discriminatory criteria which are often applied in regions where injection or extraction of fluids takes place (modified after [5]). These are:

- i. Are these events the first known earthquakes of this character in the region?
- ii. Is there a clear correlation between injection/abstraction and seismicity?
- iii. Are epicentres near wells (within 5 km)?
- iv. Do some earthquakes occur at or near injection/abstraction depths?
- v. If not, can known geologic structures channel flow to sites of earthquakes?
- vi. Are changes in fluid pressures at well bottoms sufficient to generate seismicity?
- vii. Are changes in fluid pressures at hypocentral distances sufficient to generate seismicity?

These can be useful in many cases to improve the confidence that any particular event or set of events is induced/triggered. This was the case for the 2011 Hydraulic Stimulation events (Fracking) detected in Blackpool Lancashire ([6]). More recent studies show, however, that these criteria are not appropriate in all cases. When there are many activities occurring in a region which is itself seismically active then these criteria cannot be simply applied and it is necessary to look very carefully at spatial and temporal relationships between seismicity and operational parameters associated with pre-existing faults either mapped on the surface or from seismic investigations and also statistical parameters of the seismic events themselves.

The threshold epicentral distance of 5 km used by [5] now seems to be too short compared to observed cases (e.g.[4]). Sometimes the depth of induced/triggered

events correlates well with the injection depth, however at other times the hypocentral depth can significantly exceed the injection interval (e.g. [7]). Violation of the criteria of [5] seems to occur particularly often for triggered earthquakes.

Several cases of delayed seismicity are reported in literature. Keranen et al. [7] report an 18 yr. long lag between the start of fluid injection and the occurrence of Oklahoma, US earthquake sequence from 2011. The lag inferred for the Romashkino Oil Field, the biggest oil field in Russia, was 28 yr. (from 1954 to 1982, [8]). Induced/triggered seismicity may continue even long after termination of injection operations.

The induced, and specifically the triggered, seismic response to injections is complex and variable among cases and its correlation with technological parameters is far from being fully known (e.g. [9], [10]).

2. Induced/Triggered Seismicity around the world.

Of course it is not always so easy to see which of these situations has arisen and in order to assess this we need to look at a range of scenarios, which have been observed in recent years around the world from a variety of different regions.

Because of the occurrence of a large number of recent seismic events which have a prima facie relationship to anthropogenic activities, there have recently been a number of excellent reviews in the last four years of induced seismicity. Shemeta et al to the Committee on Induced Seismicity Potential in Energy Technologies of National Academy of Sciences [11], [12] for Hydrocarbon Fields, [13] and [4] on deep high volume waste water related seismicity and [14] and [15] for induced seismicity related to geothermal projects and other types of induced seismic events in Central Europe and [16] for hydraulic fracturing activities in relation to other activities and [17] for CO₂ related gas storage activities.

It is not useful to attempt to summarise this vast volume of literature and this review will simply draw attention to some of the most significant conclusions and especially those which may be relevant to the seismicity observed in Northern Italy in 2012.

Possible causes of Induced and Triggered Seismicity fall into two main categories:

- Removal of physical support, e.g. Mining where stress change is comparable to ambient stress. Maximum Magnitudes range as high as 5.5 M_L and related to the physical strength of the rock, which is failing. This is also the case for later phases of oil and gas extraction where significant volumes of fluids have been removed so that hydraulic support from pore fluids is lacking, and subsidence and compaction processes come into play.
- Hydrological Changes to include extraction or Injection of water/Gas/Oil, which probably produces triggered seismicity, as the stress changes are small compared to the ambient stress. The magnitudes here depend on the rock strength but perhaps (although numerical modelling suggest that even a limited volume can be effective) also on the total volume of injected (and presumably extracted fluid). It has been acknowledged that although injections inducing or triggering earthquakes are only small fractions of all underground injection cases they can pose a serious risk in particular when injections are performed in naturally active regions (also e.g. [18], [4]).

In particular, the possible causes and observed magnitude ranges of relevance for the Emilia case are:

- i. Oil/gas field Extraction/Depletion (Up 7.3 M_L):
- ii. High volume waste water disposal (Up 5.3 M_L):
- iii. Geothermal operations (Up 4.6 M_L):
- iv. Cases in Debate (CiD). (Up 7+ M_L)

The most relevant of these are discussed in Appendix B.

Other categories (listed below) are not relevant for this study and they will be not discussed further.

- *Hydrofracking of low-permeability sedimentary rocks (1.0 – 3.8 M_L)*
- *Mining (1.6 - 5.6 M_L):*
- *Water injection for secondary oil recovery (1.9 - 5.1 M_L):*
- *Reservoir impoundment (2.0 - 7.9 M_L):*
- *Research boreholes testing for induced seismicity (2.8 - 3.1 M_L):*
- *Evaporite solution mining (1.0 - 5.2 M_L):*

Of critical importance in this report are earthquakes which can be related to the fluid extraction and injection activities. **Figure II.2** shows the global distribution of induced/triggered seismicity and the maximum magnitudes observed and **Figure II.3** breaks this down as a frequency plot.

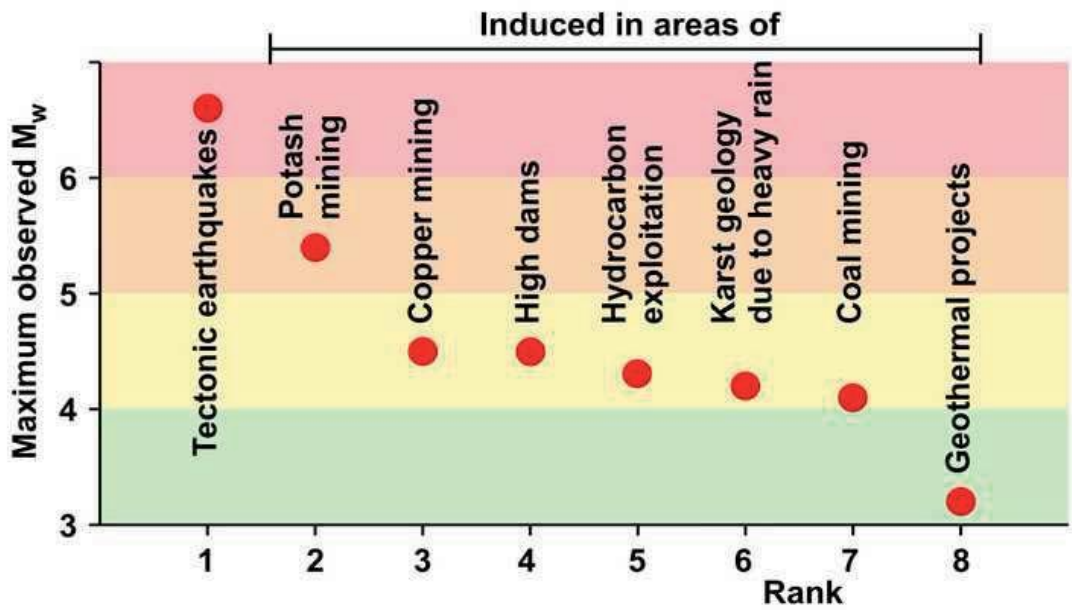
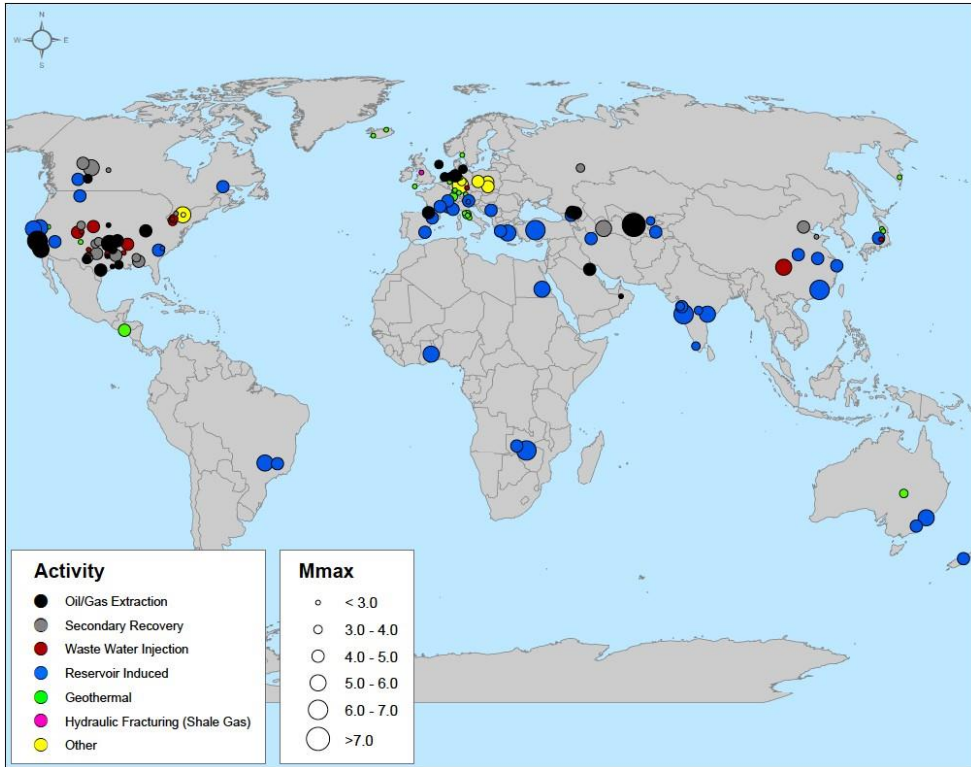


Figure II.2 (top) **Figure II.3** (bottom) Worldwide locations of seismicity likely related to human activities, with the maximum magnitude induced at each site and by type of activity, after [11] and [15].

3. Cases in Debate (CiD)

These are strong and often catastrophic earthquakes, whose origin, whether a purely tectonic or tectonic triggered by a technological activity is very controversial.

The triggering influence of human actions cannot be proved but cannot be excluded either.

The most famous CiD is perhaps the Coalinga earthquake sequence of 1983 shown in **Figure II.4** and **Figure II.5**.

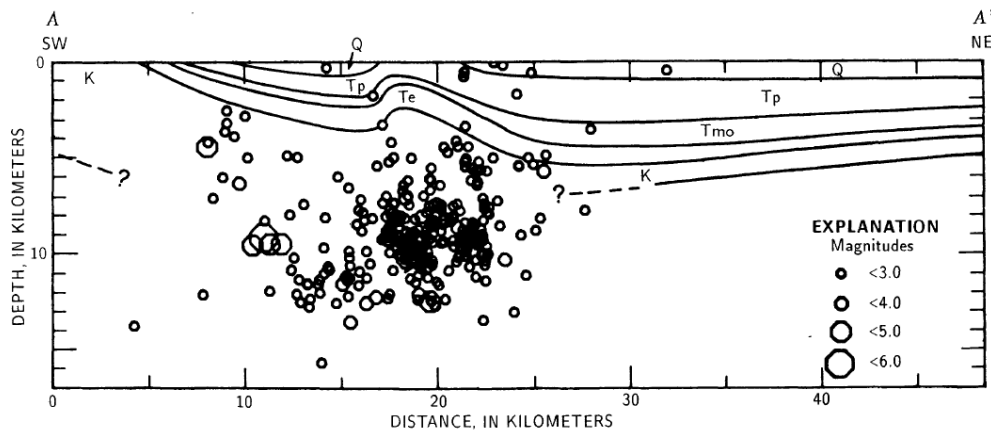


Figure II.4 Southwest-northeast geologic cross section through the Coalinga area, showing locations of the main shock and $M>3$ aftershocks for May-July 1983. ([19]).

On 2nd of May 1983, a magnitude 6.7 M_L occurred approximately 35 km northeast of the San Andreas Fault and about 12 km northeast of the town of Coalinga, California, near two major oil fields, Coalinga Eastside and Coalinga East Extension¹ in a previously aseismic (by Californian standards) region. There was considerable damage to the area including to underground wells, which were sheared. This led to speculation about a relationship between oil extraction and the seismicity. Segall [20] calculated the poroelastic stress change as a consequence of fluid extraction to be 0.01–0.03 MPa which at the time was thought to be a negligible amount in comparison with the energy of the eventual main event although current thinking would not necessarily agree.

The U.S. Geological Survey concluded that the earthquake was associated with a blind fault located on the structural boundary between the Coastal Ranges and the San Joaquin Valley (**Figure II.5**). Two additional major events occurred in the vicinity of Coalinga at Kettleman North Dome 1985 and at Whittier Narrows in 1987 directly beneath major oil fields². McGarr [21] pointed out the similarity between the three events and postulated some mechanisms for their occurrence in terms of crustal unloading.

¹ Coalinga: giant oil field discovered in 1890, cumulative production more than 912,000 million barrels, 1,646 producing wells (data from California Department of Conservation, 2006).

² Kettleman North Dome: giant oil field discovered in 1928. It is one among the major oil-producing areas of the world; cumulative production more than 458,000 million barrels, 40 producing wells (data California Department of Conservation, oil and gas Statistics, Annual Report, 2006).

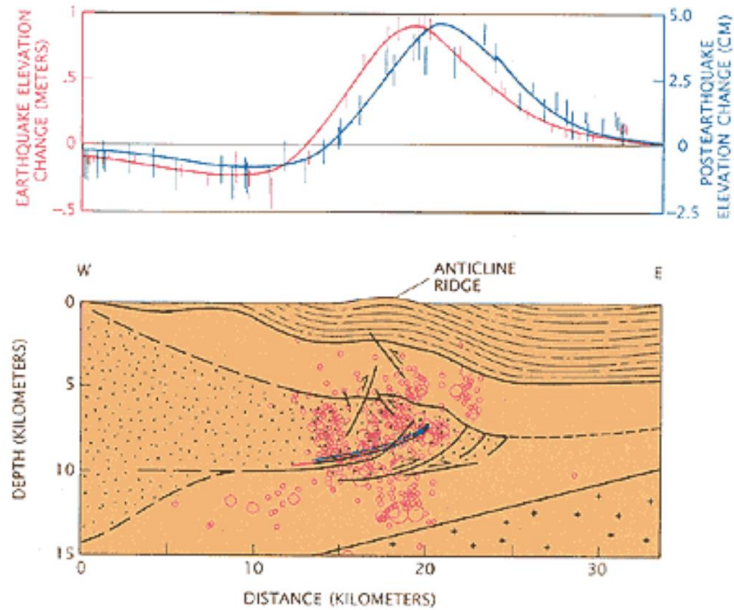


Figure II.5 Subsurface structures beneath the anticlinal sold and elevation changes over the Wilmington reservoir ([22]).

A further CiD and one of the oldest suggestions of hydrocarbon related seismicity is local to Northern Italy in the Caviaga area (**Figure II.6**) where oil and gas reservoirs are in roll-over anticlines within the blind thrusts folds beneath the Po Plain. Two earthquakes of magnitudes M 5.4 and M 4.5 were recorded on May 15th and 16th 1951 with a hypocentral depth at 5 km area in the Lodigiano, northern Italy region. These earthquakes were studied by [23] who was able to calculate directions of the first arrivals from paper-recorded data from twenty seismological stations. The authors argued that there was a possible correlation between seismic events and hydrocarbon activities. In fact in many compilations of induced seismicity, Caviaga is listed as an accepted case of anthropogenic induced seismicity³.

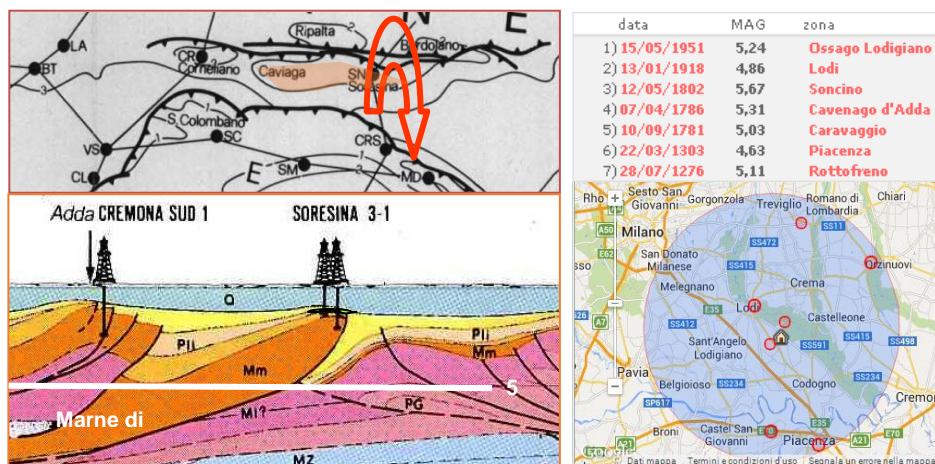


Figure II.6 Structural cross-section, location of oil and gas l of the Caviaga region, Northern Italy and historical and recent seismicity [23].

³ Caviaga: giant gas field cumulative production more than 13,000 MSm³ (2013 data). About 700 MSm³ were been produced from 1944 to 1951.

A recent CiD is from Sichuan, China where an earthquake of moment magnitude (M_w) 7.9 occurred in May 2008 with the epicentre near to a large new dam at Wenchuan and it has been suggested that the loading or even fluid percolation acted as a trigger. However the fault rupture in this event was almost 250 km long, with a large proportion of energy being released far from the influence of the reservoir pore-pressure changes but nevertheless the initial failed patch might have very well have propagated all along the fault.

4. Hydrocarbon Extraction Related Seismicity

Hydrocarbon extraction activities sometimes occur in regions which are naturally seismically active due to tectonic processes which have possibly created the structures and conditions in which oil and gas can be found. Extraction activities and the seismicity are not seen or considered to be related. Whether this is a valid assumption may be questioned in some cases but for the time being it is considered that this is true for the majority of cases. However, there are a number of authoritative reports which list a number of well-examined cases where hydrocarbon extraction has been associated (it may not be possible to use the word proven) with sometime large and damaging earthquakes. The recent IEA Report: Induced Seismicity and its implications for CO₂ storage risk, Report 9/2013 is one such publication and **Figure II.7** identifies those areas.

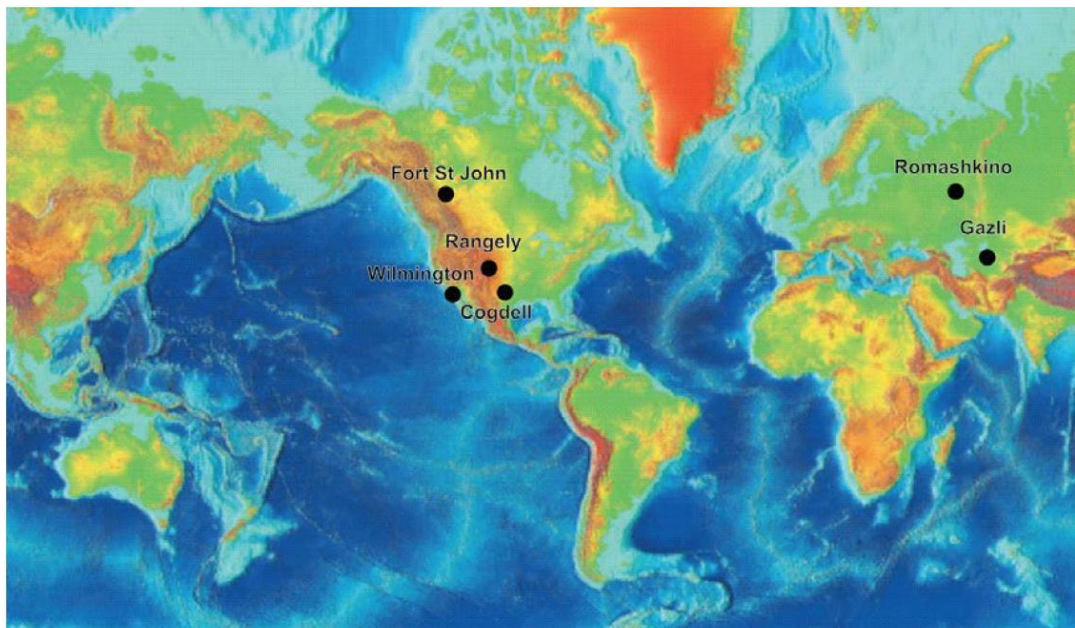


Figure II.7 Sites where Hydrocarbon extraction is firmly considered to be related to seismic activity (from IEA Report: Induced Seismicity and its implications for CO₂ storage risk, Report 9/2013).

Ottremoller et al [24] in a presentation on Ekofisk seismic event of May 7, 2001 in The North Sea also lists a number of events some of which are not included in the IEA map.

The most relevant cases are discussed below.

Rangely Colorado USA

Situated within the Rangely anticline the Rangely oil field has produced oil and gas since 1945 to the present day from the Carboniferous (Pennsylvanian) and Permian Weber sandstone, a low-permeability (12%) sandstone lying at 1700 metres

with a thickness of 350 metres. In order to enhance permeability and increase declining pressure to sustain production, water flooding was implemented from 1957 to 1986 followed by gas injection (CO₂). These procedures induced a number of relatively small earthquakes (M_L 3+) and experiments were undertaken which showed that seismicity could be triggered and then controlled by the rate of water injection and by the fluid pressure. Such simple clear and reproducible relationships have been harder to repeat or discern in other parts of the world.

Gazli , Uzbekistan

The Gazli Field (**Figure II.8**) has been actively producing gas since 1962 (average rate of 20 billion m³/y). In 1976 (twice), and 1984 large earthquakes of 6.8, 7.3 and 7.2 M_L were experienced in the region with extensive local damage, one fatality and more than 100 people injured. The producing horizons are of Cretaceous age and again water injection was trialed to attempt to halt rapidly declining production levels.

Surface subsidence was noted in these cases, which was correlatable with production rates. This is a relatively aseismic area and in fact these are the largest events recorded anywhere in central Asia. They do lie close to a major Fault, the Bukhara-Ghissar structure but the mechanisms do not show stress direction which appear to align with this feature. There is no clear consensus as to the exact mechanism if these were in fact triggered events but they are clearly a cause for concern. Activity is continuing with a sizeable event in 2006.

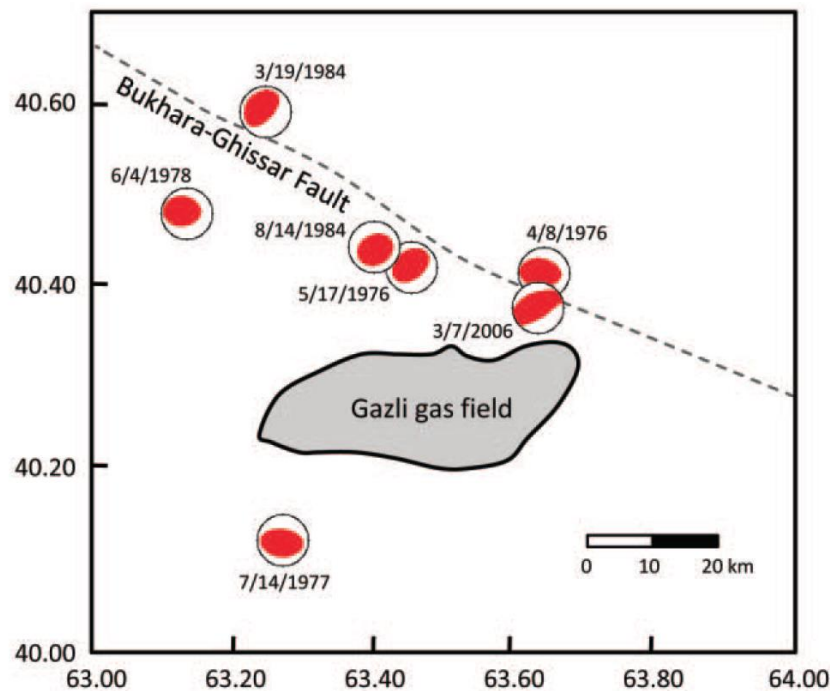


Figure II.8 The extremely large and enigmatic events, which occurred, close to the Gazli Gas field with a maximum magnitude of 7.3 M_L (after [25]).

Romashkino , FSU

The Romashkino field (**Figure II.9**) which has been operational from 1948 until the present day (total production more than 15 billion barrels), is the largest in the Volga Basin with a dimension of c 100 km by 70 km and with oil extraction from Devonian sandstone sequences at about 1800 metres depth. Again, water flooding was

implemented to enhance production from the relatively low permeability reservoir formations, commencing in 1954 with very large volumes injected (total volume of fluid injected for enhanced oil recovery – EOR – 2.13 billion m³), in fact exceeding the total extracted volume and pressures up to 25 MPa (about 250 bar) from initial values of 18 MPa.

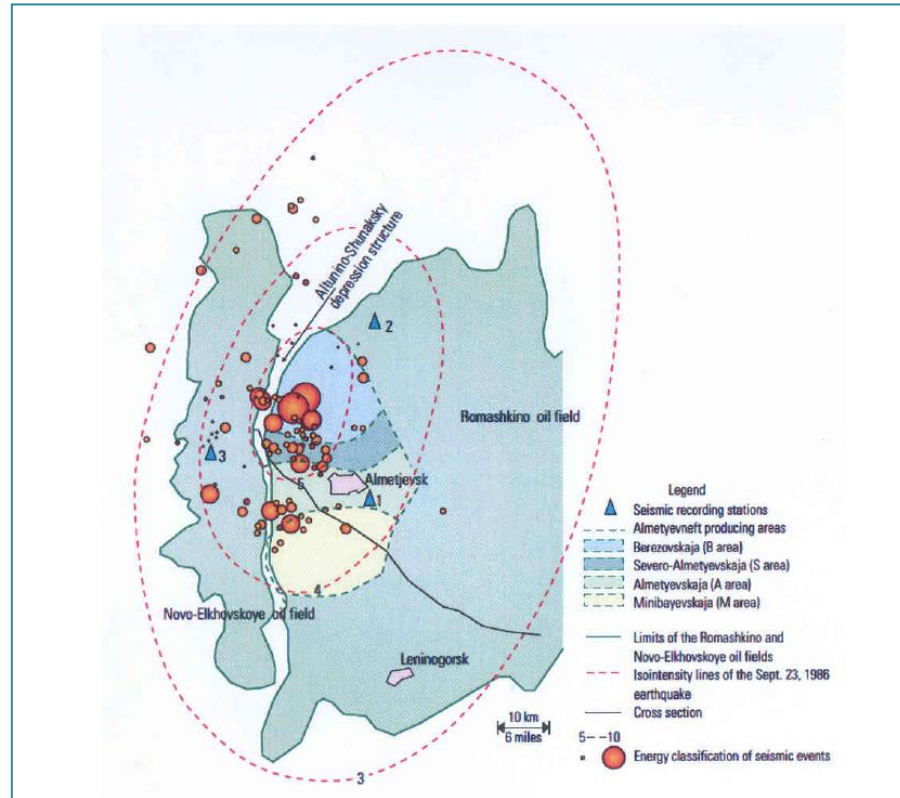


Figure II.9 Seismicity in the Romashkino Oil field region and associated geological structures ([26]).

Moderate seismicity with magnitudes of up to 4 M_L was experienced throughout the 80's and 90's and almost 400 events were detected on a local network installed in 1985. The fluid balance (excess or deficit) between extracted oil and injected water and seismicity rates was clearly correlated as shown in the **Figure II.10**

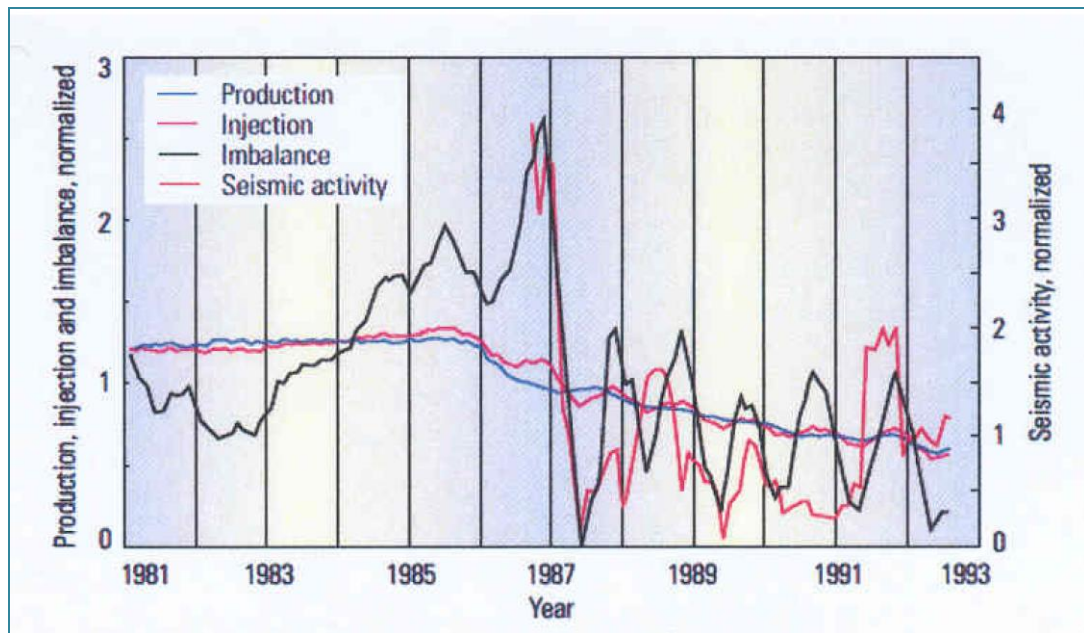


Figure II.10 Relationship between operational parameters and seismicity with a clear correlation between fluid imbalance (difference between the total volume of the extracted oil and the injected water) and the rates of seismic activity at Romashkino Oilfield ([26]).

Wilmington, California, USA

The Wilmington oil field is the largest in California and in total more than 2.5 Billion barrels of oil have been extracted over an 80 years period since 1932 from relatively deep turbiditic reservoirs, which extend down to 3200 meters. This enormous extracted volume has led to significant subsidence of greater than 9 meters with horizontal displacements of almost 4 meters in some places with extensive surface damage (**Figure II.11**). The years 1947, 1949, 1951, 1954, 1955 and 1961 saw a sequence of moderate size, shallow (0.5 km) earthquakes in the Wilmington area with magnitudes ranging from 2.4 to 3.3 M_L although it is very likely that there were many others of much lower magnitudes. In this case water injection to replace extracted volume successfully mitigated both the subsidence and the seismicity.

This led Segall to develop his theory of induced seismicity associated with surface subsidence and associated flexural stresses, which was successfully applied to the Lacq and other fields (**Figure II.12**).

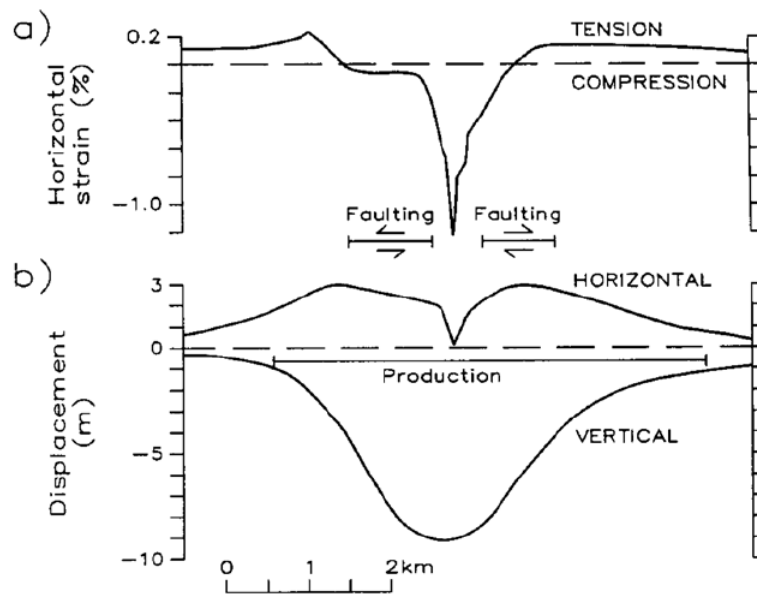


Figure II.11 Surface displacements in the Wilmington region associated with oil extraction. From Segall (1989) after [27].

Chanpura R. [28] carried out an extensive set of models to calculate the possible effects of reservoir depletion on pre-existing faults depending on their geometric relationship. The set of his final conclusions are shown in **Figure II.13** where it is clear that there are conditions for which part of the fault below the reservoir is destabilized.

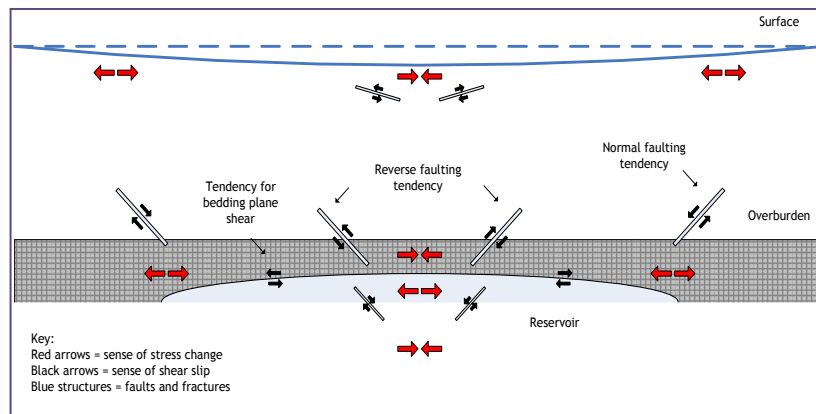
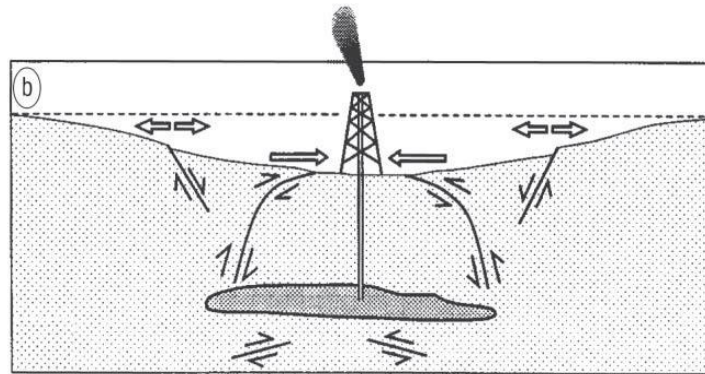
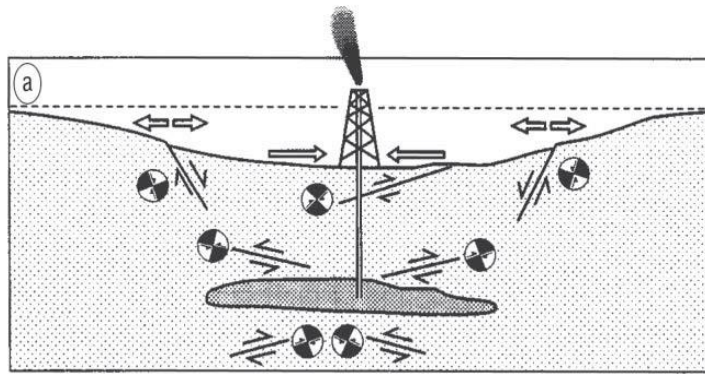
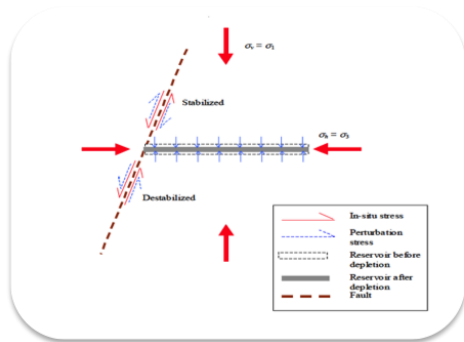
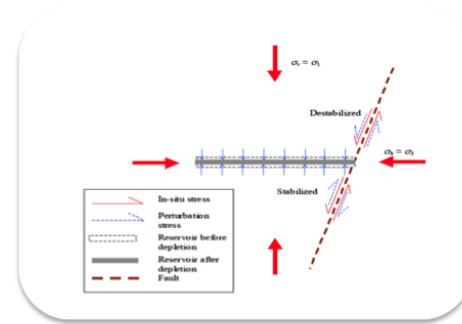


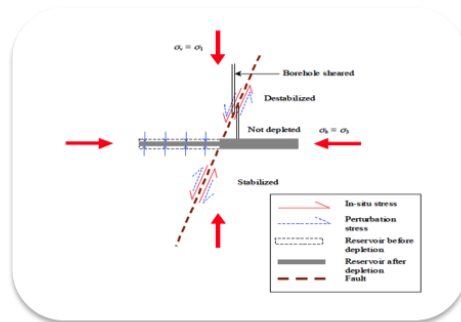
Figure II.12 Segall [29] model for deformation and seismicity associated with water/Oil extraction.



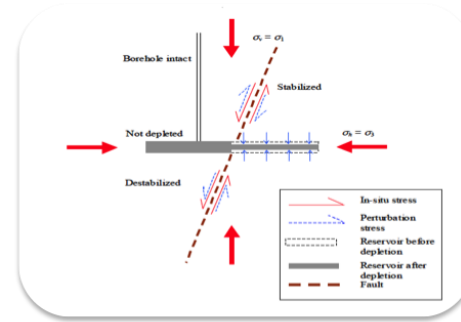
Schematics of instability of left end fault when the reservoir is depleted



Schematics of instability of right end fault when the reservoir is depleted



Schematics of instability of crossing fault when the reservoir is depleted from left to right



Schematics of instability of crossing fault when the reservoir is depleted from right to left

Figure II.13 Changes in Stress Conditions on faults as a consequence of hydrocarbon extraction and reservoir depletion.

Groningen Netherlands

More recently there has been significant seismicity (about 900 events up to 3.5 M_L) in the North of Holland, which is clearly related to the long-term depletion of the Groningen Gas Field, and to the associate compaction of reservoir; this is shown in **Figure II.14**.

The Groningen field is the largest gas field in Europe and the tenth largest in the world. It covers an area of 900 Km^2 . Gas already recovered: about 1,700 billion m^3 ; gas still recoverable: about 1,100 billion m^3 ; original reservoir pressure: about 350 bar; number of wells drilled: about 300. The reservoir is situated in the sandstones of the Upper-Rotliegend (lower Permian) at varying depths ranging from about 3,150 to 2,600 meters. The induced seismicity was observed at around this depth. The first event occurred in 1991, 28 years after the gas production started. From 1991 to 2003, 179 events with magnitudes in the range - $0.2 \leq M \leq 3.0$ was identified ([30]).

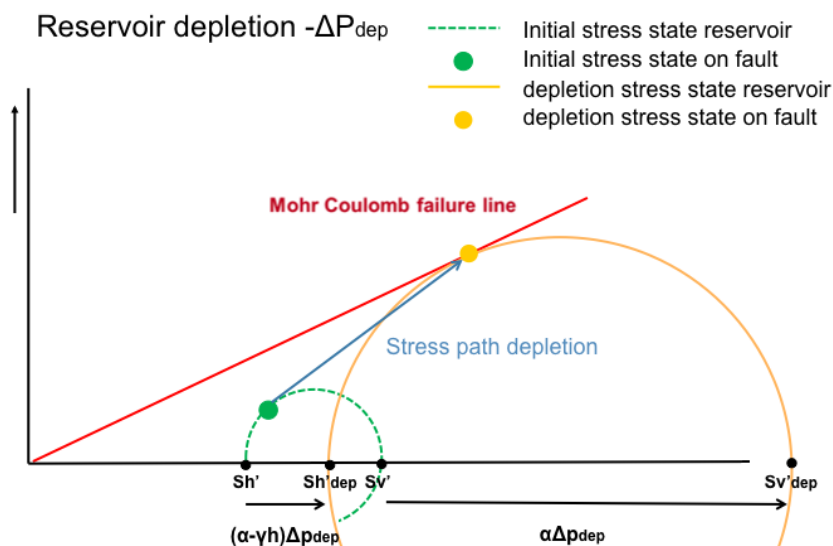
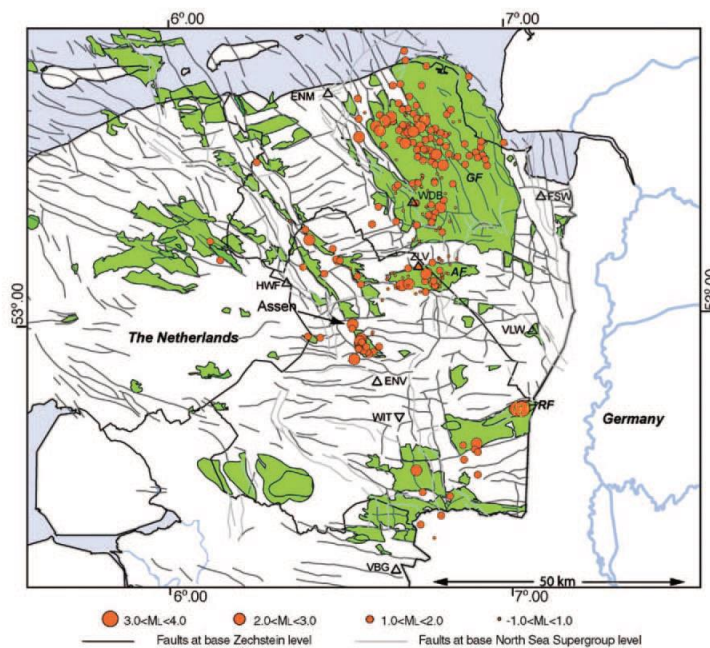


Figure II.14 Recent seismicity in the northern Netherlands over the Groningen Gas Field and the stress changes associated with reservoir depletion and changes in the stability leading to failure according to Mohr-Coulomb theory ([31] and [32]).

5. Induced Seismicity of Geothermal Reservoirs

Examples of seismicity generated by geothermal extraction and water re-injection are numerous and only a small relevant selection are described here. A good recent overview is given by Bromley and is available at:

<http://iea-gia.org/wp-content/uploads/2012/10/Bromley-Induced-Seismicity-International-Taupo-June-2012.pdf>.

However, there are some classic papers and Majer et al [33] is perhaps the best known. There are many examples of mainly low-level seismicity globally as shown in

Figure II.15 and **Figure II.16**. Immense numbers of seismic events mostly of small magnitude are generated during geothermal activities as shown in **Figure II.18** of the intense clouds of relatively low-magnitude seismic activity observed at the Soultz facility in France.

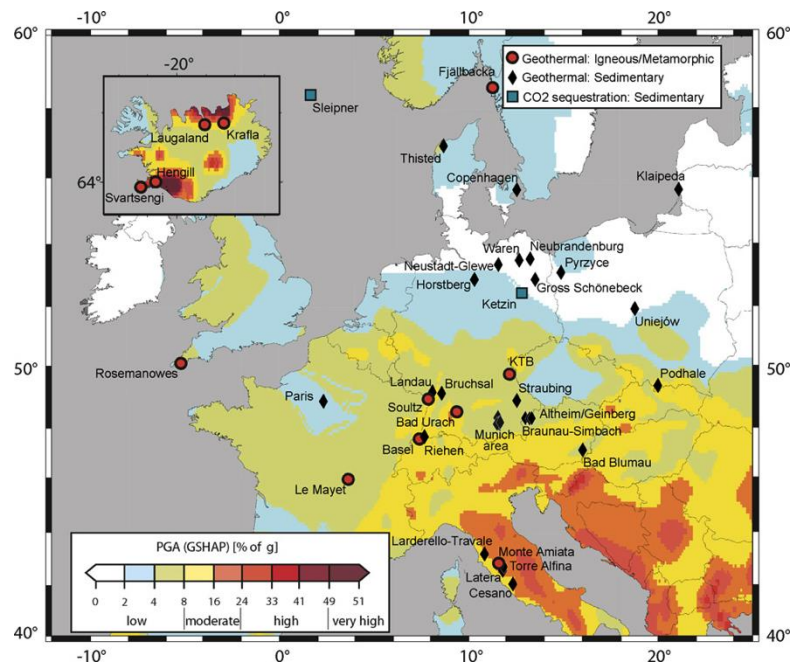


Figure II.15 Location of European geothermal injection sites ([14]).

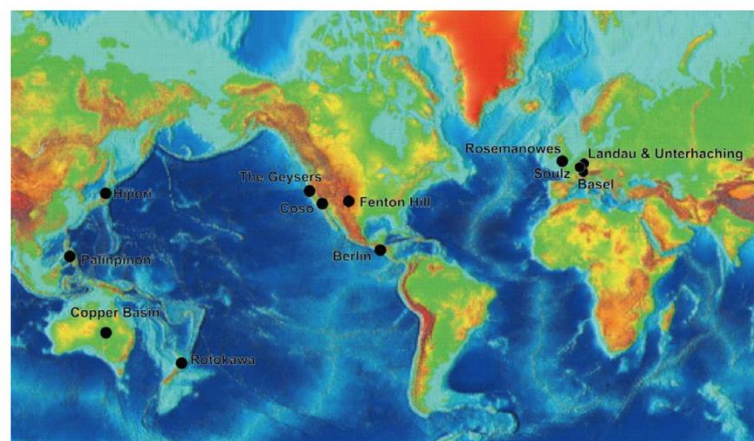


Figure II.16 Some important examples of geothermal related seismic activity.

The Geysers field in California is particularly active. Water has been reinjected and seismicity has occurred both above and below the geothermal reservoir. **Figure II.17** shows the relationships between steam and water injection and seismic activity. However, High-pressure hydraulic fracturing in Engineered Geothermal Systems (EGS) has caused seismic events that are large enough to be felt and have caused some considerable public alarm with associated very large total insurance claims in Basel Switzerland from only a 3.4 M_L event.

The correlation between activity and well-head pressure and injection rate for Basel are shown in **Figure II.19**.

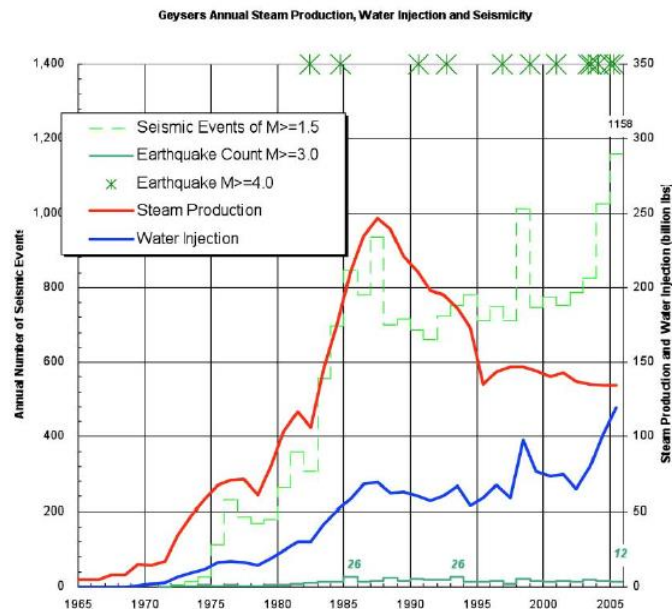


Figure II.17 Operational parameters and seismicity at the Geysers Field California.

The causes of geothermal seismicity have been vigorously debated as they appear to be more complex than those associated just with fluid changes almost certainly because of thermo-geomechanical effects and the range of suggested mechanisms are given below:

- Increased pore pressure (effective stress changes)
- Thermal stress
- Volume change (subsidence, inflation)
- Chemical alteration of slip surfaces
- Stress diffusion
- Production (extraction) induced
- Injection related

It is likely that all of these may play some part but an important recent paper by [9] has shown that for the Salton Sea Geothermal Field the most important parameter appears to be net fluid balance i.e. the difference between extraction and re-injection.

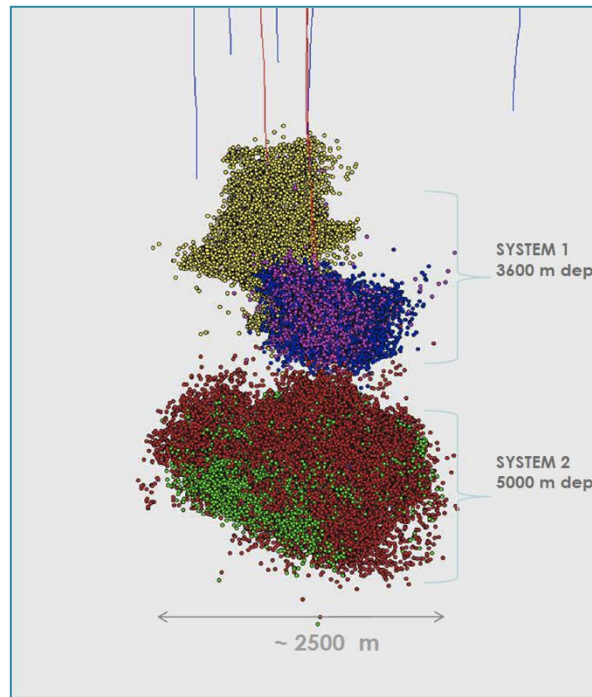


Figure II.18 Seismicity observed at Souلز-sous Foret during a 10 year period from 1993 to 2003 from Baria EGS.

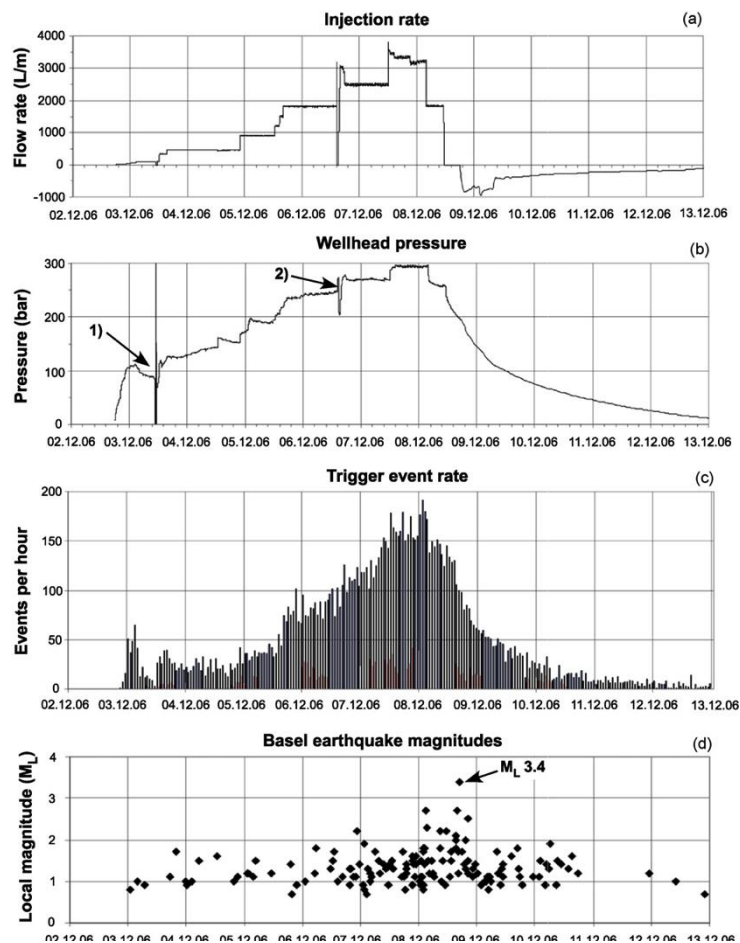


Figure II.19 Data on the hydraulic stimulation of well Basel-1. History of (a) injection rates, (b) wellhead pressures, (c) trigger event rate and (d) Basel earthquake magnitude as determined by Swiss Seismological Survey (SED). From [34].

6. Waste fluid disposal

During extraction of conventional and unconventional oil and gas and, in particular, in secondary recovery and as flow-back after hydraulic stimulation, a great deal of water (and other fluid components and solutes) are generated and in many case these have been re-injected back into the ground at sites close to extraction wells to minimize environmental impact and costs of transport and treatment. Since 2000 a significant increase in observed seismicity of moderate ($3 M_L$) to disturbing ($5.7 M_L$) earthquakes have been observed in the mid-USA as shown in **Figure II.20** and the relationship between this and the large volumes of long-term produced water injection have come under immense scrutiny. The author [4] pointed out that the clear increase from 2005 coincides with rapid increase of shale gas wells and associated increased deep waste-water injection. Between 2005 and 2012, the shale gas industry in US grew by 45 per cent each year.

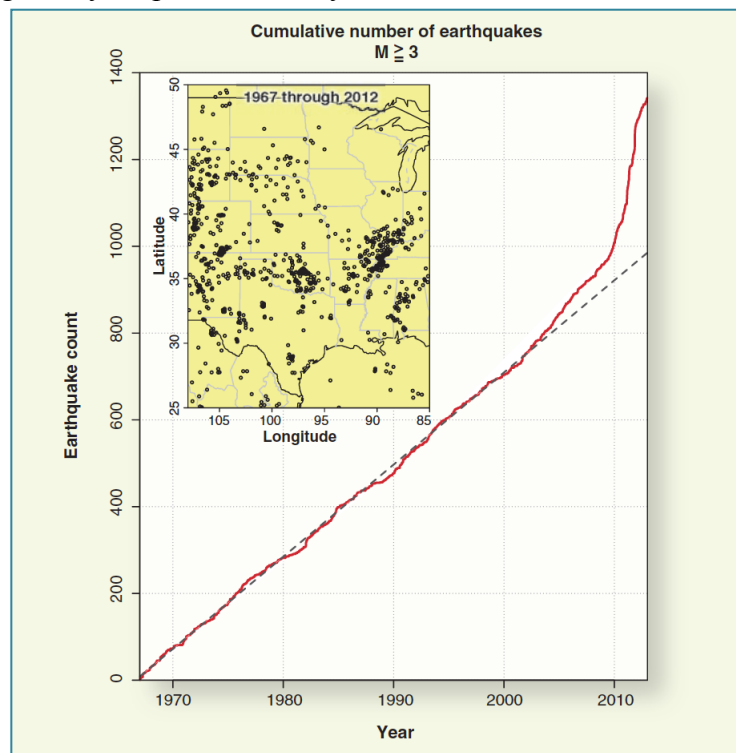


Figure II.20 Growth in the number of mid-continental earthquakes in the last decade ([4]).

Three significant earthquakes with magnitudes of 5.0, 5.7, and 5.0 (**Figure II.21**) occurred near Prague, Oklahoma, United States (on 5th, 6, and 8 November 2011) ~180 km from the nearest known Quaternary-active fault. Earthquakes with magnitudes greater than 5 are not common in this part of United States but have increased in frequency 11-fold between 2008 and 2011, compared to 1976–2007 ([7]). The primarily oil production occurred in the 1950s and 1960s and the fluid injection began in 1993. Initially, fluid was injected at zero reported well-head pressure signifying an underpressured reservoir by earlier hydrocarbon production; hence forward well-head pressure increased in steps reaching an maximum of 3.6 MPa (about 36 bar) in 2006 when the volume of water injected exceeded the volume of oil extracted; total volume injected from 1993 is about 200,000 m³.

Seismic moment exceeds that expected from the relationship of [35] and shown in **Figure II.23** by several orders of magnitude and therefore most of energy should be related to tectonic stress release. This is a potential case of fluid injection into isolated compartments resulting in seismicity delayed by nearly 20 yr from the initiation of injection, and by 5 yr following the most substantial increase in wellhead pressure.

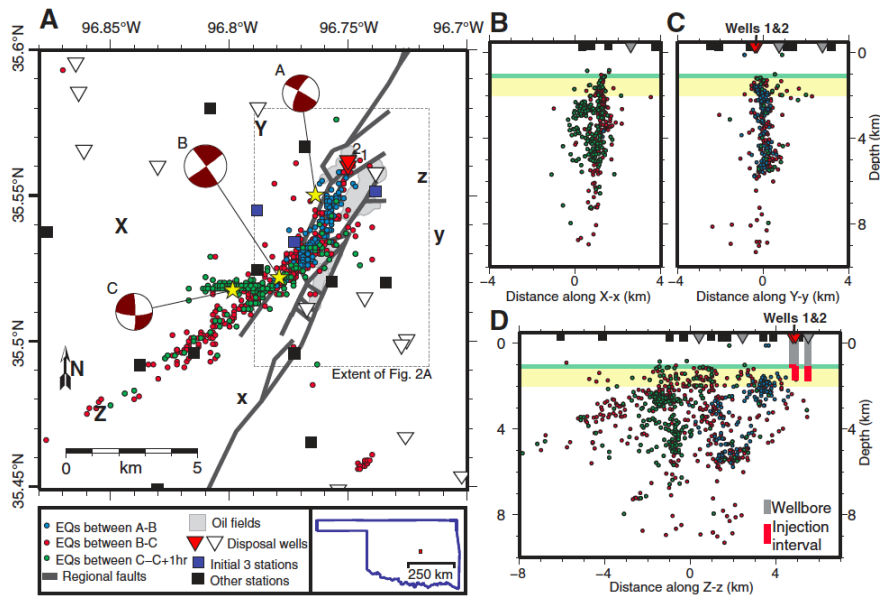


Figure II.21 Seismic centroid moment tensor mechanisms, seismic stations, active disposal wells, and oil fields in Prague Central Oklahoma, United States. Wells 1 and 2 inject near aftershocks of events. B–D: Cross sections of seismicity projected from within 4 km of plane of each section. From [7].

Usually, induced seismicity occurs fairly soon after the start of injection; seismicity began within months of injection commencing at the Rocky Mountain Arsenal⁴ ([36]), in Arkansas ([37]), and Dallas–Fort Worth (Texas) airport ([38]). However, at Prague, Oklahoma, the first significant earthquake (M_w 4.1, in 2010) did not occur until 17 years after injection commenced which has considerable significance in the context of pore-pressure diffusion processes.

Continuing injection over 18 years into subsurface compartments in the Wilzetta field may have refilled a compartment, eventually reducing the effective stress along reservoir bounding faults triggering the 2010–2011 earthquakes. Injection has continued and earthquakes with magnitudes ≥ 3.0 continue to occur.

The first event (A) of M_w 5.0, seems to have been induced by increased fluid pressure, exceeding the largest earthquake of 4.8 M_L previously known to be induced by injected fluid. Aftershocks of event A appear to deepen away from the well and may propagate into basement rocks. It is clear that injection at a relatively shallow level can have consequences for stress changes at significant depths probably into the basement.

Keranen et al [7] consider that while the second event event B, which is much larger at M_w 5.7, and event C may also be due to injection but it is also possible that they have been triggered by Coulomb stress transfer as the fault geometries are consistent with triggering by stress transfer ([39]) if the faults were close to failure, supporting the view that favorably oriented faults are critically stressed and so small- to moderate-sized injection-induced events may result in release of additional tectonic stress. The scalar moment released in this sequence exceeds predictions based on the volume of injected fluid ([35]) by several orders of magnitude, implying that there has been the release of substantial tectonic stress. The 2011 Prague, Oklahoma, earthquakes necessitate reconsideration of the maximum possible size of injection-induced earthquakes, and of the time scale considered diagnostic of induced

⁴ Rocky Mountain Arsenal: a deep well was drilled in 1961 to dispose contaminated waste-water from the production of chemical warfare.

seismicity. This point is emphasized here as this may well have relevance for the Ferrara situation.

In Paradox Valley, to decrease the salinity from the Dolores River, brine has been extracted from nine shallow wells along river and, after treating, the brine has been injected in the Paradox basin, 4.3 – 4.8 km below the surface (total injected volume: 4 Mm³) since 1991. Between 1985 and June 1996, only three tectonic earthquakes were detected within 15 km of the well and 12 within 35 km. Subsequently, hundreds of earthquakes below M_L 3 were induced during injection tests conducted between 1991 and 1995. High injection pressure (70 MPa) was required and induced earthquakes were not unexpected. The activated zone expanded, with earthquakes occurring as far away as 8 km from the injection point within a year to beyond 12 km several years later. As a precaution shutdowns of 20 days occurred to attempt to allow the fluid pressure to equilibrate, and preclude larger events; however, a M 4.3 event was induced in May 2000.

The Paradox Valley seismicity also illustrates how long-term, high-volume injection leads to the continued expansion of the seismically activated region and the triggering of large-magnitude events many kilometers from the injection well more than 15 years after commencement of injection.

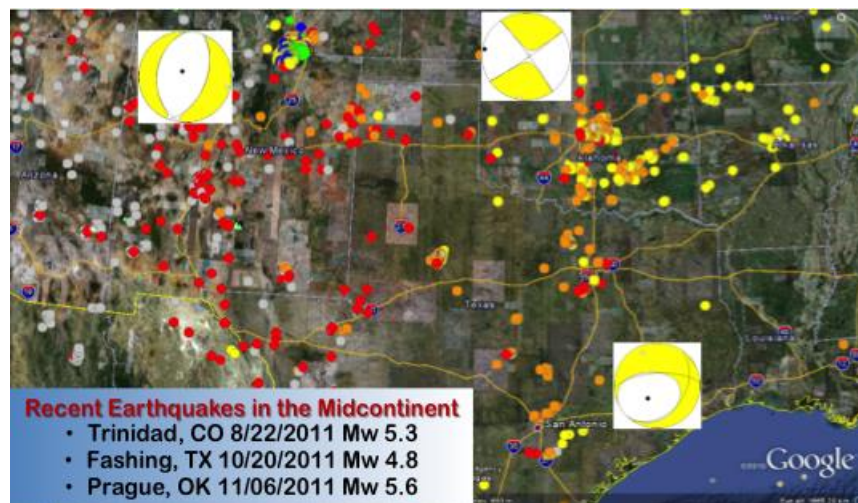


Figure II.22 A compilation of seismic events from the mid continental USA compiled by [40].

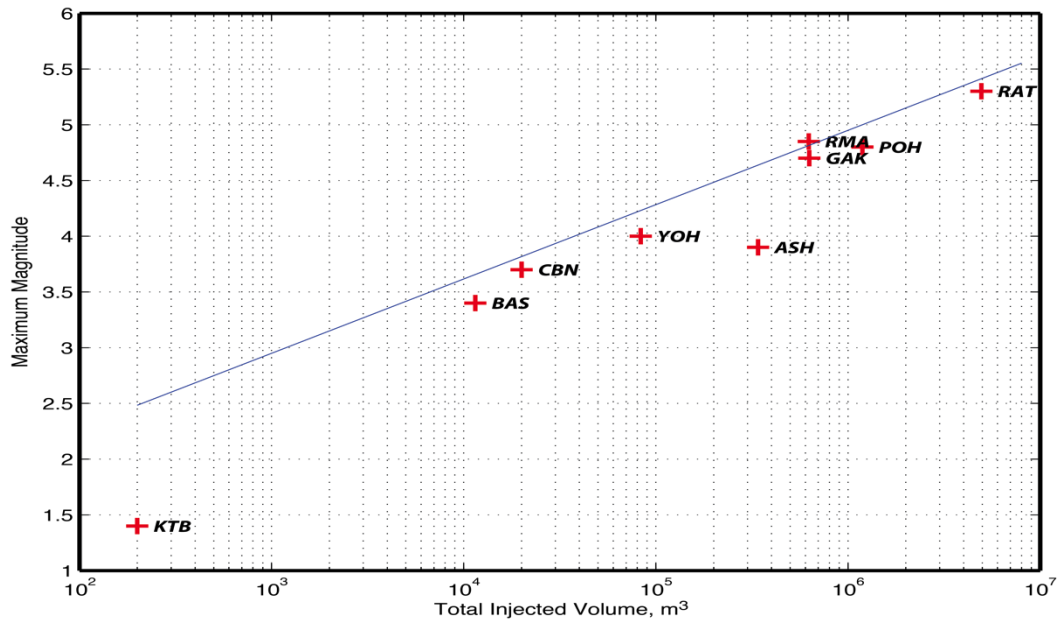


Figure II.23 Maximum Magnitude plotted against total injected volume for a number of injection sites, (Table II.1) .

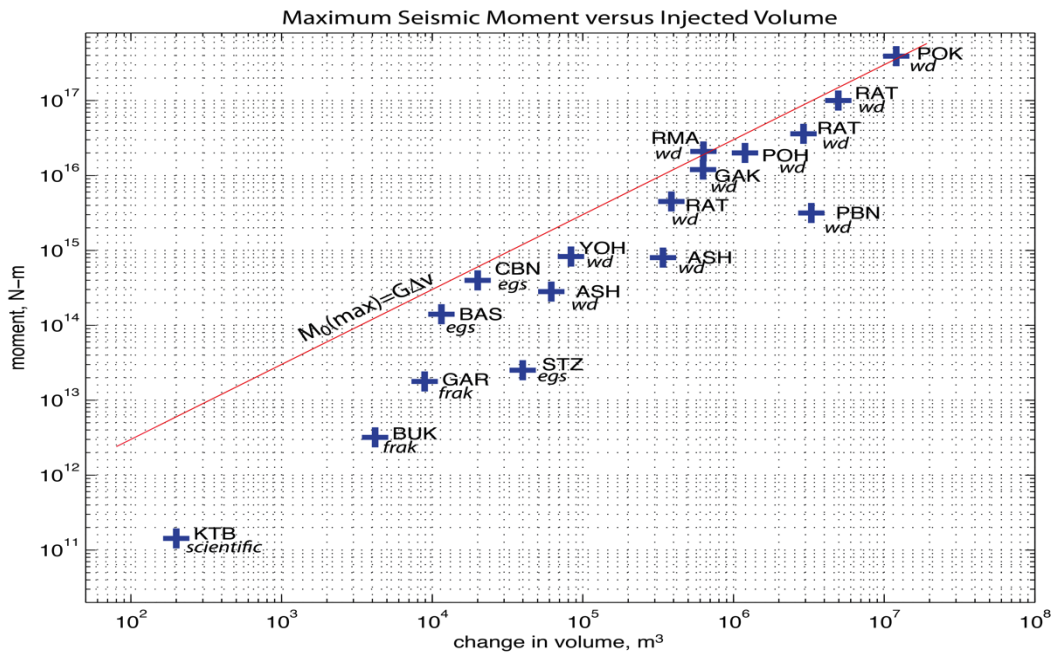


Figure II.24 Maximum Seismic Moment plotted against total injected volume for a number of injection sites, wd=water disposal and frak is hydraulic stimulation (Table II.1).

McGarr ([40]) plots the maximum magnitude (Figure II.23 from the USA) and maximum seismic moment (global Figure II.24) for against total injected fluid volume and there appears to be a reasonable correlation with both increasing and approaching the theoretical maximum of $G\Delta V$.

Table II.1 Maximum seismic moment $M_0(\text{max})$ and total injected volumes ΔV ([40]).

Event	$M_0(\text{max}), \text{Nm}$	$\Delta V, \text{m}^3$	Type*	M	Location
KTB ¹	1.43e11	200	scientific	1.4	Eastern Bavaria, Germany
BUK ²	3.2e12	4.17e3	frak	2.3	Bowland shale, UK
GAR ³	3.5e13	1.75e4	frak	3.0	Garvin County, OK
STZ ⁴	2.51e13	3.98e4	egs	2.9	Soultz, France
DFW ⁵	8.9e13	2.82e5	wd	3.3	Dallas-Fort Worth Airport, TX
BAS ⁴	1.41e14	1.15e4	egs	3.4	Basel, Switzerland
ASH ⁶	2.82e14	6.17e4	wd	3.6	Ashtabula, OH, July, 1987
CBN ⁴	3.98e14	2.0e4	egs	3.7	Cooper Basin, Australia
ASH ⁶	8.0e14	3.4e5	wd	3.9	Ashtabula, OH, January 2001
YOH ⁷	8.3e14	8.34e4	wd	4.0	Youngstown, OH
PBN ⁸	3.16e15	3.287e6	wd	4.3	Paradox Valley, CO no
RAT1 ⁹	4.5e15	4.26e5	wd	4.4	Raton Basin, CO, September 2001
GAK ¹⁰	1.2e16	6.29e5	wd	4.7	Guy, AR
POH ¹¹	2.0e16	1.19e6	wd	4.8	Painesville, OH
RMA ¹²	2.1e16	6.25e5	wd	4.85	Denver, CO no
TTX ¹³	2.21e16	9.91e5	wd	4.8	Timpson, TX
RAT2 ¹⁴	1.0e17	7.84e6	wd	5.3	Raton Basin, CO, August 2011
POK ¹⁵	3.92e17	1.20e7	wd	5.7	Prague, OK no

*frak – hydraulic fracturing; egs – Enhanced Geothermal System; wd – wastewater disposal. ¹ [41]; ² [42]; ³ [43]; ⁴ [33]; ⁵ [38]; ⁶ [44], [45]; ⁷ [46]; ⁸ [47]; ⁹ [48]; ¹⁰ [37]; ¹¹ [49]; ¹² [50], [51]; ¹³ [52]; ¹⁴ [53]; ¹⁵ [7].

McGarr considers the Painesville, Ohio, (POH) earthquake of January 1986 ([49]), in some detail. Although the distance between the two high-volume injection wells and the Painesville earthquakes at 12 km is relatively large, there are some former cases for earthquakes being induced at comparable distances from injection wells. Most of the Guy, Arkansas, earthquakes were located in the basement at distances ranging up to between 10 and 15 km from the two injection wells (disposal of hydrofracking waste fluid) implicated in this sequence ([37]).

It should be made clear that there is a significant difference between Waste Water Disposal where large volumes are injected over long periods and Enhanced Oil Recovery where only sufficient volumes required to maintain pressure to replace oil extracted are used and this is emphasized by Hitzman et al [11] :

“Intuitively, processes that withdraw fluids from a formation and reinject fluids back into the same formation are less likely to cause large increases in pore pressure. Enhanced recovery operations were found by the NAS committee to have minimal influence of induced seismicity. McGuire reported that relative to the large number of waterflood projects for secondary recovery, the small number of documented instances of felt induced seismicity suggests that those projects pose small risk for events that would be of concern to the public.

The (US National Academy of Science) committee did not identify any documented, felt induced seismic events associated with EOR (tertiary recovery). They concluded that the potential for induced seismicity is low”.

Rongchang and Huangjiachang Gas fields, Chongqing, China

In many of the cases described here the injection of waste water is carried out into deeper formations or even into basement rocks where larger magnitude events might be expected but even injection into the same reservoir from which oil and gas is being extracted can cause seismicity. A very good example of this comes from the Huangjiachang and Rongchang gas fields, Chongqing, China which is reported by [54] and [55].

The Huangchei and Rongchang gas fields⁵ are located in Sichuan Basin, that is characterized by an annual production of over 12,000 Mm³. More than 20 commercial oil and gas fields have been discovered in the Basin that is also known for the production of mine salt by pumping water.

In the Huangchei field, seismicity began to be observed at a gas reservoir in the relatively stable Sichuan Basin, China, after injection of over 120,000 m³ waste water into the depleted Permian limestone reservoir at depths between 2.45 to 2.55 km, at a wellhead pressure of up to 6.2 MPa from 9 January 2009 to July 2011 (**Figure II.25**).

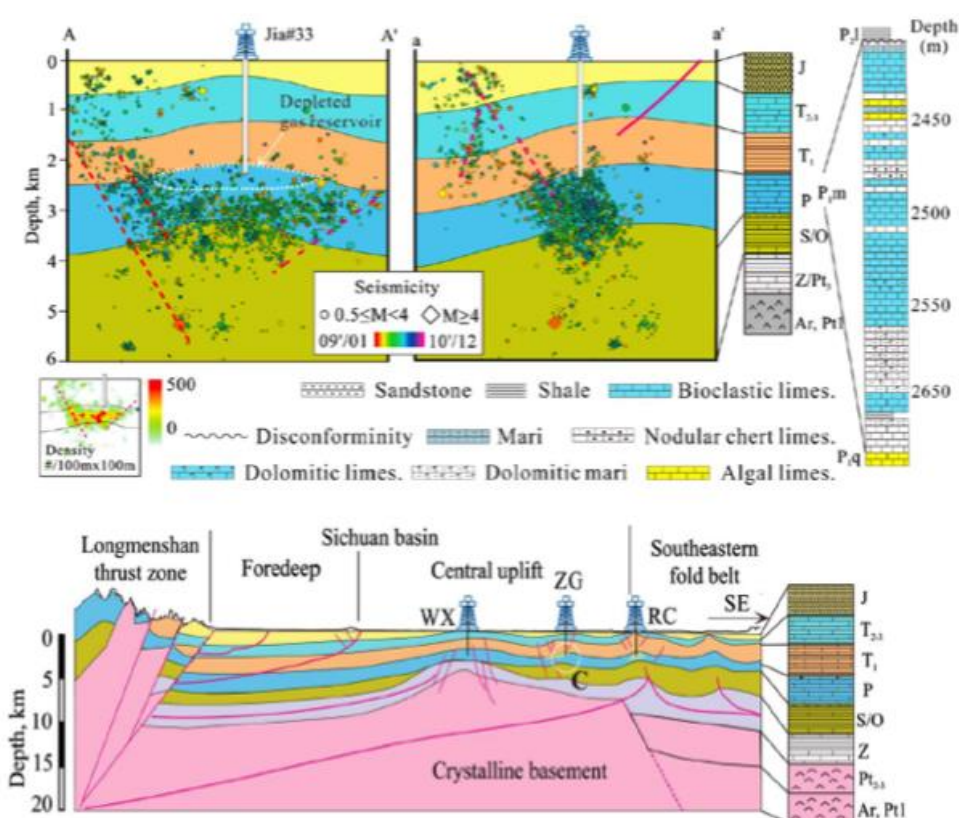


Figure II.25 Geological Cross Section across a thrust zone and its associated foreland basin (lower) and seismicity generated on the thrusts around the anticline where oil and gas have been extracted from a limestone reservoir subsequent to injection of some 120,000 m³ of waste-water at 6 MPa. After [55].

⁵ **Huangjiachang field:** since 2007 a production well was used for the injection of unwanted water that was collected through pipelines from nearby production wells. The injection rate was <300 m³/day up until April 2008, and then increased to about 500 m³/day toward the end of 2008. During this period, fluid was placed into the well under gravity flow. Since 2009, pumping under high pressure was required for injection (up to 6.2 MPa).

Rongchang field: unwanted water has been injected since 1988. The major injection well was not a gas production well (Luo-4); the water injection rate was 683 l/min. The pumping pressure was variable, with a maximum value of 2.9 MPa. The average monthly injection volume in 1988 was about 2,000 m³, increasing to about 10,000 m³ in 1990. In the following years, the average monthly injection volume varied between 6,000 and 15,000 m³. A total of more than 1Mm³ of water had been pumped into the formations.

More than 7000 surface-recorded earthquakes, up to 4.4 ML, occurred with 2 M4+, 20 M3+, and more than 100 M2+ events located at depths ranging from 2.5 to 4 km, within the Permian limestone and lying in a zone of 6 km by 2 km with a NNW trend, centred on the injection well⁶.

Lei et al. [55] consider that the induced earthquakes were due to lowering of the effective normal stress on critically-loaded, pre-existing, blind faults. It appears that despite the injection being into the extracted zone this did not appear to balance out the fluid effects and significant and prolonged activity occurred from within the faulted reservoir.

⁶ In general, the seismic activity in Zigong is thought to be associated with either the production of salt water, natural gas, or water injection. The timing and location of recent seismic activity (2009-2010) are strongly statistically correlated with fluid injections and the seismic activity falls into the category of induced earthquakes.

C. Mechanisms of Fluid Injection and Abstraction Related Seismicity

It has been known since the 1960s that earthquakes can be induced by fluid injection when military waste fluid was injected into a 3671 m deep borehole at the Rocky Mountain Arsenal, Colorado ([56]). This induced the so-called ‘Denver earthquakes’. They ranged up to M_L 5.3, caused extensive damage in nearby towns, and as a result, use of the well was discontinued in 1966. Reviews of activity often focus on selected mechanisms although there are notable exceptions ([57]). Artificially injecting fluids into the Earth’s crust induces earthquakes (e.g. [6]). Indeed this can have effects at even the smallest scales as [58] showed that very tiny pressure variations associated with precipitation can trigger earthquakes to a depth of a few kilometres. Observations of isolated swarm-type seismicity below the densely monitored Mt. Hochstaufen, SE Germany, revealed strong correlation between recorded seismicity and spatiotemporal pore pressure changes due to diffusing rain water in good agreement with the response of faults described by the rate-state friction laws. Similar results have been observed in Switzerland (**Figure II.26**).

If pore fluid is present then the induced pore pressure change is the pressure change times the Skempton’s coefficient B .

Skempton’s B coefficient is an important characteristic of a porous medium that describes the relationship between pore pressure and changes in the mean stress under undrained conditions. (B) is defined to be the ratio of the induced pore pressure to the change in applied stress for undrained conditions - that is, no fluid is allowed to move into or out of the control volume:

$$B = - \left. \frac{\partial p}{\partial \sigma} \right|_{\xi=0} = R/H = \beta_p/S_\sigma$$

The negative sign is included in the definition because the sign convention for stress means that an increase in compressive stress inducing a pore pressure increase implies a decrease in σ for the undrained condition, when no fluid is exchanged with the control volume.

Skempton’s coefficient must lie between zero and one and is a measure of how the applied stress is distributed between the skeletal framework and the fluid. It tends toward one for saturated soils because the fluid supports the load. It tends toward zero for gas-filled pores in soils and for saturated consolidated rocks because the framework supports the load.

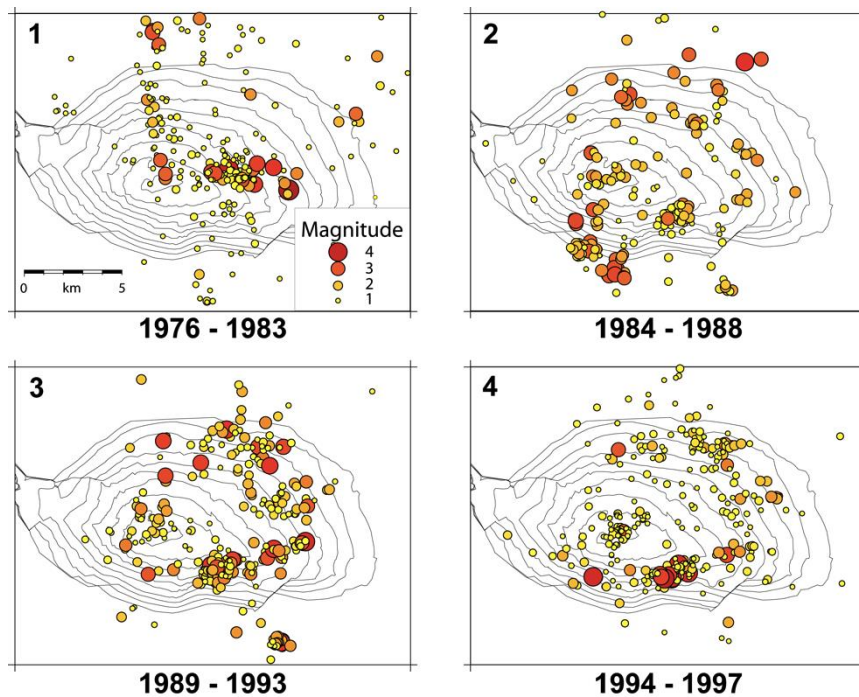


Figure II.26 Sequences of seismicity in the Lacq Gas field in the Aquitaine Basin in France from 1976 through 1997 induced by fluid extraction.

A physical causative mechanism for natural fluid-driven swarms as well as for induced seismicity is pore pressure diffusion ([59]). Increases in pore fluid pressure act to reduce fault strength, bringing pre-existing fractures closer to failure according to the Mohr–Coulomb failure criterion. The initiation of fluid injection in a region leads to substantial increases in pore fluid pressure, which build up over time and diffuse outward for significant distances and for significant times from a well. The amount and magnitude of seismicity induced therefore depends on the ambient tectonic stress, as well as local geological and hydraulic conditions. Thus, induced seismicity can continue even after injection has ceased, as was the case at the Rocky Mountain Arsenal where three ~ 4.5 earthquakes occurred the year after waste fluid injection stopped ([36];[50];[51]). Fluid injection not only perturbs stress by changing the poro-elastic condition ([60],[61]) and creates new fractures, but it also potentially introduces pressurised fluids into pre-existing fault zones, causing slip to occur earlier than it would otherwise have done naturally by reducing the effective normal stress and moving the failure closer to the Mohr–Coulomb criterion. This was first observed in the LACQ gas field in the Aquitaine Basin⁷ ([20], [61]) (**Figure II.26**).

The stress perturbation attenuates rapidly away from the sphere, over a distance of about twice the sphere radius. The stress induced inside the sphere is compressive when fluid is injected but tensile for fluid withdrawal.

Pore pressure and stress perturbation associated with fluid injection increases the risk of slip along a fault within the zone of influence. Just as injection can trigger seismicity, abstraction can also do so by the same mechanisms of poro-elastic stress diffusion. As fluid is extracted, declining pore pressures cause the permeable reservoir rocks to contract, which

⁷ The Lacq gas field in France is one of the best-documented cases of seismicity induced by extraction of fluids (Grasso and Wittlinger 1990, Segall et al. 1994). The reservoir was highly over-pressured when production started in 1957, with a pressure of about 660 bars at depth of 3.7 kilometers below sea level. The first felt earthquake took place in 1969, at a time when the pressure had decreased by about 300 bars. By 1983, the pressure had dropped by 500 bars (10 Mm³ of water were injected). 800 seismic events with magnitude up to M 4.2 had been recorded. The epicenters of 95% of the well-located events and all of the M > 3 events were within the boundaries of the gas field. The subsidence reaching a maximum of 60 mm in 1989. The gas volume already recovered is over 246,000 MSm³ (source: Total).

stresses the neighbouring crust. In the case of fluid withdrawal, the region at risk is generally outside the reservoir. The geomechanical interpretation of these is shown in **Figure II.27**.

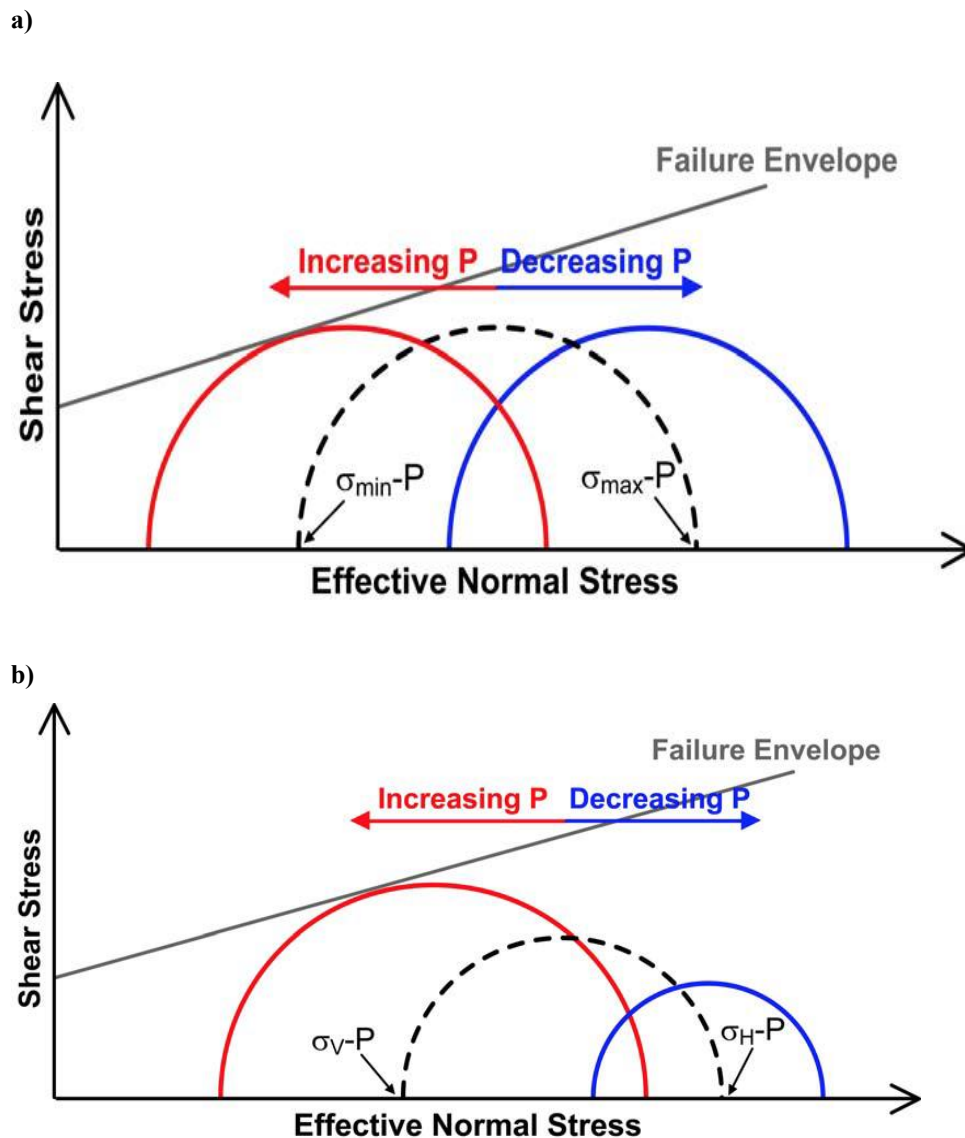


Figure II.27 a) Increasing pore pressure counteracts the normal stress leading to increased probability of failure; b) The effect of pore pressure increase (red line) and decrease (blue line) on an initial effective state of stress (dashed line) in a thrust faulting regime, from [62].

Nicol [63], somewhat before McGarr, drew the conclusion that the expected maximum magnitude is related to the total injected /extracted volume (**Figure II.28**) but in some cases where significant tectonic stress is present even larger events than are suggested by this relationship can be stimulated. He also comments on the depth to which stimulation of activity can take place with special emphasis on zones where interaction with large tectonic features may occur:

“The depths of induced seismicity and injection are generally on average, slightly deeper than the reservoir interval. These deeper events may in some cases be induced by loading or unloading of the sub-reservoir rock volume by fluid injection or extraction, respectively.

These conclusions apply equally to the largest earthquakes, which are randomly distributed within the depth range of seismicity for each site. Large magnitude earthquakes produced up to 10 km beneath large-scale hydrocarbon extraction sites (volumes >120 million m³) are a notable exception to the above conclusions. The greater focal depths for some extraction-related earthquakes have been interpreted to be a direct reflection of the fact that extraction of large volumes of fluids has the potential to induce crustal -scale deformation and seismicity”

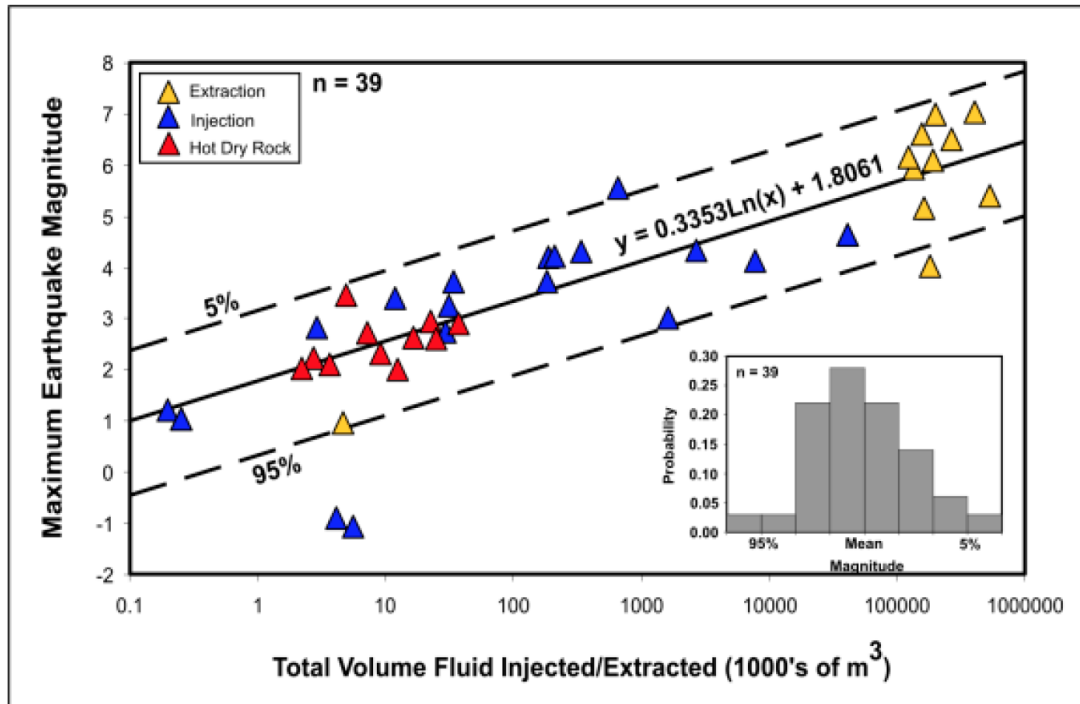


Figure II.28 Maximum magnitude and its relationship to total injected volume.

He also plots the maximum expected radius of simulation from an injection zone and this is shown in **Figure II.29** and it is clear that this can easily exceed 20km for large injected volumes where critically stressed faults of appropriate orientation exist. **Figure II.30** shows the expected time of occurrence as a function of the total operational time and it clear that near events occur rapidly but distant events may have onset times of many years.

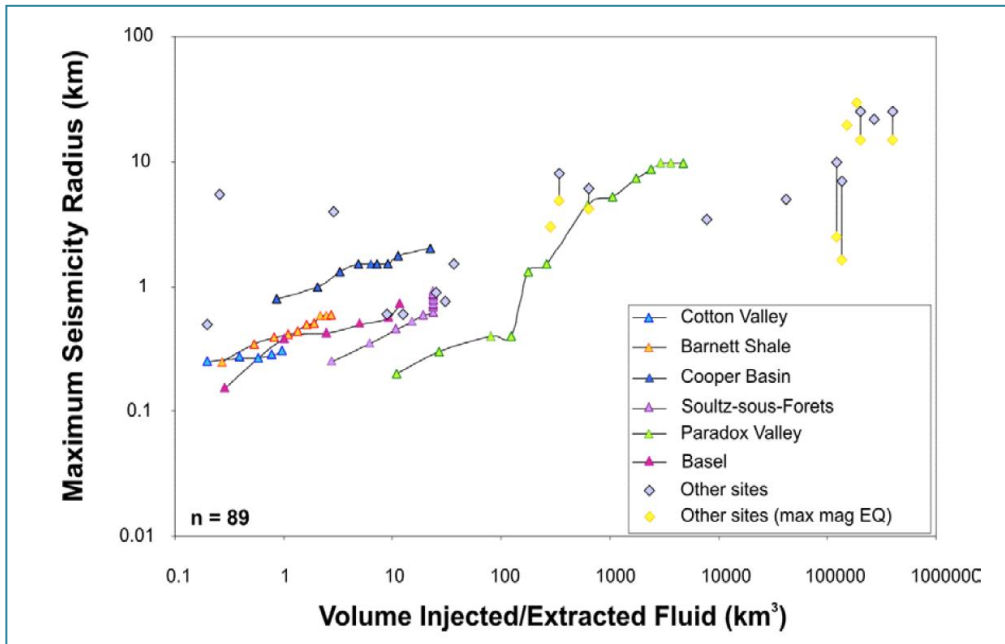


Figure II.29 Maximum radius of induced seismicity from the injection well plotted against the volume of fluid injected (from IEA 9/2013 [64] after [63]).

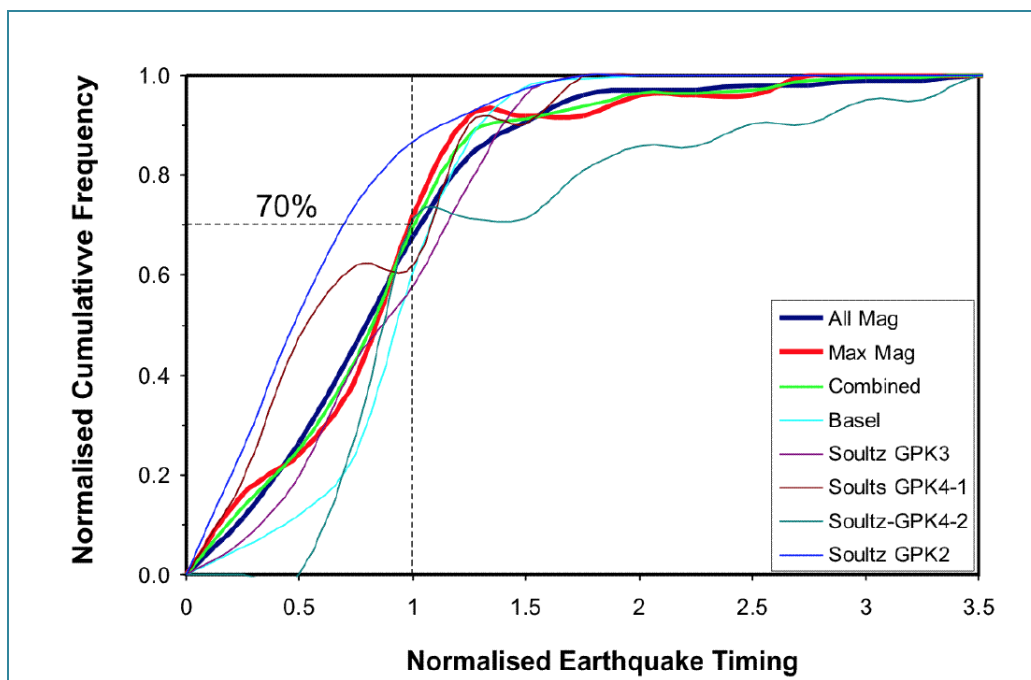


Figure II.30 Timing of induced earthquakes relative to the onset (0) and completion (1) of injection/extraction. (from IEA 9/2013[64] after [63]).

1. Stress Transfer

Whenever an earthquake happens it produces local (and distant) stress changes of two types:

- **Static:** these are permanent changes, which occur because stress has been redistributed and can lead to sufficient stress change that adjacent faults become unstable and fail with additional seismicity. The effects depend on the orientation of

both the failing fault and the receiving fault and can be calculated. A stress change of about 0.01 MPa is considered sufficient to act as trigger to another seismic event.

- **Dynamic:** these are transient effects which occur because waves carrying energy from the first seismic event travel away from the source and produce a short duration cyclic loading which can in some circumstances produced a large enough stress change to trigger an earthquake. It has been suggested by Van de Elst that even distant teleseisms from giant earthquakes may be influential in some circumstances. Again it depends on the geometry and stress state of the receiving faults.

Figure II.31 shows the consequence of stress changes on two instances of blind thrusts, which are the dominant reservoir structures in the Po Basin. If the thrust cuts the surface the stress becomes reduced but if the fault is ‘blind’ i.e. it doesn’t reach the surface, the stress is increased.

2. How do Earthquake faults fail?

Although it can appear that earthquakes are instantaneous releases of stored elastic energy they do in fact take a significant time to release their stored potential which can take some minutes in the case of giant earthquakes such as Sumatra (26 December 2004) as can be seen from the following table.

Table II.2

Mw	Moment Mo	Length	Mean Slip	Area of slip	Duration
4	10^{15} N m	1000 m	2 cm	1 km ²	0.2 s
5	3.0×10^{16} Nm	3000 m	10 cm	9 km ²	0.4 s
6	1.1×10^{18} Nm	10 km	40 cm	100 km ²	5 s
7	3.5×10^{19} N m	80 km	1 m	1000 km ²	30 s
8	1.1×10^{21} Nm	300 km	6 m	6000 km ²	150 s
9	3.5×10^{22} Nm	800 km	20 m	6×10^4 km ²	300 s

A sequential set of ‘patches’ which are strong zones which have been preventing the fault from slipping, fail one after another often progressively outwards from an initial failure but sometimes returning close in as stress changes during the event. What had seemed to be a single giant event can be thought of as a consecutive assemblage of smaller events which simply happen very close together and their cumulative effect is catastrophic.

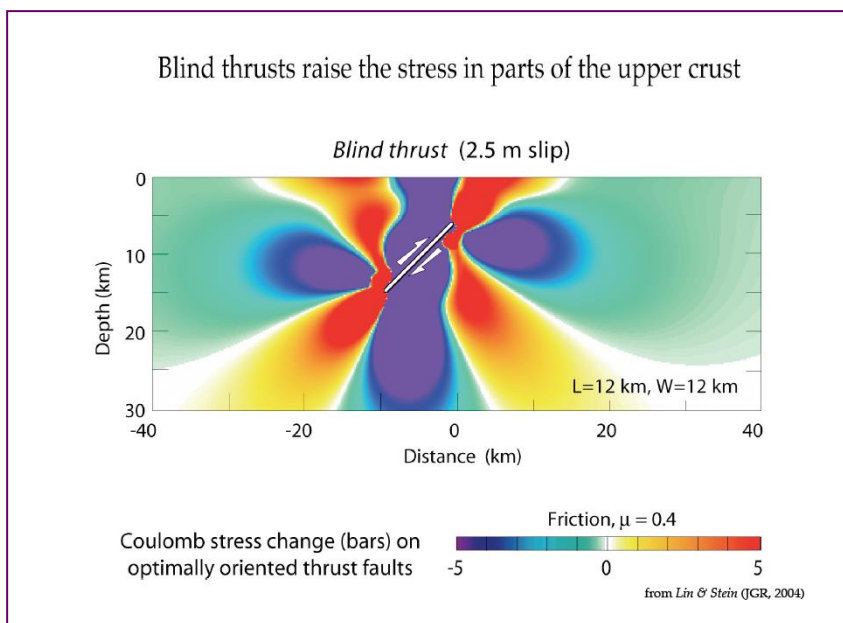
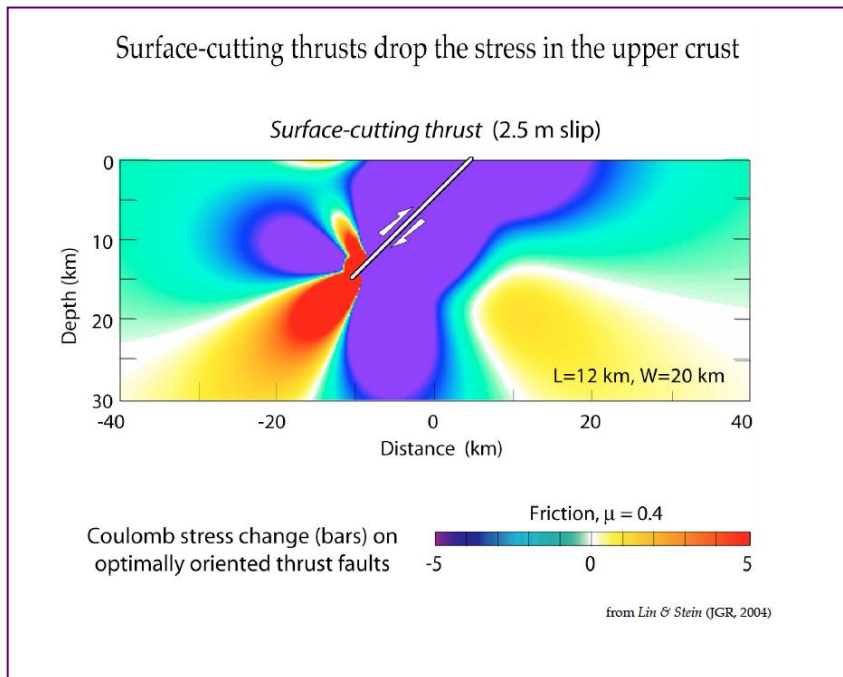


Figure II.31 Coulomb Stress changes around a surface cutting fault(top) and a blind thrust (bottom). The faults beneath the Po Basin are all Blind.

3. What is an aftershock?

It has been customary to divide earthquakes into:

- Foreshocks: i.e. occurring as precursor to a much larger ‘Mother’ event and probably on the fault surface which will eventually fully fail.
- Main Shock: The ‘Mother’ Event, with complete failure of the rupture surface.
- Aftershocks: i.e. progressively smaller events occurring on the same, or part of the same fault surface which failed in the mainshock.

The modified Omori-Utsu Law (which dates back to 1894!):

$$R(\tau) = K(c + \tau)^{-p}$$

is an attempt to describe the rate of decay (R) of aftershocks with the reciprocal of time (τ) with p being an exponent somewhere between 0.75 and 1.5 but conceptually something like unity.

Aftershock sequences are modelled by the Epidemic Type Aftershock Sequence (ETAS) model which assumes that all earthquakes are in general able to trigger subsequent aftershocks which can have even larger magnitudes than the “mother” earthquake ([65]). In the ETAS model the earthquake rate, R_{ETAS} at a location x , and time t , is the sum of a constant background rate μ and the superposition of aftershock activity from preceding earthquakes, that is,

$$R_{ETAS} = \mu + \sum_{i: t_i < t_E} \frac{K_E 10^{\alpha(M_i - M_c)}}{(t_E - t_i + c)^p}$$

The seismicity rate R of a population of faults is inversely proportional to the state variable γ describing the creep velocities of the faults:

$$R(t) = r/\tau_r \gamma(t)$$

$$d\gamma = (dt - \gamma dCFS)/A\sigma$$

where r is the background seismicity rate, τ_r the tectonic loading rate, and A is a dimensionless fault constitutive parameter ([66]). Hence, the seismicity rate depends on the evolution of the Coulomb failure stress,

$$CFS = \tau + \mu\sigma$$

where as usual, τ is the shear stress on the assumed fault plane, σ is the effective normal stress (positive for extension), and μ is the friction coefficient. This model is able to explain an induced Omori-type occurrence of aftershocks in response to a single coseismic stress step ([66]).

4. Statistical properties of anthropogenic seismicity

Statistical analyses of induced seismicity reveal collective properties, which differ from those of natural seismicity (e.g. [67]; [68]; [69]). The most predictable feature is non-stationarity; a time-dependence of induced seismic processes. An induced seismic process is partially controlled by technological operations, which vary on short-timescales resulting in time changes of the seismic process.

Natural earthquakes typically (but not always) follow the Gutenberg–Richter law which describes the relationship between the magnitude and total number of earthquakes in a region in a given time period.

$$N=10^{a-bM}$$

Where:

- N is the number of events greater or equal to M
- M is magnitude and a and b are constants

The b -value (see appendix B) is a measure of the rate of increase in number of earthquakes with certain magnitudes and is often close to 1, i.e. each increase of 1 in magnitude produces a decrease in number of events by 10.

Variations of the activity rate and/or other parameters of the seismic process, e.g. temporal changes of Gutenberg–Richter b -value suggest a non-natural origin of a seismic series ([70]). Induced seismicity should have properties, which are absent in natural seismicity: certain orderliness, internal correlations, and memory.

The magnitude distribution of induced seismicity often does not follow the Gutenberg–Richter law but is more complex and often multimodal. Out of six analyzed seismic series associated with: injection for geothermal energy production in Basel, Switzerland, injection for hydrocarbon recovery in Romashkino Oil Field in Russia, Açú dam reservoir in Rio Grande do Norte State in Brazil, Song Tranh 2 dam in Vietnam, Rudna copper-ore underground mine in Poland, Mponeng deep gold mine in South Africa; the hypothesis that their magnitude distributions follow the Gutenberg–Richter law has been rejected in every case with high to very high significance ([71]; [72]; [73]). The complexity of magnitude distribution becomes an important discriminator between induced and natural seismicity.

Even when significant deviations from the Gutenberg–Richter law for anthropogenic seismicity cases cannot be ascertained there are some subtleties such as described in **Figure II.32** from IEA Report 9/2013 [64] and **Figure II.33** from the Basel study where there seems to be a clear relationship between reservoir permeability and the b value from induced seismicity recorded from there. Low permeabilities tend to be associated with high b values and high permeabilities with low b values, which is interpreted as stress is taken up in small perhaps tensile events in shales but greater fluid percolation distance in high permeability reservoirs may facilitate stimulation of more distance on existing structures.

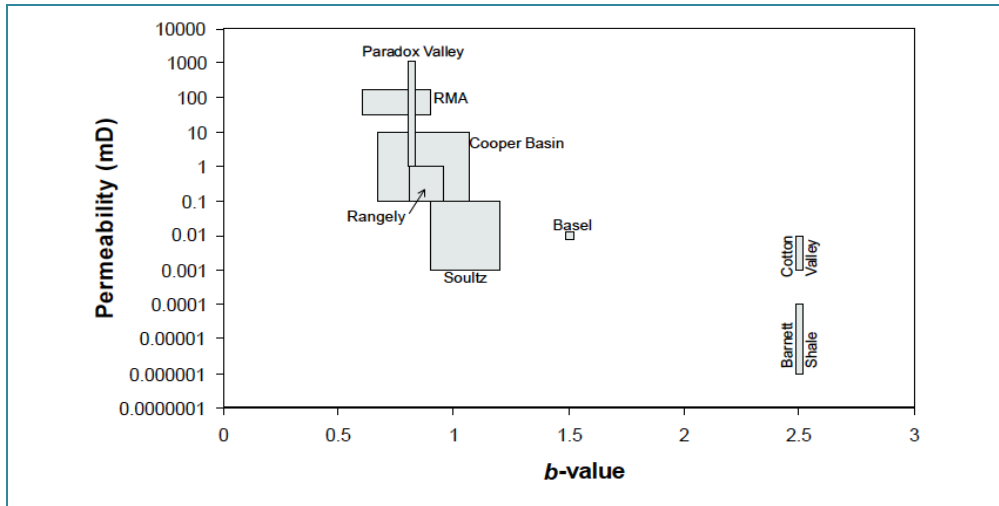


Figure II.32 Gutenberg-Richter b-values against permeability for a number of injection induced seismicity sites (from IEA9/2013 [64]).

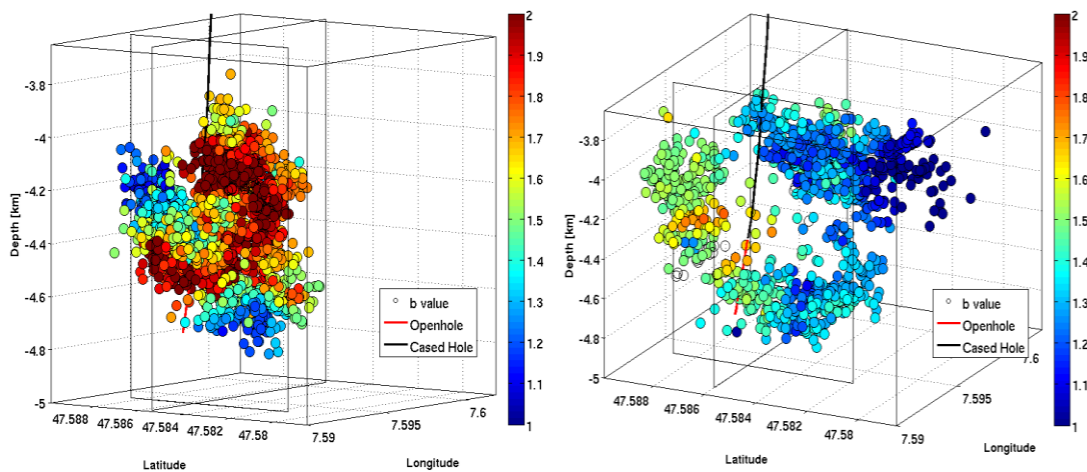


Figure II.33 Gutenberg-Richter b-values before injection (left) and after injection (right) at Basel after [74].

A comparison of b-values for a range of European seismic event groupings has been generated by [75] and is shown in **Table II.3**. The variation in b-values during the Basel swarm is shown in the visualization in **Figure II.33**, where it appears that values around 2 are seen during injection but these fall back to much lower values of around 1.1 to 1.2 in the post-injection period.

Table II.3 Comparison of b-values for a range of European seismic event, from [75]

Source of seismicity	<i>b</i> -value with $\pm\sigma$
Geothermal projects	1.94(\pm 0.21)
Natural tectonic earthquakes Long-term data	1.25(\pm 0.01)
Natural tectonic earthquakes Short-term data	1.16(\pm 0.05)
Hydrocarbon exploitation	0.93(\pm 0.11)
Coal mining	1.59(\pm 0.05)
Copper mining	2.13(\pm 0.22)
Salt and potash mining	1.02(\pm 0.09)

5. Action at a distance: the effect of fluid injection

Murphy et al. [76] describe a simulation of the effect of even a very limited injection over only 15 days to a pressure of only 170 bar on the criticality of a large fault situated outside the actual zone of injection which is a permeable reservoir but sandwiched between two impermeable layers at a depth of about 3 km (**Figure II.34** and **Figure II.35**). This numerical study showed that active faults near injection sites, even when not in direct contact with the injected fluids, could be greatly affected by stress perturbations caused by their presence. Their simulated injection induces a M_w 6.7 event with a hypocentral depth at 8 to 10+ km (**Figure II.36**) which is entirely controlled by the fault size and its previous tectonic loading and not the injected volume; the injection simply triggers the release of this stored energy.

Additionally, the injection not only advances the next sequence of earthquakes affects their size and permanently alters the size and temporal occurrence of earthquakes but also temporarily shifts the fault to a state of subcriticality (i.e. stabler) but with continuous tectonic loading the fault returns to near self-organized criticality in about 200 yr.

Their results suggest that fluid injection can trigger earthquakes whose size is dependent on the size of the fault, not the injection and that these faults do not necessary need to be in the injection site.

Table II.4 Parameters used in [76]: models of fluid injection related seismicity

Strata	D_{xx} ($m^2 s^{-1}$)	D_{yy} ($m^2 s^{-1}$)	D_{zz} ($m^2 s^{-1}$)
Cap Layer 1	0.1	0.1	0.1
Reservoir	2.0	2.0	0.1
Cap Layer 2	0.1	0.1	0.1
Boundary	0.05	0.05	0.1

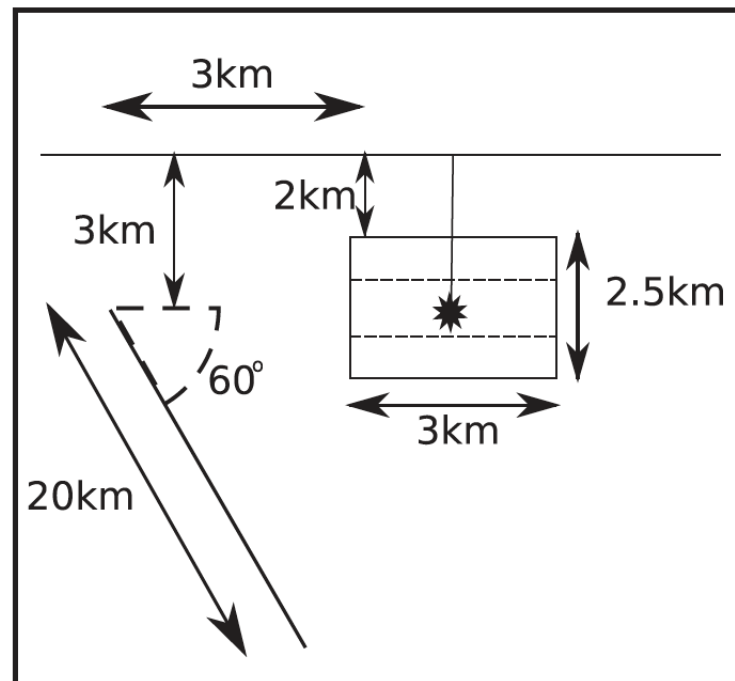


Figure II.34 Murphy et al [76] schematic of the injection site relative to a fault. The injection occurs half way along the strike of the fault which is 40 km long at a depth of 3.3 km (denoted by the star) into a reservoir which extends from 3–4.5 km. The horizontal dashed lines are the boundary between the reservoir layer and cap layers 1 and 2.

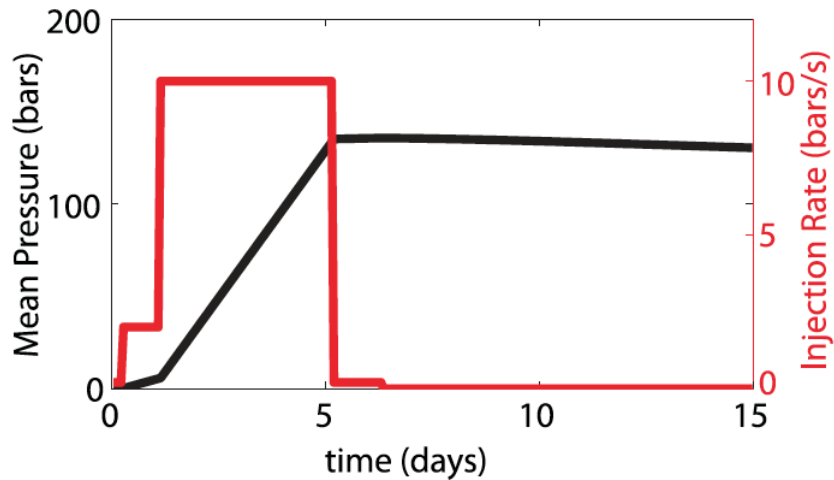


Figure II.35 Pressure injection history. Maximum injection rate (red line) is 10 Bar s⁻¹. Injection stops at 6.73 d. Mean pressure (black line) is for the whole simulation volume not just the reservoir.

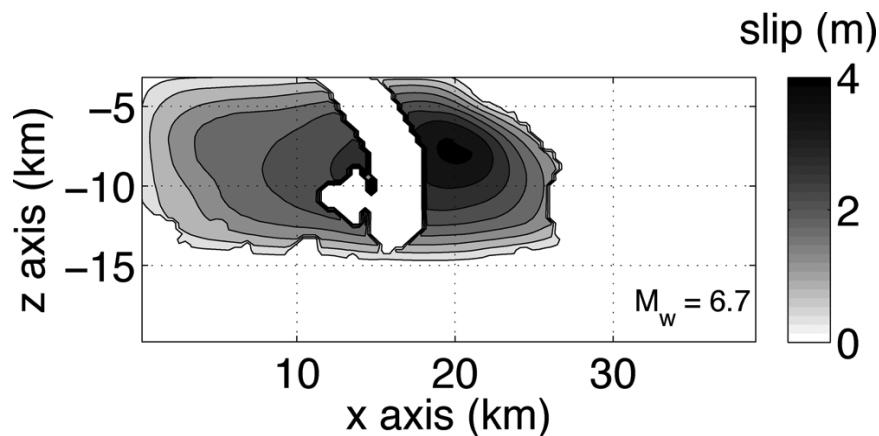


Figure II.36 Slip distribution for the induced M_w 6.7 event. Below 15 km the velocity strengthening section of the fault means no coseismic slip extends into this zone.

Summarizing then:

- Many subsurface processes which involve the injection and/or withdrawal of fluid (oil/water/gas) can induce seismicity over a range of scale from micro-seismic up to possibly magnitude 7 M_L but certainly in excess of 5 M_L .
- The onset of activity can be many years after the initiation of the fluid process.
- The location of induced activity can be tens of kilometres away from the first point of injection depending on permeability/tectonic situation/fault orientation.
- A small event can trigger a much bigger event by dynamic stress transfer and rapid coalescence of failing patches.

- Fluid injection can trigger earthquakes whose size is dependent on the size of the fault, not the injection and that these faults do not necessary need to be in the injection site.
- Large earthquakes can be considered an agglomeration of small events each of which trigger another, like dominoes nudging their neighbours. There are no mainshocks only aftershocks once the first event happens.

D. Conclusions

- Extraction and/or injection of fluids in hydrocarbon fields can, in certain circumstances, induce or trigger seismic activity
- Several authoritative reports describe well-studied cases where extraction and/or injection of fluids in hydrocarbon or geothermal fields has been *associated* with the occurrence of earthquakes, of magnitudes even higher than 5. It is difficult, sometimes not possible, to use the word *proven* in these circumstances.
- The reported cases are only a small fraction of all of the existing cases of extraction and injection of fluids and are mostly related to the additional load imposed by very large reservoirs and to the injection of large volumes of fluid (usually waste water) into surrounding rocks and not into in the same reservoir during enhanced recovery or pressure maintenance. However, some cases do exist, where earthquakes have been associated with waste-water disposal within the same reservoir where oil and gas have been extracted.
- The induced, and specifically the triggered, seismic response to injections is complex and variable among cases and its correlation with technological parameters is far from being fully known.
- The magnitude of triggered earthquakes depends more on the dimensions of the fault and its strength, rather than the characteristics of the injection.
- Recent research on stress diffusion suggests that the activated fault may also be tens of km away from the injection/extraction location, some kilometres deeper than the reservoir and several years after activities commenced.
- The greater focal depths for some extraction-related earthquakes have been interpreted to be a direct reflection of the fact that extraction or injection of large volumes of fluids has the potential to induce crustal-scale deformation and seismicity.
- Many cases of earthquake activity have been recorded during the exploitation of geothermal energy. Most of them are related to projects for the development of Enhanced Geothermal Systems where induced fractures must be produced in impermeable igneous rocks to develop permeable pathways. Several cases are also related to traditional exploitation of geothermal energy. The induced earthquakes are generally of medium to low magnitude and no more than a few km away from the extraction or injection wells.
- Exhaustive examination of all the available literature shows that the discrimination between natural and triggered/induced earthquakes is a difficult problem and does not presently have a reliable, ready-to-use solution.

III. Emilia Seismic Activity and Seismotectonic context

A. *The Emilia Seismic Activity*

The seismic sequence that struck the Emilia Region (Northern Italy) on May-June 2012 culminated in two mainshocks which occurred respectively on May 20th at 04:03:53 am local time and on May 29th, 2012 at 9:00:03 local time. These two mainshocks left about 14,000 people homeless causing damage to several villages, to the towns of Ferrara and Modena and to the economy of the region (**Figure III.1**).

The May 20th main shock had a local magnitude of M_L 5.9. It occurred in the vicinity of Finale Emilia (latitude 44.89° N, longitude 11.23° E) killing 7 people and was preceded by five foreshocks, the largest (M_L 4.1) occurring on May 20, 2012, at 01:13 local time. In this context, “foreshock” is a strictly retrospective label; an event can be so designated only after the mainshock has been identified, which requires that the seismic sequence be completed.

Then two further main events struck the region, both located to the east of the mainshock, nearer the town of Ferrara. The first earthquake occurred at 04:07 local time (M_L 5.1) and the second one (M_L 5.1), at 15:18 local time.

On May 29th, 2012, the second-largest shock, characterized by a local magnitude M_L 5.8 occurred about 12 km west of the May 20 mainshock in the vicinity of Mirandola (latitude 44.85° N, longitude 11.09° E).

INGV (Italian National Institute of Geophysics and Volcanology), using its standard procedures, assigned a focal depth of 6.3 km to the May 20 event and of 10.2 km to the May 29 event. This earthquake ruptured an adjacent thrust fault segment, located to the west.

Moment magnitude (M_w) of 5.63 [77] and M_w 6.11 (cnt.rn.ingv.it) have been computed for the May 20 event, while for the largest event of May 29 values of M_w 5.44 [77] and M_w 5.96 (cnt.rn.ingv.it) have been estimated.

During the following days, hundreds of aftershocks occurred, including M_L 5.2 and M_L 5.3 shocks at 12:55 local time and at 13:00 local time on May 29, 2012, respectively. Sometime later, a magnitude 5.1 earthquake struck at the western edge of the activated fault system on June 3, 2012, at 21:20 local time.



Figure III.1 The 2012 Emilia Sequence caused extensive damage in the Emilia region, killing 24 people and temporarily displacing more than 14,000 from their homes. The liquefaction of thixotropic soils was one of the main effects of the earthquakes [78].

In total the seismic sequence consisted of about 2,500 earthquakes of magnitude higher than M_L 1.5 distributed along a WNW-ESE elongated area of ca. 500 km² (<http://iside.rm.ingv.it>) (**Figure III.2**). As shown by the figure the seismicity generally moved from east (blue) to west (yellow).

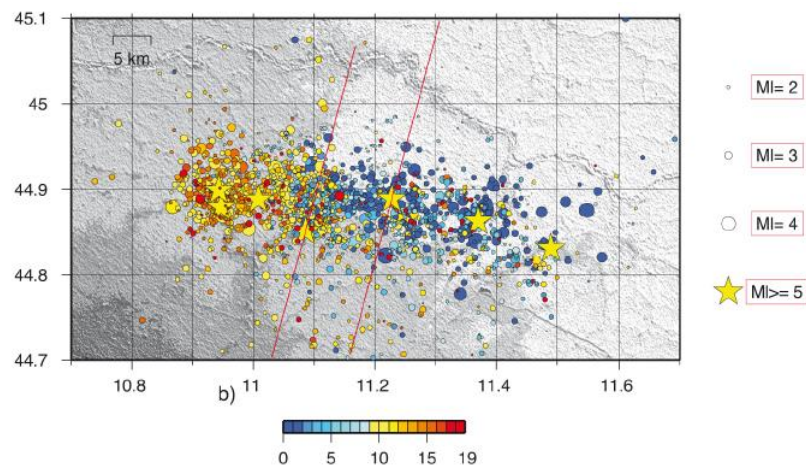


Figure III.2 Epicentral locations of the 2012 Emilia sequence in the period May 19-29, 2012. Stars show the epicenters of the events with magnitude greater than 5 and colors represent the days from the May 20 mainshock [79].

The pattern of seismicity with time is shown in **Figure III.3**.

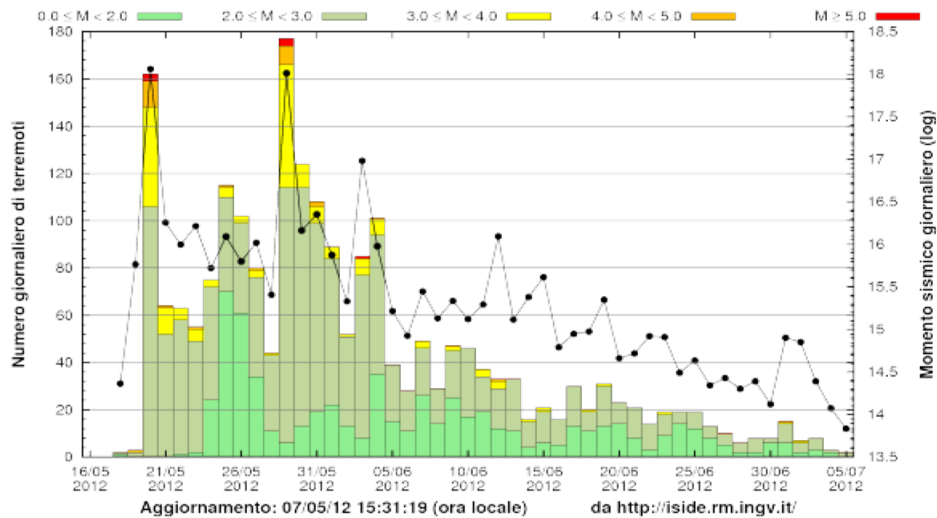


Figure III.3 Time sequence of earthquakes in the Emilia area from May 16, 2012 through July 2012. Total number of events located each day (left scale) with magnitude shown in different colors; black dots show the seismic moment release for each day (right scale).

(http://www.ingv.it/primo_piano/comunicazione/2012/05200508/)

The main event of the 20th of May was recorded by 139 stations of the Italian strong motion network (RAN), managed by the National Civil Protection, ranging from 16 km up to 650 km epicentral distance. Peak ground acceleration (PGA) recorded in the near-source region ranged from 0.01 cm/s² to 259 cm/s² ([80]). In particular the closest station at Mirandola (MRN), classified as a C site (EC8, Comité Européen de Normalisation 2004), recorded peaks of acceleration of about 0.27g. The 29th event was registered by 135 RAN stations and the closest station of MRN recorded peaks of acceleration of about 0.28g ([81]). Continuous maps of the ground motion in terms of maximum horizontal PGA, for the area of interest for the two events and developed by INGV are shown in **Figure III.4**. The maps were derived from the records available from RAN strong-motion network, using *Shakemap*TM software ([82]) converting the observed ground motions into rock-site conditions and applying the amplification factors to the rock-site estimates using values of near surface velocities, V_{S30} .

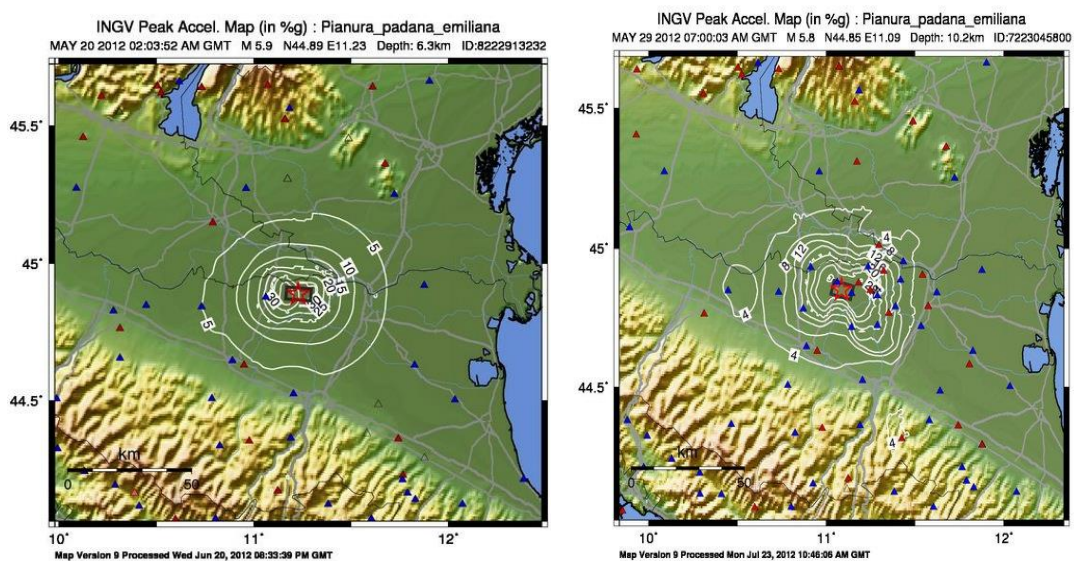


Figure III.4 Map of maximum horizontal PGA (%) relative to the two mainshocks of the Emilia sequence (available at http://cnt.rm.ingv.it/earthquakes_map.html).

From the perspective of long-term seismic hazard analysis, the Emilia seismic sequence was not a surprise. It occurred within a broad zone of historical seismicity that runs along the margin of the Po valley. The probabilistic seismic hazard model of Italy, published in 2004 by INGV (see **Figure III.5**) identified this zone as one of the country's medium seismically dangerous zones. The seismic hazard map for the Emilia-Romagna region (**Figure III.6**) clearly shows the hazard in terms of expected peak ground acceleration (PGA), for rock-site conditions, with a return period of 475 years. As shown by the figure, the area associated with the 2012 sequence is characterized by PGA ranging from 0.125g to 0.175g. Considering that those values are estimated at rock-site conditions, the estimated values are in good agreement with the recorded values mentioned above.

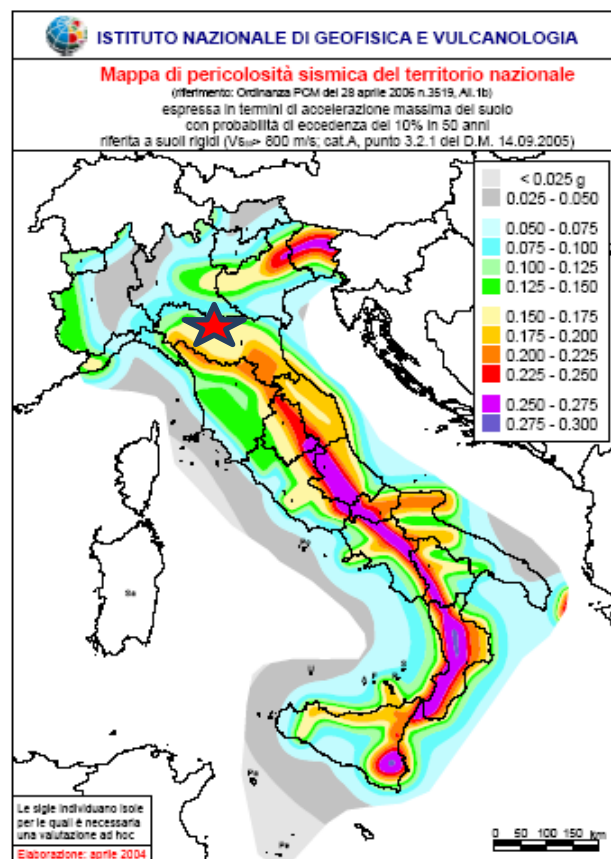


Figure III.5 The probabilistic seismic hazard map for Italy, showing the location of the 2012 Emilia seismic sequence (red star). The colors indicate the peak ground acceleration with a 10% probability of exceedance in 50 years, measured in units of surface gravitational acceleration, $g = 9.8 \text{ m/s}^2$ (available at <http://esse1-gis.mi.ingv.it/>).

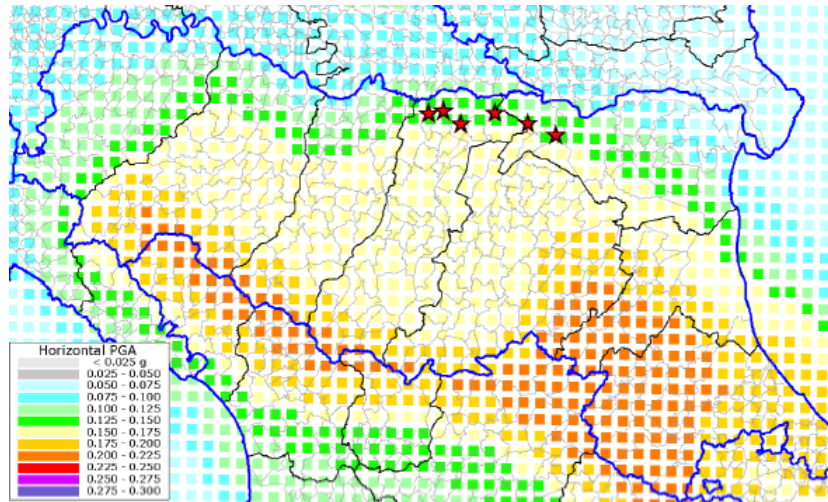


Figure III.6 Detail of the probabilistic seismic hazard map for the Emilia region. Red stars are epicenters of the events of the 2012 Emilia sequence with magnitudes ≥ 5 (available at <http://esse1-gis.mi.ingv.it/>).

1. Historical seismicity

The most relevant past earthquake activity (**Figure III.7**) was the seismic sequence in the Ferrara area, which culminated in a M_w 5.4 event in 1570. The seismic sequence lasted four years and caused severe damage in Ferrara and its surroundings ([83]).

Magnitude ca. 5.5 earthquakes are known to have occurred near Ferrara (in 1346, 1561) and in the areas of Finale Emilia-Bondeno (1574, 1908, 1986), Mantua (1901) and Cento (1922). However, this picture might be incomplete, as suggested by the recent discovery of a previously unknown earthquakes that occurred in 1639 in Finale Emilia by [84] and [85] and in 1761 on the 15th December. The latter caused damage in Mirandola [84].

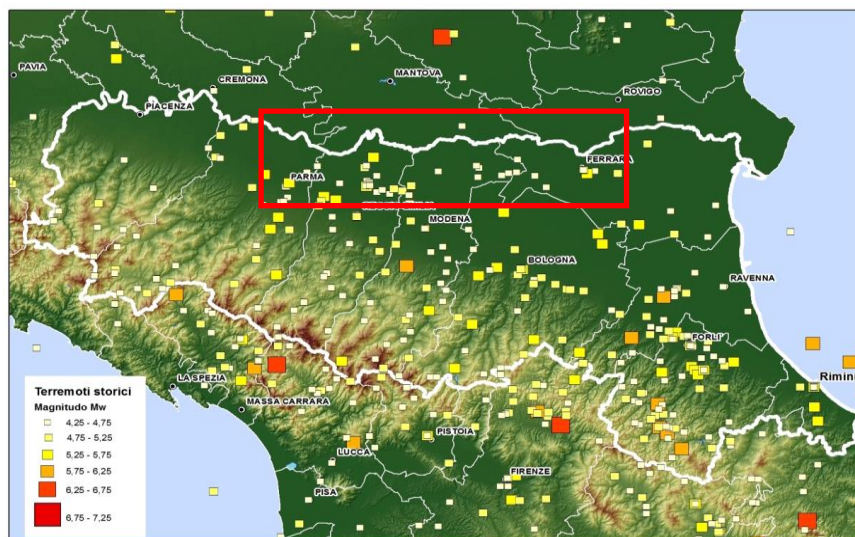


Figure III.7. Distribution of historical epicenters (Data from CPTI11-INGV) within the area hit by the 2012 sequence. The red box shows the area where recent seismicity occurred.

More recent significant seismicity occurred during April-June 1987 ([86]) across the Cavone-Mirandola structure with a sequence of low magnitude events ($2 < M_L < 4$, located at a depth of less than 4 km). This sequence of low-energy shallow earthquakes was characterized by normal faulting mechanisms (see Section B). The last medium energy event (M_w 5.4) is

the 1996 Reggio Emilia earthquake which occurred on October 15 at 09:56 GMT ([87]), which caused moderate damage in unreinforced masonry in Reggio Emilia and other small towns on the Po Plain.

2. Source parameters

INGV determined source parameters for 19 of the 32 earthquakes with $M_L > 4.0$ during the May 19, 2012, to May 30, 2012, time period, (**Figure III.8**) using a Time Domain Moment Tensor (TDMT) technique and a standard 1D velocity model.

(<http://cnt.rm.ingv.it/tdmt.html>)([88]). Most of the fault plane solutions showed dominantly reverse faulting.

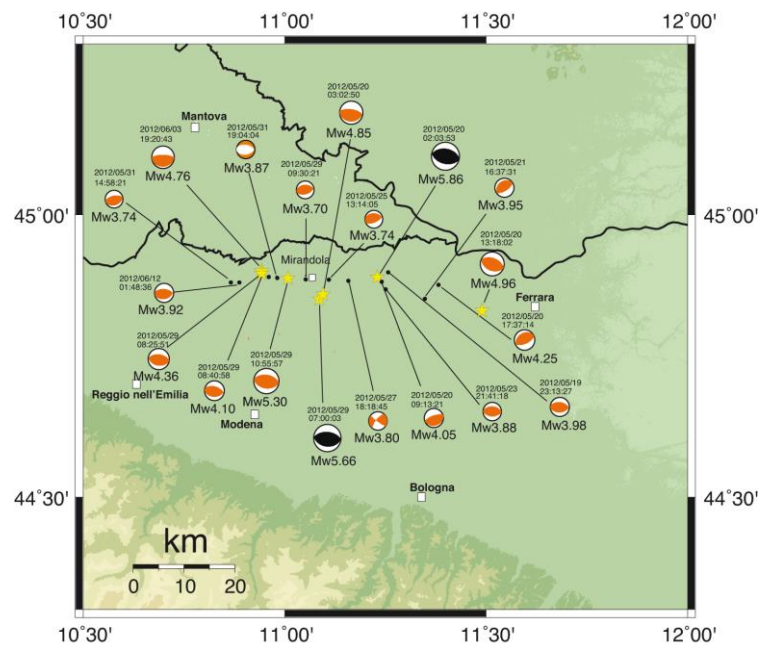


Figure III.8 Focal mechanisms of the earthquakes with $M_L > 4.0$, determined using the TDMT technique. The two mainshock mechanisms are shown in black. The yellow stars are the seven events with $M_L > 5.0$ ([88]).

A preliminary solution for the main focal parameters associated with the seven shocks with magnitude greater than 5 are given by INGV (<http://cnt.rm.ingv.it/>) and is shown in **Table III.1**. Note that the uncertainty on the depth evaluation was not reported by the authors.

Table III.1 Main focal parameter of the shocks with local magnitude greater than 5

Event	Date	Time GMT	LON	LAT	DEP (km)	MAG ($\pm\sigma$)	Dip	Strike	Rake
1	20/05/2012	2:03	11.23	44.89	6.3	5.9 \pm 0.2	45°	105°	90°
2	20/05/2012	2:07	11.37°	44.86°	5.0	5.1 \pm 0.3	45°	111°	90°
3	20/05/2012	13:18	11.49°	44.83°	4.7	5.1 \pm 0.3	45°	111°	90°
4	29/05/2012	7:00	11.09°	44.85°	10.2	5.8 \pm 0.3	45°	95°	90°
5	29/05/2012	10:55	11.01°	44.89°	6.8	5.3 \pm 0.3	45°	97°	90°
6	29/05/2012	11:00	10.95°	44.88°	5.4	5.2 \pm 0.2	45°	83°	90°
7	03/06/2012	19:20	10.94°	44.90°	9.2	5.1 \pm 0.3	45°	81°	90°

In addition, new relocation values have been recently proposed in the literature. By calibrating the 1D crustal velocity structure by using geological data and the seismic profile

App_Orient_1[77] the higher magnitude events were relocated, which moved the 29 May earthquake to an hypocentral depth of 5 km, much shallower than previous determinations.

Furthermore using the additional broadband seismic stations deployed in the epicentral area (<http://ingvterremoti.wordpress.com/2012/06/02/terremoto-pianura-padana-emiliana-intervento-della-rete-sismica-mobile/>) following the first mainshock, hypocenters were re-computed with manually revised pickings [89]. In particular, by adopting a 3D velocity model estimated by INGV instead of the preliminary and simplified 1D model used initially by them, a different depth has been estimated for the 20th mainshock giving a depth of about 10 km as compared to the 6.3 km previously estimated by INGV. The results of these new relocations are shown in **Table III.2** for events greater than 5.

Table III.2 Main focal parameter of the shocks with magnitude greater than 5

LON	LAT	DEP (km)	MAG	DATE and Time (UTC)
11.2440	44.8810	9.99	5.90	20/05/2012 2:03
11.3170	44.8047	3.47	5.10	20/05/2012 2:07
11.4045	44.8185	12.40	5.10	20/05/2012 13:18
11.0590	44.8378	9.64	5.70	29/05/2012 7:00
10.9933	44.8583	7.60	5.30	29/05/2012 10:55
10.9625	44.8545	8.65	5.10	29/05/2012 11:00

No clear indications of the error in the hypocentral location are available. Other authors [90] have re-located a selected set of earthquakes (541 events) using a simplified 1D velocity model (2 crustal layers and the Moho discontinuity). Hypocenters generally have a horizontal error of less than 1.6 km and vertical errors of less than 1.3 km. The mean depth is 7.4 ± 0.37 km for the period 20-29 May 2012 and 9.7 ± 0.41 km for the 29 May-6 June 2012 period. In any case 72% of the events are shallower than 10 km. The reported focal depths indicate that both mainshocks of 20 and 29 occurred in the upper crust; the May, 20 event seems to be shallower (5-7 km, with the exception of [89]) than the May, 29 main event (around 10-12 km).

In spite of differences in depth determination, all the calculated focal mechanisms are of compressional type occurring along thrust faults with a dip of about 45°. These solutions are consistent with the seismotectonic environment of the earthquake, described in Section 2.B, involving a complex system of blind thrust faults which accommodate motions at the WNW-ESE outer margin of the Northern Apennines. This system marks the transition between the well-established active extension zone of the Apennine chain and the buried compressive structures of the Po Plain. Earthquakes occurred on different segments of this system, for a distance of 30 km along its length. This fault system had been identified as an active structure prior to the earthquake, but was only roughly mapped even if it was included in the Italian Database of Individual Seismogenic Sources ([91], [92]).

New insights into the two main seismic events that occurred in 2012 in the Emilia region (Italy) have been provided [93] from extending the analysis from previous studies based on inversion modeling of GPS, RADARSAT-1 InSAR and RADARSAT-2 data. These data show that the displacement pattern associated with the 20 May event is consistent with the activation of a single fault segment of the inner Ferrara thrust. In contrast, the interpretation of the 29 May episode requires the activation of three different fault segments and a block roto-translation of the Mirandola anticline (**Figure III.9**).

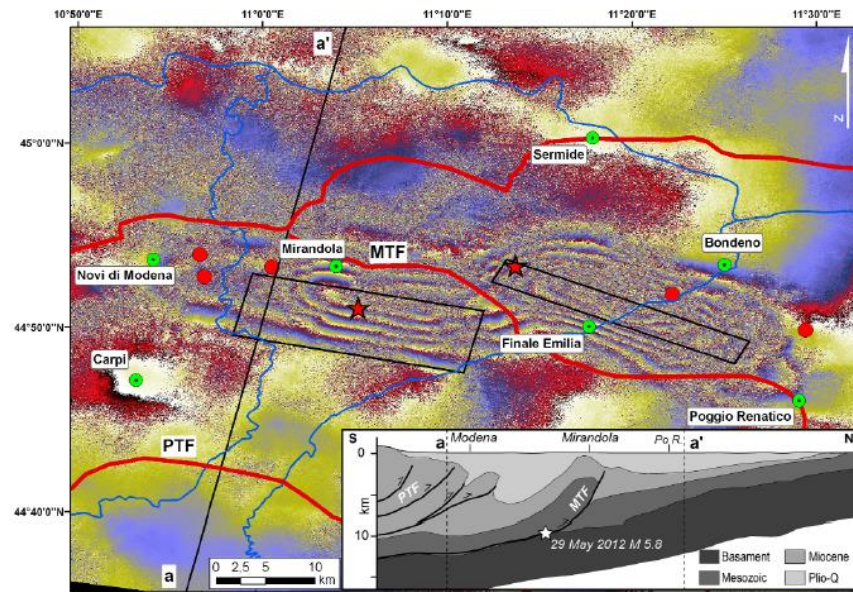


Figure III.9 Radarsat-1 wrapped differential interferogram of the region. Red stars are the position of the May 20 and 29 mainshocks; the red lines are the position of the main thrust fronts; black rectangles are the surface projection of modeled faults. Inset: The N-S simplified geological section runs across the epicentral area of the May 29 mainshock, showing the geometry of the northern Apennines buried outer thrust fronts (redrawn from [94]).

3. Coulomb Stress Transfer

Earthquakes on fault planes can trigger subsequent earthquakes at short distances from the hypocenter by transferring static stresses. In this case the occurrence of so many large earthquakes (7 earthquakes with $M > 5$, listed in **Table III.1**) in such a short time-window, may permit a possible interpretation in terms of purely tectonically triggered earthquakes. Cumulative static Coulomb Stress Changes (CSC) due to the largest earthquakes provide the most significant contribution to the total Coulomb static stress (CSS). Its computation is therefore extremely useful in order to assess the likely contributions and consequences of this earthquake swarm.

CSSs subsequent to the occurrence of each $M > 5$ event on optimally oriented fault segments, defined as the planes experiencing the maximum total stress, were computed by [96]. The evolution of static Coulomb stress changes during the sequence, obtained by the authors are shown in **Figure III.10**. It appears that each subsequent event occurred in an area of positive stress change caused by the occurrence of previous events.

Similar results were obtained by [95] who computed the stress variation caused by the main event of the May 20th, 2012 evaluating the amount of static Coulomb stress that was transferred to the region of occurrence of the May 29th, 2012, event.

The computed CSS shows that the hypocenter of the second mainshock is in the crustal region into which static stress was transferred. These results indicate that the May 29, 2012, event may have been triggered by static stressing by fault slip caused by the preceding May 20, 2012 event, (**Figure III.11**). The authors maintain that stress change calculations have been adequately validated by the observed distribution of aftershocks.

It must be pointed out that the intensity of stress transfer is strongly dependent on the transmitting and receiving fault size, which on turn depends on the earthquake's magnitude. M_w values of 5.6 and 6.1 have been computed for the May 20 main shock. The authors ([95] [96]) chose a fault area consistent with the 5.6 value. A further source of error is the assumed slip model.

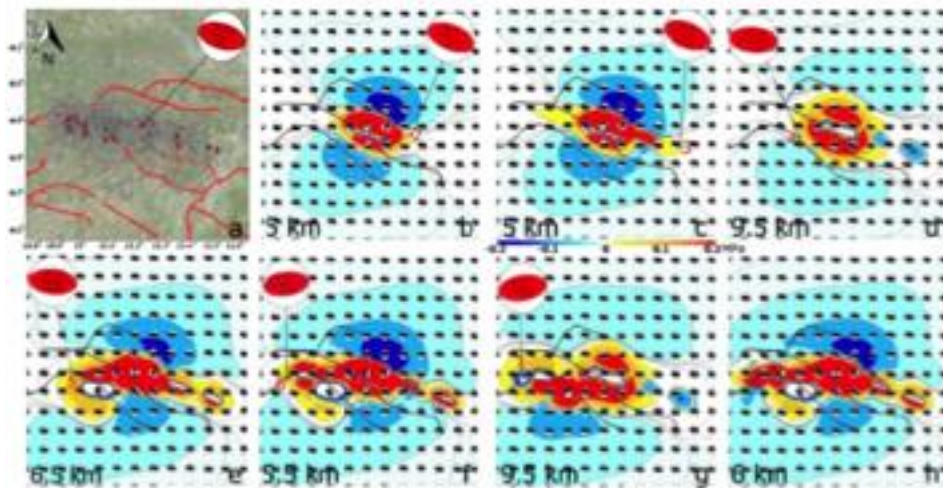


Figure III.10 Coulomb stress variation on optimally oriented fault segments obtained as a sequence of previous $n-1$ events at the depth relevant to event n (bottom left of each panel). The last panel shows the Coulomb stress variation of the 7 events (shown in **Table III.1**) at the depth of 6 km (from [96]).

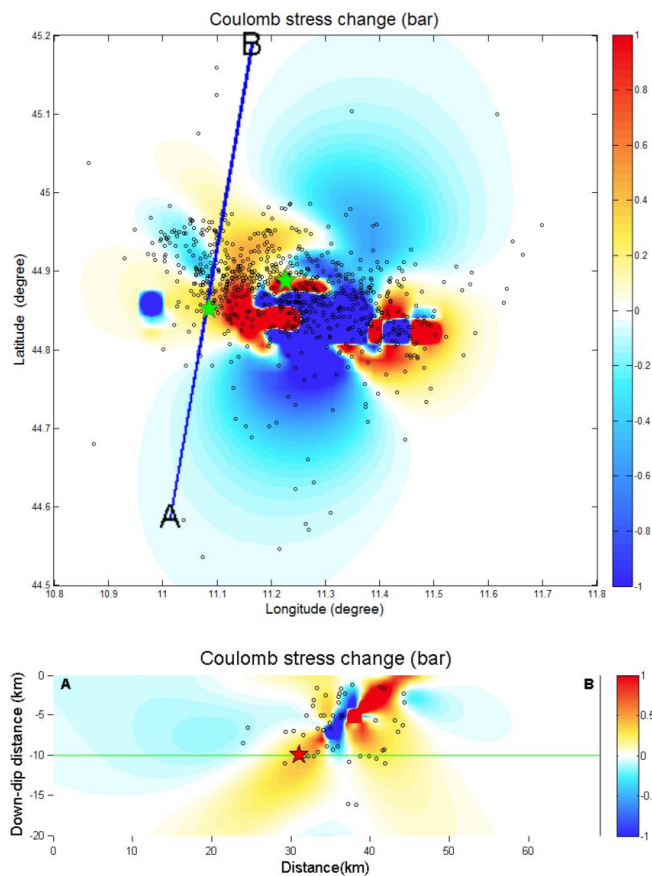


Figure III.11 Coulomb stress change at 10-km depth associated with the May 20, 2012 event. Green stars represents the two mainshock epicenters; blue areas and red areas are unloading and loading areas respectively.

Different results were obtained by [97] where cumulative changes in the static stress field were evaluated (**Figure III.12** and **Figure III.13**) starting from hypocentral locations, moment magnitudes and focal mechanism solutions of [77]. The authors argue that the Coulomb Stress Transfer effect at the locations and on the focal mechanisms of the largest subsequent earthquakes does not explain their occurrence. The symmetry of the static stress fields also differs from the asymmetries in the aftershock patterns. Therefore although static stress changes may affect the evolution of this sequence, the authors find that static stress redistribution alone is not capable of explaining the locations of subsequent events.

A dynamic triggering process caused by passing seismic waves and enhanced by source directivity was also investigated by [97]. The study indicates that dynamic triggering might be the primary factor to explain the evolution of the 2012 Emilia seismic sequence. In fact, the authors observed a correlation between the locations of aftershocks and subsequent main events with: i) the peak dynamic strain fields; ii) the local change of the permeability, as shown in **Figure III.13**.

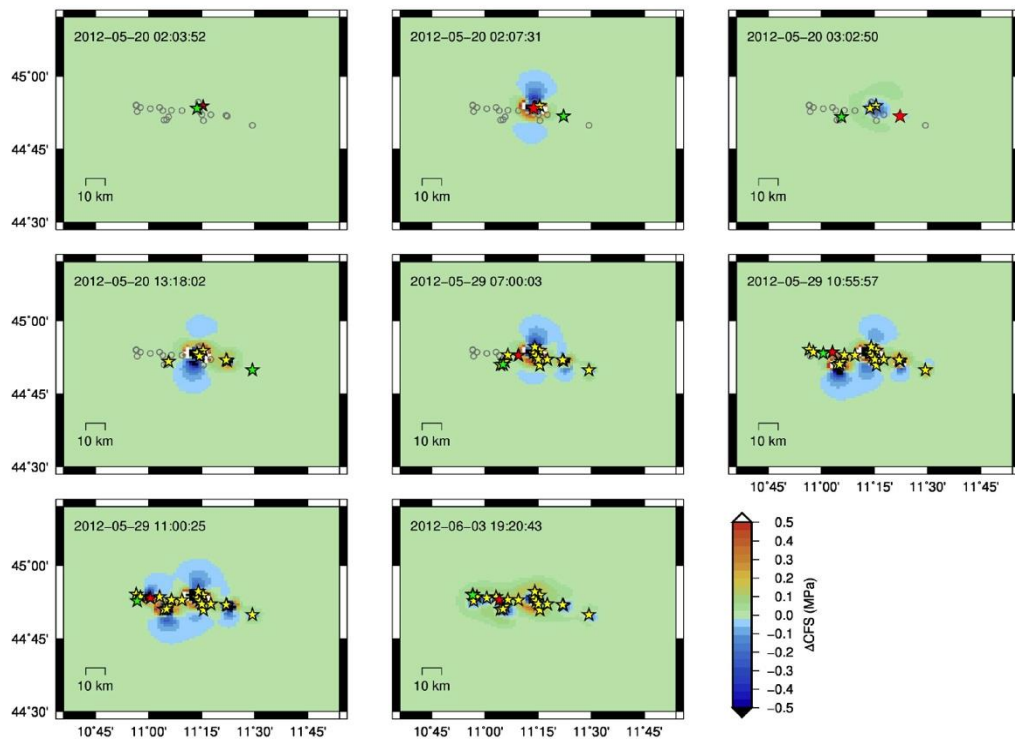


Figure III.12 Coulomb stress change at hypocentral locations and on the preferential focal mechanism of the main events of the sequence.

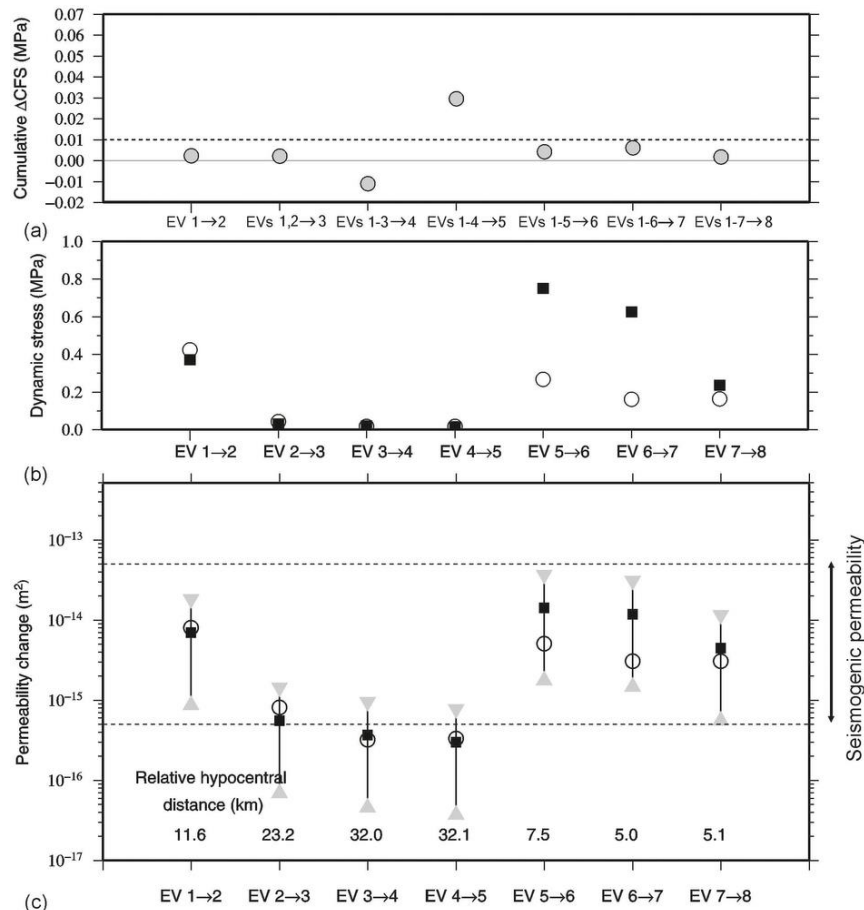


Figure III.13 a) Coulomb stress change estimated considering the contribution of all the earthquakes occurred before the target event. The dashed lines represent the commonly accepted triggering threshold for static CSC, i.e. 0.01 MPa; b) Local dynamic stress change obtained from the peak dynamic strain induced by each considered event at the hypocenter of the next main earthquake in the sequence; c) Permeability changes induced by each considered event at the hypocenter of the next main earthquake in the sequence. The local dynamic stress and permeability change are estimated both by considering the directivity effect (squares) and by ignoring it (open circles). ([97]).

4. Daily earthquake forecast for the Emilia 2012 earthquake sequence: the Epidemic Type Aftershock Sequence (ETAS) model

Time-dependent hazard models based on earthquake clustering, have been developed by seismologists to forecast seismicity over the short-term and these have been used to track the evolution of aftershock sequences in real-time. The Epidemic Type Aftershock Sequence (ETAS) model has been applied by [98] to the seismic sequence of the May-June 2012 Emilia earthquakes using the real-time earthquake data recorded by the INGV seismic network. This model is based on two physical components: a seismic background variable in space (not in time) and a second term that takes into account the triggering effects of all the previous earthquakes, as a function of the distance, elapsed time, and magnitude of the triggering event. The model allows estimation of the probability of one event at least in a specific time-space-magnitude window.

For the Emilia sequence the daily occurrence probabilities of one or more events with $M_L > 4.0$ based on the seismicity that occurred before 6:00 UTC have been provided by [99]. In **Figure III.14** results for the 20th of May (after the first main event) and the 28th of May (before the second main event) are shown. It seems that the ETAS probability distribution calculated fits the real event spatial distribution quite well.

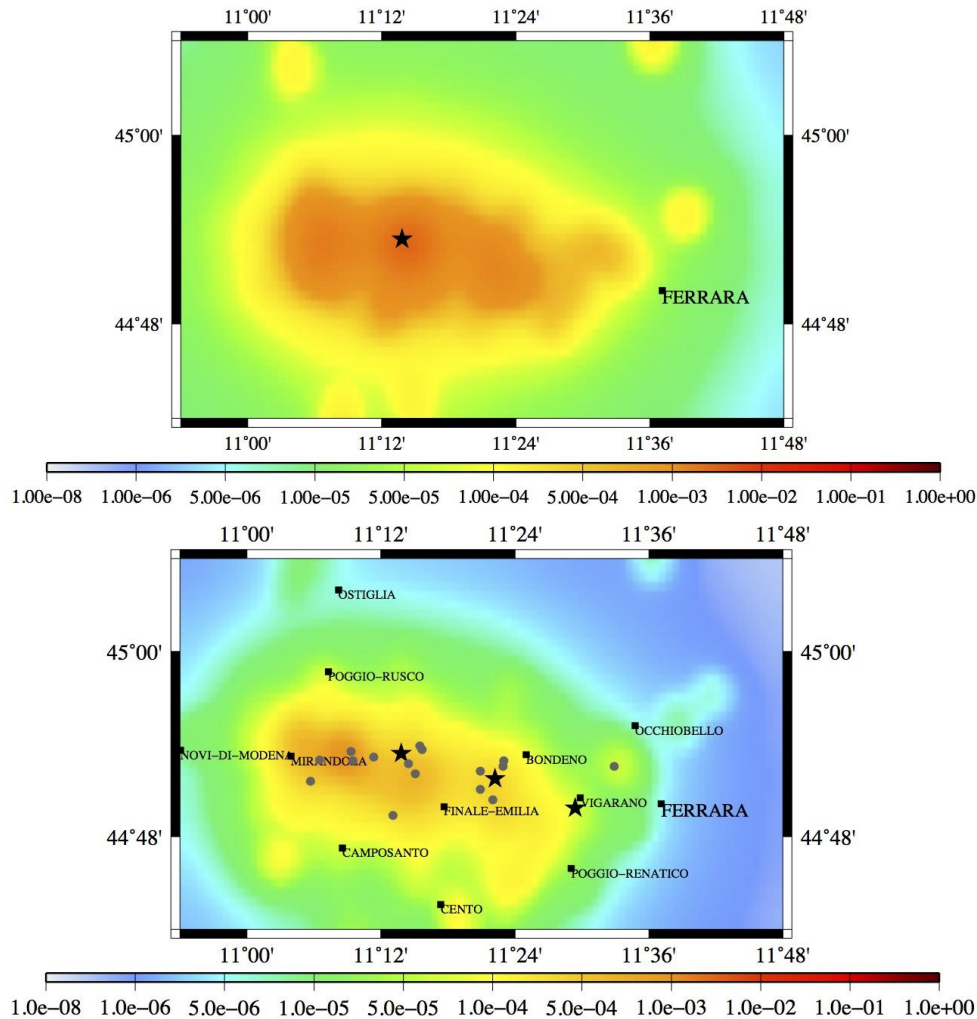


Figure III.14 Daily occurrence probability of one or more events with $M_L > 4.0$ provided at 6:00 UTC for the 20th of May (top) and the 28th of May (bottom).

B. *Seismotectonic context*

The area struck by the May 20-29 2012 earthquakes is an elliptic region about 30 kilometres long and 12 kilometres wide, which follows the crest of the buried Cavone-Mirandola anticline. The geological structures responsible for the seismic activity have been identified as thrust faults delineating the outer margin of the Northern Apennines.

In current geological literature the compressional regime which is active in the region has been associated by some authors (e.g. [100],[101],[102]) with Africa-Europe convergence, and by other authors (e.g.[103],[104],[105]) to the flexural-hinge retreat of the south-western margin of Adria undergoing passive sinking beneath the Apennines. In the second model, plate convergence would account for the compressional earthquake mechanisms present in the Southern Alps (see Friuli 1976), while passive slab sinking would justify the existence of a compressional belt along the outer margin of the Apennines and an extensional one along the Tyrrhenian side of the mountain chain (Lunigiana-Garfagnana-Mugello-Alta Val Tiberina seismogenic zones).

Figure III.15 shows that in late Miocene-Pleistocene times the slip vectors describing respectively the rigid plate motion of Africa and Europe, and the time-space forward migration of the thrust belt system in the Northern Apennines and in the Calabrian Arc, intersect each other at about 90°. This suggests the absence of any causal relation between

plate convergence and forward thrust propagation in the Apennines. Starting from the early Pleistocene-middle Pleistocene boundary, Adria became kinematically independent from the African plate and began to move counterclockwise around a rotation pole located somewhere between the western part of the Po Valley and the Genoa Gulf ([106],[107],[108],[109]). However, passive sinking accompanied by flexural-hinge retreat still continued in the Northern Apennines and in the Calabrian Arc [110], so that the tectonic regime in the Emilia-Romagna region did not undergo significant changes. The kinematic framework deduced from the geological and geophysical regional information fits the present-day seismicity pattern of Northern Italy, as well as the geodetic measurements available in the region very well.

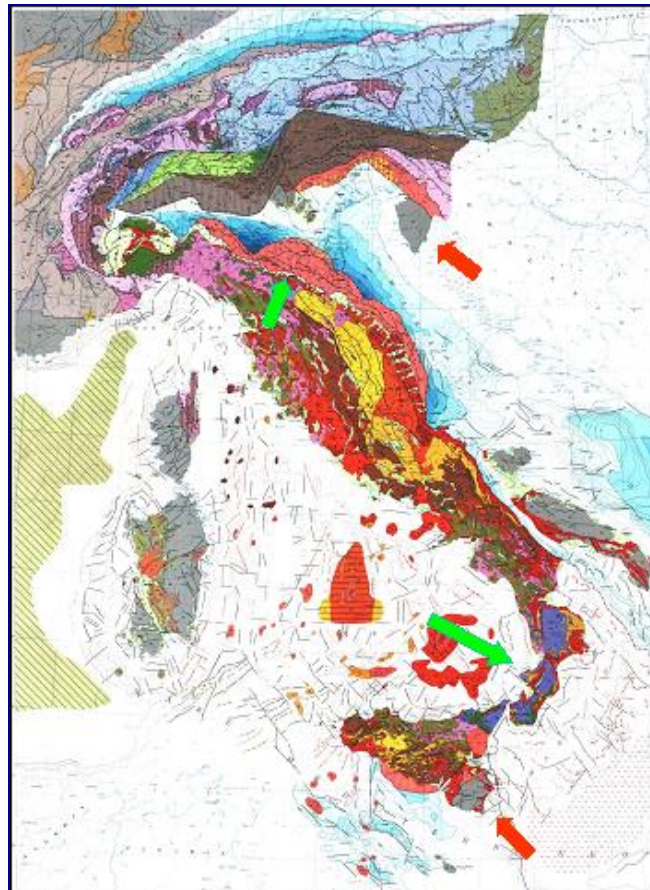


Figure III.15 Simplified structural-kinematic map of Italy showing the major tectonic feature in the Alps and the Apennines (after [111]). The orange, pink and red colours in the Apennines and Southern Alps indicate belts affected by severe deformation during Pliocene and Pleistocene times. The green arrows indicate the average direction of orogenic transport in the Northern Apennines and Calabrian Arc during late Miocene-Pleistocene times. The red arrows indicate the motion of Africa (including Adria) with respect to Europe in the same time interval following the model of [112].

Figure III.16 shows the horizontal velocities of several GPS sites in the Northern Apennines and in the Alps with respect to Adria, the latter having been assumed as a fixed reference frame. Note the opposite vergence of the mountain belts bordering the Adriamicroplate, with slip vectors indicating a tectonic transport towards the south in the Southern Alps and towards the north in the Northern Apennines. This apparent paradox may be easily reconciled when we take realise that the northwards motion of Adria with respect to Europe can account for the north-south directed vectors in the Southern Alps, whilst the flexural-hinge retreat of the inner margin of Adria is consistent with the south-north directed vectors along the outer margin of the Northern Apennines.

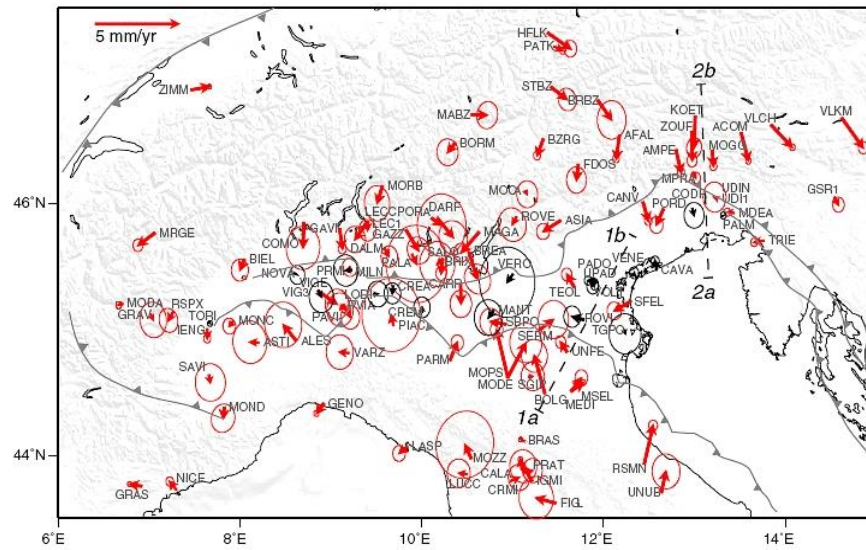


Figure III.16 Horizontal velocities of GPS sites in Northern Italy with respect to Adria (black arrows) assumed as a fixed reference frame (after [113]).

Figure III.17 shows the residual horizontal velocities of several GPS sites in Northern Italy that have been computed assuming Europe as a fixed reference frame. Finally, **Figure III.18**, shows the horizontal strain-rate field in Northern Italy deduced from the available GPS data. Converging and diverging arrows indicate the principal axes of shortening and extension, respectively.

The kinematic model derived from the geodetic measurements agrees fully with the stress field calculated by [114], which in Northern Italy is based on earthquake focal mechanisms and on borehole breakouts (**Figure III.19**).

If we look at the details of the Ferrara thrust-and-fold belt, the source area of the Emilia 2012 earthquakes, we see that the directions of the minimum horizontal stress axes deduced from borehole breakouts ([115]) appear quite dispersed (see **Figure III.20**), though the higher-quality cumulative rose diagrams approximate a W-E direction. The presence of lateral/oblique ramps (**Figure III.21**) may account for the observed local deviations of the regional maximum horizontal stress, which in the area is expected to follow a direction ranging from SSW-NNE to S-N (see also [116] and [117]). As concerns the angular relationships between the direction of the regional σ_1 and the orientations of the local maximum shearing-stress axes, we refer to [118]. In addition, some normal faulting mechanisms have been computed for low-energy shallow earthquakes in the area (see [119]). It is possible that such extensional events are related to the occurrence of collapse phenomena in the Plio-Pleistocene deposits at the rear of the growing Ferrara Folds, rather than to a change of the stress field orientation with depth as suggested by some authors (e.g. [120]).

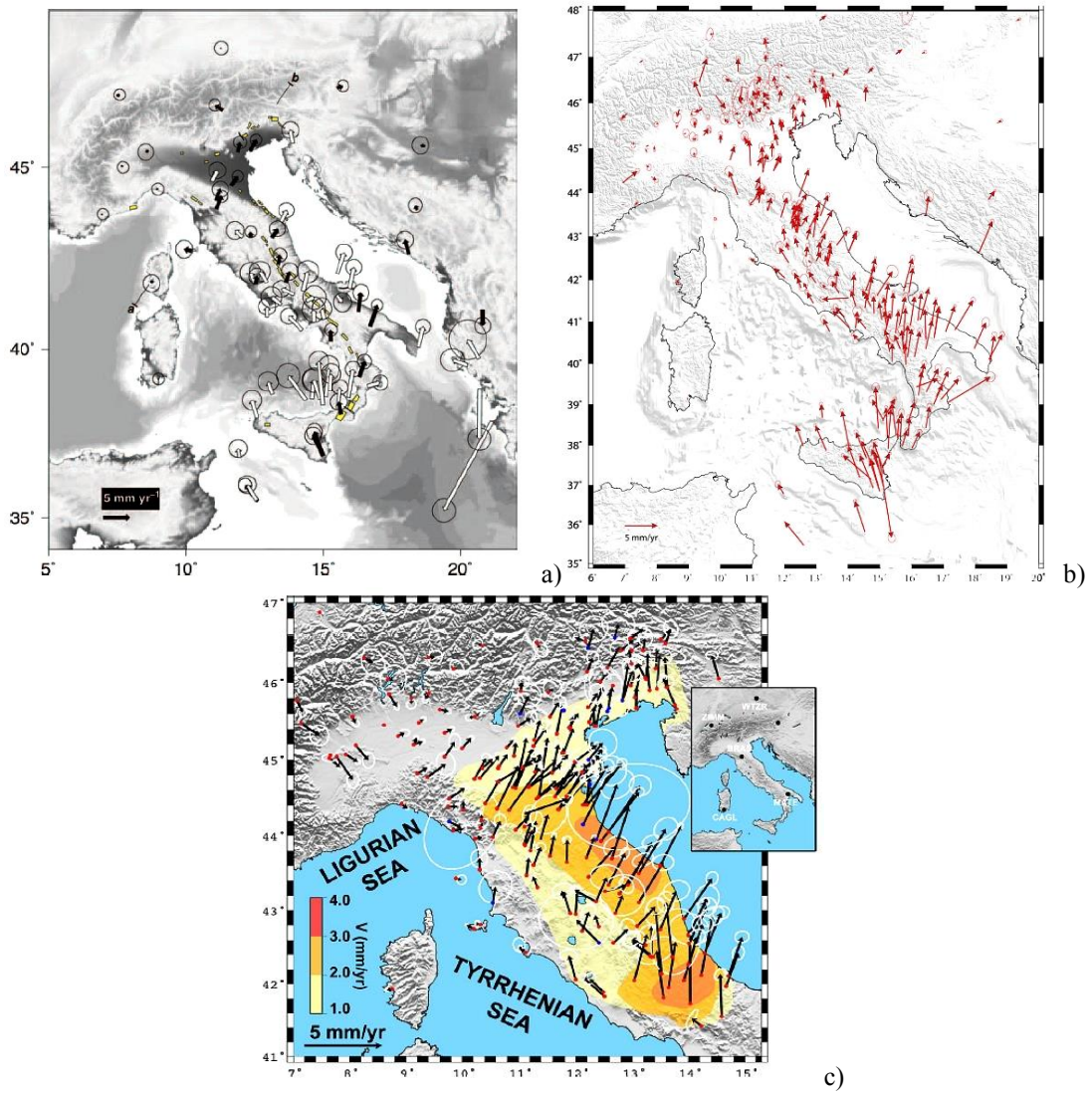


Figure III.17 Residual horizontal velocities of GPS sites in Northern Italy with respect to a fixed Europe reference frame (a after [121]; b after [122]; c after [123]).

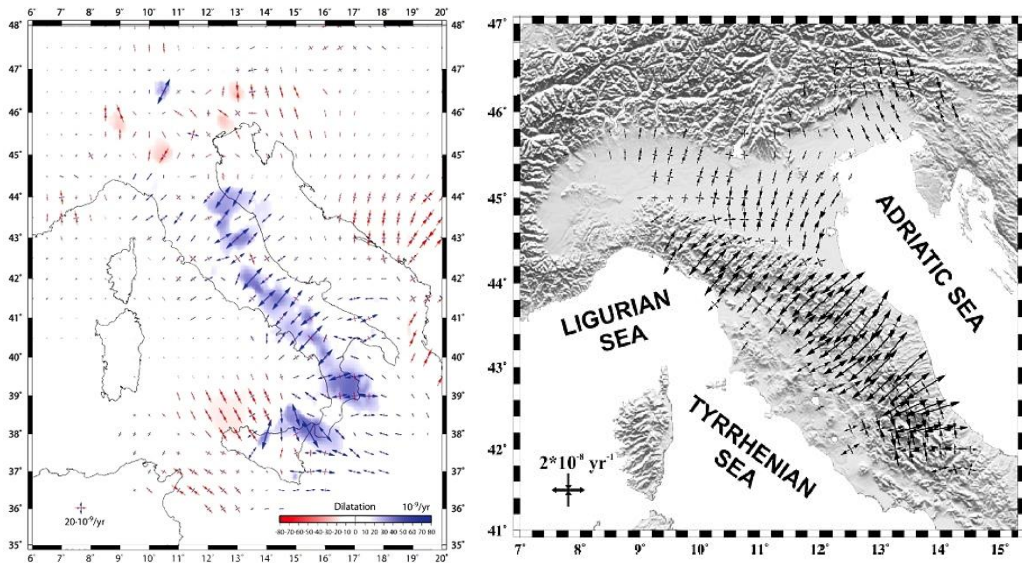


Figure III.18 Horizontal strain-rate field in Northern Italy (4a after [122]; 4b after [123]).

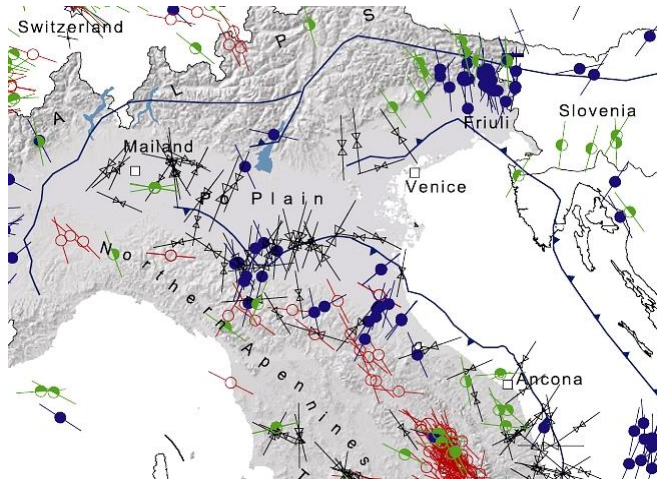


Figure III.19 Present-day stress field in Central-Northern Italy (after [114]).

A seismotectonic zonation of the Italian territory aimed at seismic hazard evaluations (e.g. [124],[125]) was completed for the first time several years ago ([126],[109]). The zonation has been subsequently, reviewed and updated ([127],[128]) but the general framework has not changed in the Northern Apennines. In all available documents the Northern Apennine region is characterized by active extensional processes along the Tyrrhenian side of the mountain chain, and by compressional processes along the Apennine foothills and along the Emilia, Ferrara, Romagna and Adriatic Folds. As concerns the Ferrara seismogenic zone, in particular, there is no difference between the models of [109] and [128], either in the polygon boundaries or in the expected predominant fault mechanism.

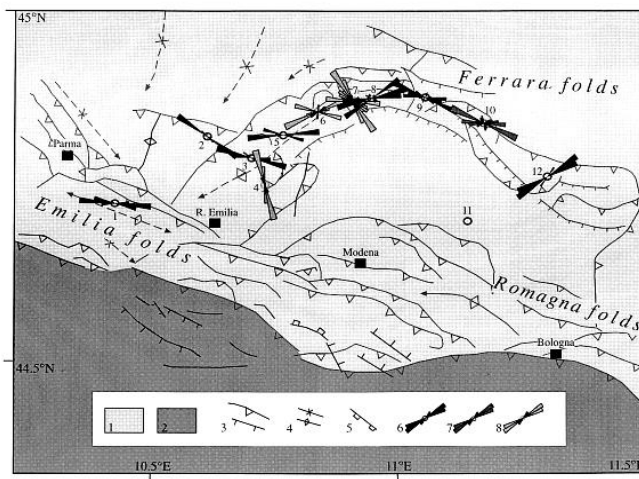


Figure III.20 Breakout results in the Ferrara thrust-and-fold belts (after [115]). Black arrows refer to B and C qualities, grey arrows to discarded D qualities.

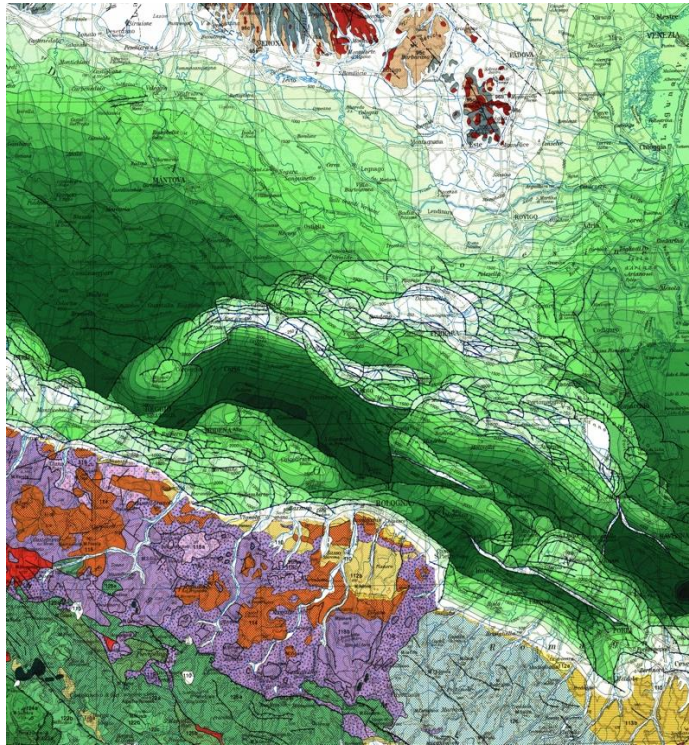


Figure III.21 Detail of the tectonic structures in the Emilia-Romagna region showing the foreland homocline, the Emilia, Ferrara and Romagna Folds and the outer margin of the Apennines. Ahead of the Apennine margin, the light-green to dark-green palette depicts the progressive deepening of the base of the Plio-Pleistocene terrigenous deposits in the foredeep basin and in the thrust-top basins developed on top of the growing folds. Both in the Romagna and Ferrara Folds W-E to WNW-ESE buried thrust fronts are intersected by a complex network of lateral and oblique ramps (after [129]).

IV. List of available information

A. Well locations and historical development

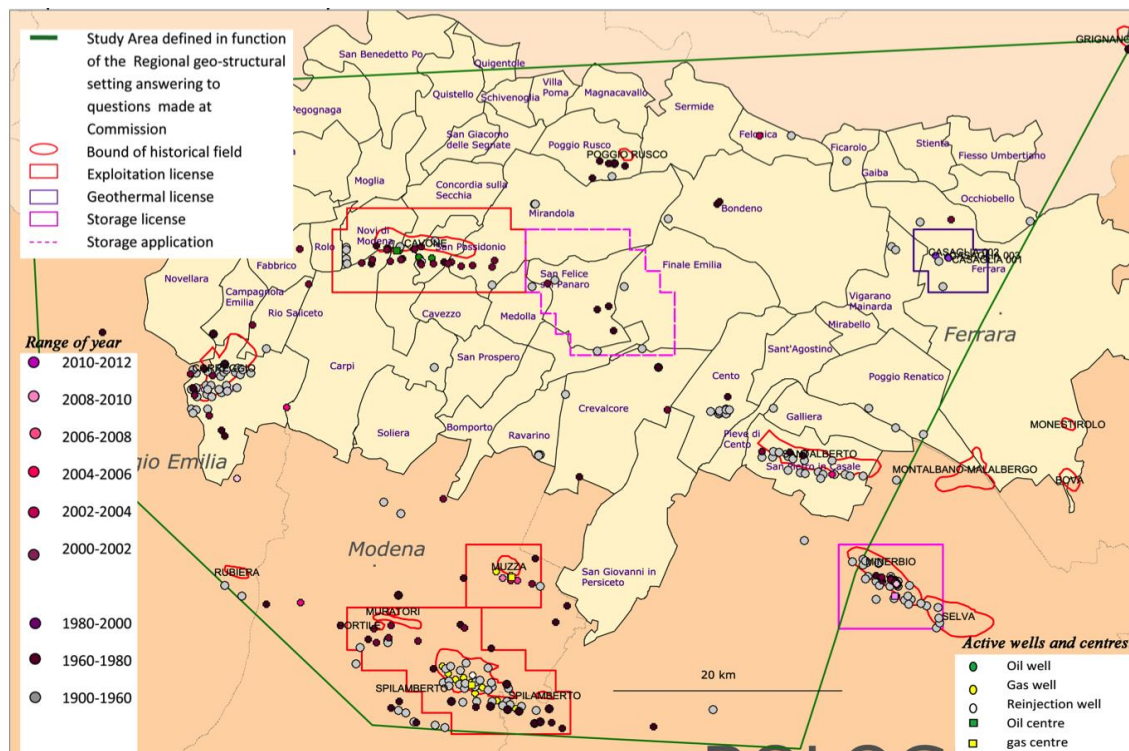
The study area (shown in **Figure IV.1**) was identified considering the particular geological context, the geostructural domain that supported the formation of hydrocarbon deposits and the exploration and production activities of oil and gas for the past several decades.

The E&P and gas storage companies, which have worked in recent years in the hydrocarbon licences under analysis, are:

- *Eni* (exploitation licences “MIRANDOLA” , “SPILAMBERTO” and “RECOVATO”, mining licence “FERRARA”)
- *Gas Plus Italiana* (exploitation licence “RECOVATO”)
- *Società Padana Energia* (exploitation licences “MIRANDOLA” and “SPILAMBERTO”)
- *Stogit* (storage licence “MINERBIO”)

The operators provided the data required by the ICHESE Commission in a strictly confidential way.

ICHESE Commission also required operational and seismic data relating to the geothermal field of Casaglia. These data were provided by Emilia Romagna Region. The list of all data provided is reported in Appendix C.



Map and Data elaboration made by Cartography Office (DIV.I) of Directorate General for Mineral and Energy Resources (DGRME-MISE) for ICHESE Commission (Roma, 2013)

Figure IV.1 Study area and historical wells.

1. Historical activity in North Italy

The mining resources in Italy are the property of the State. Hydrocarbon production activities, natural gas storage and geothermal activities are governed by licences that are given to operators with proven technical and financial capabilities. Such activities are carried out under the supervision of the Ministry of Economic Development.

Exploration and Production

Italian mining activity started in 1926 with the institution of AGIP, which became ENI in 1953. In 1941, the “Po Valley” and “Caviaga” structures were the first prospects explored.

The first oil and gas field was found in 1949 at “CORTEMAGGIORE” (Piacenza). It was followed by the discovery of the “CORNEGLIANO” gas field (Milano). The 50’s and 60’s were the most significant years for hydrocarbon exploration and production, due to several discoveries which nowadays represent most of the national production.

ENI was the first company introducing the technology of seismic surveying to Italy and, in 1980, started an exploration survey within its exclusive mining area, through the acquisition of some regional seismic lines in the Emilia Romagna Region. During the following years ENI carried out further seismic lines on the wave of advances in technological development and of the increasing exploration activity in the Italy. Discovery of new fields continued during the ’90s with the consequent drilling of several new wells.

Since the ’90s the number of drilled wells began to decline quickly due to the reduction of mining research and to the optimization of existing fields with work-over and side-track operations without drilling new wells [130] (Figure IV.2). In 2012 only 38 wells were drilled.

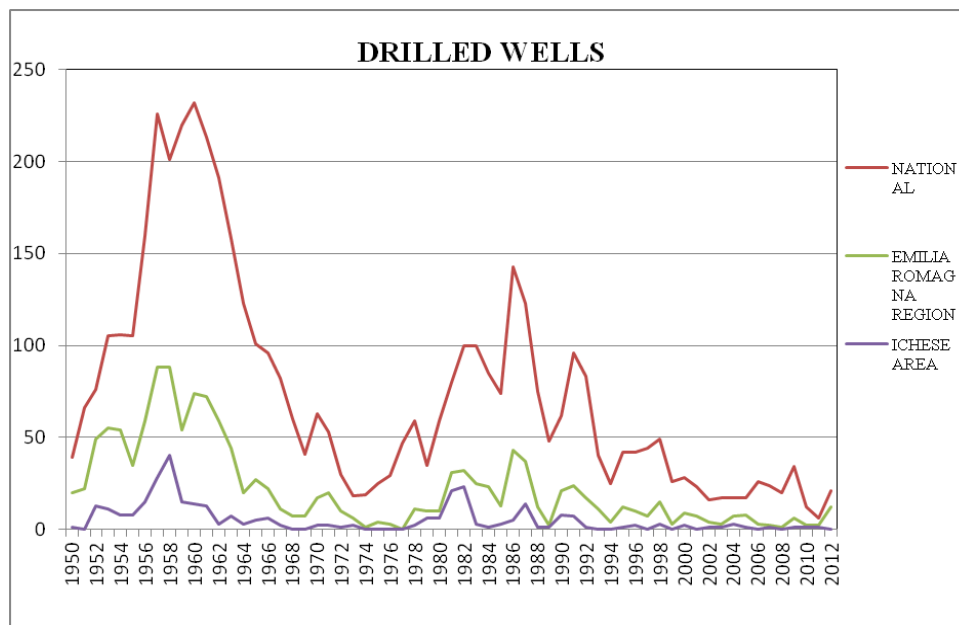


Figure IV.2 Number of historical wells drilled from 1950 to 2012.

Gas storage

The evolution of the gas market in Italy, as a consequence of the increasing availability of methane and of the development of the transportation and distribution infrastructures, led ENI to introduce a modulation storage, by converting several deposits into storage sites, starting from those of the “Po Valley”. Nowadays in Italy there are 10 active storage sites, characterized by a total working gas of 15,620 MSm³, that guarantee the continuity of gas supply to industry and civil use.

Geothermal energy

Geothermal energy represents 6% of all Italian renewable energy and about 2% of national energy production [131].

The first exploitation of geothermal heat was in Larderello (Tuscany) and in 1913 the first geothermal plant (250 kWe) was built. In Italy the first classification of geothermal resources started in 1988 after decree no. 896/1986, in order to improve knowledge of geothermal energy and to implement an inventory of the National Geothermal resources. As a result of this decree, the hydrothermal areas characterized by medium - high enthalpy ($T > 150^{\circ} \text{C}$) were identified. They cover 25% of the national territory, mainly in Tuscany, Lazio, Campania, Sicily and Sardinia. There are also several areas, like the Po Valley, characterized by low enthalpy thermal systems, potentially exploitable to produce electrical energy and most of all used directly for thermal, industrial and heating uses.

2. Historical activity in the study area

In the study area, hydrocarbon exploration activities increased from 1950 to 1990, as shown in **Figure IV.1**. Since 1900, 357 wells were drilled; 251 of them were drilled before 1980, and 94 wells from 1980 until 2000. Only 12 wells were drilled between 2000 and 2012; in particular there was one new well in the area of the “MINERBIO” storage licence and four wells in the area of the “RECOVATO” exploitation licence.

Exploration and Production

The study area includes three active licences for hydrocarbon production:

- (1) the exploitation licence of “MIRANDOLA” (121.96 km² licence area, 0.063 km² oil gathering and treatment centre) where the first oil field (Cavone) was discovered in 1972;
- (2) the exploitation licence of “SPILAMBERTO” (139.82 km² licence area, 0.003 km² gas gathering and treatment centre) whose reservoir was discovered in 1956 and
- (3) the licence of “RECOVATO” (36.75 km² licence area, 0.007 km² gas gathering and treatment centre) whose reservoir was discovered in 1987.

In 1998 the “MIRANDOLA” and “SPILAMBERTO” licences were assigned to *Eni* which was the operator until 2010, when the licence was transferred to *Società Padana Energia* company. The “RECOVATO” exploitation licence was assigned to *Eni* in 1998 and transferred to the *Gas Plus* company in 2001.

27 wells were active in the period 2010 to 2012. In particular (**Figure IV.3**):

- 7 oil wells in “MIRANDOLA” drilled in the period 1978 -1981;
- 17 gas wells in “SPILAMBERTO” and “RECOVATO” drilled in the period 1958 - 2011;
- 2 reinjection wells, one in “MIRANDOLA” and one in “SPILAMBERTO” (the latter active until 2011).

Gas Storage

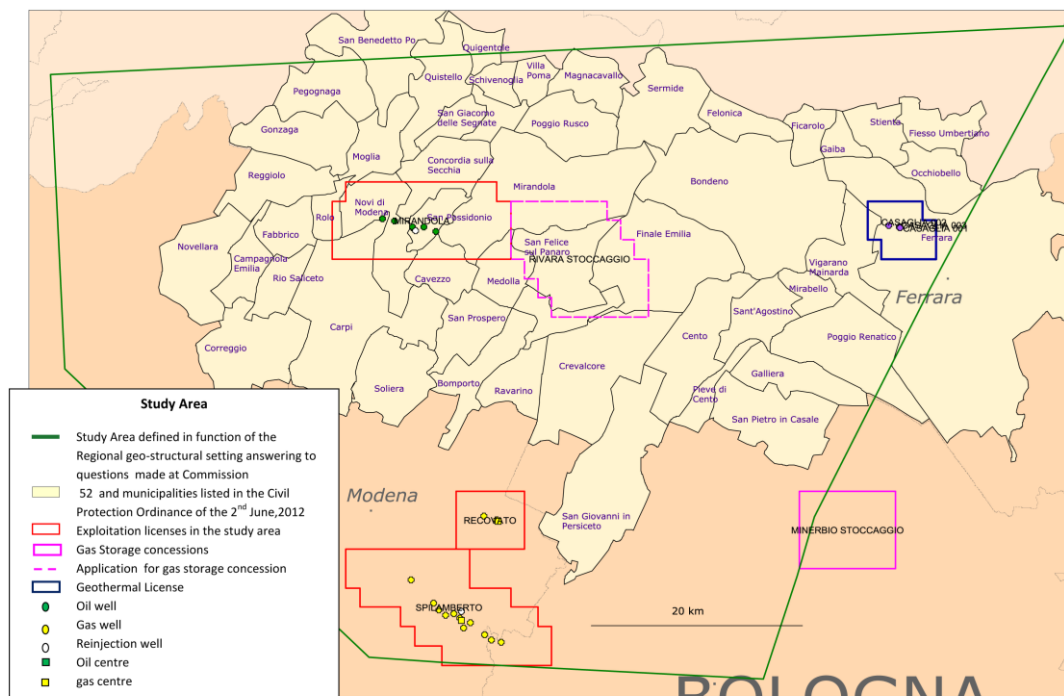
The storage plant of Minerbio is located in the south-east corner of the study area. The licence covers an area of 68.61 km² (0.044 km² gas storage gathering and treatment centre),

within the municipality of Bologna. The “Minerbio” gas field was discovered in 1956 after the drilling of the “Minerbio 1” well. Production started in 1959 and was managed by *Agip*. The field consists of 7 pools. In 1998 the hydrocarbon exploitation licence was assigned to *Eni* and one year later it was converted to storage activity. In 2002, the storage licence was transferred to *Stogit*. On July 30, 2002 the company *Independent Gas Management srl* submitted a request to be granted the storage licence in a deep aquifer, named “RIVARA-STORAGE”. The project had foreseen that storage should be carried out in fractured limestone formation, occupied by water, and should represent the first initiative of “aquifer storage” in Italy, where natural gas is usually stored underground using an already developed gas reservoir. *Independent Gas Management was unable to* acquire the elements required to assess the feasibility of the storage program (mandatory aspect for the granting of the storage project), and therefore the Ministry of Economic Development rejected the application for natural gas storage program “RIVARA-STORAGE” by the Directorial Decree of the 3rd April of 2013 (see Chapter V of this report for more details).

Geothermal field

In Emilia-Romagna Region there are no high enthalpy geothermal sources. However, in the area along the “Appenine belt”, some thermal sources have been discovered. In Ferrara and Bagno di Romagna the exploitation of low enthalpy geothermal reservoir, (about 80°-100° C), allows the directly use of heat.

In 1981 in the municipality of Ferrara, a “Geothermal Project” started in order to evaluate the possibility of utilizing the geothermal resource as a primary heat reserve for heat for the city. The project was accomplished in a joint-venture by *Eni* and *Enel*, in the mining licence “FERRARA”, where the “Casaglia 1”, “Casaglia 2” and “Casaglia 3” wells were drilled. The geothermal licence “FERRARA” was assigned to *Eni* in 1984. The licence area (31.72 km²) is located at 5 km towards North-west by the centre of Ferrara and is actually assigned to *Erga* and *Eni* (50% & 50%,) as the sole representative.



Map and Data elaboration made by Cartography Office (DIV.1) of Directorate General for Mineral and Energy Resources (DGRME-MISE) for ICHESSE Commission (Roma, 2013)

Figure IV.3 Map of active wells in the study area from 2010 to 2012.

B. Stratigraphy and standard logging data

The stratigraphic framework of the Cavone-Ferrara area has been reconstructed in detail thanks to numerous commercial wells, some of which have explored the entire sedimentary sequence from the Plio-Pleistocene terrigenous deposits to the Upper Triassic-Lower Jurassic platform carbonates. In addition, a close network of seismic profiles has provided important information about the regional architecture of the platform-and-basin system through Mesozoic times. As concerns geological times, the reader may refer to the chronostratigraphic chart of **Figure IV.4**.

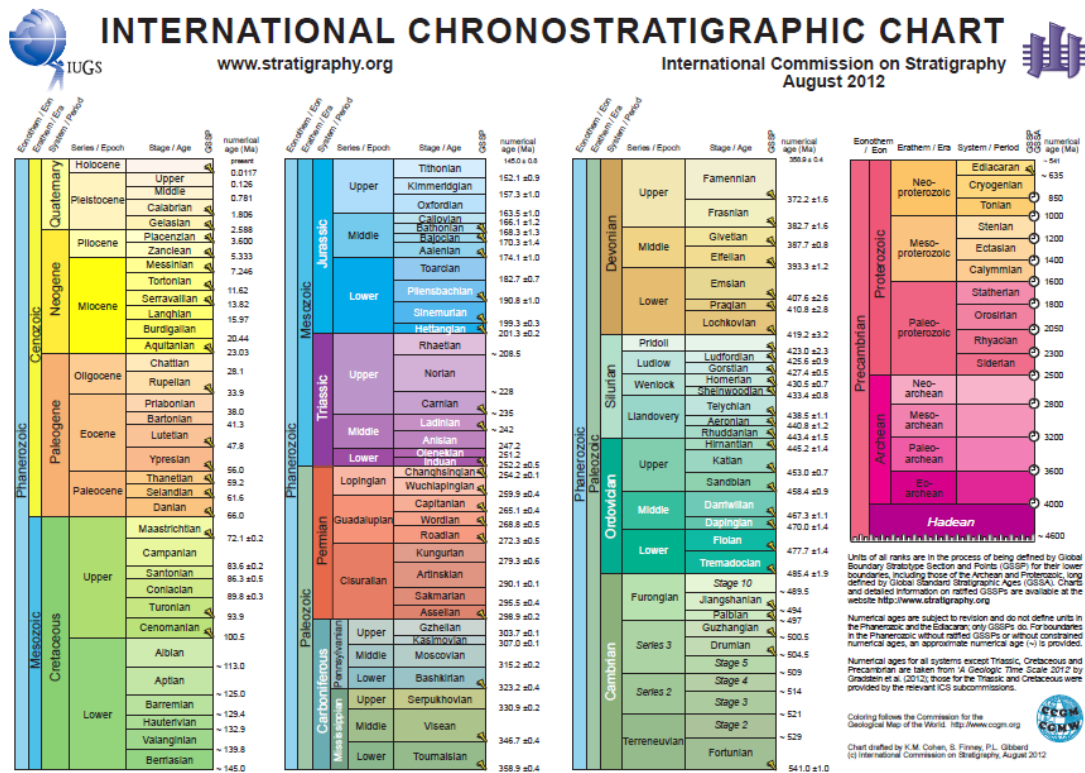


Figure IV.4 International Chronostratigraphic Chart. After [132].

Focusing attention on the study area, two paleogeographic domains may be recognized (see [133]): the Trento Platform/Plateau in the west and the Adriatic Basin in the east. These domains differentiated in Early Jurassic times (Pliensbachian) as a consequence of an extensional tectonic event that caused the dissection of an Upper Triassic-Lower Jurassic p.p. carbonate shelf and subsequently created a more or less complex platform-and-basin system. This tectonic event, widespread in the whole Mediterranean region, is related to the opening of the Atlantic Ocean (ECMA-East Coast Magnetic Anomaly dated at 195 Ma by [134]), the early rifting phases of which likely date back to 199 Ma, in correspondence to the magmatic activity peak known as the ECMA-East Coast Magnetic Anomaly, which identifies the break-up of Pangea ([135]). Before platform-and-basin differentiation, the Trento and Adriatic domains were part of a wide epeiric shelf on which peritidal carbonates accumulated during Late Triassic and Hettangian-Sinemurian times (Norian “Dolomia Principale” Fm plus Rhaetian “Calcari del Dachstein” Fm and lower Liassic “Calcari Grigi” Fm). **Figure IV.5** is a paleogeographic sketch of the eastern Southern Alps and Po Plain showing the areal distribution of the different depositional domains during the early Liassic (Hettangian-Sinemurian). The same picture provides the location of several wells used for reconstructing the standard stratigraphy of the region and the facies distribution. As concerns the study area, note that the wells have been plotted in their present-day location without any palinspastic restoration of the Ferrara Folds.

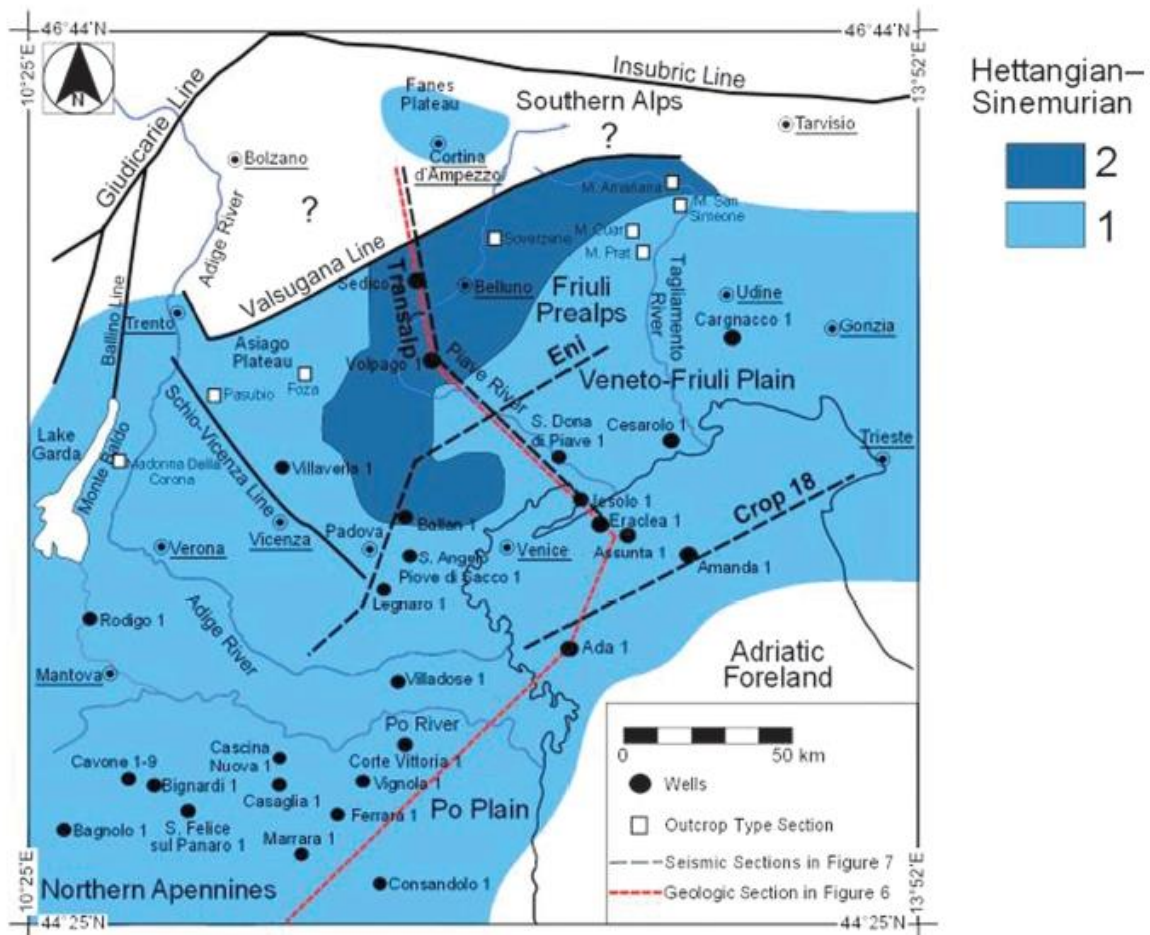


Figure IV.5 Regional sketch of the eastern Southern Alps and Po Plain showing the paleogeographic position of the Cavone-Ferrara area during Hettangian-Sinemurian (Lower Jurassic p.p.) times. After [133]. 1 Peritidal carbonates (“Calcarei Grigi”). 2 Carbonate deposits of the Belluno Basin (Soverzene Formation).

Figure IV.6 shows the region and the wells at a time (Pliensbachian) immediately following the platform-and-basin differentiation. We wish to stress the fact that the Cavone wells have crossed a sedimentary sequence whose Upper Triassic (Norian/Rhaetian)-Lower Jurassic portion is entirely composed of shallow-water carbonates until the Toarcian while the Ferrara 1 well has penetrated a stratigraphic sequence made up of Norian/Rhaetian-Sinemurian peritidal carbonates followed by Pliensbachian-Toarcian basinal carbonates. Around the end of the Toarcian, the bulk of the Trento Platform also drowned below the photic zone and became a pelagic plateau with the exception of the southern portion which persisted as a shallow-water carbonate platform until the Early Cretaceous at least (Bagnolo Platform, see [136]). A regional paleogeographic sketch referred to the Middle Jurassic is given in **Figure IV.7**. During late Mesozoic, Paleogene and early Miocene times, i.e. after the complete differentiation of the platform-and-basin system, the major sedimentation changes were closely controlled by global physical events, namely climatic changes and sea-level oscillations. In the late Miocene, the internal (southern) portions of the study area bordering the Apennine thrust front were reached by flexural subsidence and were incorporated into the foredeep basin. Sedimentation changed drastically because of a sudden and abundant siliciclastic input so that prevailing marls were substituted by prevailing sands. The northward/north-eastward time-space migration of the siliciclastic flysch deposits (see [137]) describes very well the progressive flexure-hinge retreat of the foreland plate. Between the late Miocene and the Pleistocene, finally, the foredeep basin was reached by the Apennine compression and segments of the former foreland domain were incorporated in the mountain chain. Mobile piggyback basins developed at the front of the Apennines (see,

e.g.[138]). Spectacular growth strata evident in seismic profiles clearly demonstrate the change from a foredeep-basin stage to a piggyback-basin one.

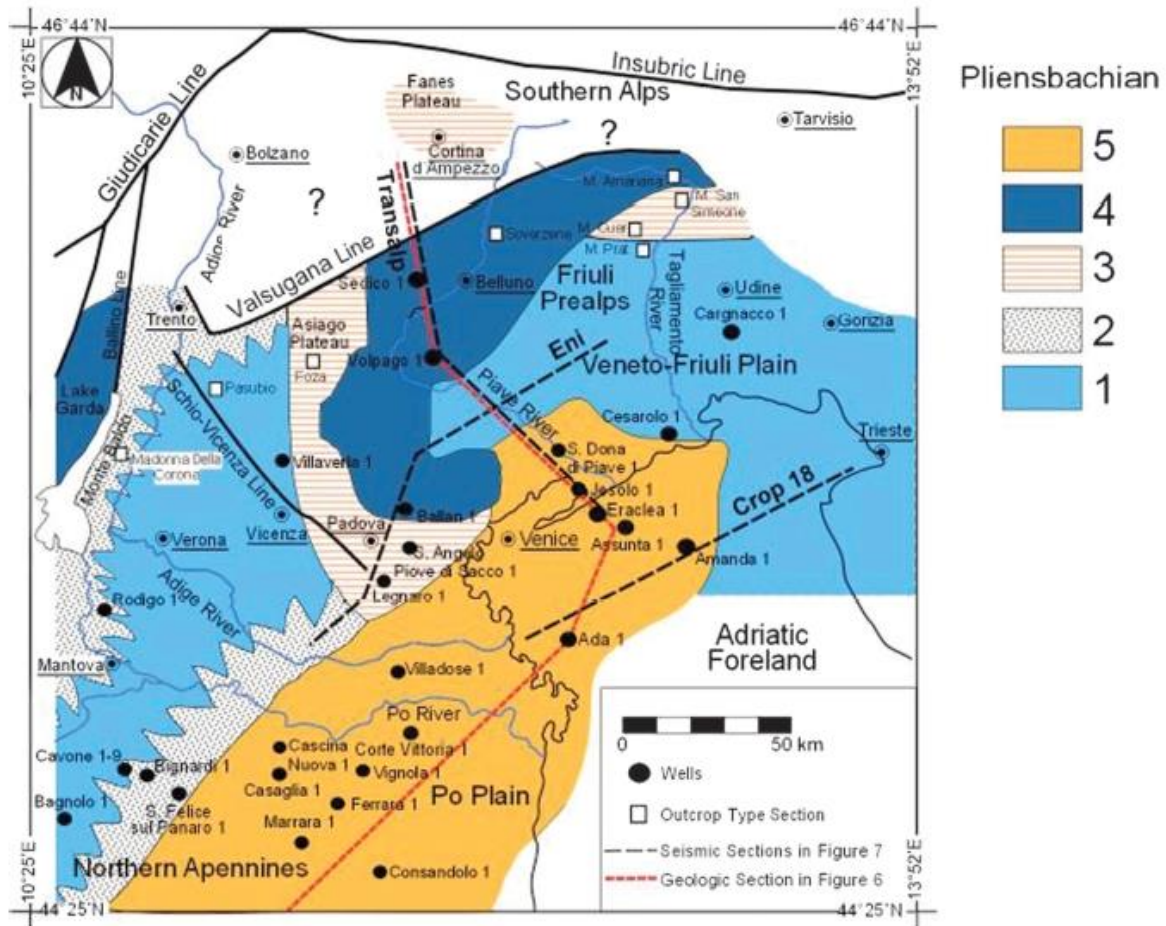


Figure IV.6 Regional sketch of the eastern Southern Alps and Po Plain showing the paleogeographic position of the Cavone-Ferrara area during Pliensbachian (Lower Jurassic p.p.) times. After [133]. 1 Shallow-water carbonates of the Trento and Friuli-Adriatic Platform. 2 Platform-edge calcarenites and lime resediments along the north-western and south-eastern margins of the Trento Platform. 3 Condensed carbonate deposits along the eastern margin of the Trento Platform and the northern margin of the Friuli-Adriatic Platform. 4 Carbonate deposits of the Lombardian and Belluno Basins. 5 Carbonate deposits of the Adriatic Basin. Note that the Adriatic Basin and the Belluno Basin had to join somewhere north Venice.

Three stratigraphic sequences displaying important facies variations during Mesozoic times give a summary of the principal characteristics of the sedimentation in the study area:

- The Bagnolo sequence, representative of a carbonate platform (Bagnolo Platform) persisting from the Late Triassic p.p. (Norian-Rhaetian) to the Early Cretaceous (Neocomian-Albian) at least. The Upper Cretaceous-Paleogene portion of the sequence is lacking, due to an erosional unconformity at the base of Messinian deposits. Consequently, the real duration of the shallow-water-platform conditions after the Albian is unknown;
- The Cavone sequence, representative of an Upper Triassic p.p. (Norian-Rhaetian)-Lower Jurassic (Toarcian) carbonate platform (Trento Platform) drowned below the photic zone around the Early Jurassic/Middle Jurassic boundary and converted into a pelagic plateau (Trento Plateau);
- The Ferrara sequence, representative of an Upper Triassic p.p. (Norian-Rhaetian)-Lower Jurassic p.p. (Hettangian-Sinemurian) carbonate platform turned into a basinal domain (Adriatic Basin) around the Sinemurian-Pliensbachian boundary.

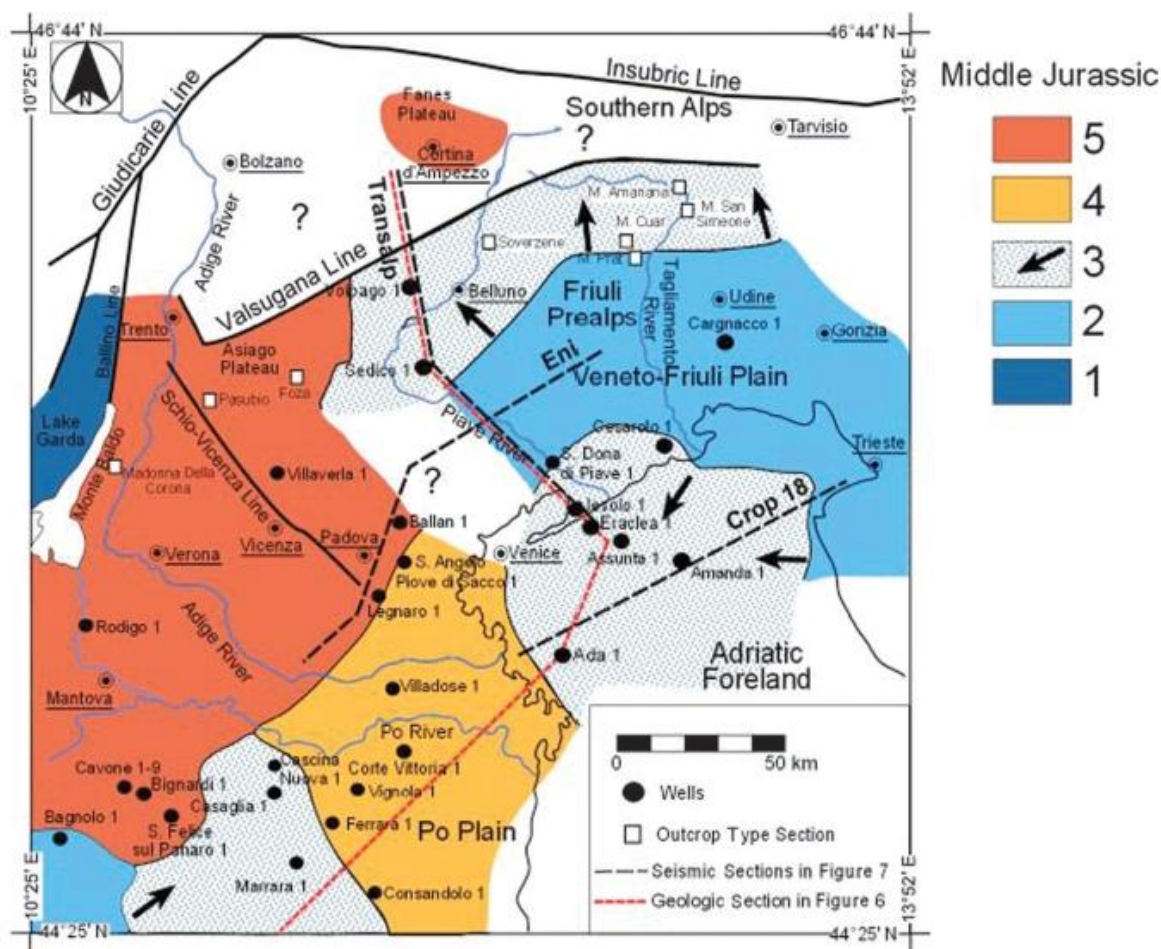


Figure IV.7 Regional sketch of the eastern Southern Alps and Po Plain showing the paleogeographic position of the Cavone-Ferrara area during Middle Jurassic times. After [133]. 1 Carbonate deposits of the Lombardian Basin. 2 Shallow-water carbonates of the Bagnolo and Friuli-Adriatic Platforms. 3 Redepleted oolitic calcarenites (arrows indicate the sense of the gravity flows). 4 Carbonate deposits of the Adriatic Basin. 5 Condensed carbonate deposits of the Trento and Fanes Plateaux (“*Posidonia*” alpina marls and marly limestones).

The Bagnolo sequence has been recognized only in the Bagnolo area. It is well documented by the composite log of the Bagnolo in Piano 2 well (**Figure IV.8**). This borehole encountered:

- 0-360 Quaternary alluvial deposits;
- 360-2196 Plio-Pleistocene marine terrigenous deposits (Porto Corsini Fm, Porto Garibaldi Fm, Santerno Clays, Asti Sands);
- 2196-4505 Messinian terrigenous deposits (Colombacci-Fusignano Fm)
- 4505 unconformity surface at the top of shallow-water platform carbonates (Bagnolo Platform) crossed from 4505 to the final depth 5733;
- 4505-4692 shallow-water limestones with *Cuneolina pavonia parva* and orbitolinids (Albian);
- 4692-5350 shallow-water limestones with *Cuneolina camposauri*, *Trocholina* spp., *Salpingoporella dinarica* and *S. annulata* (Neocomian-Aptian);
- 5350-5733 (Total Depth) shallow-water limestones with *Clypeina jurassica*, *Salpingoporella annulata*, *S. podolica* and *Thaumatoporella parvovesiculifera* (Upper Jurassic).

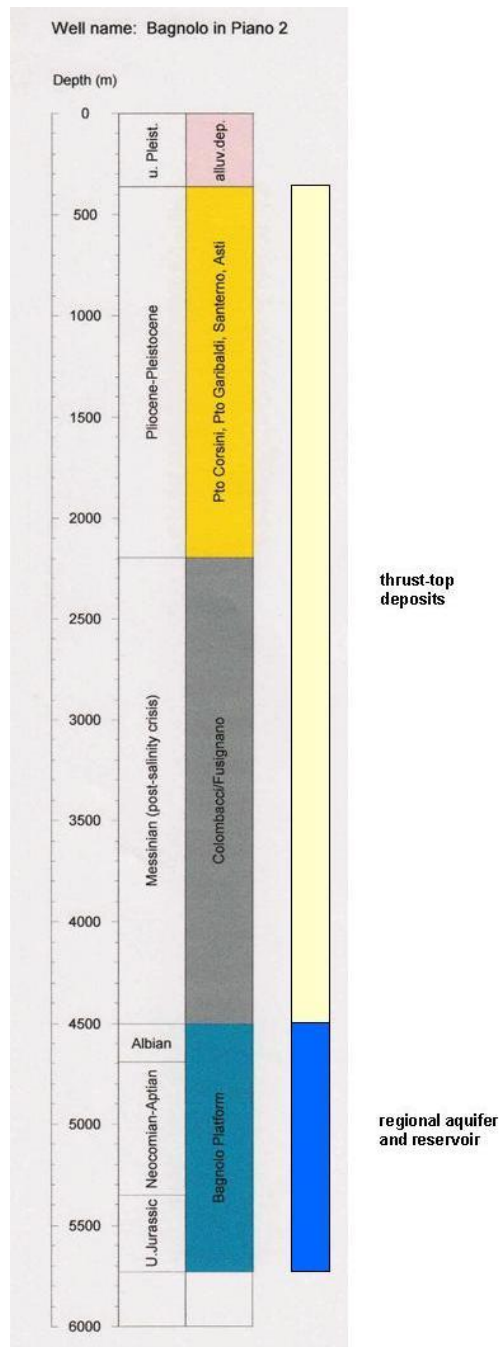


Figure IV.8 Schematic composite log of Bagnolo in Piano 1 well.

The Cavone sequence is well represented in the Cavone field (see [139]), as well as in Mirandola 1, Bignardi 1 dir and San Felice sul Panaro 1. We have chosen Cavone di Carpi 1 as a type section representative of the entire stratigraphic succession from the Norian/Rhaetian to the lower Miocene (Figure IV.9).

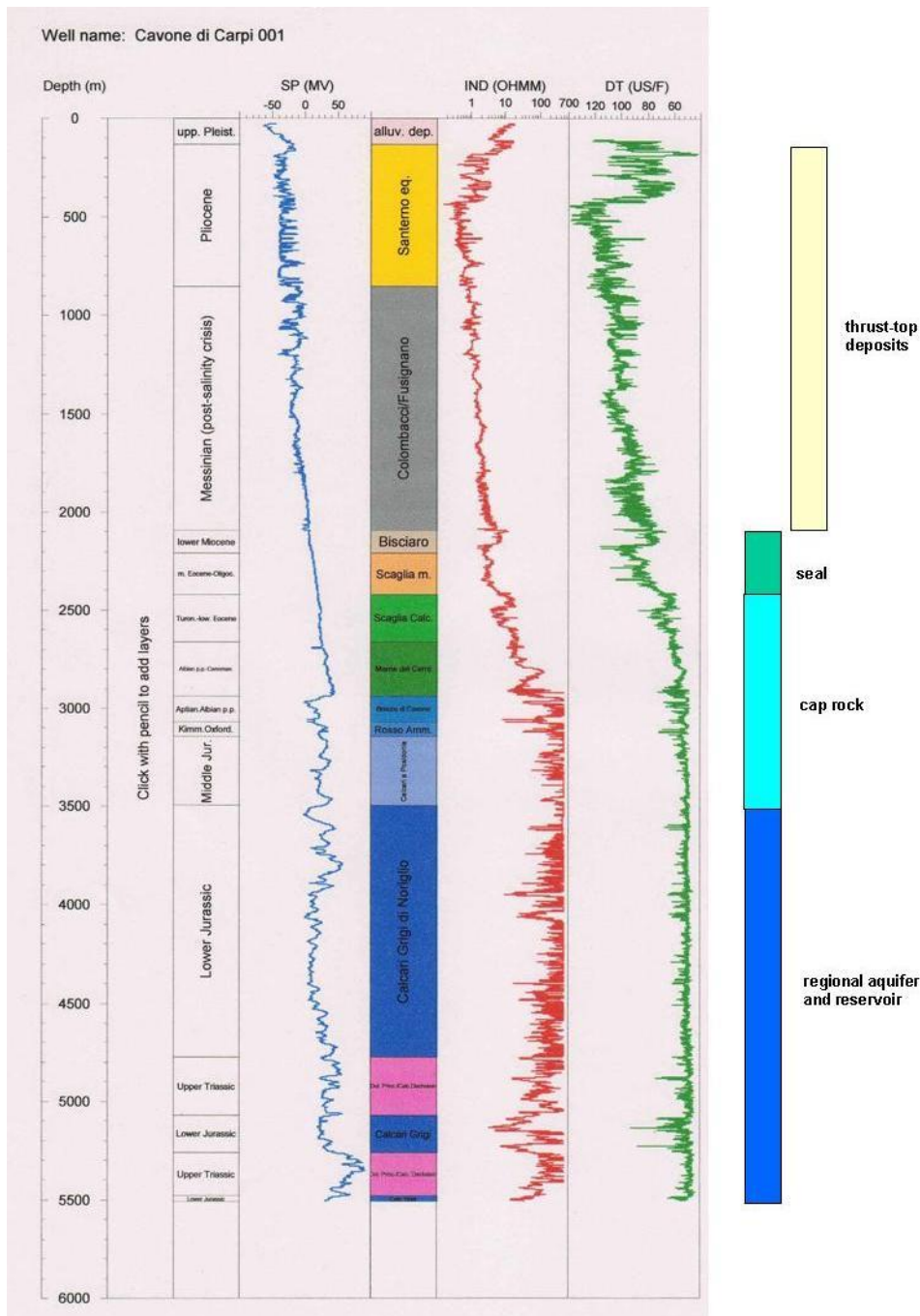


Figure IV.9 Schematic composite log of Cavone di Carpi 1 well.

Moving downsection, the borehole encountered:

- 0-130 Quaternary alluvial deposits;
- 130-857 Pliocene marine terrigenous deposits (Santerno Fm equivalent);
- 857 unconformity surface;
- 857-2093 Messinian terrigenous deposits (Colombacci-Fusignano Fm);
- 2093 unconformity surface;
- 2093-2210 marly limestones and marls with planktonic foraminifers (Bisciario Fm equivalent , lower Miocene);
- 2210 unconformity surface;
- 2210-2420 greenish-grey marls and subordinate marly limestones with planktonic foraminifers (marly member of the Scaglia Fm, Oligocene-middle Eocene);

- 2420-2860 pinkish and whitish calcilutites with planktonic foraminifers (calcareous member of the Scaglia Fm, Turonian-lower Eocene);
- 2660-2939 dark-grey and greenish marls and limestones (Marne del Cerro Fm, Albian p.p.-Cenomanian);
- 2939-3070 redeposited calcarenites and calcirudites with orbitolinids (Breccie di Cavone Fm, Aptian-Albian p.p.);
- 3070 unconformity surface;
- 3070-3145 red nodular limestones (Rosso Ammonitico Veronese, Kimmeridgian-Oxfordian);
- 3145-3495 calcilutites with pelagic pelecypods and radiolarians (Calcari a Posidonia Fm, Middle Jurassic);
- 3495-4775 shallow-water grey calcilutites and calcarenites with *Palaeodasycladus mediterraneus*, *Orbitopsella praecursor* and *Lithiotis problematica* (Calcari Grigi di Noriglio, Lower Jurassic);
- 4775-5072 intertidal dolomites (Dolomia Principale/Calcare del Dachstein, Upper Triassic);
- 5072 thrust surface;
- 5072-5260 grey calcilutites and calcarenites with *Palaeodasycladus mediterraneus* (Calcari Grigi di Noriglio, Lower Jurassic);
- 5260-5480 grey dolomites (Dolomia Principale, Upper Triassic);
- 5480 thrust surface;
- 5480-5507 (Total Depth) grey calcilutites and calcarenites with *Palaeodasycladus mediterraneus* (Calcari Grigi di Noriglio, Lower Jurassic).

The Ferrara sequence is described by the stratigraphic log of the Ferrara 1 well (**Figure IV.10**). Moving downsection, the borehole encountered:

- 0-110 Quaternary alluvial deposits;
- 110-478 Pleistocene marine terrigenous deposits (Codigoro Fm);
- 478 unconformity surface;
- 478-990 marls and subordinate sands in the upper portion of the interval (Gallare Fm equivalent, lower-middle Miocene);
- 990-1285 marls and calcareous marl (marly member of the Scaglia Fm, middle Eocene p.p.-Oligocene);
- 1285-1680 pinkish and whitish calcilutites with planktonic foraminifers (calcareous member of the Scaglia Fm, Cenomanian-middle Eocene p.p.);
- 1680-1700 marls and marly limestones (Marne a Fucoidi Fm, Aptian-Albian);
- 1700-1894 whitish and light-grey cherty calcilutites with tintinnids (Maiolica Fm, Tithonian-Barremian);
- 1894-2015 whitish and greenish cherty calcilutites rich in radiolarians, locally dolomitized (Calcari ad Aptici Fm, Dogger-Malm p.p.);
- 2015-2096 grey marls and dolomitic marls (Rosso Ammonitico Fm equivalent, upper Liassic);
- 2096-2225 calcilutites, locally dolomitized, and subordinate marls radiolarians, sponge spicules and reworked foraminifers (Corniola Fm, middle Liassic);
- 2225-2674 cherty dolomites with sponge spicules and platform-derived bioclasts and ooids (Dolomia con Selce Fm+Dolomia Oolitica Fm, lower Liassic);
- 2674-4016 intertidal grey dolomites with *Aeolisaccus dunningtoni*, *Aulotortus* sp., *Glomospirella friedli*, small *Frondicularia* sp. and algal fragments (Dolomia Principale Fm/Calcare del Dachstein Fm, Upper Triassic);
- 4016 thrust surface;

- 4016-4155 greenish-grey and reddish marls and calcareous marls with planktonic foraminifers (marly member of the Scaglia Fm, middle Eocene);
- 4155-4420 limestones and marly limestones with planktonic foraminifers (calcareous member of the Scaglia Fm, Upper Cretaceous-lower Eocene);
- 4420-4493 cherty calcilutites with tintinnids (Maiolica Fm, Tithonian-Lower Cretaceous). At the top, a few metres of black shales referable to the Marne a Fucoidi Fm (Aptian-Albian);
- 4493-4550 calcilutites and varicoloured radiolarian cherts (Calcari ad Aptici Fm, Dogger-Malm p.p.);
- 4550-4556 cherty limestones (probable Rosso Ammonitico Fm, upper Liassic);
- 4556-4743 (Total Depth) light-grey cherty dolomites with rare radiolarians and platform-derived bioclasts and ooids (Dolomia con Selce Fm+Dolomia Oolitica Fm, Lower Jurassic).

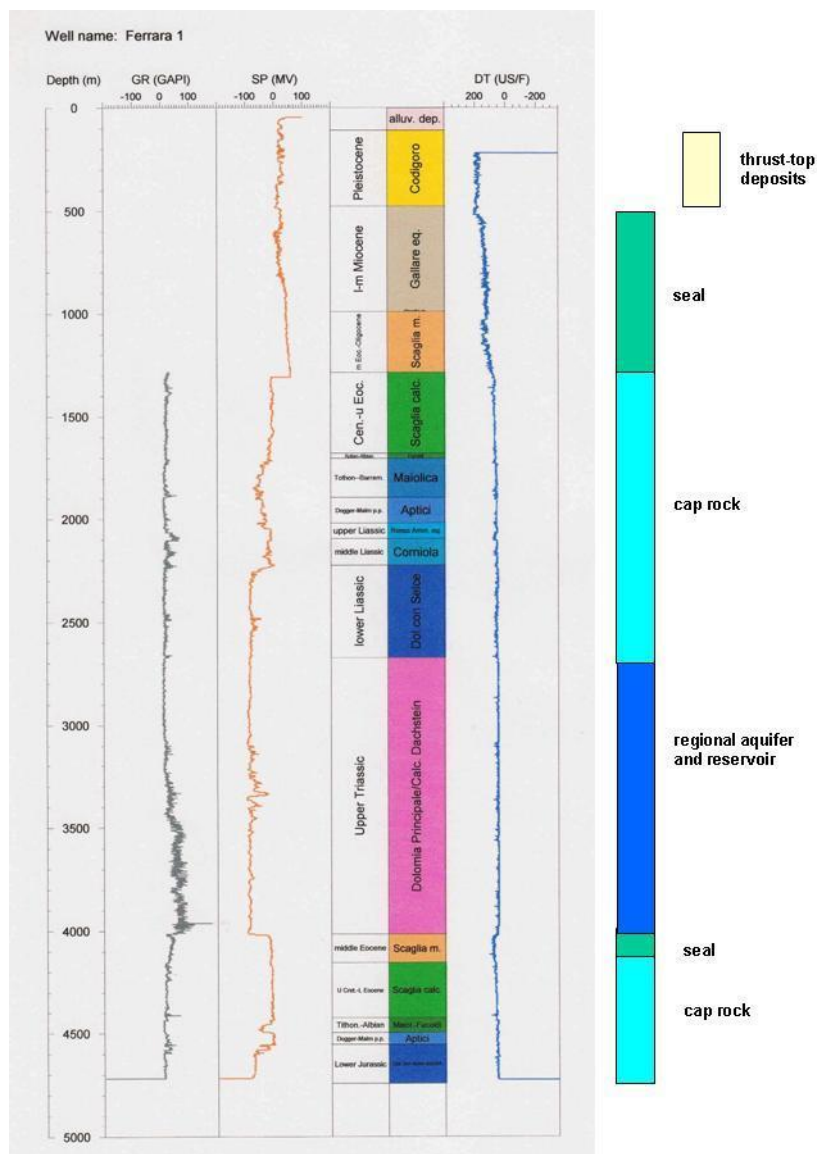


Figure IV.10 Schematic composite log of Ferrara 1 well.

In the Cavone and Ferrara sequences the Upper Triassic-Lower Jurassic platform carbonates (Dolomia Principale Fm/Calcari del Dachstein Fm and Calcari Grigi di Noriglio Fm) represent the major aquifer, as well as the potential reservoir for oil accumulation (see

Figure IV.9 and **Figure IV.10**). In the Bagnolo sequence the reservoir is made up by younger (Upper Jurassic-Lower Cretaceous) platform carbonates (Piattaforma di Bagnolo, see **Figure IV.8**). Apart from the Bagnolo in Piano, Cavone and Ferrara boreholes, the carbonate reservoir in the study area has been reached by San Giovanni 1, San Giacomo 1, Concordia 1, Bignardi 1dir, San Felice sul Panaro, Cascina Nuova 1dir, Casaglia 1 and by Casaglia 2 and 3 (drilled for geothermal purposes), as well as by Vignola 1 which is located ahead of the frontal thrust of the Ferrara Folds. In all cases, primary porosity in the shallow-water carbonates is extremely low and tectonic fracturing has been entirely responsible for the reservoir porosity and connectivity. The mechanical status of the reservoir obviously undergoes significant and abrupt lateral changes, depending on the fault distribution and fracture density. The cap rock at the top of the reservoir is made up of the pelagic lime deposits that stratigraphically overlie the shallow-water carbonates. In the case of Cavone (**Figure IV.9**) the cap rock is made up by the Calcari a Posidonia, Rosso Ammonitico, Maiolica, Breccie di Cavone (where present) and Marne del Cerro Formations, as well as by the calcareous member of the Scaglia Formation. The Rosso Ammonitico Formation has very poor porosity, even in the case of penetrative fracturing; the porosity of the Calcari a Posidonia, Maiolica and Breccie di Cavone Formations, together with the calcareous member of the Scaglia Formation, is closely controlled by tectonic fracturing; the Marne del Cerro Formation, finally, works everywhere as a true seal. In the case of Ferrara (**Figure IV.9**), the cap rock is made up by the Dolomie con Selce, Rosso Ammonitico, Calcari ad Aptici, Maiolica and Marne a Fucoidi Formations, as well as by the calcareous member of the Scaglia Formation. The porosity of these lithostratigraphic units is strictly controlled by the tectonic fracturing, with the exception of the Marne a Fucoidi Formation which plays in any case the role of seal. The complete sealing of the possible traps is everywhere assured by the marly sediments constituting the middle Eocene-early/middle Miocene portion of the stratigraphic successions (see **Figure IV.9** and **Figure IV.10**). The compositional and textural characteristics, including porosity, of the upper Miocene and Plio-Pleistocene deposits is variable in the study area, depending on the siliciclastic input which was almost entirely controlled by the tectonic activity. Actually, the upper Miocene to Pleistocene stratigraphic sequence represents a complex depositional system completely independent from the Mesozoic-lower/middle Miocene one. In this system, in which sandy reservoirs and muddy seals are patchily distributed, important traps of biogenic gas have been discovered.

C. Seismic profiles

The study area is covered by a great number of reflection seismic profiles acquired by ENI in different years (**Figure IV.11**).

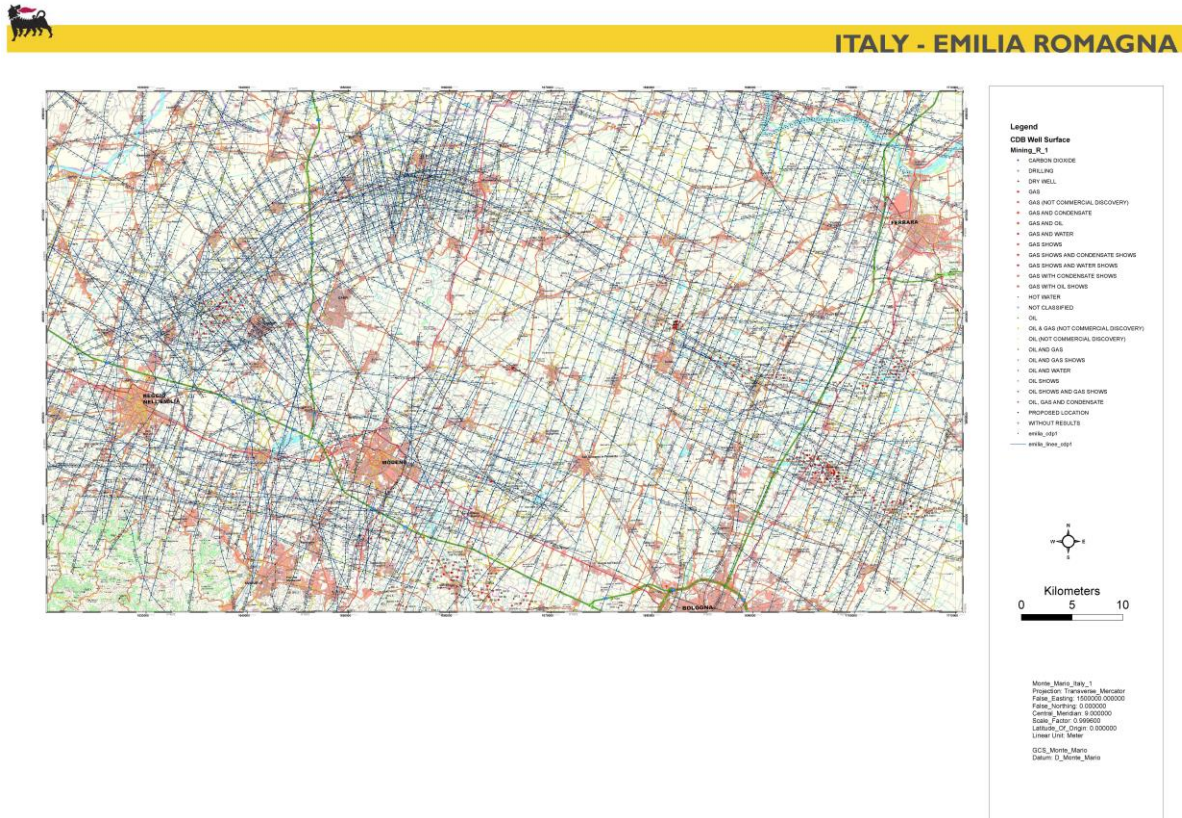


Figure IV.11 Map of the study area showing the existing seismic profiles. ENI, confidential document.

ENI kindly provided us the SEG-Y files of sixteen selected seismic lines located in the area struck by the May 20-29 2012 earthquakes. These lines (eleven dip lines and five strike lines roughly perpendicular to and parallel to the direction of the tectonic structures, respectively) have explored the Cavone and Pilastris structures in the Concordia-Mirandola area. Together with the SEG-Y files of the reflection seismic profiles, numerous well logs were also provided by ENI in a vector format (LAS files). Several wells have reached the shallow-water carbonates forming the major reservoir in the area. In addition, three regional stack lines in public domain, each one several tens of kilometres long, were available in raster/compound formats at the VIDEPI site. These regional lines, all made up of merged single profiles, cut across the entire Ferrara Arc along the profile Spilamberto-Muzza-Rivara-Pilastris (Dominio Appenninico Orientale, Section 1), the profile Bologna-Malalbergo-Casaglia (Dominio Appenninico Orientale, Section 2), and the profile Budrio-Bova-Tresigallo (Dominio Appenninico Orientale, Section 3). All spatial data, together with the principal structural lineaments of the area, have been organized in a GIS project. The entire data set relative to the available seismic profiles and wells is shown in **Figure IV.12**.

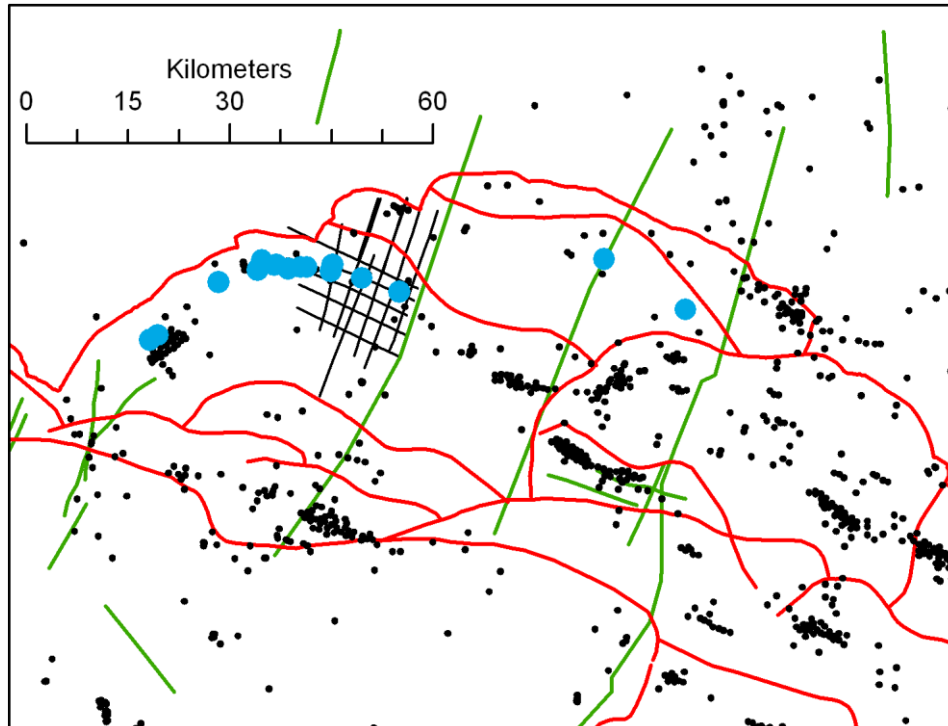


Figure IV.12 Base map of the study area showing the available wells and seismic lines. Highlighted blue spots in the Ferrara Arc indicate wells that have reached the carbonate reservoir. The latter is represented by Upper Jurassic-Lower Cretaceous shallow-water limestones in the Bagnolo sequence, by Upper Triassic dolomites and limestones overlain by Lower Jurassic limestones in the Cavone sequence, and finally by Upper Triassic dolomites and limestones overlain by lower Liassic limestones in the Ferrara sequence. Blue lines have been provided by ENI in SEG-Y format. Thicker green lines are profiles in public domain. Tectonic lineaments have derived from [111].

The SEG-Y profiles are all migrated lines moderately good in quality, with time length usually higher than 6 seconds. An example of dip line is shown in **Figure IV.13**, and an example of strike line is provided by **Figure IV.14**.

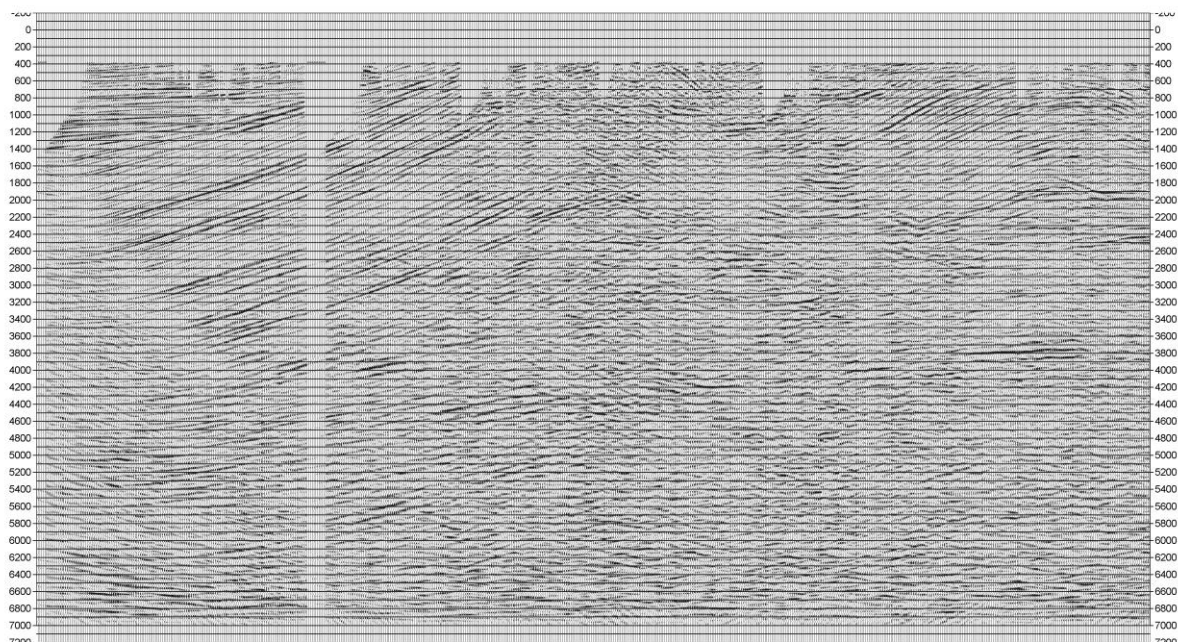


Figure IV.13 Example of dip line (MOD-74-19). The open-source software SEISEE has been used as SEG-Y viewer.

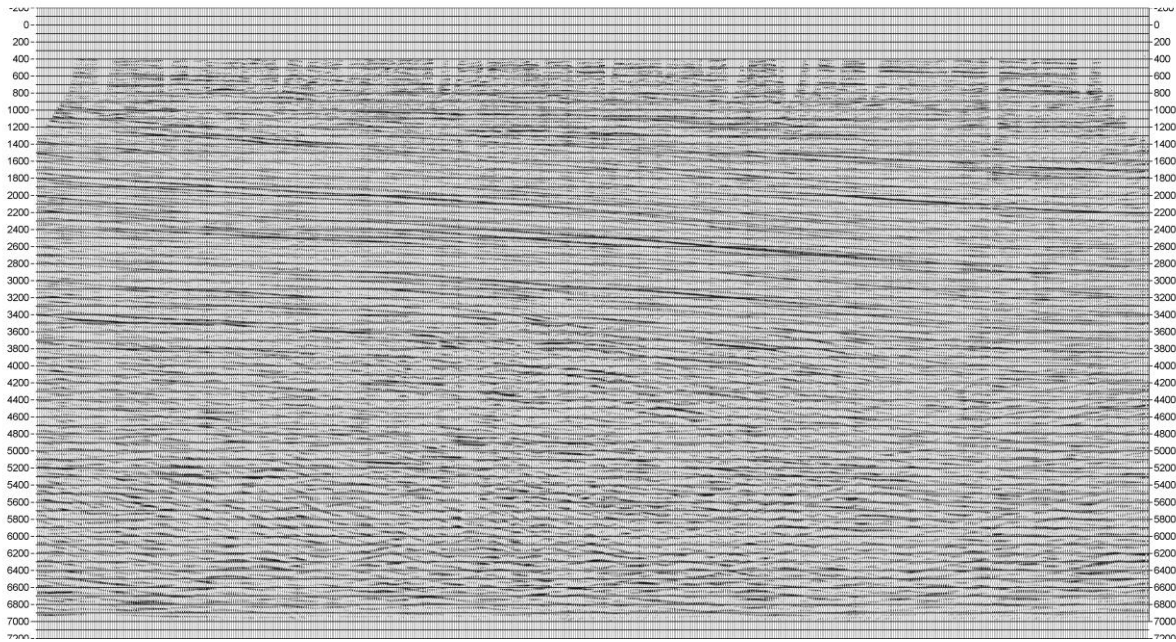


Figure IV.14 Example of strike line (MOD-74-30). The open-source software SEISEE has been used as SEG-Y viewer.

In all lines, frequencies obviously decrease while depths increase. However, also at shallow depths frequencies are relatively low, usually not exceeding 40-50 Hz and concentrating between 10 and 30 Hz at $A/F=50$. In the dip lines, frequencies show significant lateral variations. In correspondence to the Cavone structure, in fact, they are systematically lower than the whole-section frequencies, this in agreement with the rock properties of the reservoir uplifted in the nucleus of the anticline (**Figure IV.15**).

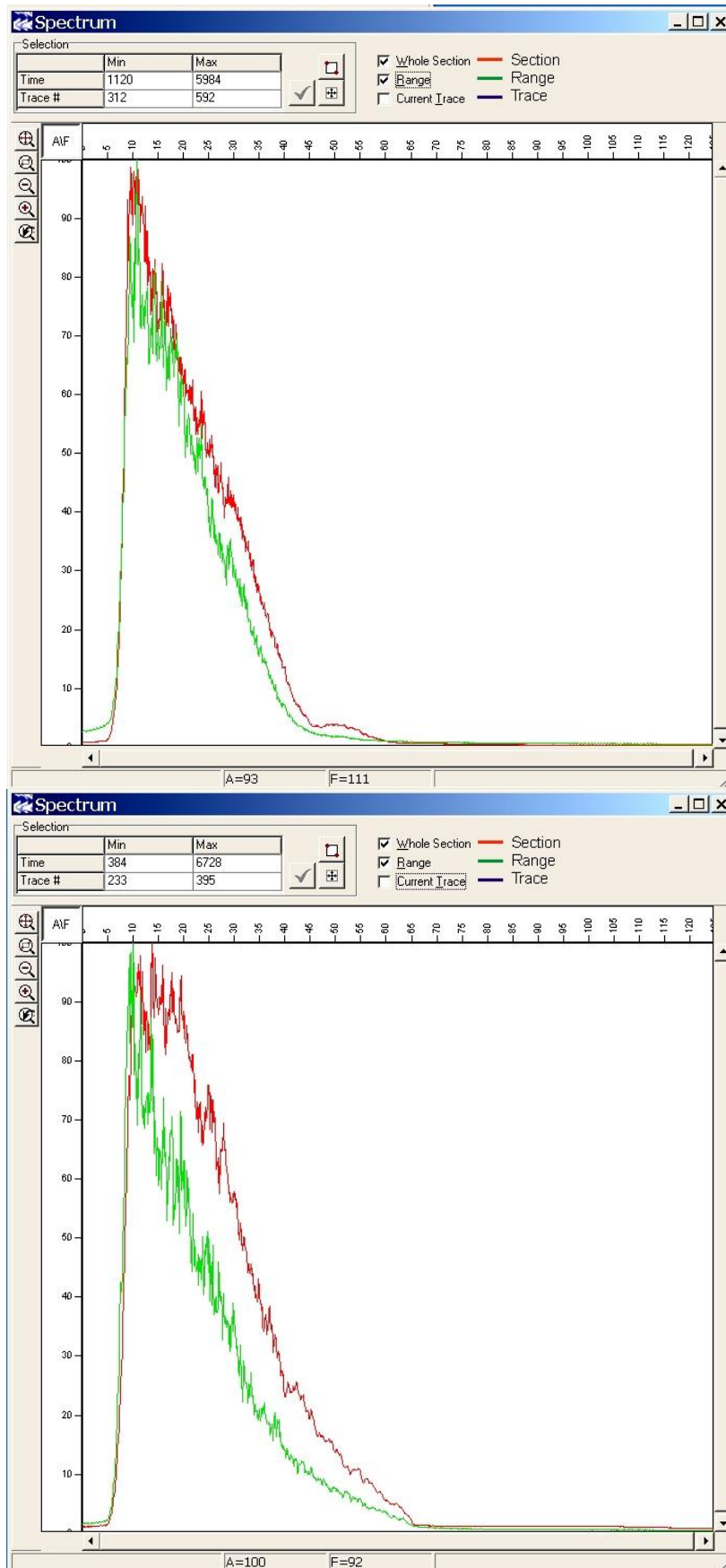


Figure IV.15 a and b. Examples of spectral curves (Amplitude/Frequency % versus Frequency) relative to dip lines (MOD-74-19 and MOD-01-EXT, respectively) showing the whole-section curves (red) and the curves in correspondence to the Cavone anticline (green). Spectrum images have been obtained using the open-source SEISSEE.

In the strike lines, on the contrary, no change in the frequencies has been observed moving along the section (**Figure IV.16**).

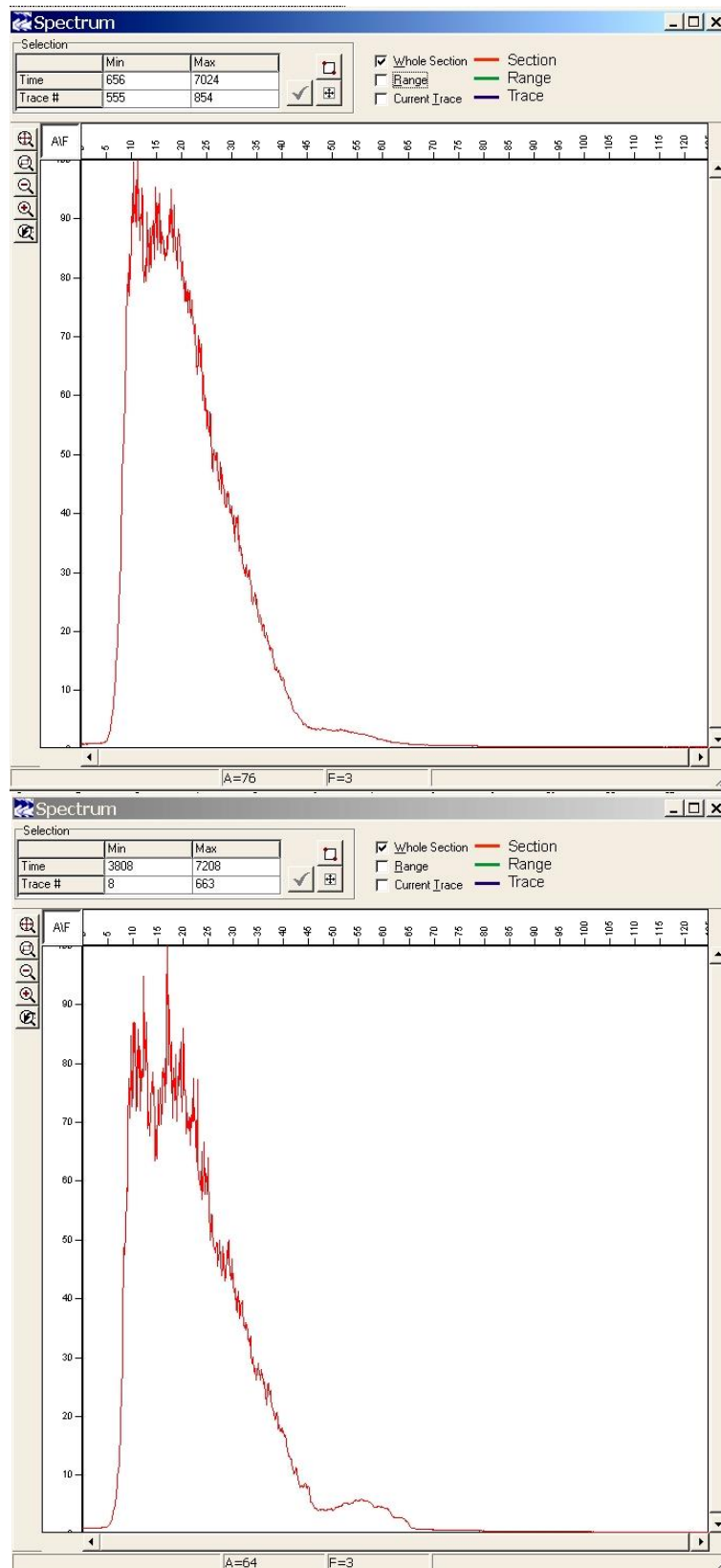


Figure IV.16 a and b Examples of spectral curves (Amplitude/Frequency % versus Frequency) relative to strike lines (MOD-74-24 and MOD-74-28, respectively). Moving along the section, no change in the shape has been observed. Spectrum images have been obtained using the open-source SEISEE.

The scarcity or the absence of high-frequency signals prevents an accurate seismic-stratigraphy analysis, discrete reflections from top and base of the explored geological layers having been strongly altered by constructive interference which has generated false attributes. The overall geometrical configuration, however, is well recognizable and consequently a quite accurate structural analysis has been possible. Results will be described in Session VII.

D. *Seismological data*

The seismological data analyzed by the Commission were provided by:

- INGV
- Companies

In particular, regarding data provided by INGV the Commission analyzed:

a) waveforms of the events with $M \geq 4$ and pickings for the events occurred during May 20 - June 6 time interval. After May 20 earthquake, additional seismic stations were deployed by INGV in the epicentral area. **Figure IV.17** shows the location of permanent and temporary seismic station around the epicentral area.

b) catalogue data taken from the Italian Seismological Instrumental and Parametric Data-Base (<http://iside.rm.ingv.it>). To maintain uniformity of the catalog, the commission used the database from 2005 as proposed by INGV (<http://iside.rm.ingv.it/iside/standard/index.jsp>)

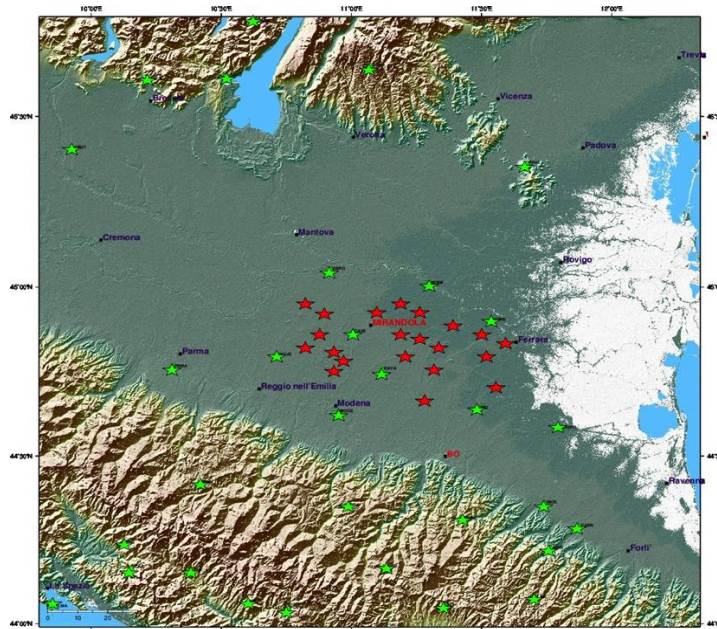


Figure IV.17 INGV permanent (green stars) and temporary (red stars) seismic stations around the epicentral area.

In the following all the data provided by the Companies are described.

1. Rivara

There is no permanent seismic monitoring system in the Rivara area. *Independent Gas Management srl* provided to the Commission (Appendix D) :

- Analysis of seismic activity available data between June, 2008 and September, 2011 and seismic hazard characterization of the Rivara area.

Data on 10 earthquakes between June 2008 and July 2010 (shown in **Figure IV.18**) and 11 earthquakes between July 2011 and September 2011 (shown in **Figure IV.19**) were processed by the Department of Geological Science of the University of Catania for the evaluation of source parameters such as earthquake localization, magnitude and focal mechanism. Results of the analysis and details on the input parameters used for the hypocentral localization and related uncertainties are reported in Appendix D.

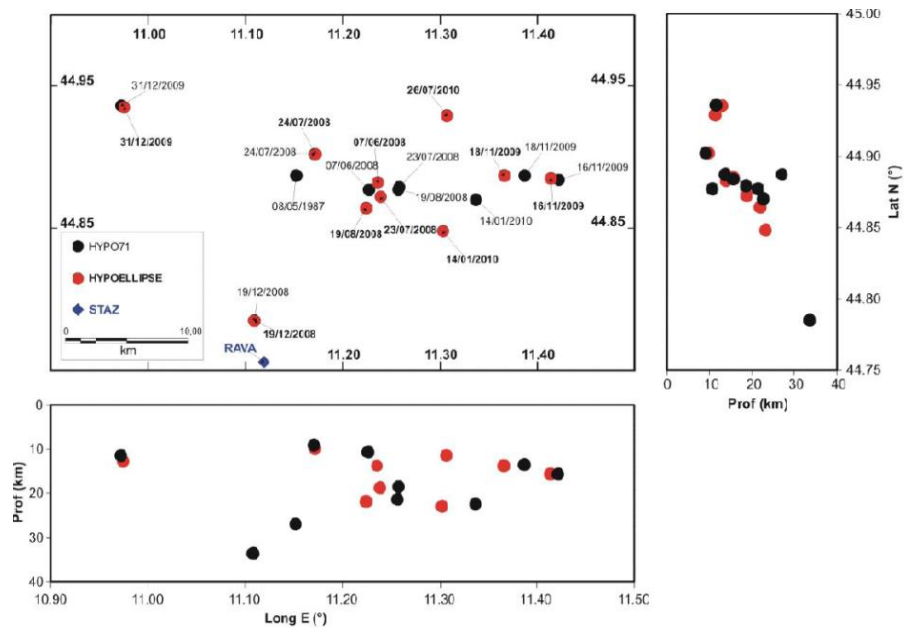


Figure IV.18 Hypocentral localization of 10 events between June, 2008 and July, 2010.

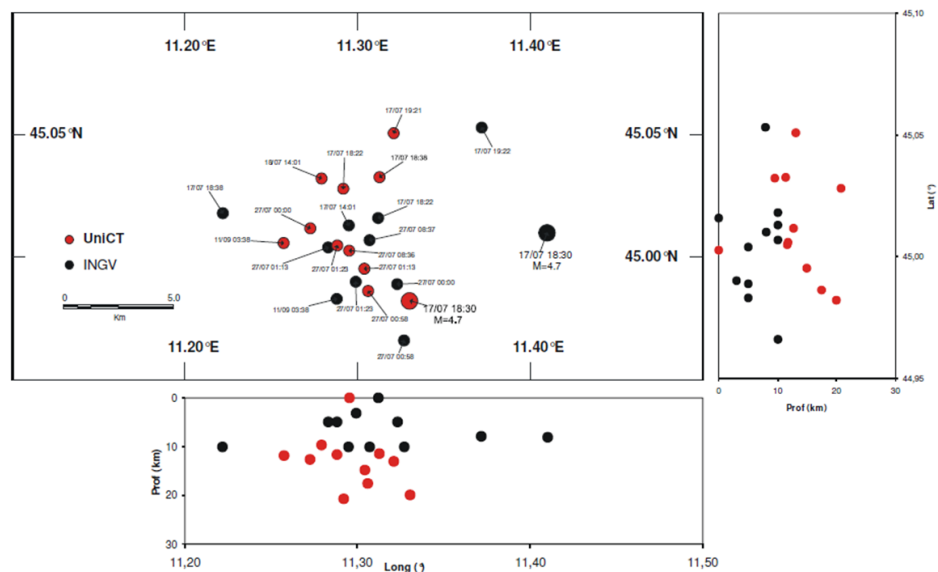


Figure IV.19 Hypocentral localization of 11 events between July, 2011 and September, 2011.

2. Minerbio

All technical data regarding the seismic monitoring system together with seismic activity and network operational data from January 2010 to December 2012, which were made available by STOGIT for the Minerbio field, are reported in Appendix D.

In particular the company provided to the Commission the following data:

- Technical and operational manual for the management of the network
- Raw and processed data from 2010 to 2012,
- Annual report from 2010 to 2012.

The Minerbio field is monitored by a local microseismic network that is formed of three stations: FIU, PAS and TOR (**Figure IV.20**) which transmit data to the ENI offices of San Donato Milanese (Milan).



Figure IV.20 Minerbio Microseismic surface network.

Each station is characterized by one seismometer (3 component Lennartz LE-3D “classic”), a recording system (Digital Lennartz Mars-88/MC system with three input channels and one monitor channel). The recorded signals on the 3 receiver channels are digitized and directly analyzed by peripheral stations through an algorithm to verify the outcome of the trigger algorithm. Events which trigger on more than one station within a specified time window are processed and interpreted.

In 2010 and 2011 the only events recorded by the network were of regional type, i.e. events characterized by epicentral distances between 10 to 100 km. For regional earthquakes, hypocentral coordinates are extracted from INGV website or obtained by integrating data from the local network and the national network when the local network records the signals before INGV stations.

In 2012, 16 local events were recorded from July to December and 13 of these were located. The 13 events, characterized by a local magnitude of less than 1.6 and depth > 5 km, are shown in **Figure IV.21** and listed in **Table IV.1** where information on the errors in coordinates and depth of the events is also provided.

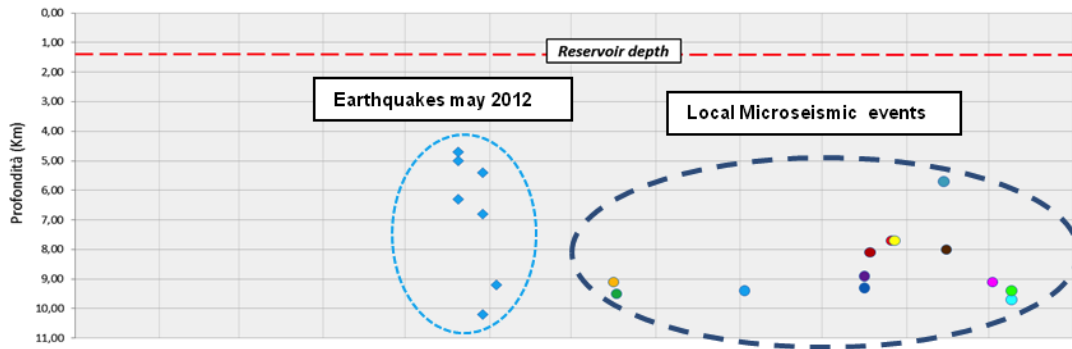


Figure IV.21 Earthquakes of May 2012 and local microseismic events recorded between July and December 2012.

Earthquakes of the Emilia Sequence (regional events with magnitude > 5) were recorded by one station (TOR) of the local network, 25-50 km from the epicentral areas. Hypocentral data of the sequence were derived from INGV.

Table IV.1 Local microseismic events recorded from July to December 2012.

Event	Date	Time (UTC)	Epicenter	Latitude_N	Longitude_E	Err. Epicenter (km)	M_L	Depth (km)	Err. Depth (km)
1	16/07/2012	22:22:12	Minerbio	44°37.65'	11° 30.01'	0.3	1.1	9.1	0.2
2	17/07/2012	04:04:01	Minerbio	44°38.65'	11° 28.07'	0.3	1.2	9.5	0.2
3	2/09/2012	22:55:14	Minerbio	44°38.43'	11° 32.22'	0.3	1.5	9.4	0.2
4	16/10/2012	16:39:19	Minerbio	44°38.29'	11° 32.05'	0.3	1.4	9.3	0.2
5	16/10/2012	16:46:28	Minerbio	44°38.46'	11° 32.28'	0.3	1.0	8.9	0.2
6	18/10/2012	04:58:09	San Giorgio in Piano	44°39.21'	11° 26.73'	0.2	1.3	8.1	0.1
7	26/10/2012	23:16:28	San Giorgio in Piano	44°39.02'	11° 26.23'	0.4	1.3	7.7	0.4
8	27/10/2012	01:40:48	San Giorgio in Piano	44°39.01'	11° 26.55'	0.2	1.0	7.7	0.2
9	14/11/2012	01:45:05	Minerbio	44°39.51'	11° 27.71'	1.7	1.4	5.7	0.7
10	15/11/2012	01:34:54	San Giorgio in Piano	44°38.66'	11° 26.89'	0.1	1.3	8.0	0.1
11	02/12/2012	01:23:59	Minerbio	44°38.55'	11° 27.00'	0.4	1.1	9.1	0.3
12	09/12/2012	03:24:36	San Giorgio in Piano	44°38.97'	11° 26.10'	0.4	1.1	9.7	0.2
13	09/12/2012	08:10:00	San Giorgio in Piano	44°38.72'	11° 26.00'	1.1	1.2	9.4	1.1

3. Mirandola

The microseismic network monitoring the Mirandola field, is managed by *ENI*. The company provided to the Commission the following data (reported in Appendix D):

- Technical data and operational manual for the management of the network;
- Raw and processed data from January 2010 to June 2012;
- Annual report from January 2010 to June 2012.

The microseismic network (shown in **Figure IV.22**) monitors the local microseismicity in the area of the Cavone field, and is composed of four stations, which transmit data to the ENI offices of San Donato Milanese (Milan). Each station is equipped with short period instruments and it is composed of one seismometer (Lennartz Le3D1 s classic) and a recorder A/D (Lennartz Mars88, 16 bit version, 3 channels).

Eleven local events, characterized by a local magnitude less than 2 and deeper than the reservoir, (shown in **Figure IV.22** and **Figure IV.23** and listed in **Table IV.2**) were recorded by the network before the 20th of May 2012. Information on the errors in coordinates and depth of the events was also provided.

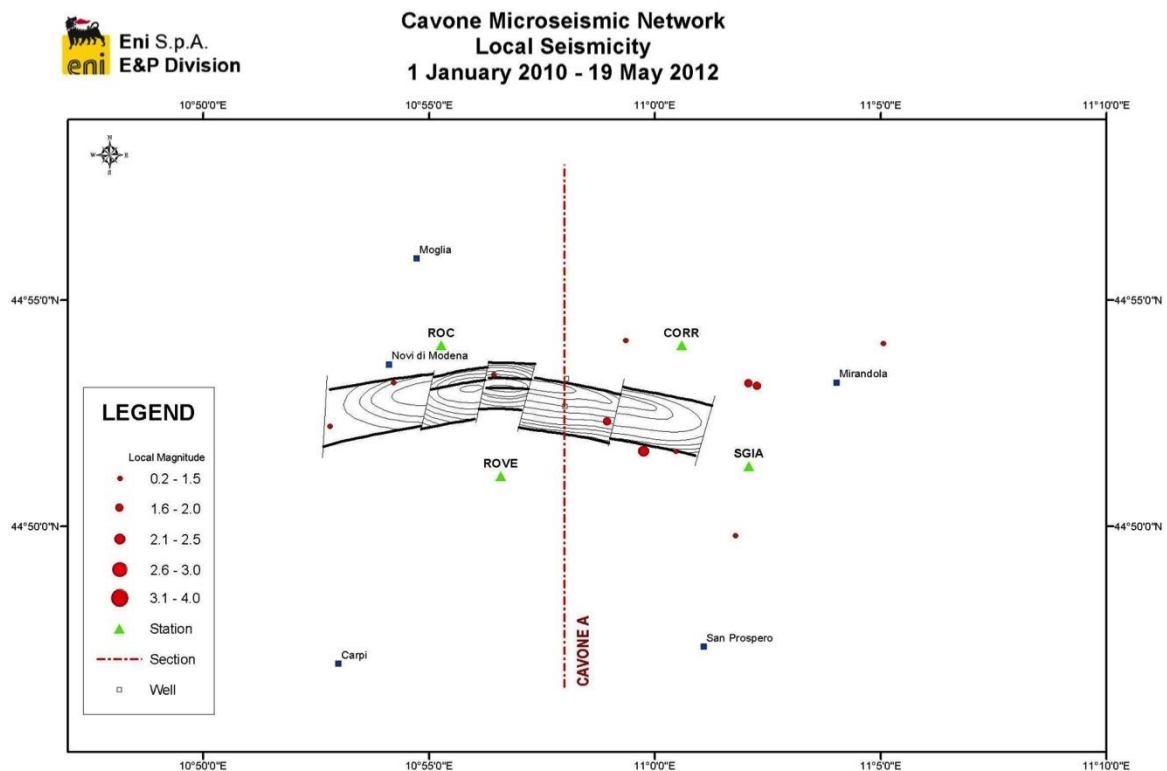


Figure IV.22 The Cavone microseismic network and local events recorded before the 20th of May 2012.

Between May 20 to June 14, 2012 due to the high level of seismic activity, it was only possible to store data for local earthquakes with $M_L > 3$ (52 events, shown in **Figure IV.23**). These events were processed by ENI and details on localization and related uncertainties are reported in Appendix D.

Starting from June 14th, 2012, two stations were out of commission and so from then localization was no longer possible.

Table IV.2 Local microseismic events recorded from January 2010 to May 19, 2012.

Event	Date	Time (UTC)	Epicenter	Latitude_N	Longitude_E	Err. Epicenter (km)	M _L	Depth (km)	Err. Depth (km)
1	02/01/2010	07:43	Mirandola	44°52.32'	10°58.94'	1.5	1.9	9.8	0.7
2	09/02/2010	00:03	Novi di Modena	44°53.17'	10°54.21'	0.3	0.5	5.3	0.1
3	10/02/2010	12:43	Novi di Modena	44°53.35'	10°56.43'	0.9	1.2	5.5	1.5
4	01/10/2010	02:34	Mirandola	44°54.10'	10°59.35'	4.5	0.2	10.0	5.0
5	11/03/2011	08:11	Mirandola	44°51.65'	11° 0.46'	0.3	0.5	6.0	0.5
6	06/04/2011	00:44	Novi di Modena	44°52.28'	10°52.84'	0.9	0.4	4.9	0.2
7	23/10/2011	10:11	Mirandola	44°51.65'	10°59.75'	0.9	2.0	8.0	1.0
8	11/12/2011	21:52	S.Prospiero	44°50.06'	11°02,1'	0.3	1.2	11.2	0.3
9	21/03/2012	22:41	Mirandola	44°53.16'	11° 2.08'	0.7	1.8	5.4	0.1
10	22/03/2012	01:06	Mirandola	44°53.16'	11° 2.08'	0.8	1.7	5.4	0.2
11	13/04/2012	23:54	S.Felice al Panaro	44°54.05'	11° 5.06'	0.5	1.0	7.9	0.6

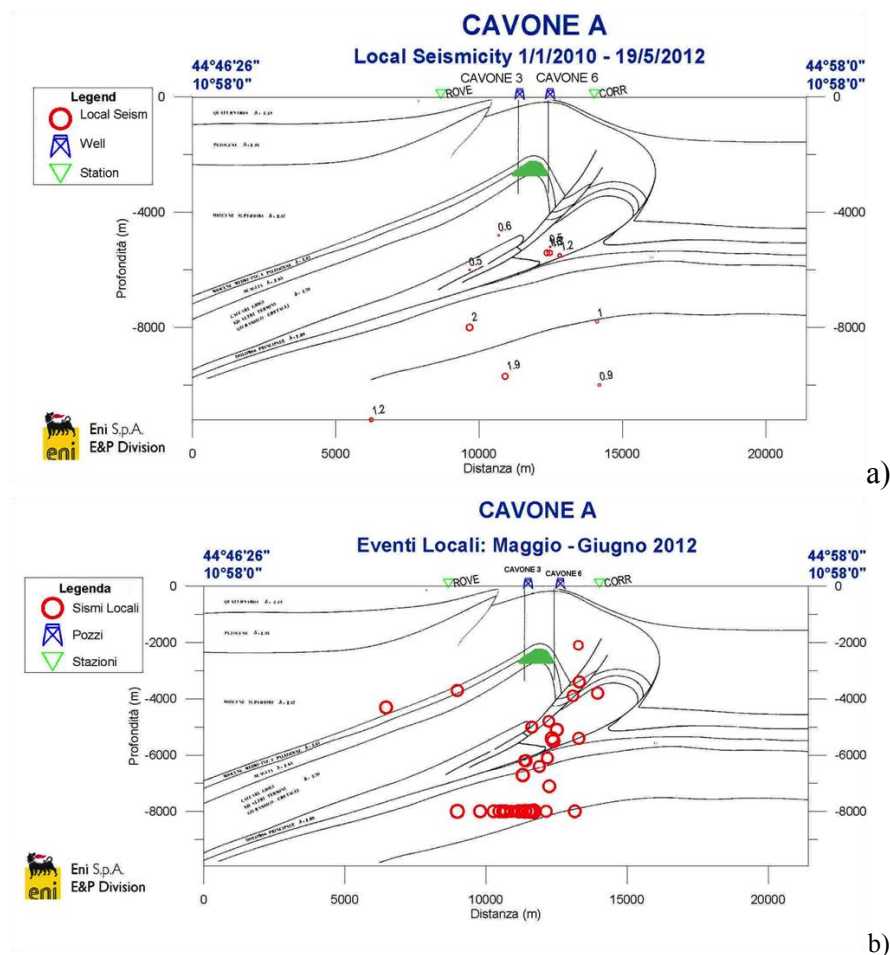


Figure IV.23 Hypocentral distribution of local events recorded by the network a) before May 20, 2012; b) after May 20012.

4. Casaglia

The local microseismic network at Casaglia is managed by the Department of Physics and Earth Science of the University of Ferrara. The data provided to the Commission (Appendix D) are the following:

- list of earthquake recorded from March 2010 to 16th September 2013;
- technical details of the local network.

The network consists of six permanent stations arranged as in **Figure IV.24**. The station “PON” is equipped with a three-component seismometer, while all the other have a vertical component seismometer. The network layout was designed in order to obtain the maximum precision, in recording earthquakes with epicenters inside or at least near to the network and to estimate the most significant parameters, namely magnitude and hypocenter depth.

The signal is sampled continuously through an A/D converter (16 bit), with an internal timer at a sampling frequency of 80 Hz. Digital data are modulated and transmitted via FM telemetry to a workstation, housed at the heat-exchange plant of HERA, the geothermal heating operator.

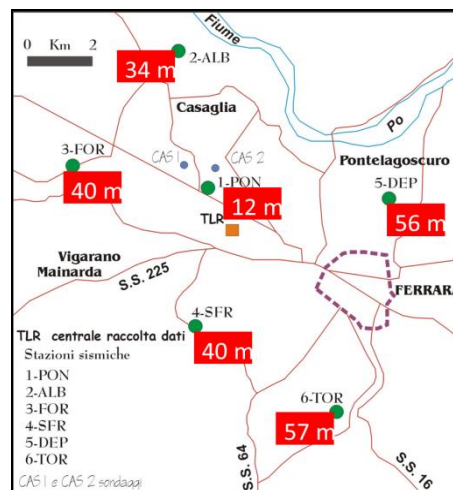


Figure IV.24 Casaglia microseismic network and station depth (in red).

Detailed information on the 69 earthquakes recorded by the network from March 2010 to September 2013 are reported in Appendix D. The 69 events, shown in **Figure IV.25** are characterized by magnitudes ranging from 0.5 to 5.8 and hypocentral depth ranging from 0.5 km to 34 km. The highest magnitude events are those belonging to the May-June 2012 sequence. For some events, data on hypocentral depth were derived from INGV or fixed at a default value because of the limited quality of the data.

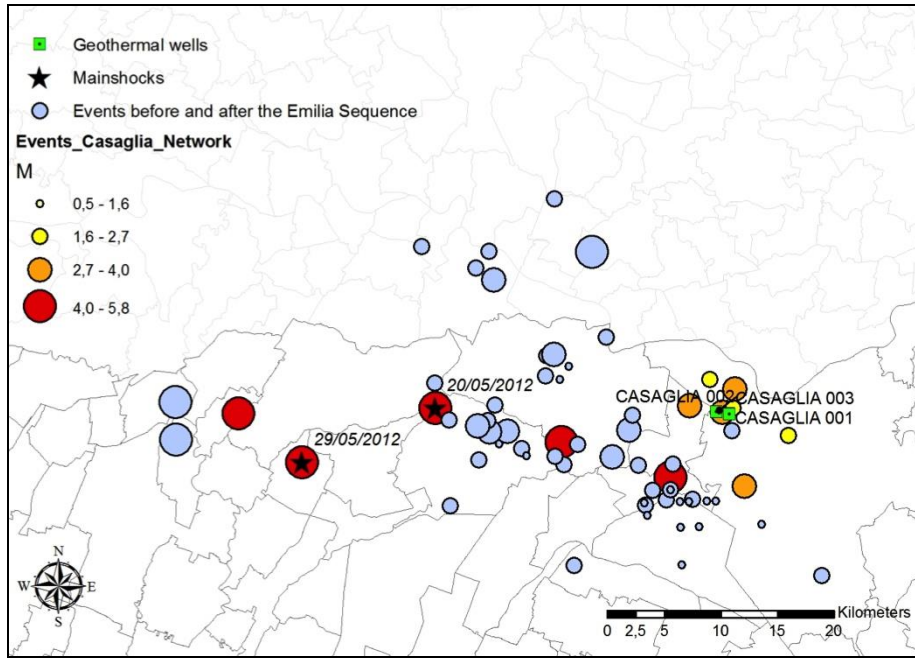


Figure IV.25 Distribution of events recorded by the Casaglia network from March 2010 to September 2013.

E. Production and injection data

1. Exploration and Production

The hydrocarbon fields of “CAVONE” and “SPILAMBERTO”, located in the ex - ENI exclusive mining zone (Law 136/1953)⁸, were assigned as exploitation licences named “MIRANDOLA” and “SPILAMBERTO” after the privatization of the company in 1995. Since 1980, Cavone has produced 2.79 Mtonnes of oil (19,551,000 barrels) and 73 MSm³ of gas (481,800 boe). The original recoverable reserves were estimated at 3.0 Mm³ from a total resource of 15 Mm³; the residual reserves in 2012 are about 0.16 Mm³ after recovery of 3.06 Mm³. Spilamberto has produced 3,779 MSm³ of gas⁹ (24,941,400 boe)¹⁰. Since 1996, “RECOVATO” has produced 355 MSm³ of gas¹¹(2,343,000 boe).

In 2012, there were 26 active wells in the three licences (listed in **Table IV.3**): 8 productive wells and 1 water reinjection well in “MIRANDOLA”; 13 gas productive wells in “SPILAMBERTO”; 4 gas productive wells in “RECOVATO”.

Table IV.3 Active wells in the three licences.

EXPLOITATION LICENCE	WELL NAME	DRILLING YEAR	DEPTH (m)	USE
MIRANDOLA	CAVONE 002	1978	4096	Production
MIRANDOLA	CAVONE 004	1978	3255	Production
MIRANDOLA	CAVONE 007 DIR	1980	3101	Production
MIRANDOLA	CAVONE 008 DIR	1980	3061	Production
MIRANDOLA	CAVONE 009	1980	3234	Production
MIRANDOLA	CAVONE 013	1984	3230	Production
MIRANDOLA	CAVONE 014	1985	3400	Reinjection
MIRANDOLA	CAVONE 017	1986	3310	Production
MIRANDOLA	SAN GIACOMO 1	1981	3700	Production
SPILAMBERTO	S.MARTINO 001	1987	1207	Production
SPILAMBERTO	S.MARTINO 002	1987	1008	Production
SPILAMBERTO	SPILAMBERTO 007	1958	1630	Production
SPILAMBERTO	SPILAMBERTO 008	1958	1512	Production
SPILAMBERTO	SPILAMBERTO 010	1958	1546	Production
SPILAMBERTO	SPILAMBERTO 016	1958	1364	Production
SPILAMBERTO	SPILAMBERTO 017	1959	1615	Production
SPILAMBERTO	SPILAMBERTO 019	1959	1350	Production
SPILAMBERTO	SPILAMBERTO 020	1959	1639	Production
SPILAMBERTO	SPILAMBERTO 021	1959	1710	Production
SPILAMBERTO	SPILAMBERTO 023	1959	1502	Production
SPILAMBERTO	SPILAMBERTO 026	1960	1545	Production
SPILAMBERTO	SPILAMBERTO 029	1960	1417	Production
RECOVATO	MUZZA 001 DIR A	2005	1792	Production
RECOVATO	MUZZA 003 X DIR A	2007	1813	Production
RECOVATO	MUZZA 004 DIR*	2002	1257	Production
RECOVATO	MUZZA 005 DIR	2011	1800	Production

⁸ Law for “Insitution of the Ente Nazionale Idrocarburi (E.N.I.)”.

⁹ Elaboration of historical production data available at the Ministry of Economic Development, Directorate General for Mineral and Energy Resources.

¹⁰ In Spilamberto field the production began in 1959 and 7,759.20 MSm³ were produced from 1959 to 1980.

¹¹ Elaboration of historical production data available at the Ministry of Economic Development, Directorate General for Mineral and Energy Resources.

MIRANDOLA

Since the beginning of its activity (1980), 22 wells have been drilled and 3 of them have been closed throughout past years. The total surface of the field is about 15 Km². The reservoir pressure at the discovery was 296 kg/cm² and it has remained stable during the whole life of field due to aquifer. The activity of the 22 wells from their drilling to 2010 is described in detail in **Table IV.4**.

Table IV.4 Activity of each well

Well name	Activity of each well
Cavone 1	Productive from March, 1986 to February, 1996
Cavone 2	Productive from March, 1980. The well didn't work for two times intervals: from January to August 1981 and from November 1998 to August 1999.
Cavone 3	Productive from April, 1986 to January, 1990 with discontinuous production.
Cavone 4	Productive from July, 1980 The well didn't work for many time intervals: in 1980/1981, 1984/1985 and 2000/2002
Cavone 5	The well was completed for water disposal because of its location in deep structural formations. The water injection started from March, 1994 until July, 1997
Cavone 6	The well was drilled to the North of the field, out of the structure. It was closed (there is no production)
Cavone 7	Productive from June, 1982 . The well didn't work for two time intervals: on 2003 and on 2005/2006
Cavone 8	Productive from June 1981. The well didn't work during many time intervals, the most important are: on 2002/2003 and on 2005/2007.
Cavone 9	Productive from December 1980.
Cavone 10	Productive from June, 1983 to September, 1993. The well didn't work during many time intervals, the most important was: on 1983/1986 and on 1990/1992.
Cavone 11	Productive from August, 1982 to June 1989. After it was closed for water disposal. The water injection started in March, 1994 and it ended in February, 1998.
Cavone 12	Productive from November, 1982 to October 1987. The well didn't work during long time intervals. The most important production period was from 1983 to 1985.
Cavone 13	Productive from July, 1984 to January, 2009. The well didn't work during many time intervals: on 1988 and on 2000/2002.
Cavone 14	Used for water disposal from January, 1993.
Cavone 15	Productive from June 1987 to April, 1995.
Cavone 16	Productive from October, 1987 to June, 2004. The well didn't work during the time interval 2000/2002.
Cavone 17	Productive from December, 1987.
Cavone 18	The well was drilled in the Western part of the structure. It resulted in water and for this reason it was abandoned. There is not production.
Cavone 19	Productive from September, 1987 to November, 1993.
Cavone 20	The well, drilled in the eastern part of the field, resulted in water due to the deep of the structure. It was abandoned. There is not production
Cavone 21	productive from August, 1988 to October, 1989.
S.Giacomo 1	Productive from June, 2005.

Figure IV.26 shows the oil, gas and water production from 1980 to 2012. In 1982 the yearly oil production reached a peak of 200,000 tonnes (1,372,770 barrels); then, due to the natural depletion of the field, the production gradually decreased to 30,623 tonnes (214,360 barrels) in 2012. A stable trend is observed in the period 2010-2012, (**Figure IV.27**), except for a decrease from November 2010 to April 2011 and two negative peaks in December 2011 and June 2012. From November 2010 to April 2011 the oil production decrease by about 12% respect the previous months (2,600 tonnes in October 2010; 2,300 tonnes in November 2010) and the water volume reinjected decrease by 22% (11,600 m³ in November

2010; 9,000 m³ in October 2010). In May 2011 the production and reinjection return to the November 2010 values.

In December 2011 the oil production decreased by 24 % compared to the previous month values (2,557 tonnes in November 2011; 1,932 tonnes in December 2011). In January 2012 the production returns to the previous data; than it goes upward to 3,338 tonnes in March 2012.

Finally, the production slows down until June 2012 when it reaches the lower rate of 1,863 tonnes.

These variation can be explained by analyzing the production of each well. In fact, “Cavone 13” and “Cavone 4” wells were not active at all in 2011. These two wells were put on stream on 10th February 2012 and then the production was stopped again on May 2012. At the same time the production of “S. Giacomo 1” well was also stopped. The negative peak of production, in May 2012, may be explained by the fact that all the producing wells were shut off after the second seismic event as a precautionary measure (data on production of each well can be found in Appendix D).

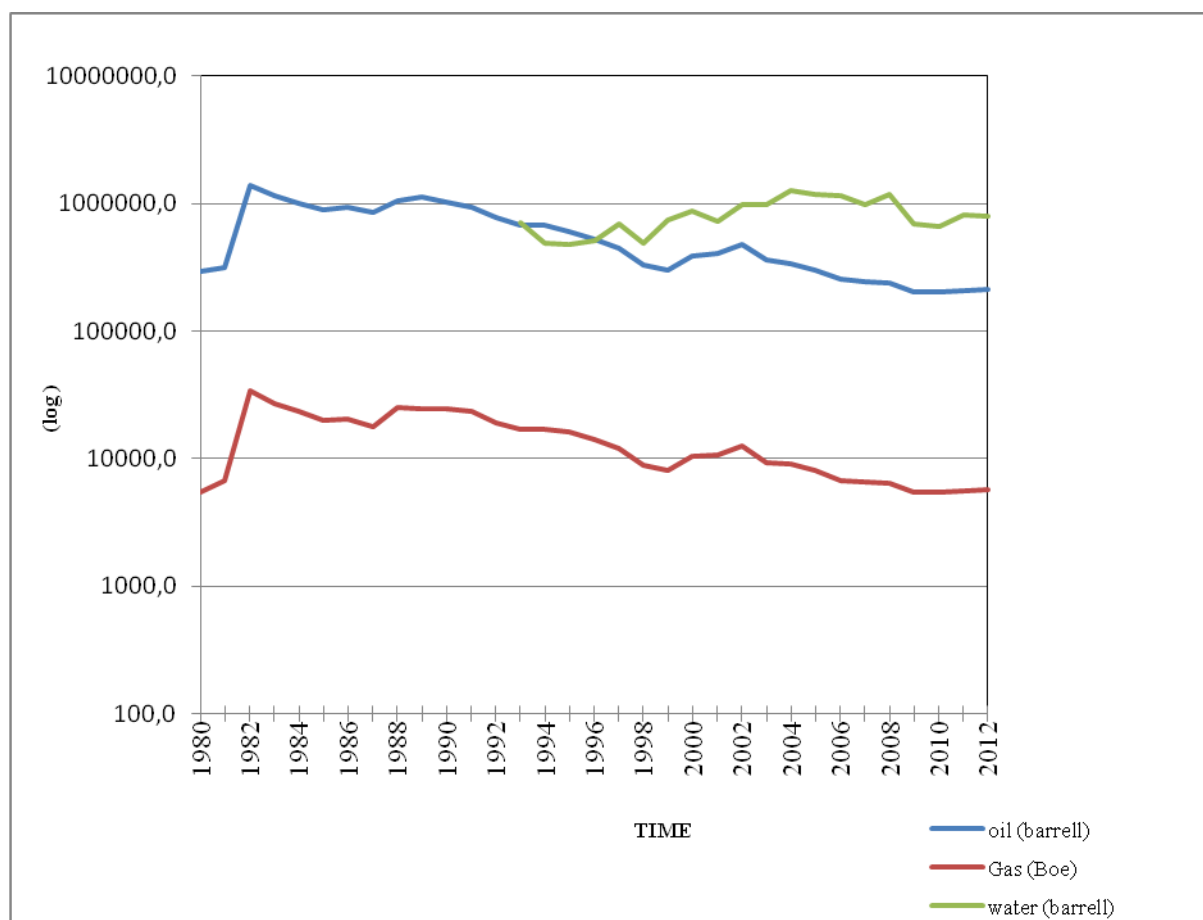


Figure IV.26 Oil, gas and water yearly production from 1980 to 2012 in the Cavone field.

The water reinjection activity associated with hydrocarbon production is authorized by the local competent authority (Provincia di Modena and Provincia di Ferrara as forseen by the Regional Law n.3/99 “*Delega autorizzativa alle province per il rilascio della autorizzazione allo scarico nelle unità geologiche profonde delle acque risultanti dall’estrazione di idrocarburi*”, and by the Regional Law 5/2006) that establishes the volume limit permitted to be reinjected for each licence. The volume of water reinjected in “Mirandola” authorized by the Municipality of Modena is 219,000 m³/year¹².

¹² Determina n° 775 del 20/08/2007 Provincia di Modena

The “Cavone 14” reinjection well, drilled in 1985, was completed to allow the disposal of the produced water, after the interpretation of injectivity tests performed in May-June 1985. The reinjection started in 1993 and the total volume reinjected from Cavone field and S.Giacomo reservoir is 2.85 Mm³.

Since 2005, Cavone 14 well receives the water produced by the S.Giacomo reservoir in addition to the water of the Cavone field. The total contribution of S.Giacomo reinjection water is 0.074 Mm³ (2,5% on total volume).

Water reinjection activities are commonly used in the oil industry practice to increase the capacity and/or recovery factor of the oil and, as in this case, to dispose of water linked to hydrocarbon production.

The water is reinjected into the geological producing formation and more precisely in the depth interval ranging from 3,302 – 3,367 m (MD- Measured Depth).

The choice of this particular interval was dictated by the consideration that it is located, certainly, below the water oil contact, estimated at approximately 3,100 m (TVD-True Vertical Depth).

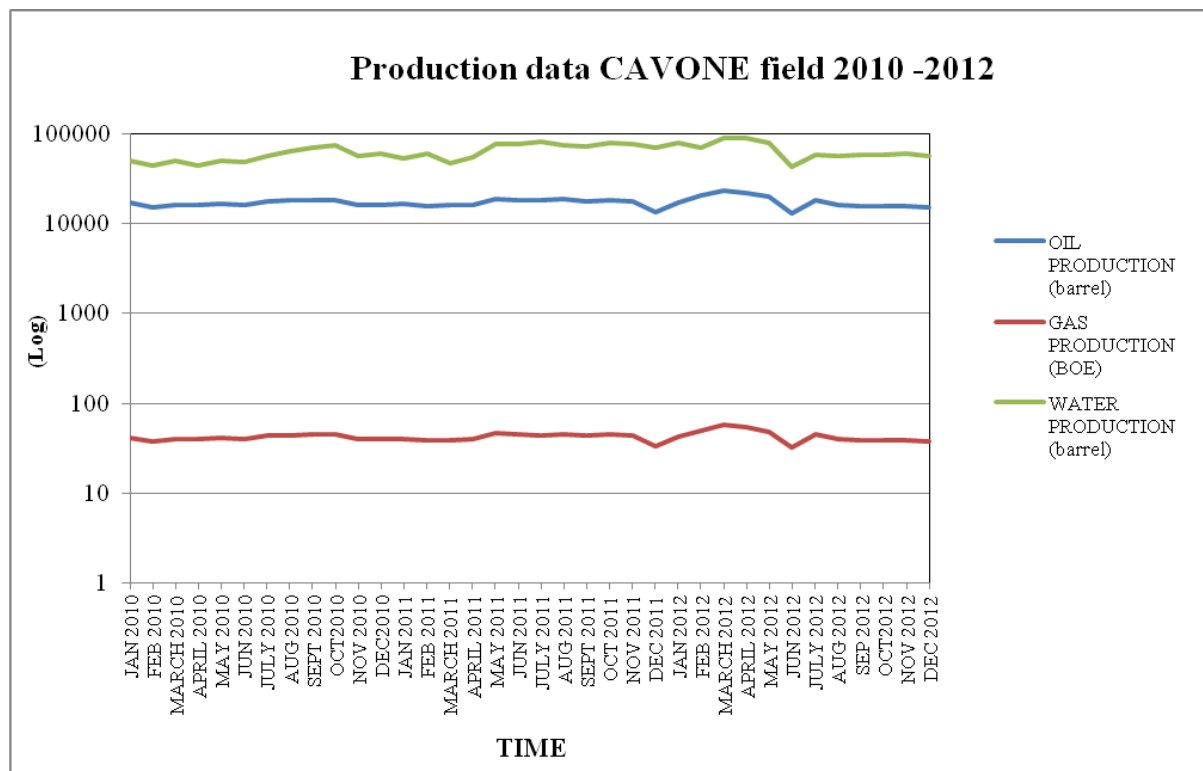


Figure IV.27 Oil, gas and water monthly production from 2010 to 2012 in the Cavone field.

The water injection activity is characterized by an alternation of 3 days of injection (on average) and 2 days off (on average) (data on water injection can be found in Appendix D). From 2010 to 2012 the total reinjection volume of water in “MIRANDOLA” was about 362,000 m³ (**Figure IV.28, Figure IV.29, Figure IV.30**).

The injection water volume is not directly measured but it is quantified on pump cycles. In fact the piston pump used for reinjection is a volumetric pump operated by an electric motor, working at fixed speed. The pump discharge is constant and equal to 25 m³/h (600 m³/day), while the water production rate is variable. A water storage system is thus necessary, and also a discontinuous reinjection cycle.

Hence injection water volumes are obtained by multiplying the working hours of the piston pump by its theoretical discharge 25 m³/h considering the volumetric efficiency of the pump (typically 96-98%).

Even if the water volume produced follows the hydrocarbon production, however it tends to increase at the end of the production life, as is common in hydrocarbon activity.



Figure IV.28 Yearly injection Volume 1993-2012 Cavone 14.

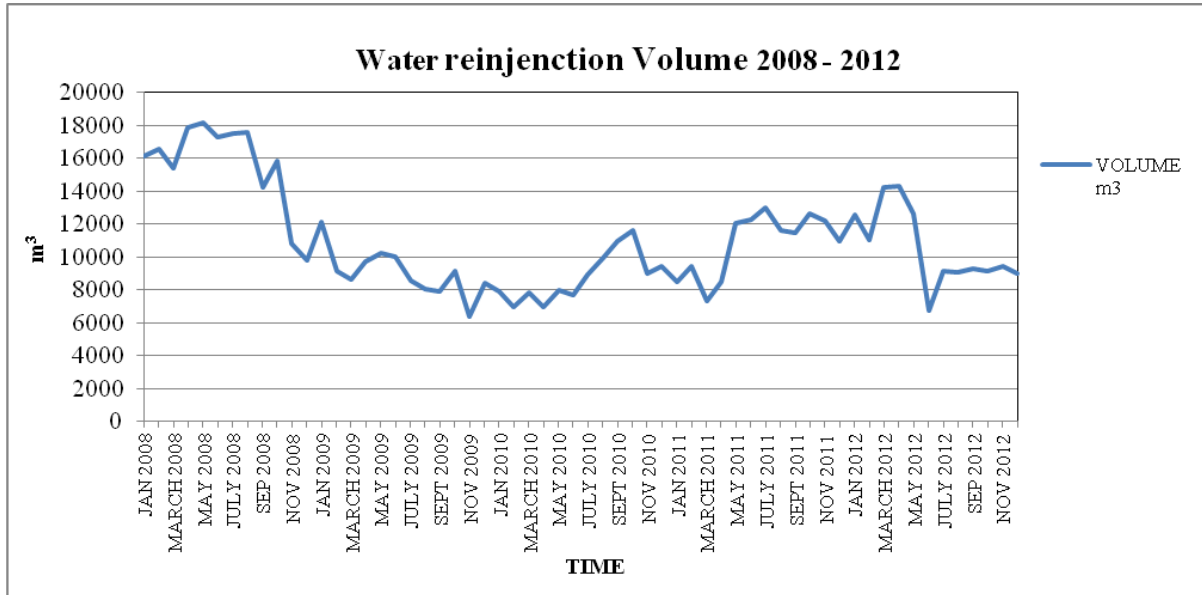


Figure IV.29 Monthly water injection volume 2008-2012.

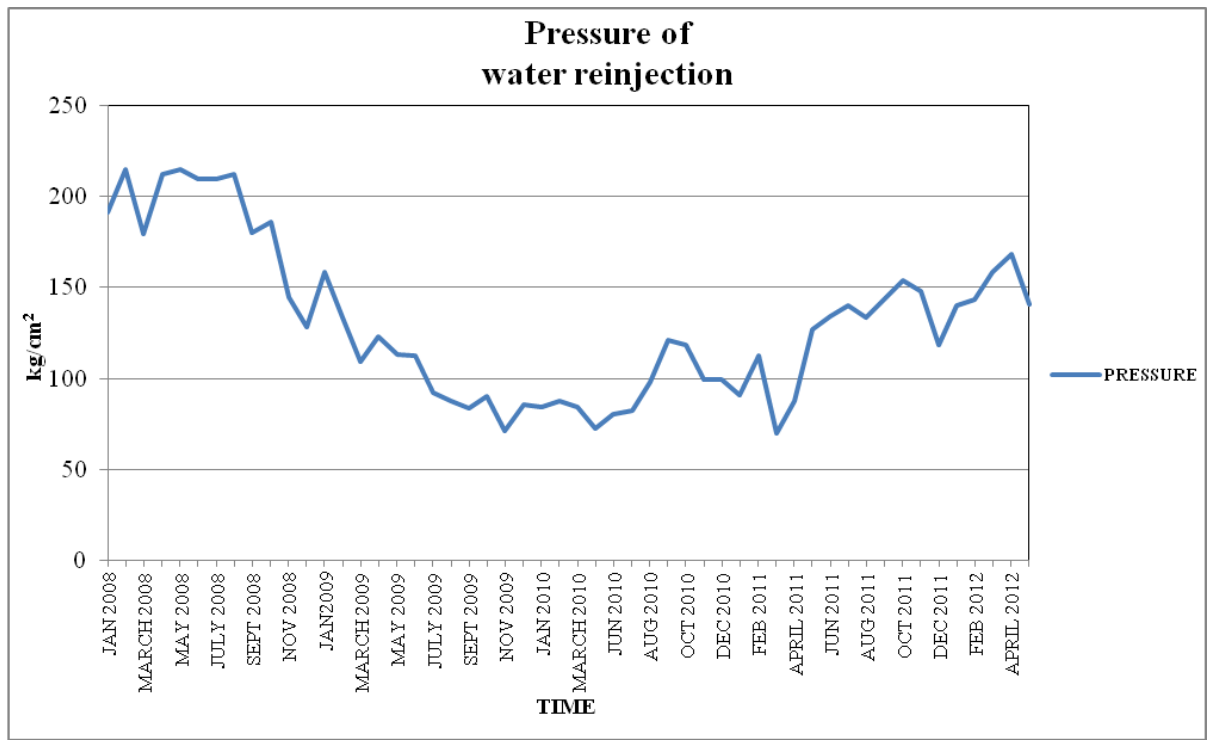


Figure IV.30 Pressure of water injection (Kg/cm²).

SPILAMBERTO

From 1980 to 2012 the yearly gas production of Spilamberto field was affected by two positive peaks (1983; 1991) followed by a decrease, probably due to the effect of the Oil and Gas crisis.

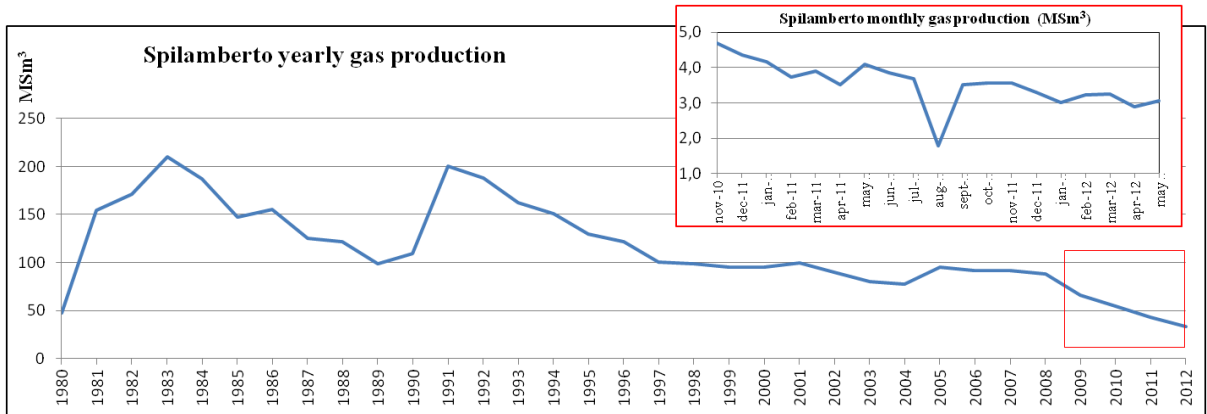


Figure IV.31 Spilamberto yearly gas production (from the beginning of its activity) with a particular of the monthly production from 2010 to 2012 (in the red rectangle).

The gas production of “SPILAMBERTO” was affected by a decrease from November 2010 to May 2012. This was due to the natural depletion of the field during the production lifetime. The decrease of about 2 MSm³ of production, between June and August 2011, was due to the shut off of three wells: “Spilamberto 23”, “Spilamberto 26” and “Spilamberto 29” wells. On September 2011 “Spilamberto 23” and “Spilamberto 29” wells were put on stream again while “Spilamberto 26” well did not resume until May 2012.

From 2010 to 2012 the total reinjection volume of water in “SPILAMBERTO” was 268 m³.¹³ The reinjection well “Spilamberto 09” in 2012 did not work and the reinjection water volume was zero from November 2011 to May 2012.

RECOVATO

From 1996 to 2012 the yearly gas production of Recovato had a constantly increasing trend.

The gas production of “Muzza” field was characterized by stable production from November 2010 until January 2012 when “Muzza 1” and “Muzza 3” wells stopped production. The increase from May 2012 was due to the new “Muzza 5” well coming on stream (Figure IV.32).

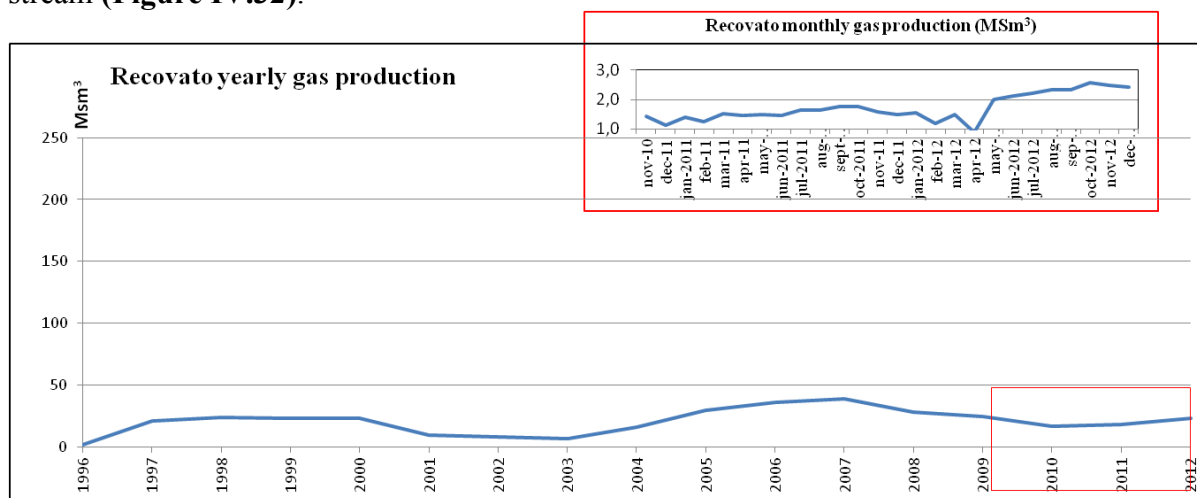


Figure IV.32 Recovato yearly gas production (from the beginning of its activity) with a particular of the monthly production from 2010 to 2012 (in the red rectangle).

2. Gas storage

The “Minerbio” storage field, discovered with the drilling of the “Minerbio 1” well, started production in 1959, managed by Agip. It consisted of 7 pools of which only one was productive; for this reason, in 1975, the C pool was converted to storage activity.

In 1998 the hydrocarbon exploitation licence was assigned to ENI (due to group restructuring) and one year later (1999) it was converted totally to storage activity. In 2002, the storage licence was transferred to Stogit.

In the “Minerbio” field 84 wells were drilled. 36 of them were drilled in the early years of hydrocarbon production (from 1959 to the ‘80s) while the others were drilled during the storage operations. In May, 2012 the number of active storage wells was 51 as listed in Table IV.5.

From 2010 through 2012 the total gas storage was 5,16 Msm³ and the total gas put in the national network was 5,47 Msm³.

¹³ Elaboration of historical production data available at the Ministry of Economic Development, Directorate General for Mineral and Energy Resources.

Table IV.5 Active wells in “Minerbio”

WELL NAME	DRILLING YEAR	DEPTH (m)	USE
MINERBIO 032	1963	1450	Development well
MINERBIO 034 DIR	1966	1461	Development well
MINERBIO 035	1967	1486	Development well
MINERBIO 037 DIR	1979	1265	Storage well
MINERBIO 038 DIR	1979	1267	Storage well
MINERBIO 039 DIR	1981	1234	Storage well
MINERBIO 040 DIR	1981	1236	Storage well
MINERBIO 041 DIR	1980	1235	Storage well
MINERBIO 042 DIR	1981	1247	Storage well
MINERBIO 043 DIR	1981	1249	Storage well
MINERBIO 044 DIR	1981	1260	Storage well
MINERBIO 045 DIR	1981	1254	Storage well
MINERBIO 046 DIR	1981	1271	Storage well
MINERBIO 047 DIR	1981	1294	Storage well
MINERBIO 048 DIR	1981	1270	Storage well
MINERBIO 049 DIR BIS	1981	1281	Storage well
MINERBIO 050 DIR	1981	1284	Storage well
MINERBIO 051 DIR	1981	1285	Storage well
MINERBIO 052 DIR	1981	1288	Storage well
MINERBIO 053 DIR	1981	1296	Storage well
MINERBIO 054 DIR	1982	1253	Storage well
MINERBIO 055 DIR	1982	1268	Storage well
MINERBIO 056 DIR	1982	1229	Storage well
MINERBIO 057 DIR	1982	1256	Storage well
MINERBIO 058 DIR	1982	1235	Storage well
MINERBIO 059	1982	1240	Storage well
MINERBIO 060 DIR	1982	1260	Storage well
MINERBIO 061 DIR	1982	1247	Storage well
MINERBIO 062 DIR	1982	1252	Storage well
MINERBIO 063 DIR	1982	1237	Storage well
MINERBIO 064 DIR	1982	1244	Storage well
MINERBIO 065 DIR	1982	1247	Storage well
MINERBIO 066 DIR	1982	1251	Storage well
MINERBIO 067 DIR	1982	1239	Storage well
MINERBIO 068 DIR	1982	1257	Storage well
MINERBIO 069 DIR	1982	1244	Storage well
MINERBIO 070 DIR	1982	1250	Storage well
MINERBIO 071 DIR	1982	1259	Storage well
MINERBIO 072 DIR	1982	1263	Storage well
MINERBIO 073 DIR	1982	1250	Storage well
MINERBIO 074 DIR	1982	1251	Storage well
MINERBIO 075 DIR	1983	1244	Storage well
MINERBIO 076 DIR	1983	1256	Storage well
MINERBIO 077 DIR	1990	1248	Storage well
MINERBIO 078 DIR	1990	1248	Storage well
MINERBIO 079 DIR	1990	1250	Storage well
MINERBIO 080 DIR	1990	1256	Storage well
MINERBIO 081 DIR	1990	1249	Storage well
MINERBIO 082 DIR	1990	1250	Storage well
MINERBIO 083 DIR	1990	1249	Storage well
MINERBIO 084 DIR	1990	1259	Storage well

3. Geothermal energy

The “FERRARA” geothermal licence was assigned to ENI in 1984. The licences (50% - 50%) are ERGA and eni-Geothermal Activity that is the operator.

The “FERRARA” geothermal licence covers an area of 31.72 km² and it consists of 2 production wells, “Casaglia 2” “Casaglia 3” and, 1 injection well, “Casaglia 1” (as listed in **Table IV.6**).

Table IV.6 Active wells in “Ferrara”

WELL NAME	USE	DRILLING YEAR	DEPTH (m)
CASAGLIA 1	Reinjection	1955	3799
CASAGLIA 2	Production	1981	1960
CASAGLIA 3	Production	1995	1950

The geothermal fluid is extracted by two pumps inside the “Casaglia 2” and “Casaglia 3” production wells. After the extraction, geothermal fluid is circulated through a heat exchanger and then it is filtered and reinjected inside the reinjection well “Casaglia 1” is located at a distance of 1 km from the two production wells. The water reinjection activity is authorized by the local competent authority which establishes the volume limit of 400 m³/h (3,5 Million m³/y) for “Casaglia”.

The plant started to work on 1995.

The annual production and reinjection volume in the field, from 1995 to 2012, are shown in the following figures (Appendix D) . From 2010 to 2012 the total volume reinjected in “Casaglia” field was about 6,818,805 m³.

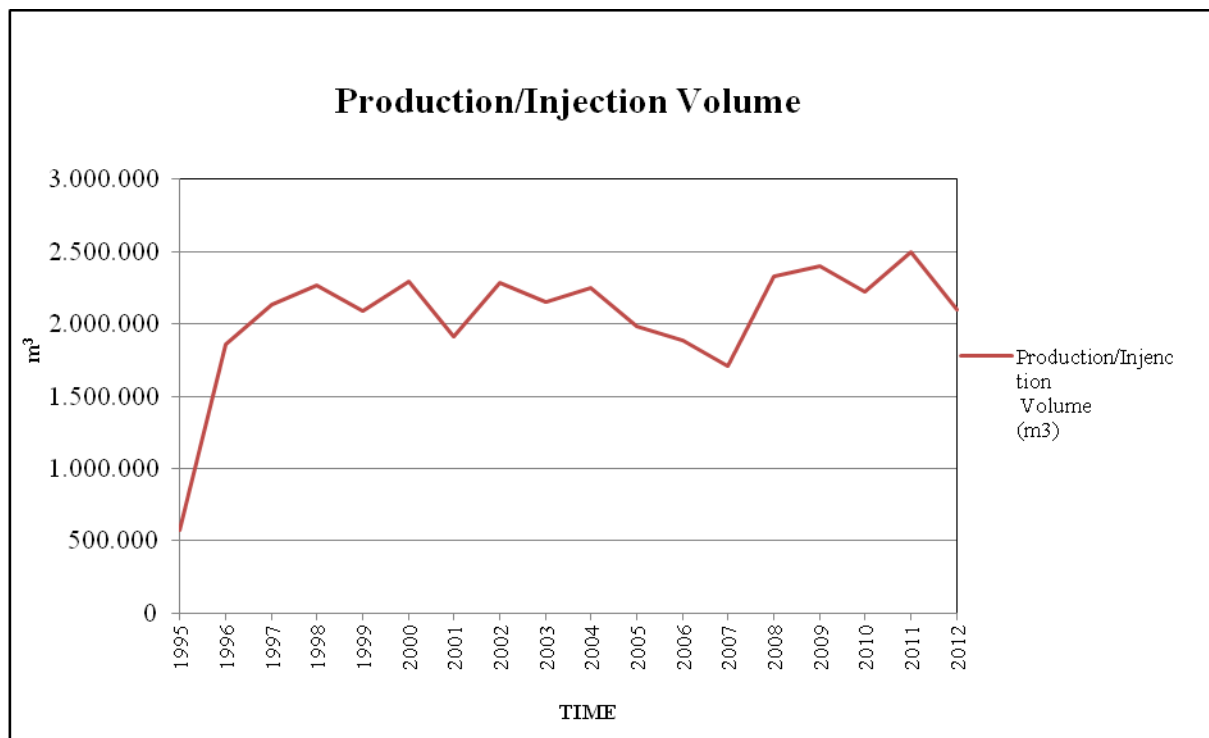


Figure IV.33 Production/Injection yearly volume of water in Casaglia field.

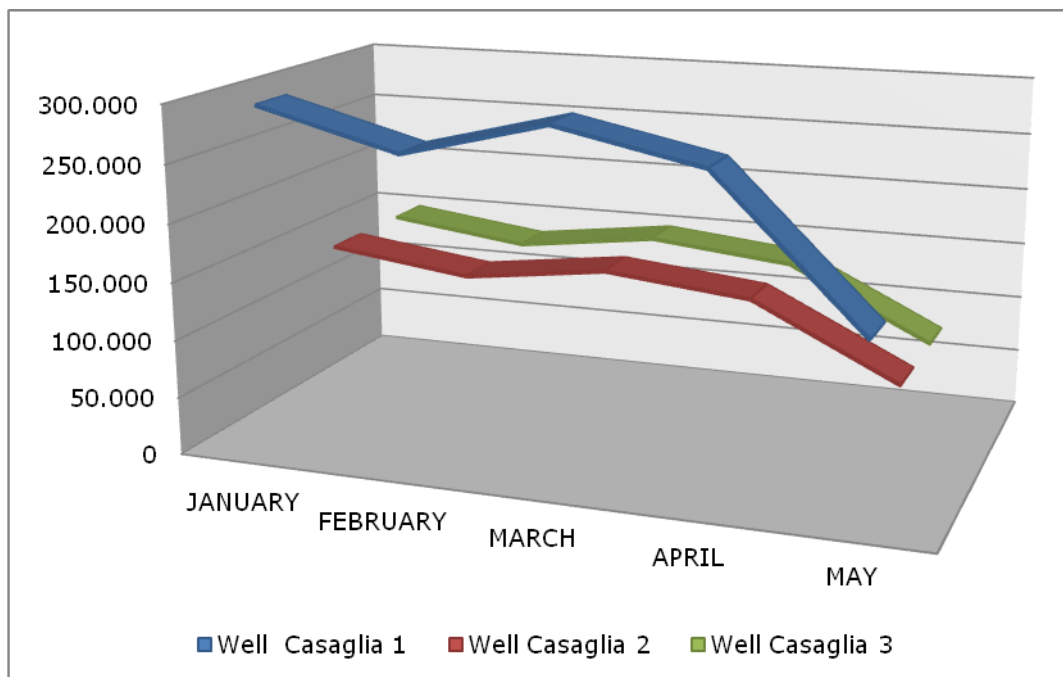


Figure IV.34 Production/Injection monthly volume of water in Casaglia field.

As mentioned before, the Municipality of Ferrara authorizes a maximum reinjection flow rate in “Casaglia 1” well of less than 400 m³/h¹⁴. The reinjection flow rate is equal to the total production volume of each well, “Casaglia 2” and “Casaglia 3” (less than 200 m³/h for each wells)¹⁵. The pump capacity in the production wells is a function of the amount of heat requested by Hera S.p.A.

The Production/Injection Volume from January to May 2012 are shown in **Table IV.7** for each well.

The pressure, from January 2012 to May 2012, was 13 kg/cm² for the production wells and 6 kg/cm² for reinjection well.

Table IV.7 Production/Injection Volume January- May 2012

	Well Casaglia 2	Well Casaglia 3	Well Casaglia 1
MONTH (year 2012)	PRODUCTION VOLUME (m ³)	PRODUCTION VOLUME (m ³)	INJECTION VOLUME (m ³)
JANUARY	148,434	148,434	296,868
FEBRUARY	132,382	132,382	264,764
MARCH	148,100	148,100	296,200
APRIL	135,250	135,250	270,500
MAY	74,025	74,025	148,050

¹⁴ P.G n°995/12 of 16/01/2012 Provincia di Ferrara

¹⁵ Data submitted by Eni

F. Reservoir

The hydrocarbon reservoirs of Minerbio, Recovato, Spilamberto and Mirandola, included in the studied area were operative during the May 12 seismic sequence. The main characteristics available for each reservoir are summarized in the following.

The available data concerning these reservoirs are reported in Appendix D and listed in Appendix C.

1. Minerbio

The gas underground storage field of Minerbio is located 35 km SE of Finale Emilia and 30 km S of Ferrara. The original gas-water contact depth lies at about 1500m. Data provided includes a 3D seismic survey, drilling and completion plan, well logs and profile from the well Minerbio 85 dir, daily volume and pressure for each single well and pressure measurement between 2010 and 2012. Microseisms recorded by the monitoring network, raw and processed data are provided, as well as recording stations characteristics and locations.

Subsidence monitoring data are also available for vertical and horizontal component, compared with storage activity.

2. Recovato

Recovato hydrocarbon concession lies 35 km S-SW of the town of Finale Emilia, covering an area of 36,75 km², where 4 wells are actively producing (Muzza 1 Dir A, Muzza 4 Dir A and Muzza 5 Dir). The field produces gas from layers located at a depth between 1150 m and 1760 m, characterized by good reservoir rock (porosity 25-30%). The operator states that only a small amount of associated water is produced, therefore no reinjection is performed. Monthly production history, production model, and reservoir parameters for all the 4 wells are available, plus detailed logs from well Muzza 5 Dir.

3. Spilamberto

Spilamberto concession is located 18 km SSE of Modena and 45 km S-SW of Finale Emilia, it spans over an area of 140km², oriented NW-SE. The wells reach depths up to 1800m. A reservoir study (static, geological and dynamic model) from 1999 based on a previous study of 1992 is available. At the time of the study the field was producing gas from 11 wells, in the 2 years preceding the Finale Emilia earthquake there were 17 wells in production. The associated water was reinjected in the well Spilamberto 9 until 2011. The 1999 reservoir study notes some inconsistencies between the field behavior and the expected behavior, based on the previous geological model. Cumulative production has been higher than the expected recoverable gas in place. The reservoir study describes the model history matching for the production history of each well.

Monthly production data and monthly pressure data for the months between November 2010 and May 2012 are available for the productive wells, while daily data for pressure and volume reinjected have been provided for the same period of time. Additionally, the production tests from the 17 producing wells are available.

4. Mirandola

The Mirandola concession spans over an area of 122 km² and is composed of two independent fields: the Cavone oil field and the San Giacomo oil field. Since this is the only field that can correlate hydraulically with the seismic events, it will be presented in more detail. The reservoir reaches depths of ca. 2900m, covering an area of ~18km². The two fields

lay one adjacent to the other, sharing the tectonic setting and they seem to be separated by a N-S sealing fault/system of faults. The Cavone oil field is divided in 5 blocks, an aquifer underlies the reservoir and interacts laterally with the field. In addition, vertical connectivity to the aquifer may act at some distance from the fault, in the central part of some of the blocks.

Reservoir properties (porosity and permeability) and extensive rock sample analysis have been measured on more than 1500 m of core recovered from the main expected productive layers. Other permeability values were derived from pressure history matching of a hydraulic model of the reservoir and measured field data. These permeability values of two layers are at least 2 orders of magnitude higher than the highest value obtained from fractured samples. In this model no account was taken of potential compaction-driven pressurization. Another explanation for the much higher model values is the existence of one or more high-conductive fault and/or fractures within the system.

MIRANDOLA: detailed information

The Cavone oil field produces from a Mesozoic carbonate reservoir at a depth of circa 2900m. The reservoir lies within an anticline displaced by reverse faulting, in a fold-fault system verging North, intersected by thrust faults oriented E-W.

The field is divided into 5 blocks (A to E), separated by a set of strike slip faults oriented N-S, plus the San Giacomo reservoir (block F). There are no indications of hydraulic connectivity of this latter reservoir with respect to the first 5 blocks. A hydraulic connection between the adjacent blocks (A to E) is possible. A lateral aquifer seems to be in hydrological connection with these blocks. An aquifer bounds the field to the west and under the reservoir, where it has been reached by different wells (18-01-10-05-19-09-15 and 14). The water-oil contact is 3130 m below sea level throughout the reservoir. Some wells have reached that depth, but have not encountered, the aquifer; instead oil bearing formation was present, especially in blocks C-D-E that are located at a shallower depth.

The San Giacomo field (one well drilled) (block F) does not seem to communicate with the Cavone field. The pressure response between producing Cavone wells and San Giacomo well could not be measured reliably, the original oil water contact depth is 3056m and reservoir initial pressures are different. Therefore it is hypothesised that the 2 reservoirs are independent.

The original static pressure of the reservoir was 296 kg/cm² to 2990 m depth, in the Cavone -1 well (BRECCE formation). Not all the faults are expected to be seals and the evidence for that is the pressure response between wells due to production and the relative increase in water production. The source of water is assumed to be due to vertical flow through the faults, from the underlying aquifer to the oil-bearing layers. The productive formations are the deeper "Calcari grigi di Noriglio", comprising the layers Oolitico, Nor-A, Marker and Nor-B, and the shallower "Brecce di Cavone", present only in the western part and composed of a porous layer (Packstone s.s.) and a tight layer (Brecce S.s.). The formation "Marne del Cerro" acts as cap rock, as low horizontal and low vertical permeabilities have been measured from samples,

In the following figures, we can see the spatial distribution of the block and of the drilled wells (**Figure IV.35**) and the field configuration (**Figure IV.36**) where the wells can be seen, ordered from west to east and producing units can be identified (water content in parenthesis).

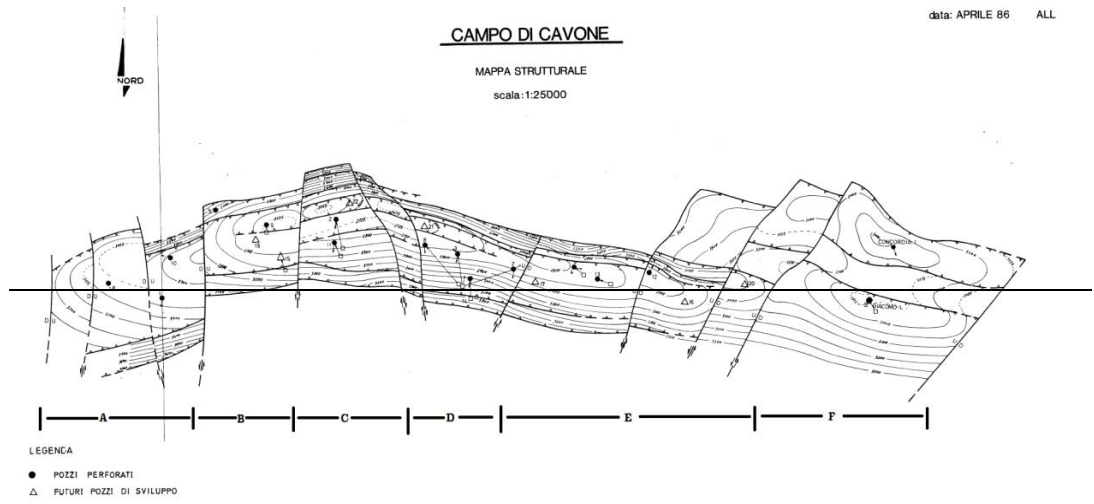


Figure IV.35 Structural map (modified from Fig. 1 report AGIP 1986, Appendix D). The field extends roughly 12 km longitudinally and 1.5 km (average length of the blocks) in direction N-S.

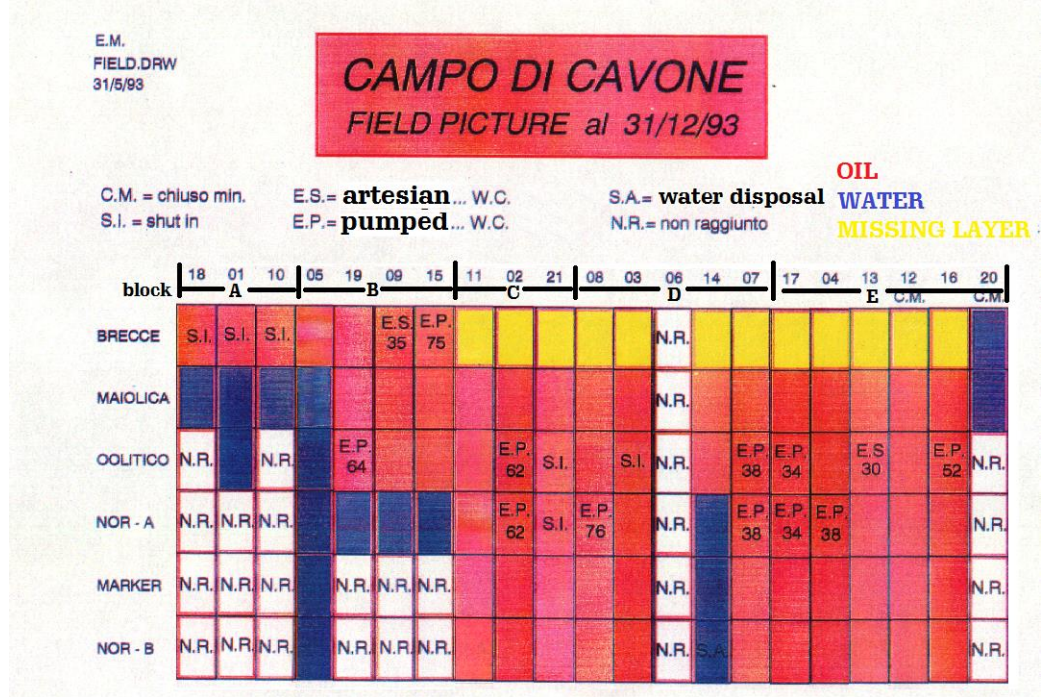


Figure IV.36 Field picture, wells re-ordered west to east (well 6 drilled out of reservoir), (modified from Fig. 4 report AGIP 1994, Appendix D).

It is interesting to note that same layer may lie at different depth according to which block they belong to, therefore, it is assumed that their physical properties are similar but their fluid content is different. As an example, the Oolitic layer can be found at a depth of 3500m in well 1, belonging to block A, while in the wells 21-8-3, located in block B, the same layer can be found at a depth of ~2800m, being respectively water and oil bearing. With respect to this, it is important to stress that the faults oriented E-W, generated during the compressive tectonic phase will be associated with horizontal fracture generation (maximum stress horizontal N-S, minimum stress vertical), enhancing communication among wells completed in the same layer or immediately above/below, while the tensile regime is associated with vertical fractures (the vertical stress is the highest). **Figure IV.37** shows the two different settings. The current tectonic regime in the area is compressive, the aquifer seems to act mainly laterally, from the West gradually diffusing to the East, while the tensile

faults (oriented N-S) should put the deeper aquifer in communication with the productive layers.

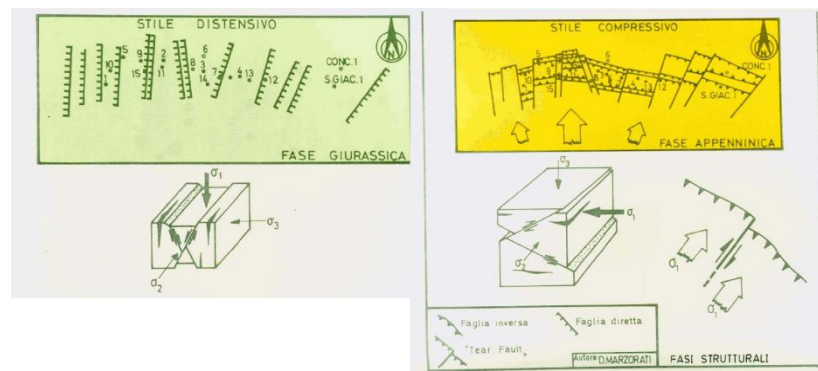


Figure IV.37 Tectonic setting and fracture generation (modified from Fig. 8 report AGIP 1986).

A total of 240 cores has been collected from the different wells, for a total length of 1543.3 meters. Routine analyses have been performed (porosity, permeability, density) and for some of the oil bearing layers water/oil relative permeability, static pressure effect on porosity, capillary pressure curves plus triaxial compression testing were made. Values for primary porosity are corrected taking into account confining stress (lab measurement). A detailed discussion about the origin of the fracture has been carried out for the layers OOLITICO; NOR-A, MARKER, NOR-B, finding tectonic and intrinsic reasons for different behaviour of the different layers and to evaluate micro- or macro-fracturing of the units. Data from this analysis are from petrographic logs from wells 2-3-7-11-12-13-14 and from triaxial compression measurements performed in the lab.

The results must be upscaled correctly to compare the permeability values from samples to reservoir.

- OOLITIC and NOR-B presents intense micro-fracturing, while macro-fracturing is usually higher in NOR-A (more plastic behavior due to clay content);
- Micro and macro-fractures tends to be closed with depth, increased tangential stress load from the rock and stronger aquifer interaction;
- Macro-fractures in NOR-A are more frequent (6 fractures/meter) in the northern flank of the field, becoming more sparse gradually going south (2 fractures/meter);
- Macro-fractures in NOR-B and OOLITIC are more frequent (3-4 fractures/meter) in the hinge zone, disappearing to the south flank, where porosity for the OOLITIC units as well disappears due to diagenetic effects and/or for different textures;
- Micro-fractures are more frequent on the north flank, disappears in the south flank, and are always open in the hinge zone (although less dense).

The measured permeability (k) and porosity (ϕ) are summarized in **Table IV.8**, the model permeability values are given when they differ from those measured in the samples:

Table IV.8 Summary of porosity (ϕ) and permeability (k) values. The numeric k is necessary to get a good history matching based on ~1 year of production data from different wells for the model proposed in the report (see chapter 7).

LAYER	Primary ϕ	Primary k	Sec. ϕ	Sec. k	Numeric k	notes
BRECCE	0.09	10 mD (horizontal and vertical)	----	----		
MAIOLICA	<0.02	<1 mD	0.005			Values registered for 80% of 840 samples
OOLITICO	0.09	100 mD (vertical > horizontal)	Only in the transition between blocks		17600 mD	Samples from well 13. Interaction water and formation
NOR-A	[95%]<0.04 [5%] 0.05	[95%] fractured [5%] 5 mD	0.05 "moldic"	0.2 - 300 mD	4400 mD	Reservoir "water-wet"
MARKER	0.005 - 0.01	0.1 - 0.2 mD	0.01 -0.02	0.1 - 100 mD		Fractured close to frontal or back thrust faults
NOR-B	[95%]<0.04 [5%] 0.05	[95%] fractured [5%] 5 mD	0.05 "moldic"	0.2 - 300 mD		Reservoir "oil-wet"

The fracturing trends analyzed earlier support the suggestion of the high permeability values from numerical model matching. The values of transmissivity (obtained by Horner analysis) and extrapolated permeability calculated from production test of some of the wells can be found in **Table IV.9**. When multiple intervals are tested at the same time, the permeability cannot be clearly assigned to each layer. Variation of the transmissivity value in the order of Darcy*m are recorded for the same interval at different times in well 7. Values may have been influenced by acid stimulation treatment or other activities performed on the wells.

The permeability values for the OOLITIC formation obtained from this evaluation are still much lower than the values of the numerical model, although they are higher than those obtained from the rock sample analysis.

Reservoir pressure measurement are available for some of the wells, with at least a couple of values per year, for the years between 1978 and 1985 in the AGIP 1986 report (Appendix D).

Table IV.9 Transmissivity and extrapolated permeability (associated with the depth interval being tested, in parenthesis), obtained from different wells in different intervals. Min-max value in parenthesis when obtained from multiple layer testing.

WELL & Date		MAIOLICA	OOLITICO	NOR-A	NOR-B
2 20.4.78	Trans (mD*m)			23100	
	Depth tested (m)		2723.9-2744.0	2744.0-2764.7	3086.1-3123.9
	Permeability (mD)			293.9 mD	
2 25.5.78	Trans (mD*m)				359
	Depth tested				2983.6-3001.5
	Permeability				20 mD
2 2.9.78 10.9.78	Trans (mD*m)			3760	6615
	Depth tested			2792.6-2802.5	2948.8-2954.8
	Permeability			379.8 mD	1102.5 mD
2 18.3.80	Trans (mD*m)		72500		
	Depth tested		2730.9-2758.7	2792.6-2802.5 2873.2-2884.1	
	Permeability			1491.8 mD	

2 28.3.80	Trans (mD*m)		72680	
	Depth tested		2730.9-2758.7	2792.6-2802.5 2873.2-2884.1
	Permeability		1495.5 mD	
3 13.10.78	Trans (mD*m)	204000		
	Depth tested	2822.3-2835.2	2835.2-2860.0	2860.0-2863.8
	Permeability	4915.6 mD		
3 4.7.80	Trans (mD*m)		13015	
	Depth tested		2971.7-2977.6 2982.6-2992.5 3010.3-3015.2	
	Permeability		628.7 mD	
3 16.11.80	Trans (mD*m)			1036
	Depth tested			3056.0-3066.8 3075.6-3088.2
	Permeability			44.3 mD
3 20.3.83	Trans (mD*m)			1169
	Depth tested			3056.0-3066.8 3075.6-3088.2
	Permeability			49.9 mD
7 5.6.82	Trans (mD*m)		13936	
	Depth tested		2842.0-2844.3	2844.3-2849.2 2888.2-2895.4 2902.6-2913.5 2930.0-2938.6
	Permeability		411.1 mD	
7 1.4.83	Trans (mD*m)		20600	
	Depth tested		2842.0-2844.3	2844.3-2849.2 2888.2-2895.4 2902.6-2913.5 2930.0-2938.6
	Permeability		607.7 mD	
8 7.7.82	Trans (mD*m)			240
	Depth tested			2921.4-2941.6
	Permeability			11.9 mD
8 23.7.82	Trans (mD*m)			330
	Depth tested			2921.4-2942.8 2971.8-2977.6 2982.0-2987.7
	Permeability			10 mD
11 1.6.81	Trans (mD*m)	11558		
	Depth tested	2907.7-2931.6		
	Permeability	483.6 mD		
11 15.9.82	Trans (mD*m)		1120	
	Depth tested		2897.4-2908.6	
	Permeability		121.7 mD	
13 5.6.84	Trans (mD*m)			46
	Depth tested			3002.2-3017.2
	Permeability			3 mD
13	Trans (mD*m)		21000	

23.6.84	Depth tested		2851.9-2859.9		
	Permeability		2625 mD		
MIN-MAX PERMEABILITY		483-(4915)mD	(293.9)-2625 mD	121.7-628.7 mD	3-1102.5 mD

However, rather poor information about the geomechanical behavior of the reservoir and surrounding rock is given in the report: apparently, no mechanical properties of the cap rock and of the overburden have been considered or investigated.

The measured elastic properties of the reservoir rock is the "energia potenziale elastica", units Kg/cm² which can be converted to Pa, however the derived value is of kPa order of magnitude, so it does not seem to represent Young's modulus or any elastic properties. Other AGI/TEPE reports can provide details of the mechanical testing. Using this, compressibility (Cf) ranges from 0,255 GPa⁻¹ to 6,25 GPa⁻¹. The MARKER layer provide vertical sealing between NOR-B and NOR-A. The aquifer push from the bottom seems to be stronger for the well in the central part of the field, farther from the faults.

Geochemical analysis on the fluids shows some unexplainable results (Sulphur content is always higher in the NOR-B oil than in OOLITIC and NOR-A) and water salinity is higher (<45 gr/L vs 29 gr/L) for wells closer to the fault (this may be due to communication with the upper SCAGLIA CALCAREA formation, lying above the MARNE DEL CERRO cap rock). Evaluating the density of oil after some production time shows how all the levels apart from the NOR-B tends to produce lighter oil with time. This is consistent with the OOLITIC layer being the source of the oil and with the NOR-B being vertically separated from the other layers.

In **Table IV.10** the porosity for each layer and the wells producing from each block are shown. From production tests, it is possible to obtain a model of well communication as follows:

- NOR-A and OOLITIC layers behave differently than the NOR-B layer. The difference is smaller where the main faults are present (wells 7-4-13-12);
- where the MARKER layer is more intact, wells completed in the NOR-B layer presents pressure much higher than NOR-A and close to initial field pressure (wells 8-3-14-13, well 13 was in communication also with other wells)
- wells 7-13 (OOLITIC) and 4 (NOR-A fractured) are hydraulically communicating, with fast increase of pressure to a value close to the well 12 pressure (NOR-B) ;
- wells 9 (MALM + DOGGER fractured) and 2 (OOLITIC) show the same pressure, with recovery this value increases much slower;
- there is interference among all the wells in the OOLITIC (2-7-13);
- there is interference between 7-13 (OOLITIC and) and 4 (NOR-A fractured), 12 (NOR-B) which is not producing.

Table IV.10 GBV and NBV are respectively Gross Bulk Volume and Net Bulk Volume, OOIP is Oil Originally In Place.

C A V O N E

BLOCCHI	FORMAZIONI o LIVELLI	Ø %	S % _w	G.B.V. ₆ m ³ x10 ⁶	N.B.V. ₆ m ³ x10 ⁶	O.O.I.P. ₆ x f.ne Sm ³ x10 ⁶	O.O.I.P. ₆ x blocco Sm ³ x10 ⁶	O.O.I.P. %	WELLS
A	BRECCE	9.0	35.0	----	44.0	2.83	2.83	18.2	18 - 10 1
B	BRECCE	7.0	35.0	----	16.0	0.80			5 - 9 19 - 15
	OOLITICO	5.5	25.0	----	6.0	0.27			
	NOR-A poroso	5.0	25.0	141.62	8.64	0.35	2.12	13.6	
	NOR-A fratturato	0.5	0.0	141.62	89.5	0.49			
	NOR-B poroso	5.0	25.0	22.34	3.71	0.15			
	NOR-B fratturato	0.5	0.0	22.34	12.13	0.06			
C	OOLITICO	5.5	25.0	----	9.4	0.42			2 - 11 21
	NOR-A poroso	5.0	25.0	251.4	17.6	0.72			
	NOR-A fratturato	0.5	0.0	251.4	152.35	0.84	3.49	22.4	
	NOR-B poroso	5.0	25.0	264.06	21.12	0.87			
	NOR-B fratturato	0.5	0.0	264.06	117.11	0.64			
D	OOLITICO	5.5	25.0	----	6.87	0.31			8 - 3 14 - 7
	NOR-A poroso	5.0	25.0	170.93	14.52	0.59			
	NOR-A fratturato	0.5	0.0	170.93	80.51	0.44	2.75	17.7	
	NOR-B poroso	5.0	25.0	136.72	23.78	0.98			
	NOR-B fratturato	0.5	0.0	136.72	79.43	0.43			
E	OOLITICO	9.0	25.0	----	22.93	1.70			17 - 4 13 - 12 16 - 20
	NOR-A poroso	5.0	25.0	277.50	36.79	1.51			
	NOR-A fratturato	0.5	0.0	277.50	123.76	0.68	4.38	28.1	
	NOR-B poroso	5.0	25.0	100.00	7.5	0.31			
	NOR-B fratturato	0.5	0.0	100.00	32.8	0.18			
T O T A L E							15.57	100	
S . G I A C O M O									
F	OOLITICO	5.5	25.0	----	1.0	0.04			
	NOR-A poroso	5.0	25.0	19.53	0.51	0.02			
	NOR-A fratturato	0.5	0.0	19.53	3.30	0.02	0.08		
	NOR-B poroso	5.0	25.0	----	----	----			
	NOR-B fratturato	0.5	0.0	----	----	----			
T O T A L E C A V O N E E S . G I A C O M O							15.65		

G. Other

Additional data has been requested to attempt to understand the dynamic behavior regarding pressure and subsidence due to human activities. In particular, for the Cavone field, new data were requested regarding well interference and behavior of block F in order to integrate the information available in AGIP reports of 1986 and 1994 (Appendix D). Società Padana Energia offered to perform a month-long interference test, with bottom pressure readings in the injection well; however the amount of additional new data that could have been collected were of limited interest, because some of the wells are technically inaccessible in order to host the bottom hole pressure recorders.

To evaluate if relevant changes in stresses were taking place in the underground due to human activities, subsidence data were requested .

1. Subsidence

Available data regarding subsidence for the study area are:

(i) Isokinetic lines for the time window 2006-2011 from the Regional Agency for Prevention and Environment of Emilia Romagna region (*Agenzia Regionale per la Prevenzione e l'Ambiente*, ARPA, <http://www.arpa.emr.it/>), **Figure IV.38**

(ii) Subsidence/uplift measurements of the activities in the Minerbio storage field provided by Stogit (Appendix D).

(iii) Subsidence recording from 3 GPS station located close to the Cavone reservoir and a levelling survey performed in 2006 and repeated in 2008 provided by ENI (Appendix D).

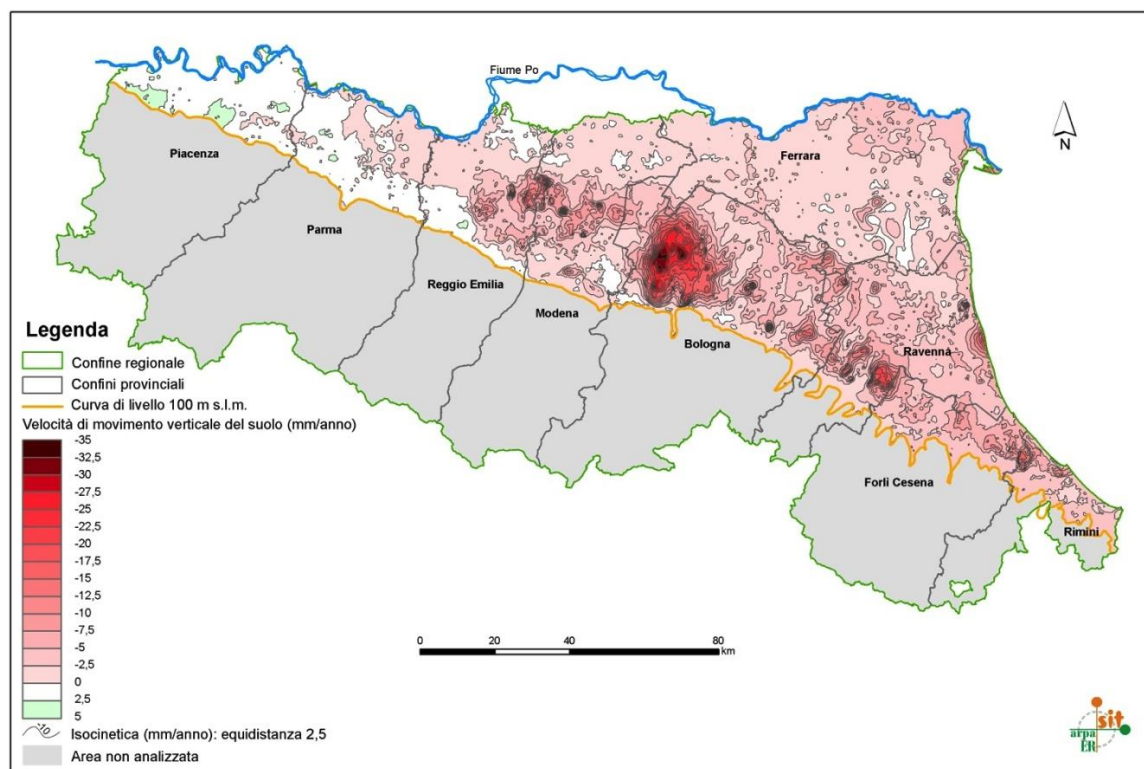


Figure IV.38 Subsidence rate map for the time window 2006-2011 provided by ARPA, <http://www.arpa.emr.it/>.

(i)

As shown in **Figure IV.39**, subsidence rates for the area are minimal. In particular:

- Mirandola : <2.5 mm/year
- Spilamberto: <10 mm/year
- Rivara:<2.5 mm/year
- Recovato: <2.5 mm/year
- Minerbio: <7.5 mm/year
- Ferrara: <2.5 mm/year

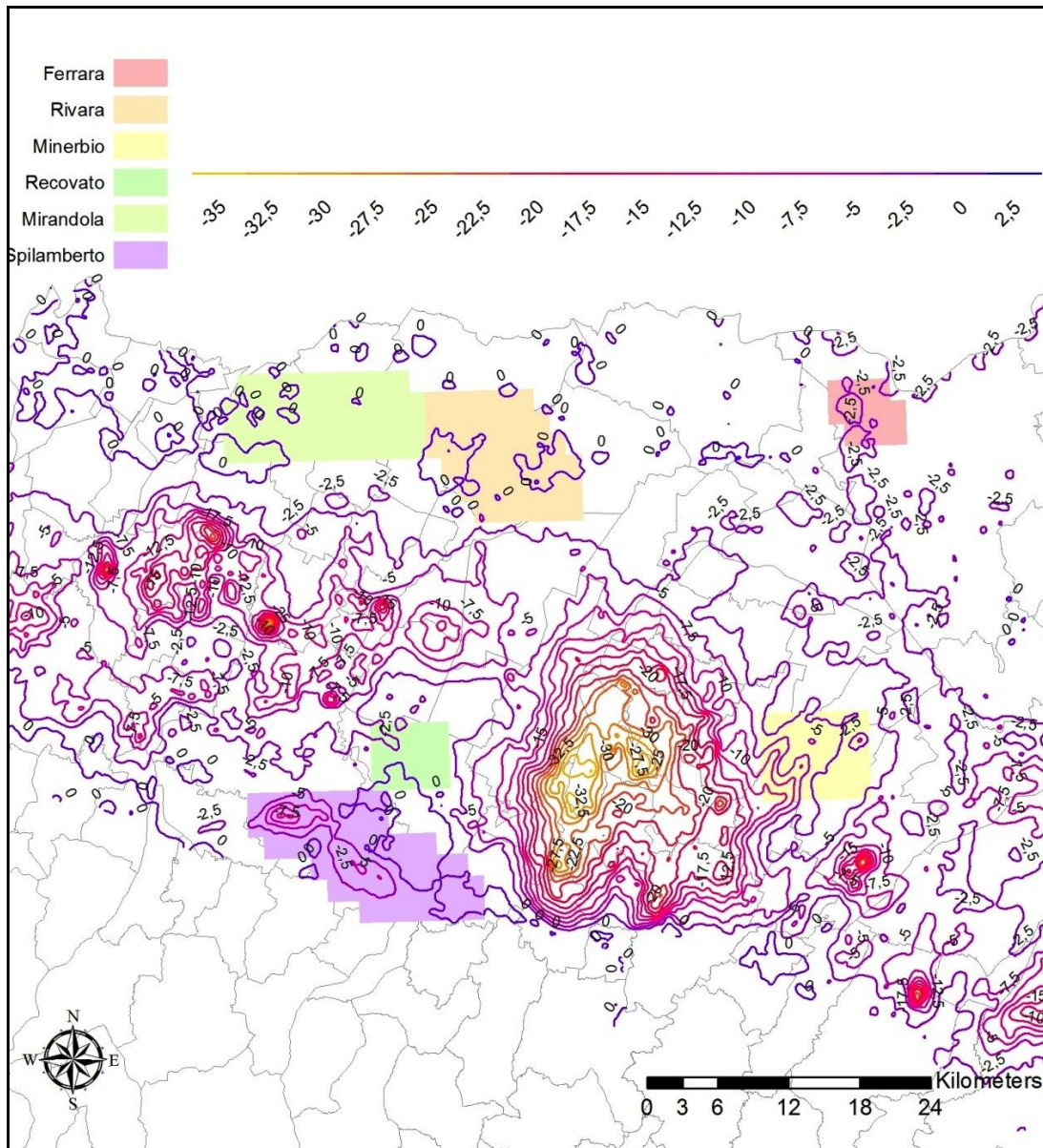


Figure IV.39 Subsidence rate map and licences in the study area.

(ii)

The interferometric analysis in the field of Minerbio performed by Stogit for the period October 2003 - November 2012 shows a slight negative trend (-0.46 mm / year) of the area occupied by the field. CGPS System (Continuous Global Positioning System) data acquisition (December 2008 - December 2012) recorded slightly higher altimetric values of -

1, 7 mm/y. In any case results of subsidence monitoring in Minerbio field do not appear to show significant anomalous behaviour.

(iii)

The leveling survey provided by ENI was performed in the vicinity of the well SG1 and it is very accurate (orders of magnitude higher than what can be achieved from satellite or GPS) (see **Figure IV.40**). Unfortunately the data were of limited use, since the measurements performed in 2008 could not be absolutely referred to the same reference point as the measurements performed in 2006. The correction of the data would have been a very extended procedure and not possible in the time frame within which the commission was operating.

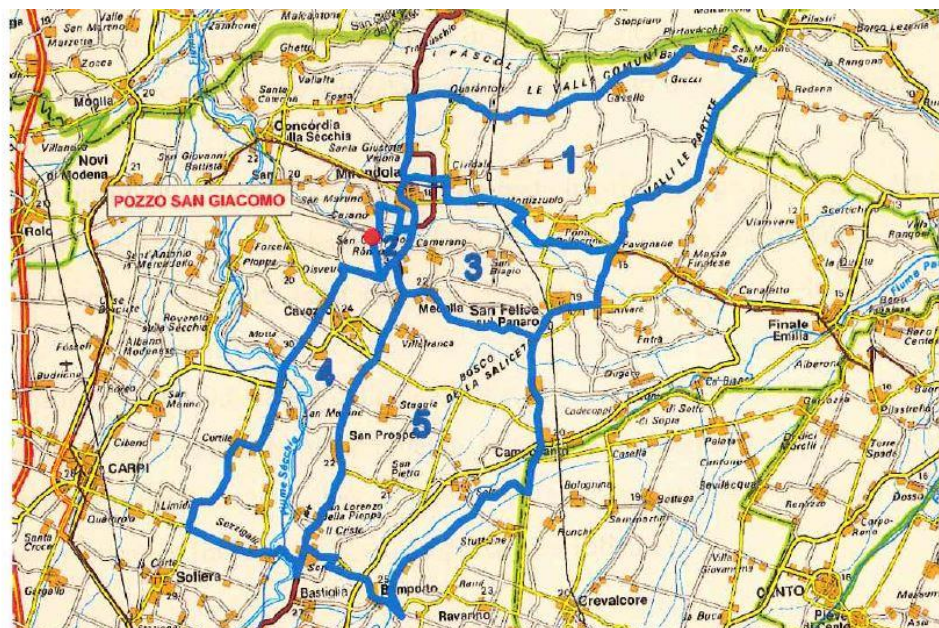


Figure IV.40 San Giacomo survey network (provided by ENI).

Generally, the subsidence data does not show significant difference from the expected natural rate of subsidence in the Po Valley.

V. Answer to the first question

In this section, after a brief description of the “RIVARA-STORAGE” project and of the documents provided by the company *Independent Gas Management srl* and by the Ministry of Economic Development, we provide the answer to question 1) of the Decree no. 5930 December 11, 2012 of the Head of the Department of Civil Protection of the Presidency of the Council of Ministers [*Is it possible that the seismic crisis in Emilia has been triggered by the recent researches at the Rivara site, particularly in the case of invasive research activities, such as deep drilling, fluids injections, etc.*]

A. The “RIVARA-STORAGE” project

On July 1st, 2002 the company *Independent Gas Management srl* submitted a request for the granting of a storage licence in a deep aquifer, named “RIVARA-STORAGE”. The project had proposed natural gas storage in a fractured limestone formation occupied by water. The project, would have represented the first initiative of “aquifer storage” in Italy, where natural gas was stored underground using depleted gas reservoirs.

On September 8, 2006, the company submitted to the Ministry of Environmental and Protection of Land and Sea (MATTM) the request of environmental compatibility, pursuant to Article 21 of the Legislative Decree no. 152/2006.

On August 3, 2007, the Environmental Impact Assessment (EIA) Technical Committee expressed a negative interlocutory judgment to the *Independent Gas Management project*. Several supplementary documents were therefore submitted by the company, which had meanwhile made a joint venture with *ERG Power & Gas* establishing the company *ERG Rivara Storage srl*.

On February 17, 2012, the MATTM issued the EIA Decree n.32, expressing the positive assessment of environmental compatibility with prescriptions, limited to the storage program assessment at the feasibility stage, pursuant to Article 3, paragraph 7 of the Ministerial Decree January 21 2011, despite the negative opinions expressed by Emilia Region, on August 1, 2007 and 8 February, 2010.

On February 29, 2012, the company updated the application for the grant, dated 2002, by delivering to the Ministry of Economic Development (MISE), the request for the authorization to carry out the research program under the aforementioned Article 3, paragraph 7.

On March 27, 2012, the MISE requested the agreement of the Emilia Region for the authorization but the Region again refused the aforementioned request of agreement by the resolution no. 512 on April 23, 2012.

Pursuant to the current legislation, the refusal of the Emilia Region represented an impediment to the successful conclusion of the authorization procedure for the research phase. Therefore on August 6, 2012 the MISE rejected the request of the research program.

On July 2, 2012, *ERG Rivara Storage srl* lodged a formal request to the Regional Administrative Court of the Emilia Region to annul the aforementioned resolution no. 512.

On November 2012, *ERG Power & Gas* left the joint venture and the company returned to be managed completely by *Independent Gas Management srl*.

The Ministry of Economic Development, due to the impossibility of assessing the feasibility of the storage program (mandatory aspect for the granting of the storage project), also rejected the application for natural gas storage program “RIVARA-STORAGE” by the Directorial Decree dated April 3, 2013.

B. Review of the available documentation

1. Description of the available data

Following the request of the Commission, on 25 June, 2012, *Independent Gas Management srl* provided all the technical data and scientific reports related to the design of the natural gas storage of Rivara. These data are completely reported in the Appendix D. In particular the company presented to the Commission the following documents:

- Rivara Project reports: summary, chronology and presentations.
- Technical data and reports: subsurface study, subsidence assessment report, report for EIA, physical model, analysis of seismic data, physical data of the aquifer, description of the microseismicity network project, seismic profiles, stress-strain state of reservoir, reservoir simulation, paleogeographic and paleotectonic study, geochemical study, geomechanics parameters and a 3D reservoir geomechanics study, risk assessment study.
- Master's Thesis on Rivara (by local residents).
- Others: technical standards and regulations on Underground Gas Storage (UGS) in aquifer risk assessment studies of UGS, scientific papers, worldwide UGS statistics.

In addition, on June 19, 2013 the MISE presented an official statement (Appendix D) providing a declaration in which it is officially stated that, with respect to the Rivara storage project, the Ministry has not authorized any kind of mining activity (“*[.] it is evident that this Administration has not authorized any mining activity in the area related to the Rivara storage project*”) and that no mining activities were carried out in the past 30 years (“*[.] The central and the territorial offices of the Ministry have no evidence of mining activities carried out in the past 30 years and that the last well drilled in the area has been the “Bignardi 1 DIR” in 1981, but with complete shutoff of well in June 1982*”). The Ministry also provided the Commission with a complete report on the Rivara permit procedure.

2. Answer to the question

After a critical review of the available information provided by the Company, no contradictions were found of the statement that no kinds of mining activities have been performed at the Rivara site in the recent years.

The answer to the first question is therefore: NO.

VI. How the Commission addressed question two

In this section, the approach used to answer to the question 2) of the Decree [*Is it possible that the Emilia seismic crisis has been triggered by activities for the exploitation and utilization of reservoirs carried out in recent times in the close neighbourhood of the seismic sequence of 2012?*] is provided.

After reviewing the extensive literature on the issues and evaluating the available data for the area of interest as reported in Chapter 2-4, the Commission has decided to focus its attention on the exploitation licence of “MIRANDOLA” and the geothermal field of “FERRARA”.

Both are very close to the location of the May 2012 seismic sequence; the Cavone fields, belonging to the Mirandola licence, are about 20 km west of the main shock of May 20, and close to the events exceeding 5 M_L of May 29 and June 3. Two other large shocks, exceeding 5 M_L , which occurred on May 20, were displaced towards the Casaglia geothermal field, which is about 20 km North-East of the May 20 main shock epicentre. Moreover extraction and deep waste water injection activities (to a depth of about 3 km) have been continuous for several years in Mirandola and re-injection has been performed at Ferrara for geothermal purposes.

The Minerbio field is a gas storage reservoir; Recovato and Spilamberto are gas production fields. Although extraction activity has been continuous at Cavone, Recovato and Spilamberto up to and including the onset of the sequence of earthquake in May 2012, the Cavone 14 well was the only site carrying out continuous waste-water injection before and during the 2012 seismicity. In fact, from November 2011 to May 2012 the “Spilamberto 09” reinjection well was not operative.

Moreover, whereas the Cavone reservoir is located within Mesozoic carbonatic formations and may be connected to underlying thrust faults, the other reservoirs are in Plio-Pleistocene formations above some impervious units; consequently the connection with seismogenic structures is highly unlikely.

Minerbio

Structural framework

This occupies the western portion of the Selva tectonic structure, an anticline emerging from a wide structural depression located south of the Consandolo-Monestirolo tectonic structure. Minerbio is located in the hangingwall of a thrust separating the Consandolo-Monestirolo anticline from the Selva and Budrioanticlines (see **Figure VI.1**). Note that the Consandolo-Monestirolo anticline links westwards with the Cavone-Rivara anticline.

Drilled stratigraphic succession

Plio-Pleistocene terrigenous deposits. The deepest borehole, the Minerbio 24 well, stopped in lower Pliocene sands and clays, at a depth of 2357 metres, without reaching the Miocene part of the stratigraphic succession.

Storage reservoir

Plio-Pleistocene sands at a depth of 1000-1500 metres.

Possible influence on the seismogenic structure(s)

The seismogenic structures lie at depths greater than the depth of the Consandolo-Monestirolo reservoir. The Minerbio reservoir for gas storage is composed of Plio-Pleistocene deposits that are separated from the Consandolo-Monestirolo carbonate reservoir

by at least one impermeable interval consisting of the middle Eocene-lower/middle Miocene marly deposits of the Consandolo-Monestirolo stratigraphic sequence. This shaly interval forms a barrier that makes any direct hydraulic connection with the seismogenic structure(s) unlikely.

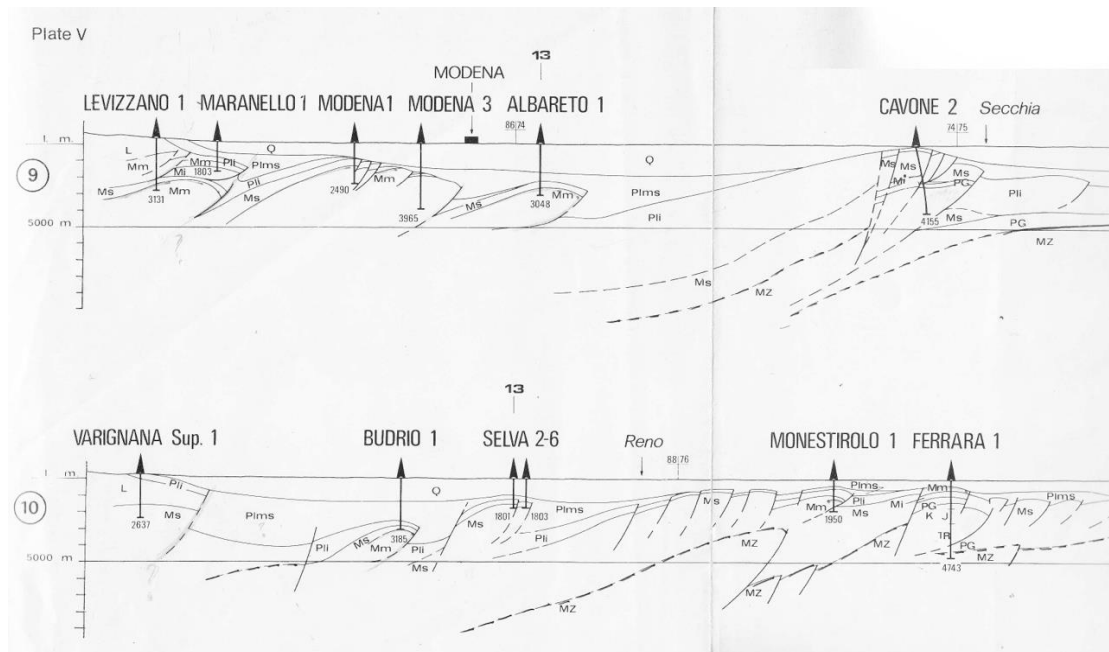


Figure VI.1 Structural framework from [140].

Recovato (Muzza)

Structural framework

This is the Castelfranco Emilia-Albareto structure, an anticline located SW of the Selva structure, in the hangingwall of the Cavone-Rivara anticline (see **Figure VI.1**).

Drilled stratigraphic succession

Plio-Pleistocene terrigenous deposits (sands and clays). The deepest borehole (Muzza 2, total depth 2103 m) reached the upper Messinian Fusignano Formation. The latter is unconformably overlain at the depth 2013 m by Plio-Pleistocene sands and clays.

Gas reservoir

Plio-Pleistocene sands; gas production at a depth of 1300-1500 metres.

Possible influence on the seismogenic structure(s)

The seismic sources lie at depths greater than the depth of the Cavone-Rivara reservoir. The Muzza gas reservoir is separated from the Cavone-Rivara reservoir by at least one impermeable interval corresponding to the middle Eocene-lower/middle Miocene marly deposits of the Cavone-Rivara stratigraphic sequence. This shaly interval forms a barrier that makes direct hydraulic connection with the seismogenic structure(s) unlikely.

Spilamberto

Structural framework

The Modena structure, is an anticline located in the hangingwall of the Castelfranco Emilia-Albareto structure and in the footwall of the Apennine nappe front (see **Figure VI.1**).

Drilled stratigraphic succession

The Spilamberto 2 well (Total Depth 2420 m) reached sands and conglomerates referred to the upper Miocene Cortemaggiore Formation. The latter is unconformably overlain at a depth of 1330 metres by Plio-Pleistocene terrigenous deposits.

Gas reservoir and re-injection

Upper Miocene sands and subordinate conglomerates of the Cortemaggiore Formation at a depth of 1150-1400 metres.

Possible influence on the seismogenic structure(s)

The seismic sources lie at depths greater than the depth of the Cavone-Rivara reservoir. The Spilamberto gas field lies in the hangingwall of the Castelfranco Emilia-Albareto structure and the latter is separated from the Cavone-Rivara reservoir by at least one impermeable interval corresponding to the middle Eocene-lower/middle Miocene marly deposits of the Cavone-Rivara stratigraphic sequence. This shaly interval forms a barrier that makes any direct hydraulic connection with the seismogenic structure(s) unlikely.

A. Methodology

Although at present it is not possible to discriminate unequivocally between induced, triggered and natural tectonic earthquakes, the possible interactions between seismicity and production has been analyzed in order to evaluate the possibility that the Emilia seismic crisis has been triggered by activities in the field of Mirandola and Casaglia.

By considering the production activity of the two fields in the context of the complex structural framework and prior seismicity, it seems unlikely that the Emilia sequence was completely induced, i.e. the stress changes which have been generated by the activities for the exploitation and reservoir utilization and geothermal production are not sufficient to create new failures in previously unfaulted rock. Consequently the Commission focused on the possibility that the main shocks of May 20 and 29 and the following sequence were triggered, i.e. that human activity may have contributed to the tectonic stress already existing on the fault system.

In order to have a homogeneous picture of the characteristics of seismic activity of the geological information and on the operations of extraction and injection of fluids, the Commission decided to re-process the most significant available data.

1. Analysis performed by the Commission

Starting from available data and studies from literature summarized in the previous chapters, the activity of the Commission was focused on:

Structural framework and seismological analysis:

- *Reevaluation of the main available reflection seismology and well logging data to check the tectonic model of the area and to build a 3D velocity model to be used for the re-location of seismic activity (section 7.A).*

The use of a 3D model is required by the strong asymmetry of the shallow geological structures along on N-S direction.

- *Relocation and recalculation of the focal parameters and Coulomb stress transfer using the developed 3D model (section 7.B)*

Static stress transfer within the crust is a physical process through which a sufficiently large earthquake can induce/trigger other earthquakes on nearby favorably oriented seismogenic structures. Therefore the changes in the Coulomb failure function (CFF) of each main event of the Emilia sequence have been estimated in order to evaluate whether they have contributed to bring the faults of the May 29/June 3 events closer to failure.

Analysis of the Mirandola field:

- *To check the available physical model of the reservoir of Mirandola (section 7.C)*

The oil and gas field in Cavone is the closest to the May 2012 sequence focal area, at distances comparable with other cases of triggered seismicity due to fluid injection and/or fluid production, although the net produced volumes in Mirandola are much lower than in other known cases (less than two or three orders of magnitude compared to the volume of Lacq and Groningen¹⁶). However, the injected waste-water volumes at $2.6 \times 10^6 \text{ m}^3$ are comparable and in fact exceed some cases in the US where triggered/induced seismicity has been shown to occur, as shown in **Figure VI.2**.

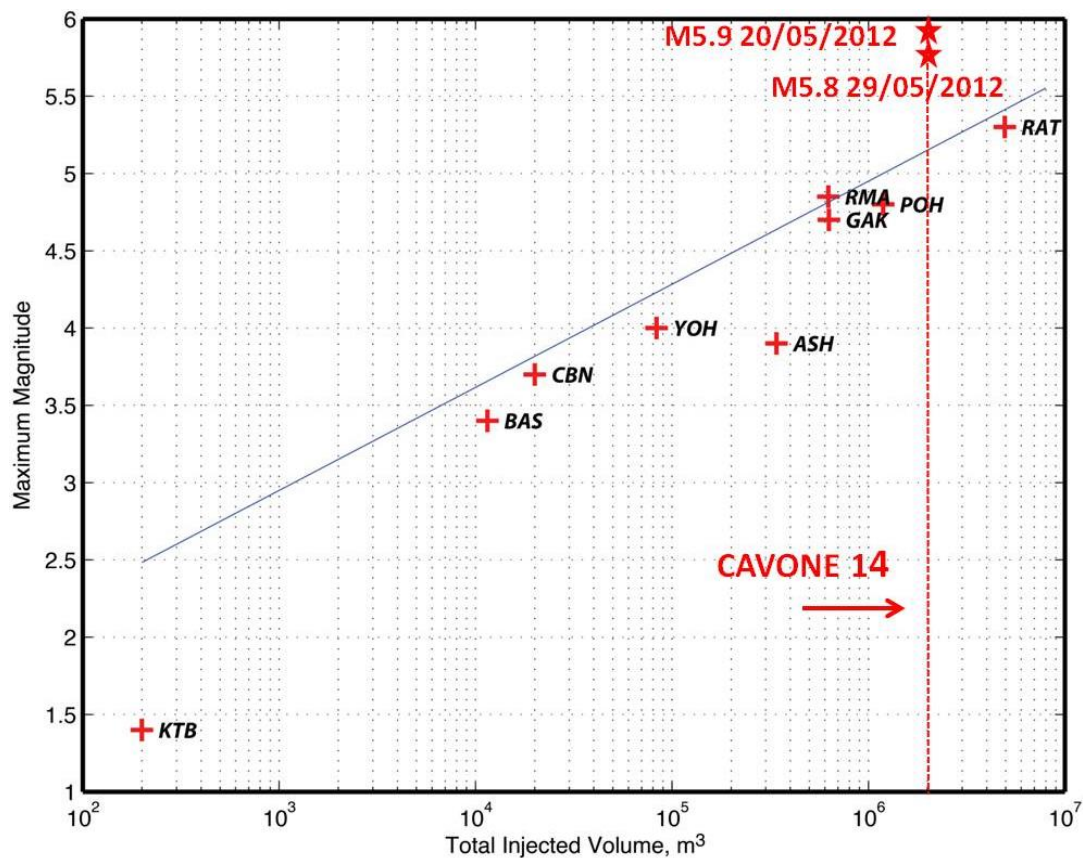


Figure VI.2 Maximum Magnitude plotted against total injected volume for a number of injection sites [40] and for the Cavone field.

¹⁶ About 3 Mm^3 have been extracted from Cavone field; 780 Mm^3 from Lacq and $6,300 \text{ Mm}^3$ from Groningen (at the Pressure and Temperature of the fields).

Although the current state of knowledge does not allow to make exact forecast, both dynamic and a static analysis are necessary to determine if spatial and temporal correlation between field operations and observed seismicity can be backed by one or more physical processes. Reservoir pressure and production may be sustained by compaction or driven by an aquifer, subsidence may be induced by change in pore pressure or in temperature, the change in shear and normal stress acting on faults may be due to diffusing overpressure or by induced deformation in the rock mass.

It is not uncommon or unexpected to observe delay or time- and rate-dependent response to re-injection or production of fluids in/from the reservoir and in the surrounding rock formations.

To understand the processes involved, how the perturbation in stress and strain induced by fluid production or injection are acting on the rock mass, which at the very end can be observed in different processes such as subsidence, reservoir compaction, permeability reduction, various sources and types of data are needed.

In the case studies presented fluid injection and reservoir depletion have been associated with triggered seismicity, however the causes of processes depending on them (for example subsidence and variation in injection pressure) and through which they reactivate the fault may be different. Both fluid injection and pore pressure decrease are taking place in Cavone reservoir (with depletion happening in a single compartment), it is then worthwhile to investigate both aspects

Due to the local compressional tectonic setting, reservoir depletion may induce stress changes large enough to trigger earthquakes, hastening the natural seismic cycle. Although the regional subsidence in the area is very low (less than 1 mm per year), the lack of local reliable dynamic data (subsidence or horizontal displacement) around wells SG1 and C14 does not allow us to evaluate dynamically the stress changes or to distinguish a possible depletion driven subsidence.

Because of the lack of static pressure readings for well SG1 during the 5 years of production we can only evaluate static stress changes induced by a given reservoir depletion. A value of 1 MPa is assumed, based on production from other nearby wells. The approaches of [141] and [142] will be followed.

- *Statistical analysis of seismicity and production data of Mirandola (section 7.D)*

Statistical analyses of induced/triggered seismicity may reveal collective properties which differ from those of naturally seismicity such as non-stationarity and time-dependence of seismic processes (e.g. [143], [144]) . Therefore a statistical analysis of seismic parameters has been performed.

Moreover in order to evaluate possible statistical correlations between seismicity and operational activities, an investigation of the spatial and temporal relationships between seismicity and production parameters has also been carried out.

Analysis of the Casaglia field:

- *To analyze the possible influence of the geothermal activity in Casaglia (section 7.E)*

Any possible influence of the geothermal activity in Casaglia at the location of the main shocks of the 20th and of the 29th of May has been investigated. Since volume balance is maintained in the far field (local imbalance may be present between the injection/production point) the only candidate for triggering of earthquakes are the

thermo-elastic stress changes arising from differences in temperature between extracted and re-injected fluid. A dynamic simulation has been performed by [145], to evaluate the thermo- and poro-elastic stress changes induced by a geothermal doublet having a temperature drop of 80 K, with the aid of a finite element numerical model. To compare the stress change inside the crust with observable quantities, the subsidence associated with 30 years of operation has been calculated and then the yearly rate extracted, to be compared with the natural subsidence/uplift rate.

VII. Processing of seismic and production data

A. Velocity model and identification of significant faults

1. Structural interpretation of reflection seismic profiles

The Ferrara Arc has been usually interpreted, in the geological literature, as a fault-propagation-fold system grown in the hangingwall of blind thrusts at the front of the Northern Apennines (see among many others [146], [94], [147], [140], [148] and references therein). We have revised the structural architecture of the area struck by the May 20-29 2012 earthquakes by interpreting a network of reflection seismic profiles kindly provided by ENI in SEG-Y format and three regional lines in public domain available in raster/compound format at the VIDEPI site. The seismic lines have been calibrated by means of several commercial wells, some of which have reached the buried carbonate reservoir. The SEG-Y profiles have been imported in a Kingdom Project together with the LAS curves of the wells located close to the traces of the seismic lines. In this project the most significant horizons and faults have been traced and finally time-structural maps referred to the picked horizons and time-structural maps referred to the most significant thrust surfaces have been produced.

Some of the analysed boreholes have encountered one or more tectonic repetitions due to the existence of thrusts at the base of the carbonate reservoir (see wells Casaglia 1, Cavone di Carpi 1, Concordia 1, Ferrara 1 and San Giovanni 1). Among these wells, Concordia 1 resulted particularly useful to calibrate the seismic lines imported in the Kingdom Project and to tie these lines to the regional line Dominio Appenninico Orientale Sezione 1, which cuts across the Cavone-Camurana-Spada structure in the Rivara area and the Pilastrri-Ferrara structure not far from its western termination.

Figure VII.1 is a schematic columnar section of Concordia 1 with the principal wirelog curves. After having crossed a thick succession of Pliocene-Messinian terrigenous deposits, the borehole encountered a Cenozoic-Mesozoic section typically referable to the Cavone sequence. Moving downsection, the stratigraphic succession is represented by the Gallare Formation (here including the Paleogene marly member of the Scaglia Formation and the equivalent of the lower Miocene Bisciaro Formation), the Turonian-middle Eocene calcareous member of the Scaglia Formation, the Aptian-Cenomanian Marne del Cerro Formation and a Middle Jurassic-Neocomian condensed sequence 63 metres thick which overlies the shallow-water-carbonate reservoir here represented by the Lower Jurassic Calcarei Grigi di Noriglio Formation. The condensed section, which is part of the cap rock, includes the Maiolica, Calcarei ad Aptici and Calcarei a *Posidonia* Formations. At the depth 3852, a thrust surface separates the Calcarei Grigi di Noriglio Formation from an underlying basinal marly sequence of Paleogene age attributed to the Gallare Formation. The latter has been penetrated for more than 1000 metres without reaching the base. **Figure VII.2** shows the seismic line MOD-74-17 the upper half portion of which has been calibrated by the wells Concordia 1 and San Giacomo 1. The legend of the mapped horizons is provided in **Figure VII.3**

The thrust surfaces crossed by the aforementioned wells at the base of the carbonate reservoir have all been interpreted, in the current geological literature, as blind reverse faults responsible for the growth of fault-propagation folds in the hangingwall block. Following such an interpretation, the Cavone-Camurana-Spada and the Pilastrri-Ferrara structure would represent two independent ramp anticlines floored by two different reverse faults which would root somewhere in the basement following roughly parallel trajectories (see, among many others, [148] and references therein).

Well name: Concordia 001

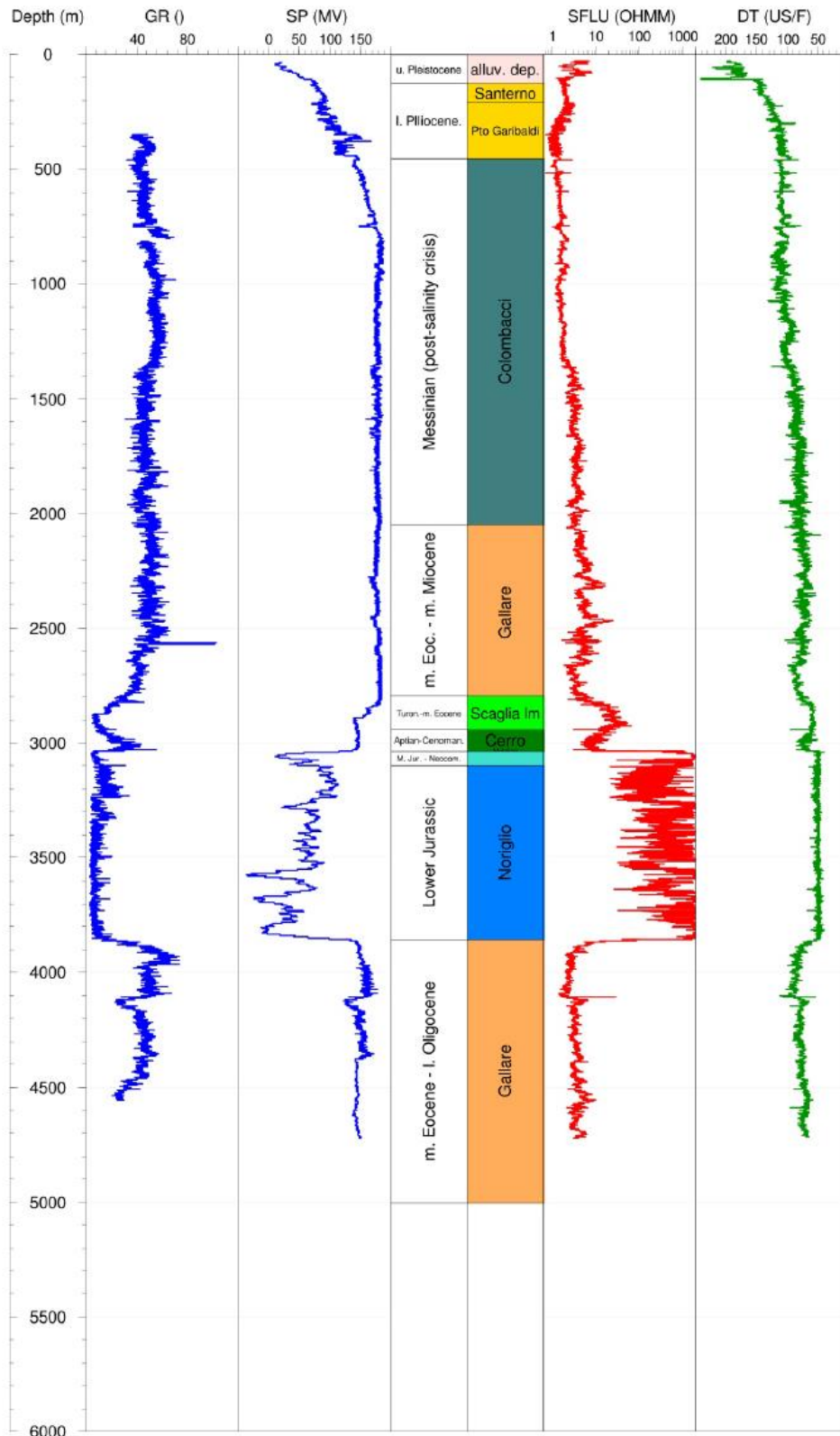


Figure VII.1 Columnar section and wirelog curves of Concordia 1. Note the tectonic repetition of the Gallare Formation due to the presence of a thrust surface at the depth 3852.

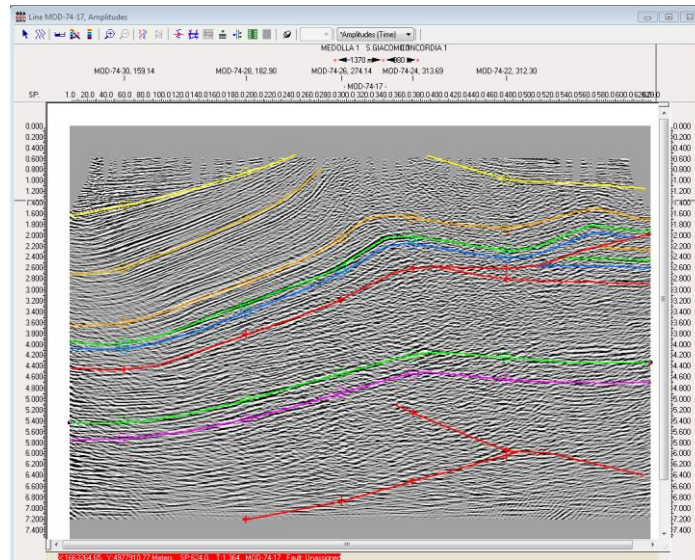


Figure VII.2 Geological interpretation of the seismic line MOD-74-17 showing the Concordia anticline and the thrust surface responsible for the tectonic repetition encountered in the Concordia 1 well (see legend of the mapped horizons in **Figure VII.3**). The stratigraphic sequence in the footwall of the thrust derives from the well Corte Vittoria 1 (T.D. 6118) located in the foreland area ahead of the Pilastrri-Cavone and Ficarolo structures.

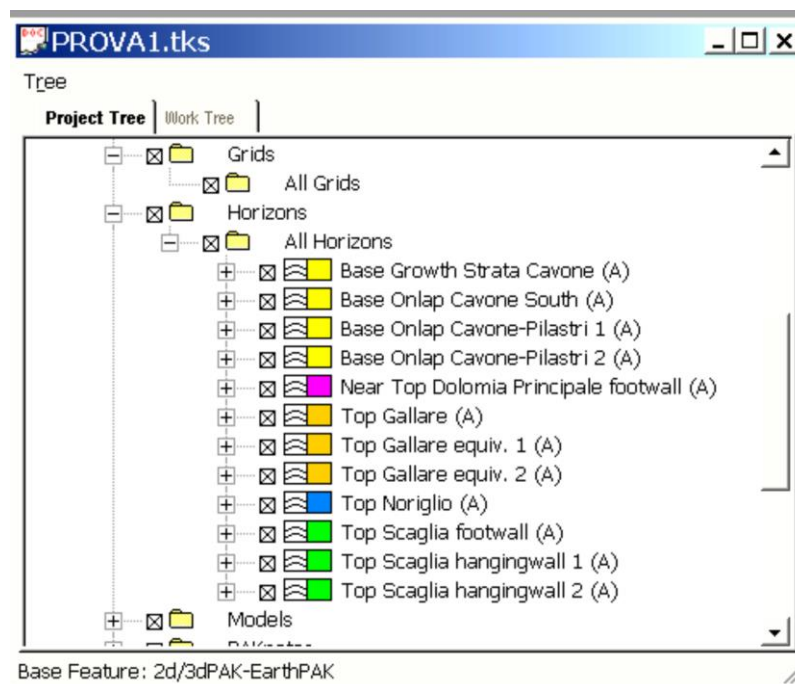


Figure VII.3 Legend of the mapped horizons. The Gallare Formation refers to the Lower Miocene-middle Eocene marly deposits in the footwall of the main thrust whilst the Gallare equivalent refers to the coeval deposits in the hangingwall (Gallare equivalent 1 and Gallare equivalent 2 in the hangingwall and in the footwall of the major breach enucleated from the main thrust, respectively).

The structural interpretation is quite different. Over the entire Ferrara Arc a major thrust surface, which follows a typical flat-ramp-flat trajectory, is responsible for a long-wave fault-bend-fold structure developed in the hangingwall block. This structure has been complicated by the existence of one or more breaches enucleated from the base thrust, which have propagated ahead of the Cavone structure as second-order thrust(s) and backthrust(s) with associated short-wave detachment and fault-propagation folds.

Figure VII.4, Figure VII.5 and Figure VII.6 are images of the seismic lines MOD-74-19, MOD-74-21 and MOD-74-23, respectively, with our interpretation. **Figure VII.7 and Figure VII.8** show the seismic lines MOD-74-25 and MOD-01-EXT with our interpretation (a) and the interpretations of Regione Emilia-Romagna (b) and Erg Rivara Storage (c), respectively.

At greater depths, all the interpreted lines show the existence of blind thrusts and backthrusts which determinate folding in the footwall of the major thrust surface. In our interpretation, both the shallow thrust responsible for the Cavone anticline and the deep thrusts/backthrusts cutting across the footwall of the first-order structure may act as seismogenic faults, focuses being separated by a non-seismogenic layer, If our interpretation is correct, the shallow seismogenic structures and the deeper ones have no hydraulic connection since they are separated by a thick layer of marly deposits referable to the Gallare Formation which are a seal and therefore constitute a real barrier for fluid circulation.

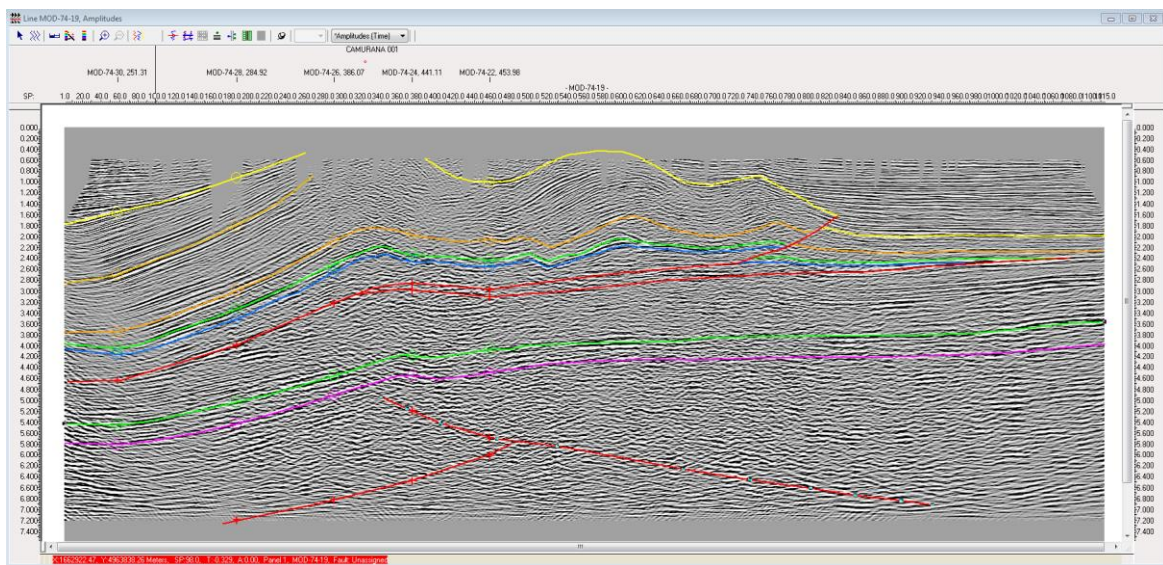


Figure VII.4 Geological interpretation of the seismic line MOD-74-19.

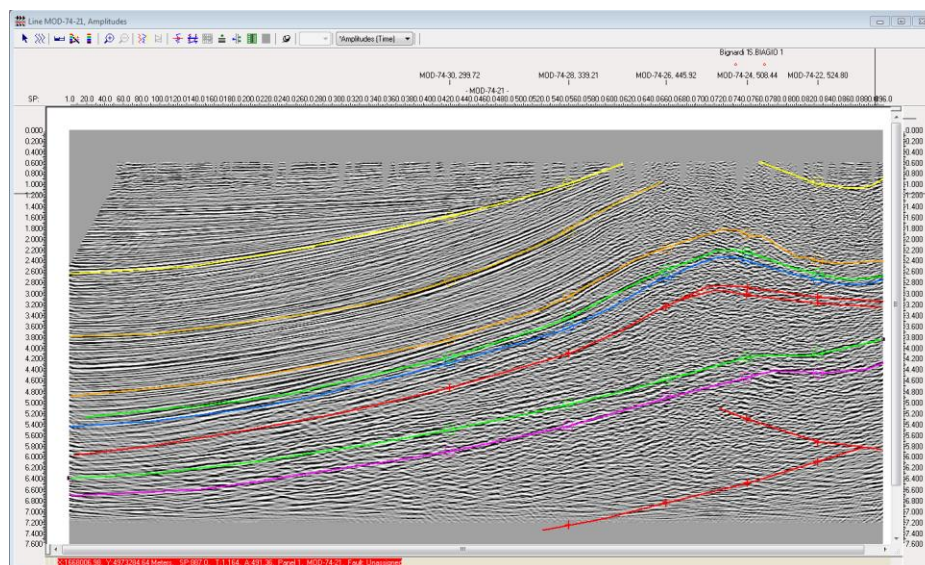


Figure VII.5 Geological interpretation of the seismic line MOD-74-21.

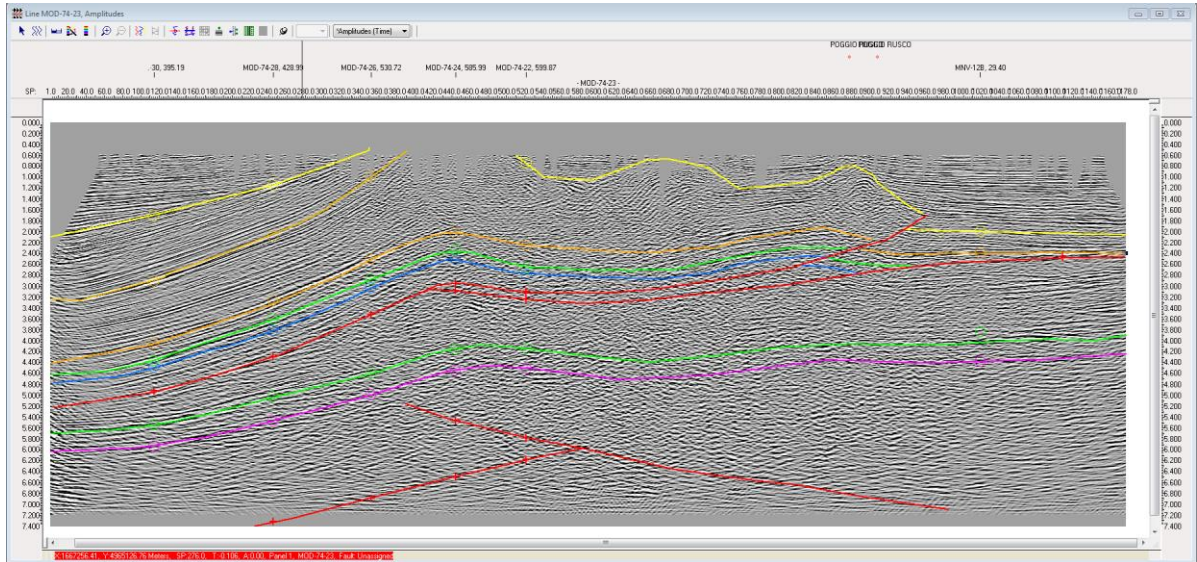


Figure VII.6 Geological interpretation of the seismic line MOD-74-23.

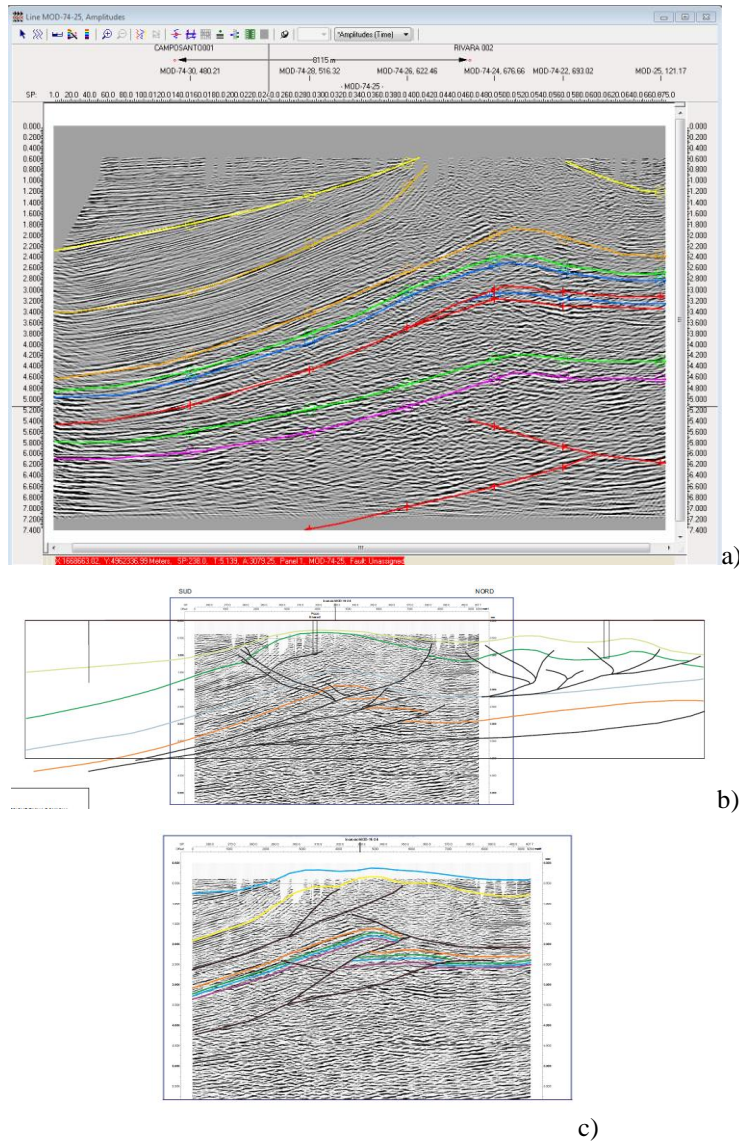


Figure VII.7 Seismic line MOD-74-25 according to our interpretation a) and according to the interpretations of Emilia-Romagna Region (b) and Erg Rivara Storage (c). Interpretations (b) and (c) after ERG RIVARA STORAGE (2009), Appendix D.

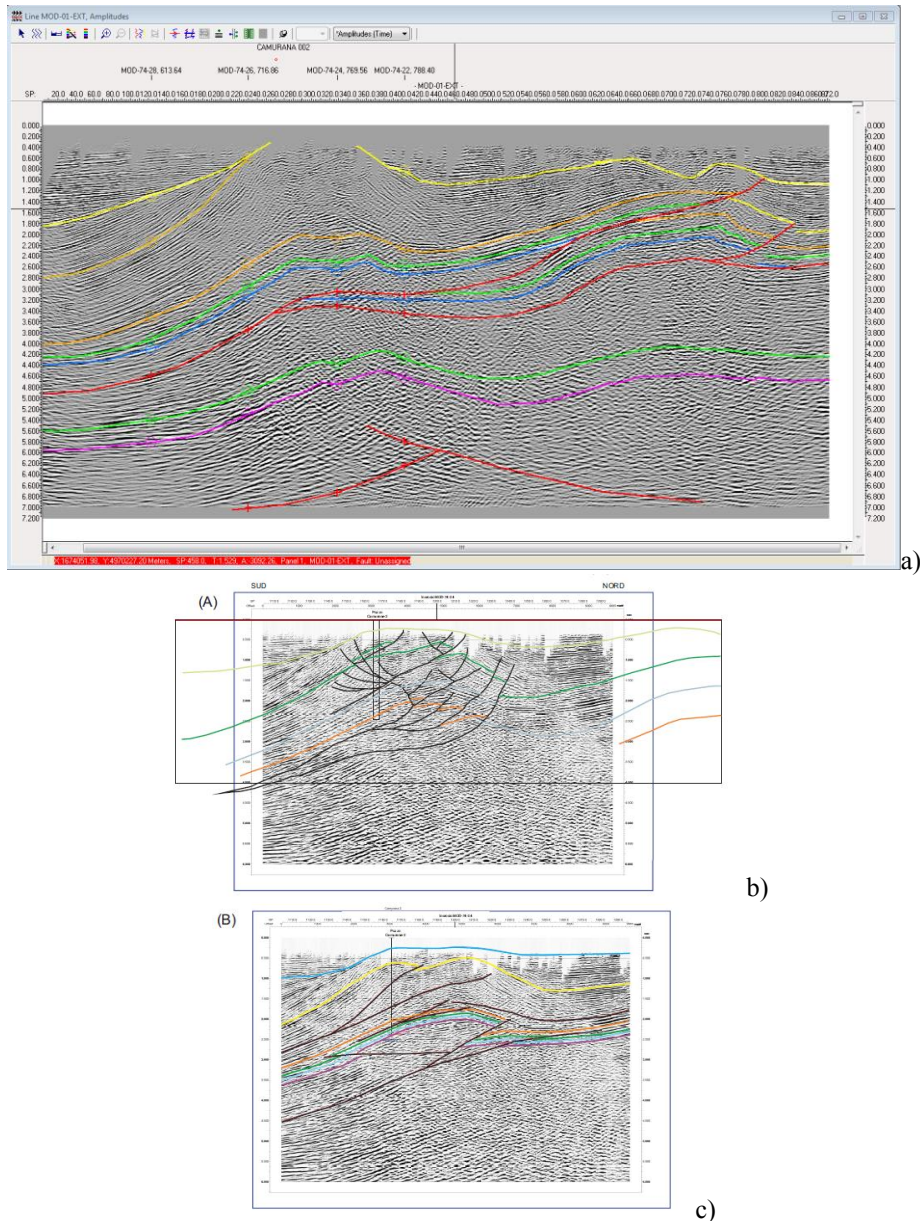


Figure VII.8 Seismic line MOD-01-EXT according to our interpretation a) and according to the interpretations of Emilia-Romagna Region (b) and Erg Rivara Storage (c). Interpretations (b) and (c) after ERG RIVARA STORAGE (2009), Appendix D.

2. Velocity model and identification of significant faults

A unique velocity model, such as the model applied by the National Institute of Geophysics and Volcanology to the entire Italian territory, is unsuitable for a reliable hypocentre determination of the seismic events that struck the study area on May 20-29 2012 because of the occurrence of strong lateral heterogeneities related to local and regional structural complexities. Consequently, it was decided to elaborate a new velocity model representative of the real geological structure of a wide area surrounding the registered earthquakes. In this area, three structural domains can be distinguished (**Figure VII.9**):

- a foreland domain (Padan Foreland), structurally characterized by a homoclinal ramp gently dipping towards the south;
- a mountain chain segment, corresponding to the Modena-Forli Apennine margin, the bulk of which is constituted of rootless nappes overlying a deep-seated duplex system;
- an intermediate domain, corresponding to the Ferrara Arc, made up of a thrust-and-fold system buried beneath undeformed or gently deformed Plio-Pleistocene deposits.

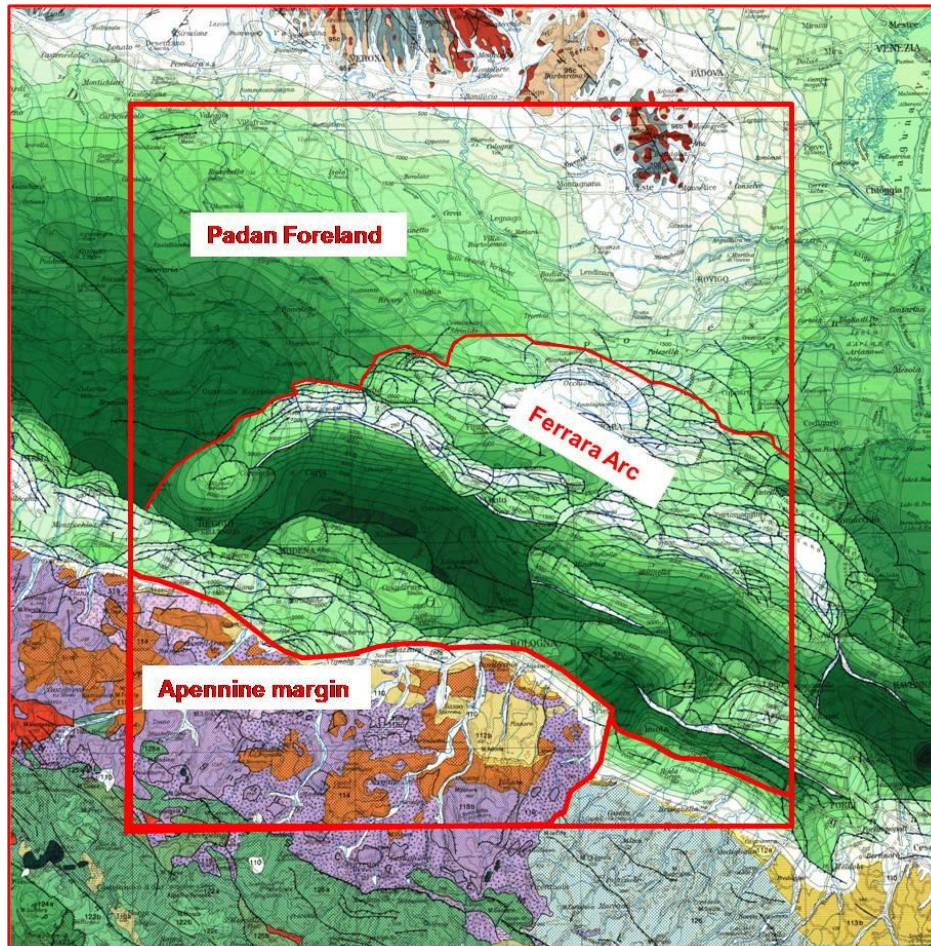


Figure VII.9 Area selected for a new velocity model (red square). In this area, three first-order structural domains have been distinguished: the Padan Foreland, the Ferrara Arc and the Apennine margin. The light-to-dark-green colour-bar is representative of a progressive deepening of the base of the Plio-Pleistocene deposits in the foreland homocline, in the Ferrara thrust-and-fold belt and in the Apennine deep-seated frontal tectonic structures (Emilia Folds) buried beneath rootless nappes (violet). Along the Apennine margin the nappe pile is overlain by thrust-top deposits of Plio-Pleistocene age (orange and yellow). Base map from [129].

Moving from the northern to the southern portion of the foreland domain the major lateral variation is represented by the progressive thickening of the low-velocity upper layer (about 2 Km/sec) which consists of Plio-Pleistocene deposits lying on top of a Meso-Cenozoic sedimentary sequence assumed to have a rough isopachous trend. This layer changes in thickness from less than 500 metres to more than 6500 metres. The pre-Pliocene stratigraphic succession is represented by Upper Triassic and Lower Jurassic p.p. shallow-water carbonates overlain by Lower Jurassic p.p.-Eocene p.p. deeper-water carbonates. The deeper-water carbonates, in turn, grade upwards into an Eocene p.p.-Miocene marly/shaly sequence. The Miocene part of this sequence (which may include Messinian evaporites, where present) is unconformably overlain by Plio-Pleistocene terrigenous deposits. Due to the progressive deepening of the base of the Plio-Pleistocene deposits, and consequently the progressive thickening of the low-velocity upper layer, we have divided the foreland area (including in this partition also the most external thrust sheets of the Ferrara Arc mostly made up of

Neogene sediments) into four polygons (polygons 1-4 in **Figure VII.10**). The Ferrara Arc, in turn, has been also divided into four segments corresponding to the Bagnolo-Cavone and Pilastrri-Ferrara ridges (polygons 6-7 and polygon 5, respectively) and to the backlimb of the Cavone ramp anticline plus Emilia Folds (polygon 8). The Apennine margin, finally, has been divided into two polygons corresponding to the Emilia and Romagna segments (polygons 9 and 10, respectively).

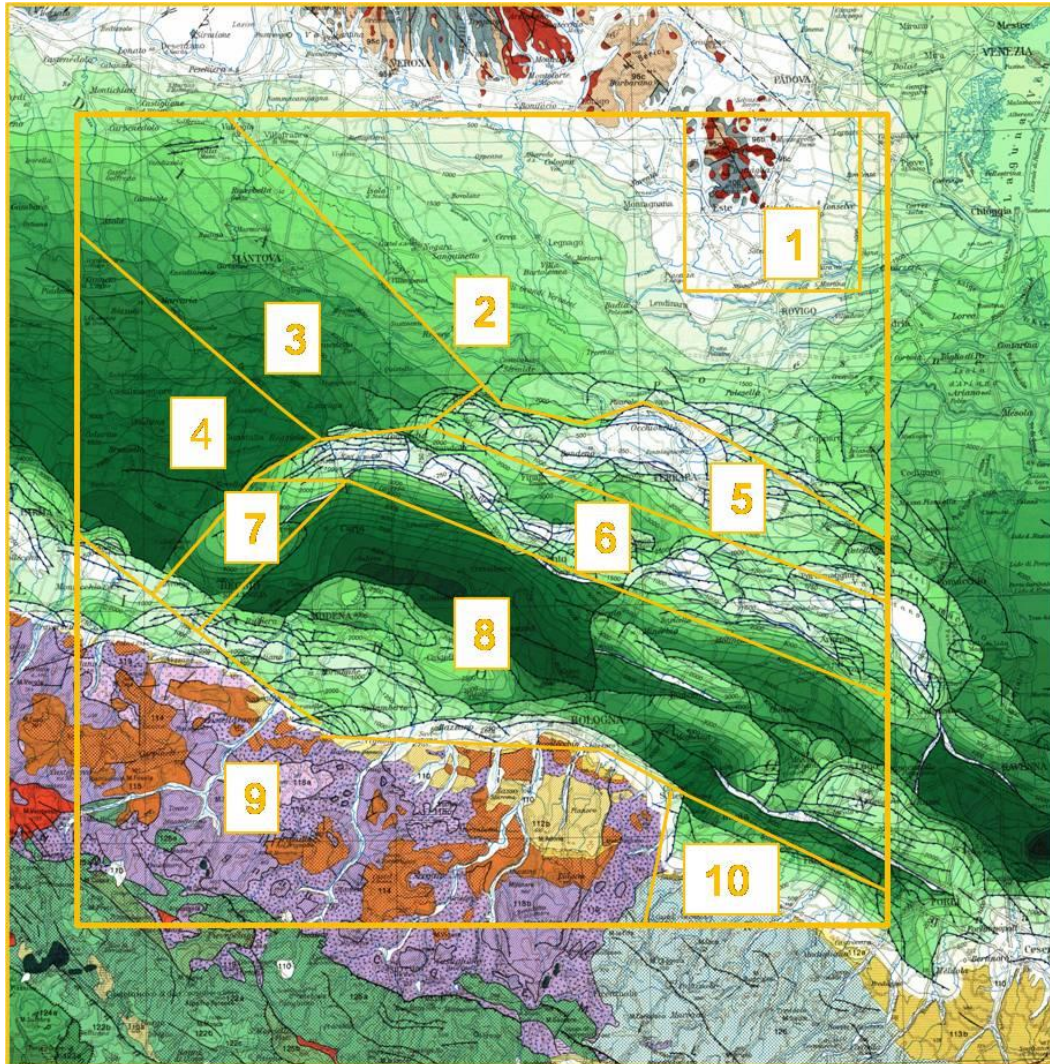


Figure VII.10 Polygons with different velocity functions that have been used for earthquake relocation. See discussion in text.

Here, we will provide the polygon vertices of the adopted velocity model expressed in kilometeric coordinates WGS 1984 UTM Zone 32N:

- Polygon 1 - Colli Euganei

1.1	728.128,682	5.025.796,047
1.2	727.864,098	5.008.035,856
1.3	699.652,844	5.007.705,126
1.4	699.222,895	5.025.035,369

- Polygon 2 - Foreland homocline northern portion

2.1	731.171,397	5.025.895,266
2.2	733.486,505	4,958.327,162

2.3	704.150,770	4.978.237,098
2.4	683.910,104	4.977.972,514
2.5	622.989.670	5.023.117,136
• Polygon 3 - Foreland homocline, central portion		
3.1	622.989.670	5.023.117,136
3.2	677.220,542	4.983.084,495
3.3	655.393,643	4.980.967,824
3.4	662.721,346	4.977.448,859
3.5	649.889,029	4.973.585,934
3.6	606.047,483	5.008.960,797
3.7	605.888,733	5.022.719,158
• Polygon 4 - Foreland homocline southern portion		
4.1	606.047,483	5.008.960,797
4.2	649.889,029	4.973.585,934
4.3	638.600,118	4.970.663,385
4.4	619.318,569	4.951.811,785
4.5	606.717,762	4.961.601,388
• Polygon 5 - Casaglia-Ferrara Ridge		
5.1	677.220,542	4.983.084,495
5.2	683.910,104	4.977.972,514
5.3	704.150,770	4.978.237,098
5.4	733.486,505	4,958.327,162
5.5	733.618.797	4.954.060,748
5.6	662.721,346	4.977.448,859
5.7	655.393,643	4.980.967,824
• Polygon 6 - Cavone Ridge		
6.1	662.721,346	4.977.448,859
6.2	733.618.797	4.954.060,748
6.3	734.026,697	4.940.744,462
6.4	668.145,316	4.963.723,571
6.5	655.207,165	4.967.057,327
6.6	638.600,118	4.970.663,385
• Polygon 7 - Bagnolo in Piano Ridge		
7.1	638.600,118	4.970.663,385
7.2	649.928,717	4.967.533,578
7.3	624.687,416	4.947.531,038
7.4	619.318,569	4.951.811,785
• Polygon 8 - Backlimb of the Cavone Ridge and Emilia Folds		
8.1	649.928,717	4.967.533,578
8.2	655.207,165	4.967.057,327
8.3	668.145,316	4.963.723,571
8.4	734.026,697	4.940.744,462
8.5	735.257,012	4.906.732,207
8.6	695.648,808	4.925.385,369
8.7	645.920,271	4.930.822,567

8.8	624.687,416	4.947.531,038
-----	-------------	---------------

- Polygon 9 - Emilia Apennine segment

9.1	606.717,762	4.961.601,388
9.2	645.920,271	4.930.822,567
9.3	695.648,808	4.925.385,369
9.4	707.674,145	4.919.829,108
9.5	703.110,073	4.903.041,262
9.6	607.661,445	4.900.501,257

- Polygon 10 - Romagna Apennine segment

10.1	707.674,145	4.919.829,108
10.2	735.257,012	4.906.732,207
10.3	735.376,075	4.903.914,389
10.4	703.110,073	4.903.041,262

Referring to the single polygons, the assigned velocities between the surface and a depth ranging from 12000 to 15000 meters are provided (depths in meters; velocities Km/sec):

- Polygon 1 - Colli Euganei

0.00-500	3.5-4.0 km/sec
500-1500	5.0
1500-4000	5.5-6.0
4000-10000	6.0-6.2

- Polygon 2 – Foreland homocline northern portion

0.00-1500	2.0 km/sec
1500-3000	3.5
3000-4000	5.0
4000-6500	5.6-6.0
6500-12000	6.0-6.2

- Polygon 3 – Foreland homocline, central portion

0.00-3000	2.0 km/sec
3000-4500	3.5
4500-5500	5.0
5500-8000	5.5-6.0
8000-12000	6.0-6.2

- Polygon 4 – Foreland homocline southern portion

0.00-5500	2.0-2.3 km/sec
5500-7000	3.5
7000-8000	5.0
8000-10500	5.5-6.0
10500-15000	6.0-6.2

- Polygon 5 – Casaglia-Ferrara Ridge

0.00-4000	5.0 km/sec
4000-5000	3.5-4.0
5000-6000	5.0

6000-8000	5.5-6.0
8000-15000	6.0-6.2

- Polygon 6 – Cavone Ridge

0.00-2500	2.5-2.8 km/sec
2500-4000	4.8-5.0
4000-5000	4.0-4.5
5000-8000	5.0
8000-10000	5.5-6.0
10000-15000	6.0-6.2

- Polygon 7 – Bagnolo in Piano Ridge

0.00-4500	3.0 km/sec
4500-6000	5.0
6000-7000	4.0-4.5
7000-11000	5.0
11000-13000	5.5-6.0
13000-15000	6.0-6.2

- Polygon 8 – Backlimb of the Cavone Ridge and Emilia Folds

0.00-6500	2.5-3.0 km/sec
6500-7500	3.5-4.0
7500-11500	5.0
11500-13500	5.5-6.0
13500 -15000	6.0-6.2

- Polygon 9 – Emilia Apennine segment

0.00-6000	3.0-3.5 km/sec
6000-8000	4.0-4.5
8000-11500	5.0
11500-13500	5.5-6.0
13500.15000	6.0-6.2

- Polygon 10 - Romagna Apennine segment

0.00-1500	2.0 km/sec
1500-3500	3.0
3500-5500	4.0-4.5
5500-11500	5,0
11500-13500	5.5-6.0
13500-15000	6.0-6.2

Though the proposed model is not a real 3D model, it has helped very much in the re-determination of the hypocentral depths of the major seismic events in Emilia-Romagna registered in May 2012, and thus contributed to the discrimination between inactive and active fault segments. Referring to the May 20 earthquake (Magnitude 5.9), the shallow depth of the focus (5.3 ± 1.0 Km) allowed us to correlate the source with a well-defined segment of the thrust controlling the Cavone-Mirandola ramp anticline. A time-depth conversion of the section, in fact, locates the thrust segment on which the earthquake hypocenter has been projected at a depth of 4000-4500 meters. Note that the thrust interpreted as an active surface is a major breach nucleated from the Cavone-Mirandola base thrust. This breach appears to be responsible for a tectonic repetition of the Cavone stratigraphic succession (the blue, green

and orange horizons represent the top of the Noriglio, Scaglia and Gallare formations, respectively). Referring to the May 29 earthquake (Magnitude 5.3), the significantly greater depth of the focus (9.3 ± 0.9 Km/sec) points to a correlation between the source and a deep-seated blind thrust (hypocenter projection at about 10.000 meters)) which concurred to the growth of a thrust-propagation fold in the footwall of the Cavone-Mirandola thrust. The stratigraphic succession of the footwall block has been defined by using the well Corte Vittoria 1 (Total Depth 6118 m) which is located in an undeformed foreland area in front of the Ficarolo thrust sheet (**Figure VII.11**).

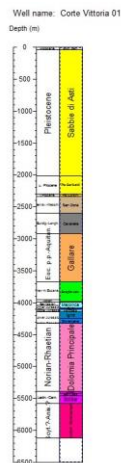


Figure VII.11 Corte Vittoria 1 well.

Figure VII.12 and **Figure VII.13** show the proposed correlation between the above seismic events and the recognized tectonic structures. If the geological interpretation is correct, there is no hydraulic connection between the rock volumes interested by the earthquake rupture. Actually, the entire sedimentary succession sandwiched between the Scaglia Formation present in the footwall of the Cavone-Mirandola thrust (green horizon overlying a violet horizon which approximates the top of the Dolomia Principale Formation) and the Noriglio Limestone plus Dolomia Principale formations present in the hangingwall (rock volumes between the blue horizon and the Cavone-Mirandola thrust) is composed of impermeable marly/shaly sediments which form the seal of the deep-seated reservoirs not reached by the wells drilled in the area.

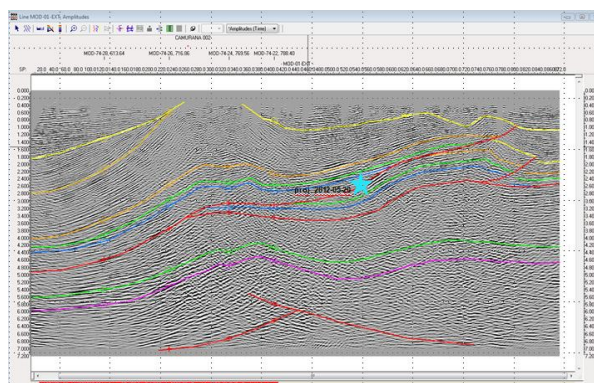


Figure VII.12 Seismic line MOD-01-EXT showing the major tectonic features present in the epicentral area of the May 20 earthquake. The picture evidences the thrust that likely represents the causative fault of this event.

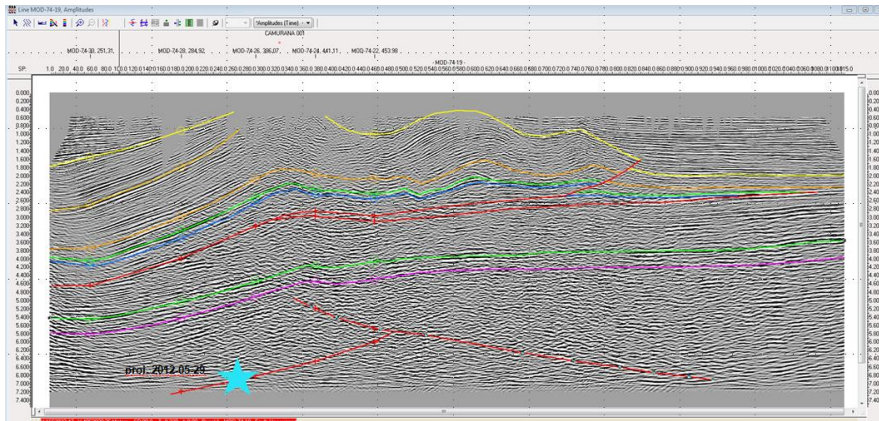


Figure VII.13 Seismic line MOD-74-19 showing the major tectonic features present in the epicentral area of the May 29 earthquake. The picture evidences the thrust that likely represents the causative fault of this event.

B. Relocation focal mechanism and tectonic stress transfer

1. Earthquake location and focal parameters

120 earthquakes of $M > 1.5$ have been recorded by the INGV seismic network during the seven years preceding the main shock of May 20. Forty-four of these events have been selected because of their spatial proximity to the May 2012 event. They have been relocated using the previously described 3D velocity model and a probabilistic earthquake location method based on a non-linear global search procedure ([149]) applied to the INGV database of travel-time picks (inside.rm.ingv.it).

Furthermore, a revised database of the 2012 Emilia sequence was provided by INGV to the Commission. 31 events of the sequence, which have a magnitude $ML > 4.0$ have been relocated. The travel times have been calculated using a method based on the finite difference solution of the eikonal equation ([150]), which is valid for a 3D heterogeneous medium. The non-linear global search method in a 3D environment has the advantage that it does not require the computation of partial derivatives, which is very difficult in complex media. The earthquake locations are strongly dependent on the ratio between the velocity of P-waves and S-waves (V_p/V_s), thus an analysis to evaluate the best ratio to be used in the location procedure has been performed. A $V_p/V_s = 1.81$ has been selected, this value being the best ratio obtained by the minimization of the final residual distribution.

The solution, expressed as a PDF (probability density function), provided the uncertainty in the location due to the picking and travel-times calculation error and the network-event geometry. The maximum likelihood point of the complete non-linear PDF is selected as an “optimal” hypocenter and the uncertainty of the solutions has been evaluated in terms of 68% confidence ellipsoid major semi-axis length ([151]), obtained by SVD (singular value decomposition) of the covariance matrix. The uncertainty has been defined as ERH (uncertainty in the epicenter position) and ERZ (uncertainty in the hypocenter depth).

The results of the earthquake re-locations are shown in Appendix E and in **Figure VII.14** and **Figure VII.15**.

The main result of the earthquake’s relocation using the new 3D velocity model (see section 7.A) is that the focal depths of most of the events are significantly shallower than those computed with standard methods. In particular, the seven earthquakes with $M \geq 5$ show depths ranging from 4.2 to 10.2 km (May 20 mainshock at 5.3 km; May 29 mainshock at 9.3 km) with uncertainty ranging from 0.8 to 1.3 km. The earthquake’s epicenters define more closely an E-W elongated strip with a smaller scatter in the N-S direction compared with locations with standard methods.

An estimation of the focal parameters including compressional and tensional axes for the re-located earthquake sequence has been performed using both moment tensor analysis, and a grid search mechanism determination algorithm. In both these procedures, the maximum likelihood hypocenter solution determined by global search earthquake locations and the corresponding ray take-off angles in the 3D velocity model have been used. The uncertainties in the take-off angles are due both to hypocenter errors, to the open geometry of the network and picking errors, and to unknown features of the velocity model, and also to small scale heterogeneities. The dependence of the take-off angle on hypocentral depth is analyzed to evaluate the variability of take-off angles from errors in depth. The variability of the take-off angle to the error in depth is more evident for stations close to the epicenter for very shallow earthquakes, but in any case it can be estimated to be lower than 10%.

The maximum likelihood solutions for the focal parameters (strike, dip, rake) of the fault plane are reported in Appendix E. Due to the high level of noise affecting most seismic stations located in the Po valley, a robust focal solution has been evaluated only for a subset of selected events (44 earthquake for the pre-sequence database; the 7 events with magnitude

$M > 5$; 24 earthquakes for the database of events with $4.0 \leq M \leq 5$ database). Focal mechanism confirm the existence of a thrust fault system according to the previous evaluations. The range of values for the strike (φ), dip (δ) and rake (λ) are:

$$\begin{aligned}\varphi &= 80^\circ \div 120^\circ \\ \delta &= 30^\circ \div 55^\circ \\ \lambda &= 80^\circ \div 110^\circ\end{aligned}$$

In particular an increase in the fault dip has been observed after the May 29th mainshock; in fact, the fault dip increased from an average value of 35° to an average value of 45° . This increase in the dip fault could indicate that May 29th event occurred on a different fault system (Mirandola thrust) with respect to the May 20th earthquake (Ferrara thrust). This consideration is in agreement with what observed taking into account the depth of the hypocenters and the analysis of the seismic reflection profiles.

Results for the 7 events with magnitude $M > 5$ are summarized in **Table VII.1** (Local magnitudes are from INGV database).

Table VII.1 .Main focal parameters of the shocks with magnitude greater than 5.

Event	1	2	3	4	5	6	7
Date	20/05/2012	20/05/2012	20/05/2012	29/05/2012	29/05/2012	29/05/2012	03/06/2012
Time GMT	2:03	2:07	13:18	7:00	10:55	11:00	19:20
LON	11.253°	11.344°	11.464°	11.068°	10.985°	10.930°	10.919°
LAT	44.885°	44.853°	44.826°	44.854°	44.872°	44.875°	44.903°
DEP (km)	5.3	4.2	4.8	9.3	4.2	10.2	8.9
Er H (km)	1.3	1.5	1.2	0.8	0.8	1.0	1.1
Er Z (km)	1.0	1.3	0.9	0.9	0.9	1.1	0.8
MAG	5.9	5.1	5.1	5.8	5.3	5.2	5.1
Dip	38°	40°	33°	34°	33°	37°	35°
Er Dip	6°	5°	6°	5°	7°	6°	8°
Strike	99°	104°	114°	97°	105°	90°	95°
Er Strike	12°	10°	12°	10°	11°	10°	11°
Rake	85°	87°	97°	93°	100°	102°	95°
Er Rake	11°	13°	9°	10°	10°	11°	9°

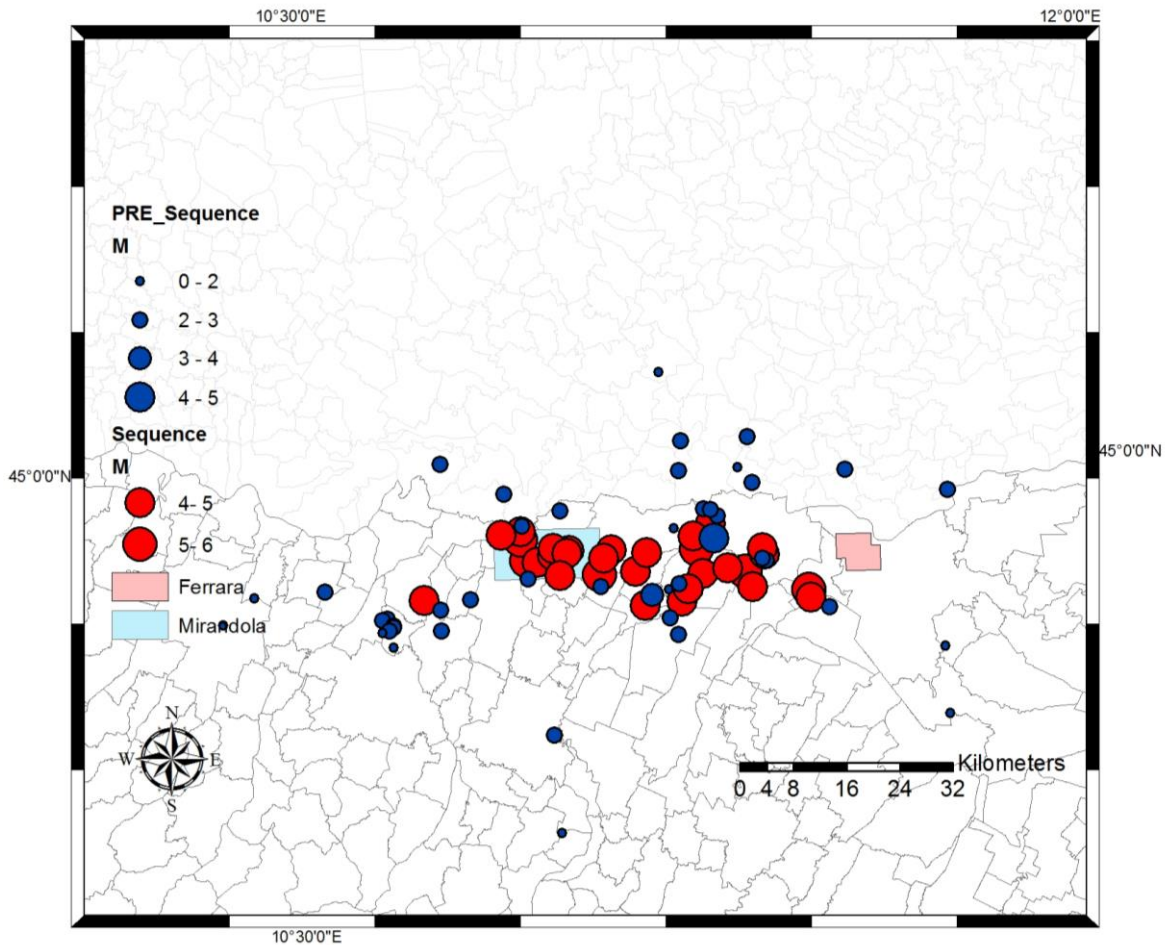


Figure VII.14 Relocations of events from 1.1.2005 to 19.05.2012 (blue circles) and events with $M \geq 4$ of the Emilia sequence (red circles).

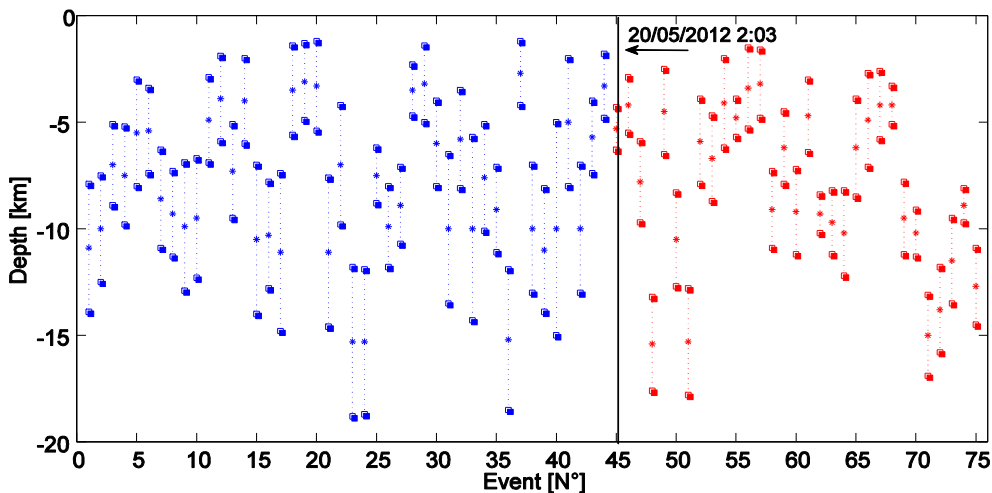


Figure VII.15 Hypocentral depths and related uncertainty (\pm errz) of events from 1.1.2005 to 19.05.2012 (blue stars) and events with $M \geq 4$ of the Emilia sequence (red stars).

2. Coulomb stress transfer within the Emilia seismic sequence

It is well known that earthquake ruptures induce stress changes on neighboring faults that can alter the probability of occurrence of future earthquakes (see e.g., [152], [153], [154], [155], [156], [157], [158], [159] and many others). Static stress transfer within the crust is a

physical process through which a large earthquake can induce/trigger other earthquakes on nearby favorably oriented seismogenic structures (e.g., [159]).

All the results available in literature up to now suggest that in the case of the Emilia sequence, the two main events ruptured on two neighboring faults (or even different patches on the same blind fault, as suggested by [160]). The static stress changes caused by the displacement of a source fault embedded in an elastic half-space have been evaluated; in particular, the change in the Coulomb failure function (CFF, or Coulomb stress) is resolved on specified target failure planes (receiver faults) following the approach described by [161], [162] and [163].

Considering the Coulomb failure criterion, $\Delta CFF = \Delta\tau_s + \mu' \Delta\sigma_n$, the failure is postulated to be promoted when the Coulomb stress change is positive. Here, ΔCFF is the change in failure stress on the receiver fault caused by slip on the source fault(s), $\Delta\tau_s$ is the change in shear stress (reckoned positive when shear occurs in the direction of fault slip), $\Delta\sigma_n$ is the change in normal stress (positive if the fault is unclamped), and μ' is the effective coefficient of friction on the fault.

Seven events with $M > 5.0$ (the same as used in [164]), and shown in **Table VII.2** have been selected. Lateral variations are notable even in the order of a few kilometers; therefore, the uncertainties related to the source parameters (e.g., hypocenter locations, fault plane orientation) as well as other model parameters as the friction coefficient and the geometry (width/length ratio) of the fault, can play an important role in the results obtained.

Table VII.2 Seismic events with $M > 5$ considered for the stress transfer analysis

Event No.	Date	Time (GMT)	M_L
1	20/05/2012	02:03	5.9
2	20/05/2012	02:07	5.1
3	20/05/2012	13:18	5.1
4	29/05/2012	07:00	5.8
5	29/05/2012	10:55	5.3
6	29/05/2012	11:00	5.2
7	03/06/2012	19:20	5.1

Considering the variability range for the results found in the literature for the source modeling of those events (e.g., [164], [165], [166], [167], [160]), a new analysis of the effects of uncertainties in the input model parameters on the CFF calculations has been performed. In particular the ΔCFF has been evaluated on the (receiver) fault plane of the event 4 (May 29, 2012 mainshock) after the occurrence of the first three events on May 20, 2012 (**Table VII.2**). The main effort has been to assess the effects of the uncertainties in some of the parameters characterizing the source of the main event (event 1: on May 20, 2012) and those defined for the fault plane of the event 4 (May 29, 2012), and considering it as the receiver fault. The procedure adopted has been to perform Monte Carlo sampling from predefined distributions characterizing the uncertainties on the input parameters to produce randomized stress calculations. A total of 1500 models were sampled separately considering Gaussian and Uniform distributions. The source solutions and associated uncertainties that we have considered are those obtained in this report (**Table VII.3**). The selected uncertain parameters to be assessed and their values (mean value and range) are listed in **Table VII.4**.

Table VII.3 Source parameters (and uncertainties) obtained in this report.

DATE	Time	Latitude	Longitude	Depth	Horiz. error	Vert. error	Strike	Strike error	Dip	Dip error	Rake	Rake error
120520	0203	44.885	11.253	5.3	1.3	1.0	99	12	38	6	85	11
120520	0207	44.853	11.344	4.2	1.5	1.3	104	10	40	5	87	13
120520	1318	44.826	11.464	4.8	1.2	0.9	114	12	33	6	97	9
120529	0700	44.854	11.068	9.3	0.8	0.9	97	10	34	5	93	10
120529	1055	44.872	10.985	4.2	0.8	0.9	105	11	33	7	100	10
120529	1100	44.875	10.930	10.2	1.0	1.1	90	10	37	6	102	11
120603	1920	44.903	10.919	8.8	1.1	0.8	95	11	35	8	95	9

Table VII.4 Summary of the Input Parameters for the Randomized Stress Calculations. The central values and variation ranges are also presented.

Parameter	Central value	$\pm\sigma$
Parameters of the main event of 20 May 2012 (source fault)		
Latitude (center of the fault)	44.885°	± 1.3 km
Longitude (center of the fault)	11.253°	± 1.3 km
Depth (Km)	Range from 4.0 to 7.0 Km	
Strike (°)	99.0°	$\pm 12.0^\circ$
Dip (°)	38.0°	$\pm 6.0^\circ$
Slip (m)	0.4m	± 0.10 m
Rake (°)	85.0°	$\pm 11.0^\circ$
Friction coefficient	Range from 0.4 to 0.8	
Fault length (Km)	Range from 9.0 to 21.0 Km (conserving an area of 100 Km ²)	
Parameters of the main event of 29 May 2012 (receiver fault)		
Latitude (center of the fault)	44.854	± 0.8 Km)
Longitude (center of the fault)	11.068	± 0.8 Km
Depth	from 8 to 10 km	
Strike (°)	97	$\pm 10.0^\circ$
Dip (°)	34	$\pm 5.0^\circ$
Rake (°)	93.0	$\pm 10.0^\circ$
Fault length (Km)	Range from 7.0 to 12.0 Km (conserving an area of 40 Km ²)	

Three different tests have been performed: first, the results obtained without considering uncertainties in the input parameters are presented. This corresponds to obtaining the Δ CFF using the central values reported in **Table VII.4**. The second case shows the results when we consider the uncertainties in the location, orientation slip and friction coefficient of the fault planes of both the source (event 1) and receiver (event 4) faults. Finally, the third case considers uncertainties in the same parameters as in the second case, but also introduces uncertainties in the geometry (W/L ratios) of both faults (keeping the resulting area of the fault plane constant).

Case 1: Coulomb stress calculations for fixed parameter values

Case 1 concerns the solution obtained when we assume fixed parameter values (i.e., without taking into account the uncertainties in the model parameters). **Figure VII.16a** shows the distribution of ΔCFF in a layer located at 10 Km depth (dashed line in **Figure VII.16b**) that intersects the fault plane of the receiver fault of interest (that of event 4). **Figure VII.16b** is a cross section in the direction XY represented in **Figure VII.16a**, where it is possible to see the receiver fault plane located close to a boundary zone of positive and negative ΔCFF values. This proximity to this transition zone between $\Delta\text{CFF}>0$ (and then areas of promoted failure) and $\Delta\text{CFF}<0$ (zones where failure is inhibited) provides further support to the necessity to consider uncertainties in the stress change analyses.

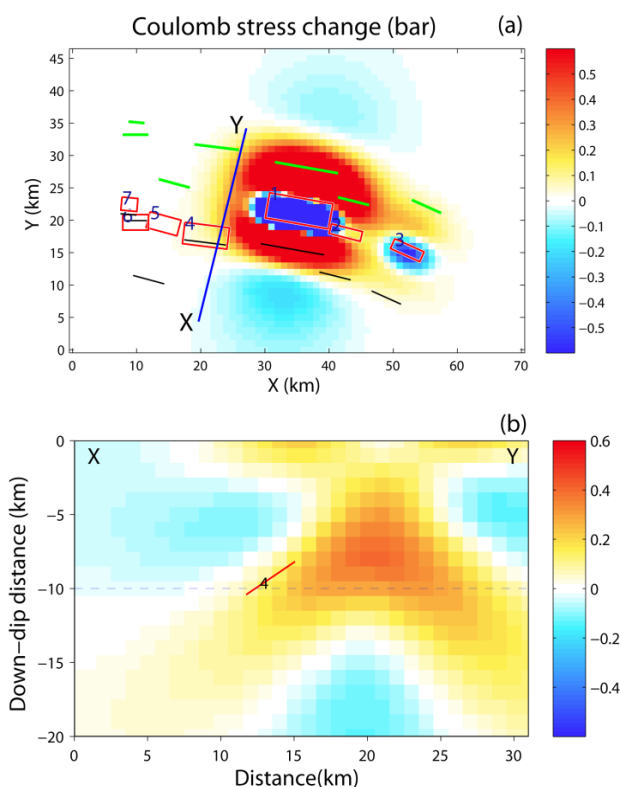


Figure VII.16 Cumulative stress changes due to the first three events calculated on the fault plane of event 4 (a) Horizontal ΔCFF projection on a layer located at a depth of 10km. Projections of the faults are represented by red rectangles. (b) Cross section (in the line XY represented in the panel a), where it is possible to see the intersection with the fault 4 (red line).

Considering in particular the ΔCFF values resolved for the specific fault planes of the receiver faults (4 to 7 in this solution), the results obtained are summarized in **Table VII.5**. Looking at the ΔCFF obtained for the receiver fault of interest (source of event 4), the average value of ΔCFF on the whole fault area is 8.61×10^{-2} bar. In the following sections we discuss the effects on the ΔCFF parameters of the uncertainties in the input parameters and compare the results with this value.

Table VII.5 Summary of Δ CFF values calculated for the element's rake (fourth column) and for the optimum rake (Δ CFF and optimum rake values are presented in the fifth and sixth columns, respectively). Δ CFF values for the other receiver faults (5 to 7) are presented for reference.

Event No.	Date	Time (GMT)	Δ CFF individual rake (bar)	Δ CFF for optimum rake (bar)	Optimum rake (°)
4	29/05/2012	07:00	8.61×10^{-2}	1.10×10^{-1}	60.4
5	29/05/2012	10:55	2.81×10^{-2}	2.83×10^{-2}	95.3
6	29/05/2012	11:00	9.10×10^{-3}	1.21×10^{-2}	68.1
7	03/06/2012	19:20	8.70×10^{-3}	8.70×10^{-3}	95.7

Case 2: effects of uncertainties in the focal parameters

Using Monte Carlo sampling, 1500 scenarios of model parameter values of the source and receiver faults parameters (location: latitude, longitude, depth of the center of the plane, orientation: strike and dip, slip (only source fault): value and direction, and friction coefficient) were generated and used to compute the randomized Δ CFF value. The results presented here were obtained by modeling the parameter uncertainties using a Uniform distribution with boundary values defined using the respective ranges and central values defined in **Table VII.4**.

Δ CFF were calculated for each of the sampled scenarios and the results were plotted as histograms and exceedance probability curves (defined as $1 - \text{CDF}$) to represent the probability that a given Δ CFF value is exceeded. **Figure VII.17** shows the results obtained for the Δ CFF values obtained for the receiver fault with respect to the individual rake (i.e., in the direction of the rake, left plots), and those obtained for an optimal rake (right plots). The curves plotted at the top directly provide the probability that any Δ CFF value is exceeded, and from these we can estimate that the probability that Δ CFF > 0 (and then, that failure in fault 4 could be promoted by the stress change produced by the previous events) is about 0.9 for the individual rake solution, and about 0.95 for the optimal rake. It is worth nothing that the Δ CFF value obtained considering the fixed parameters and shown in the previous paragraph is located within the 90% confidence interval defined for Δ CFF.

Case 3: same as previously but s introducing uncertainties into the fault geometry

Finally, for the third case we consider the uncertainties in the same parameters as in the second case, introducing also uncertainties in the geometry (W/L ratios) of both faults (keeping constant the resulting area of the fault plane). As in the previous case, **Figure VII.18** shows the results obtained for the Δ CFF values obtained for the receiver fault with respect to the individual rake (left), and the values obtained for an optimal rake (right). In this case the probability that Δ CFF > 0 (and therefore, that failure in fault 4 could be promoted by the stress change produced by the previous events) is about 0.8 for the individual rake solution, and about 0.9 for the optimal rake.

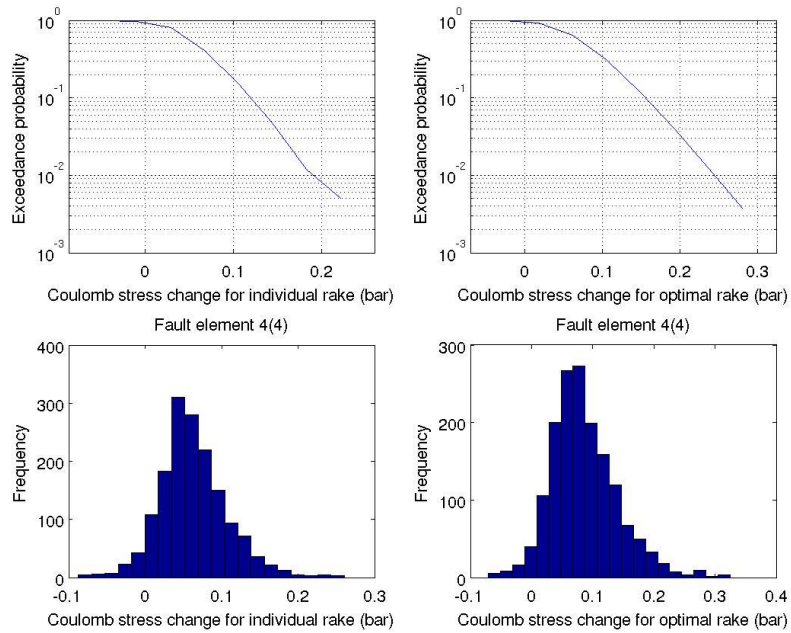


Figure VII.17 Exceedance probability curve and histogram of the CFF calculated for the individual rake (i.e., the rake direction of the fault 4 rupture, left), and for and 'optimal rake' (e.g., rake in which CFF is maximized, right).

In this case, adding the uncertainties in the fault plane geometry, the values of CFF obtained reach values with about one order of magnitude higher than those obtained in the previous cases (in the case 1, but also in the cases considering other source locations as those presented in [164] and [168]).

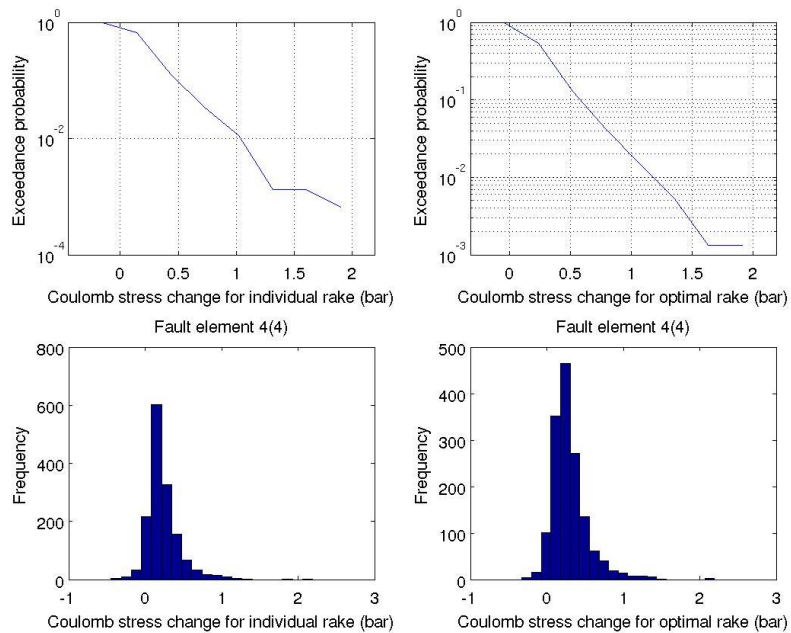


Figure VII.18 Exceedance probability curve and histogram of the CFF calculated for the individual rake (i.e., the rake direction of the fault 4 rupture, left), and for and 'optimal rake' (e.g., rake in which CFF is maximized, right).

It can be seen that the uncertainties in the parameters of orientation of the fault (strike and dip), which are in the in the order of 5° to 12° , have little effect on variations of the ΔCFF

values. Likewise, given the fault location uncertainties, the depth looks more sensitive to the resulting uncertainties in ΔCFF . Even though we have not carried out a separate analysis of the effects of the uncertainties in the friction coefficient, it looks like these uncertainties in the defined range have little effect with respect to the other uncertainties considered. Conversely, when considering uncertainties on the fault geometry (in terms of W/L ratio), the range of variation of the ΔCFF values increases by about one order of magnitude (see e.g., **Figure VII.18**). Note that in this case the fault areas were kept constant but uncertainties in the area could be considered as well so the uncertainty range could further increase.

Case 4: considering the effects of uncertainties in the fault plane area

All the three cases analyzed up to now have considered a constant fault plane area. In order to assess the effects of uncertainties in the fault plane area (added to all the other uncertainties considered in the case 2 of the previous section), in this section we consider four scenarios resulting from the combination of two limit values of fault plane areas for the first event (May 20, 2012), and two limit values of fault plane area for the main event of May 29, 2012 (acting as source and receiver faults, respectively, as in the previous exercises). The limit values for the fault areas have been determined as the maximum and minimum area reported in literature for the source of the two events. The four scenarios are summarized in **Table VII.6**.

Table VII.6 Summary of the four scenarios defined to assess the effects of uncertain fault areas

Scenario No.	Source fault area (km ²)	Receiver fault area (km ²)
1.	34	22
2.	34	68
3.	100	22
4.	100	68

Figure VII.19, Figure VII.20, Figure VII.21, and Figure VII.22 summarize the results obtained for this test (one for each scenario). In all of the cases, the probability that $CFF > 0$ is $> 80\%$. In particular, $p(CFF > 0) \sim 80\%$ in the scenario 1, whereas $p(CFF > 0) \sim 90\%$ in all the other three scenarios. It is worth noting that these results are in full agreement with the results already found in the previous section, i.e., that considering the uncertainties in the model parameters to calculate the Coulomb failure criteria, the probability that CFF is positive (and then, that the fault plane of the main event on May 29, 2012 was located in an area in which rupture was stimulated) is $> 80\%$.

Another interesting observation that can be drawn from these scenarios is in the relationship between the range of variability of the obtained values of CFF (for a given scenario) and the fault plane area. In fact, looking at the range of values of CFF obtained for the different scenarios (see e.g., the exceedance probability curves in Figures 6 to 9), it is worth noting that for the first two scenarios the maximum CFF values are smaller than the maximum values obtained for the other two scenarios (i.e., 3 and 4). In fact, the maximum CFF value obtained in the scenarios 1 and 2 simulations are, respectively, ~ 0.5 and ~ 0.4 ; conversely, the maximum CFF values for the scenarios 3 and 4 are ~ 1.3 and ~ 2.0 , respectively. Note that the first two scenarios were simulated adopting a smaller area for the source fault respect to the source area used for simulations in scenarios 3 and 4, highlighting the important effect of the source fault area on the (absolute) value of the CFF.

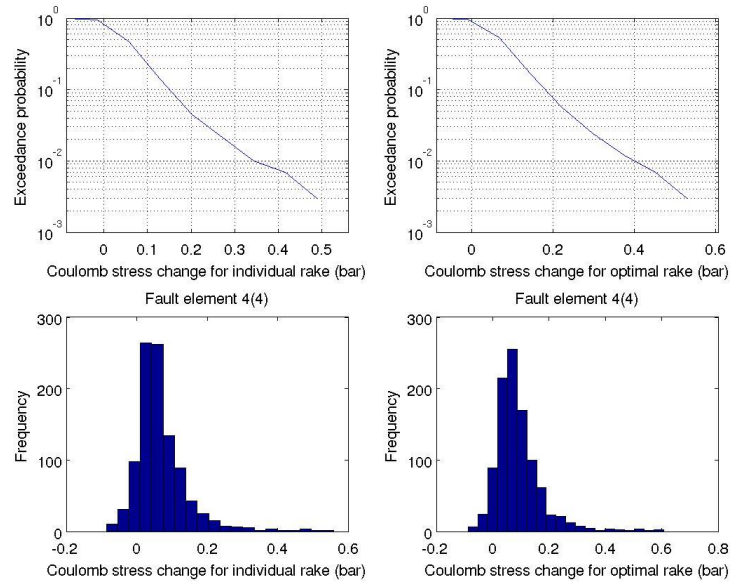


Figure VII.19. Exceedance probability curve and histogram of the CFF calculated for the individual rake (i.e., the rake direction of the fault 4 rupture, left), and for and 'optimal rake' (e.g., rake in which CFF is maximized, right). Scenario 1: Area source fault: 34km^2 ; area receiver fault: 22km^2 .

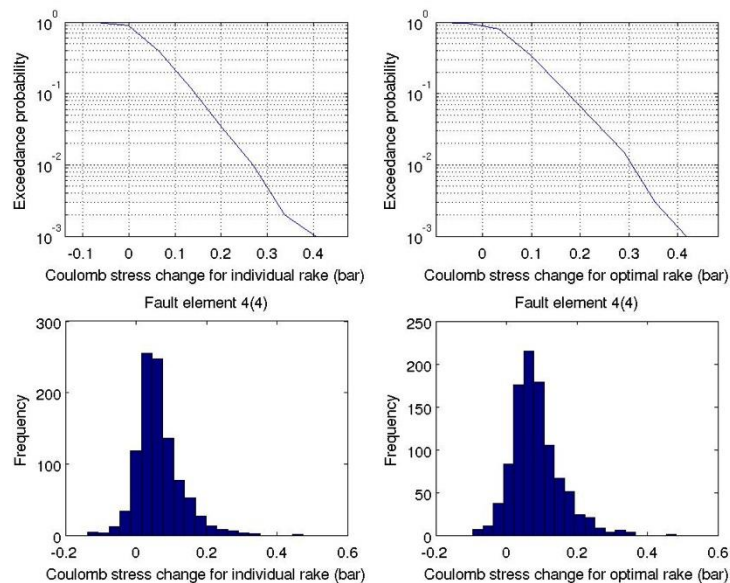


Figure VII.20 Exceedance probability curve and histogram of the CFF calculated for the individual rake (i.e., the rake direction of the fault 4 rupture, left), and for and 'optimal rake' (e.g., rake in which CFF is maximized, right). Scenario 2: Area source fault: 34km^2 ; area receiver fault: 68km^2 .

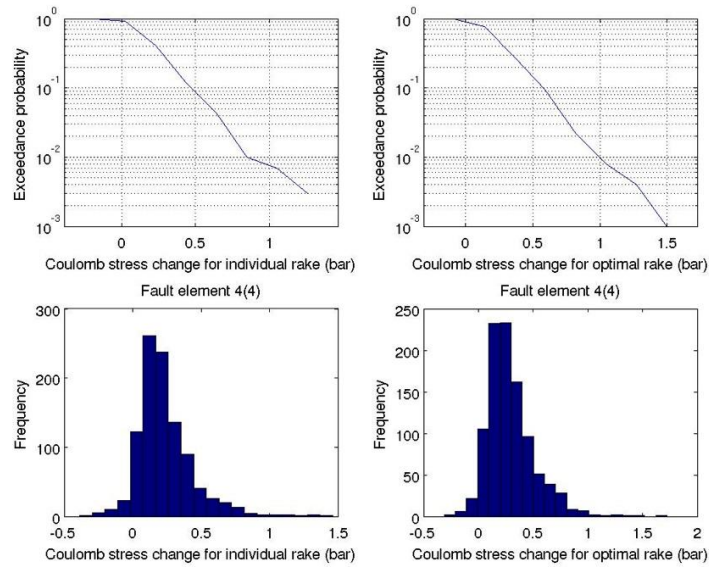


Figure VII.21 Exceedance probability curve and histogram of the CFF calculated for the individual rake (i.e., the rake direction of the fault 4 rupture, left), and for and 'optimal rake' (e.g., rake in which CFF is maximized, right). Scenario 3: Area source fault: 100km²; area receiver fault: 22km².

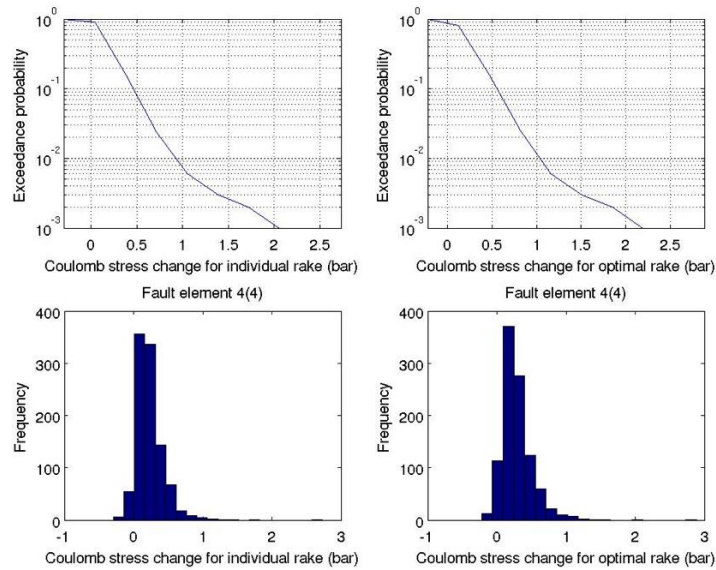


Figure VII.22 Exceedance probability curve and histogram of the CFF calculated for the individual rake (i.e., the rake direction of the fault 4 rupture, left), and for and 'optimal rake' (e.g., rake in which CFC is maximized, right). Scenario 4: Area source fault: 100km²; area receiver fault: 68km².

C. Reservoir model

1. General overview

The Cavone reservoir spans over an area of more than 15 km² and at a depth of about 2900m. It can be divided in 6 blocks (A-F), being called “block A” the most western one and “block F” the most eastern one. Production started in 1980, in 1987 the blocks A-E were in production and in 2005 the block F was put into production through the well San Giacomo1.

Oil bearing rocks are located in different units and even the same rock unit can be at different depth, depending on the well location. The same rock unit may be oil producing in one block and water producing in another.

All the water filtered out of the production fluid is reinjected into the aquifer in the well Cavone 14, located in block D. Water is reinjected at hydrostatic pressure into a deep confined aquifer. From the pressure recordings (wellhead) an increase in injection pressure is visible, for the days where pumping is 600 m³, the pressure goes up roughly 5 bar per day, while during no flow period, pressure goes down roughly 10 bar per day (reading values before and after the pause in re-injection). The injection pressure, lower than the minimum horizontal stress, excludes the possibility of unintentionally created new fractures. The decay in the overpressure indicates rapid dissipation of pore pressure, therefore the pressure perturbation will be acting only locally around the well.

In a compressional tectonic regime, triggering of earthquakes outside the reservoir volume is promoted by the reduction of pore pressure in the reservoir, therefore water injection in Cavone case may even stabilize the seismogenic reverse faults. It must be noted that reservoir depletion may be a triggering cause for earthquake, but there is no 1 to 1 connection between pressure decrease and triggering of seismicity.

With available informations, the blocks A-E are hydraulically connected, block F seems to represent an independent compartment with respect to the other 5 blocks. The extraction of fluid from well SG1 (with the ratio water-to-oil up to 8 to 1) and the reinjection of produced water into well Cavone14 then creates an imbalance in block F. The hydraulic model provided by ENI has been analyzed to investigate the permeability and the hydraulic behavior of the reservoir, while a semi-analytical mechanical model has been developed to evaluate if depletion in block F can be a trigger even without having direct hydrologic connection [4].

2. Hydraulical model

In order to understand the hydraulic behavior of the Cavone field during production, a numerical model was built by ENI to match production history for the years 1979-1985 and to forecast the future behavior of the reservoir. This "black-oil" model takes into consideration the relative saturation of the water/oil component and pressures. The model is based on the values obtained from the well cores for porosity of the layers and for the relative and absolute permeability.

Values have been introduced into a grid of 35 cells in the x direction times 9 cells in the y direction (**Figure VII.23**) and 6 layers. The cells are then grouped in 9 units (**Figure VII.24**), with blocks cut by normal faults oriented N-S, to introduce different permeability values for the same layer to match interference between wells and field behavior.

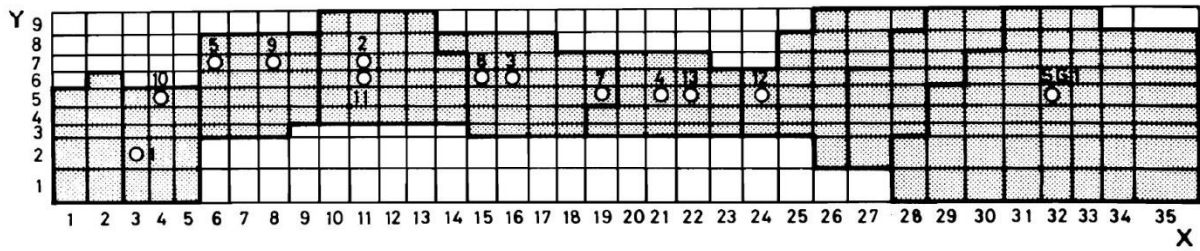


Figure VII.23 Numerical model grid of the field.

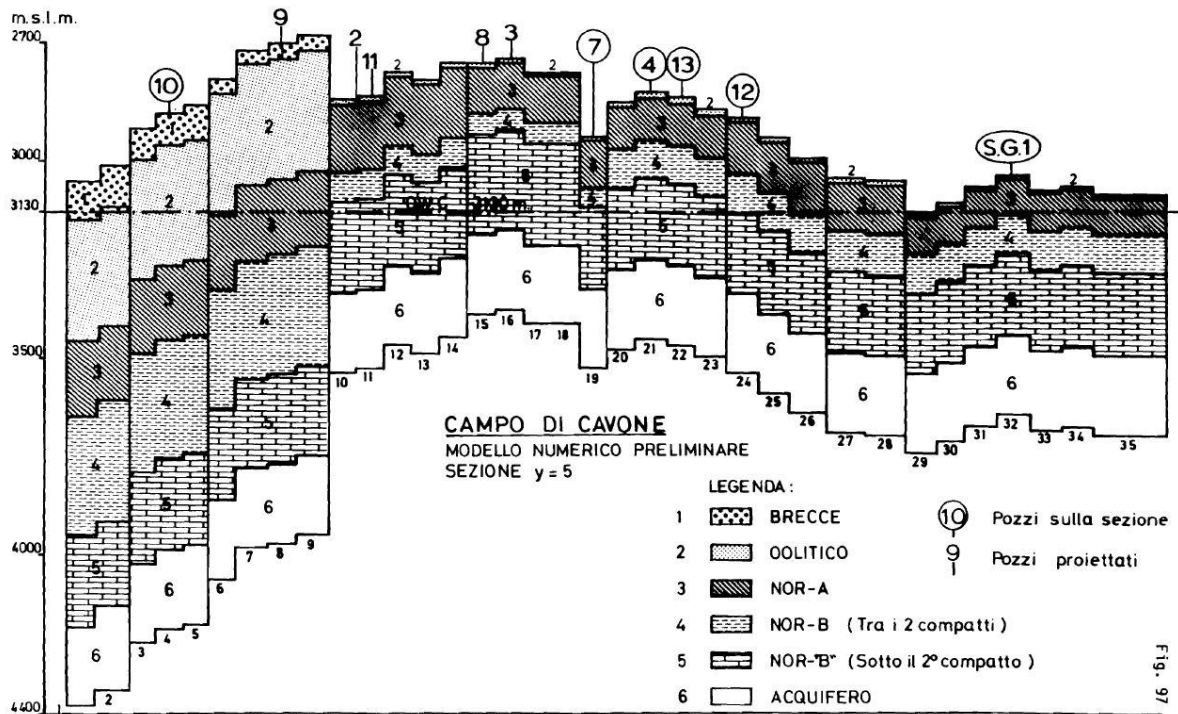


Figure VII.24 Section of the model, with the 6 layers. Circled numbers are the wells that lie in the plane of the section, the others are projected.

The model is a single-porosity type and therefore faults and fractures are taken into account only as increased permeability and averaged porosity for the cell. In the model hydraulic communication between the well SG1 and the Cavone wells is possible.

The model reproduces fairly well the first 6 years of production of the reservoir and it confirms the sealing zone between the Cavone wells and San Giacomo wells, since pressure decline/increase computed for well SG1 due to the activity in the blocks A-E are not consistent with recorded field data, implying that the communication with block F is much poorer or even absent.

The conclusion from the model of the ENI authors is that compressibility of the rock/fluid system, obtained from rock samples, is not sufficient to sustain pressure. Therefore, in the Eastern and Western parts of the field a strong lateral aquifer is acting to sustain pressure in oil producing wells of blocks A-E. It is not clear how this laterally acting aquifer is introduced into the model, probably as a boundary condition.

The underlying aquifer influence is limited to the NOR-B layer, especially for the wells located in the central part of the blocks. The assumption of a strong lateral aquifer also requires high permeability in the layers OOLITICO and NOR-A. The authors say this is proven by high transmissibilities recorded in production tests from wells 3-7-2. This has to be considered with some care because the permeability value used in the model is 3 times higher

than an average estimate of permeability from the reported production tests. Unfortunately, vertical inflow from overburden units is excluded by model definition, since the cap rock is included in the model as a top boundary condition.

However in our point of view, the strong lateral aquifer is still only an assumption and is not a confirmed phenomenon. Otherwise, vertical faults separating the blocks should play a role and results from production tests should not be generalized because their values may be restricted by the single tested well. Water produced from some wells close to the faults presents salinity compatible with water from the overburden unit "SCAGLIA CALCAREA", showing possible vertical flow of water, even from the overburden units.

In addition, the model is only hydraulic, therefore subsidence/compaction effects cannot be evaluated. It is our recommendation that a coupled hydro-mechanical model should be implemented to take into account possible pressurization from subsidence/compaction and changes in permeability from the fractures. A coupled model can also evaluate the effects of injection and production from blocks A-E and the production from block F, since the balance between volume injected/produced plays a significant role and different subsidence/compaction scenarios will arise considering how much fluid is produced and re-injected or transferred into each block.

From the AGIP report of 1994 (Appendix D), we know that when the MARKER layer is intact, wells completed in the NOR-B layer present pressures much higher than NOR-A and close to initial field pressure even after some production. This does not hold true for wells completed in OOLITIC layer or NOR-A layer. The SanGiacomo1 well is drilled in the central part of the block F, close to the hinge, where the marker layer is expected to be intact, hydraulically separating the layers NOR-A and NOR-B.

For the Cavone field, we can see the different trend in **Figure VII.25**, with a stronger decline in pressure for the well producing from OOLITIC and NOR-A: it must be added that the recovery in pressure also depends on the reinjection of water. In the same picture, the pressure readings for well SG1 varies with time but they are not dependent on expected (calculated via history matching model) pressure changes due to production from the other wells.

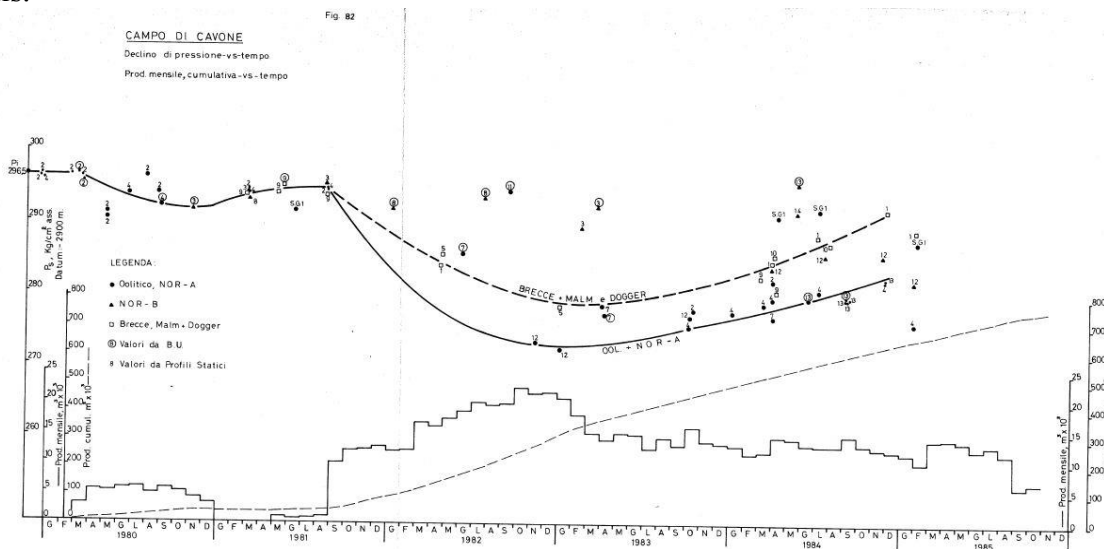


Figure VII.25 Static pressure recording and production curves at the beginning of the production in Cavone.

In conclusion, the hydraulic model, the production and the injection pressure recordings show that:

- small reservoir pressure drop and increased water content with production mean the reservoir communicates laterally and vertically with the aquifer;
- the rocks surrounding the reservoir and hosting the aquifer show good porosity and permeability, therefore overpressure due to water re-injection will decay rapidly;
- water can move vertically through some of the faults;
- contiguity of aquifer and reservoir in the blocks E-F does not imply communication.

3. Geomechanical model

The well-known picture (**Figure VII.26**) from Segall [141] regarding depletion, states that:

- normal faulting is promoted on the side of the reservoir;
- reverse faulting is more likely to occur above/below the reservoir.

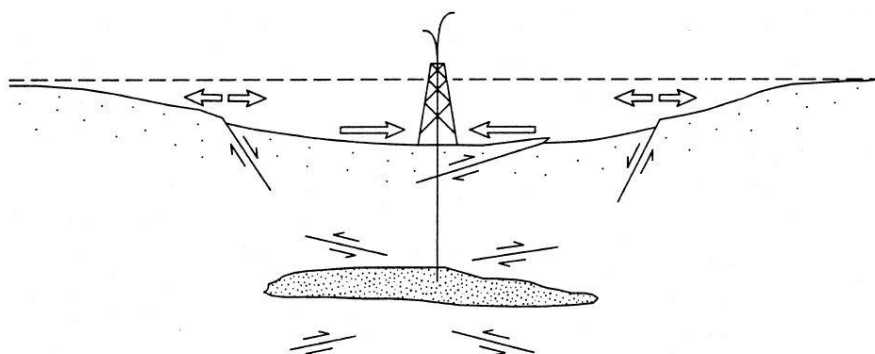


Figure VII.26 Different behaviour of stress changes (direct pressure increase can re-activate any faulting in any location) from [141].

This can be re-interpreted as:

- extension of the overburden bringing thrust faults to a more stable state (if normal faulting is promoted, thrust faulting is inhibited);
- compression of the overburden bringing thrust faults to failure;

Therefore, if only thrust faulting is taken into account, reservoir depletion may induce seismicity by stress change mainly below/above the reservoir whereas pressure diffusion can be more or less isotropic in promoting seismicity.

A conceptual model of Cavone field divided in 6 blocks (**Figure VII.27**) can help describing the temporal and spatial changes in the operations and in the reservoir behaviour. The amount of subsidence recorded above hydrocarbon reservoir generally depends linearly on the pressure decrease in the reservoir, however a delay of up to 10 years has been observed between the start of depletion and the time subsidence start taking place. Unfortunately, the subsidence profile recorded by means of geometric levelling along paths located in proximity of well SG1 in the years 2006 and 2008 are not directly comparable

among them (due to problems with the absolute reference point location). Since the well started production in 2005, even if those readings were comparable they may not yet represent the correct subsidence development of the field. A precise evaluation of subsidence-depletion cannot be achieved also due to missing data about rheological properties of the overburden.

To evaluate the stress changes that can be induced we will follow the approach of [141] and [142]. These approaches are based on the inclusion theory, reservoir allowing for calculation of stress and strain in an elastic media due to a deformed inclusion (the depleted). Since the pressure in block A-E is assumed to be maintained by the aquifer, the mechanical model mimics only the block F. Area of the reservoir in block is assumed to be 1 km x 1km and thickness 20m, on the base of **Table VII.7**. Regarding pressure drop, a trend similar with what happened in the blocks A-E in the first 2 year of production (i.e. without reinjection) is expected in San Giacomo compartment. We assume therefore a pressure drop of 10 bar in block F due to the production which started in 2005 (cumulative oil and water produced until May 2012 from block F ~90'000 m³, close to the cumulative production from January 1980 to December 1981 in the other five blocks).

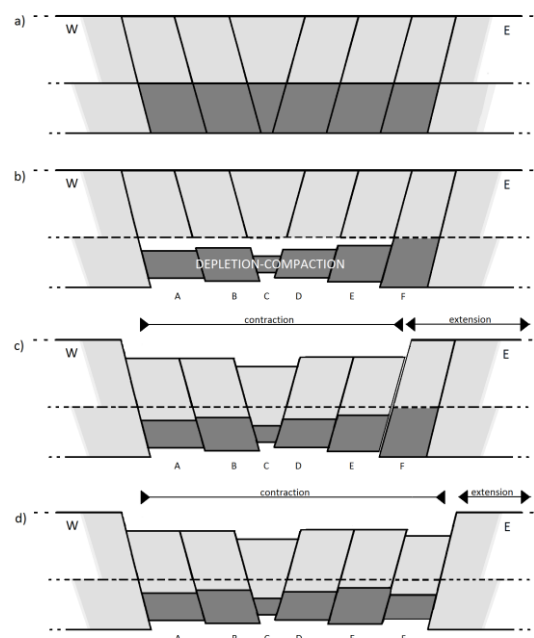


Figure VII.27 Conceptual model of deformations along the W-E axis. The dipping of the faults separating blocks is exaggerated. Dark gray represents oil bearing units. (a) initial situation; (b) first depletion and reservoir compaction, blocks A-E, years 1980-2005, block F remains pressurized because hydraulically separated; (c) San Giacomo 1 (SG1) well enters into production, depletion of block F starts; (d) change in stress regime above block F → change from stabilization to promotion of shearing of reverse fault.

The presence of a free surface changes the distribution of the stresses with respect to the zone above the reservoir, so the problem to be solved can be reduced to the elastic strain inclusion in a half-space, unless the width of the reservoir is much smaller than the depth. **Figure VII.28** shows a sketch of the problem to be solved.

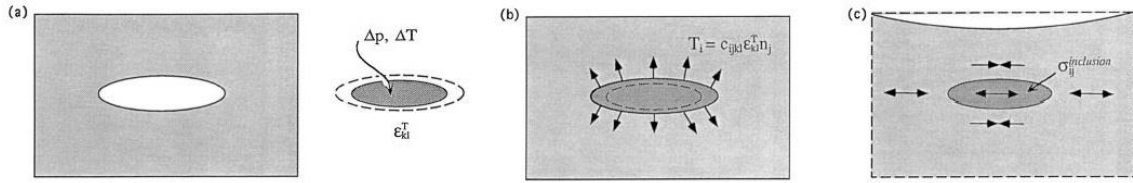


Figure VII.28 Schematic illustrating the sequence of steps needed to compute the stress in the reservoir. (a) The ellipsoidal reservoir is removed from the earth. Fluid and heat are extracted causing the pore pressure and temperature to change by Δp and ΔT ; respectively. This causes the reservoir to undergo a ‘transformation’ strain T_i : (b) Tractions are applied to the boundary of the reservoir such that the elastic strain is equal and opposite to the transformation strain. At this point the reservoir fits exactly back into the earth. (c) The reservoir is glued back in place and the surface tractions relaxed. This results in a uniform stress within the reservoir $\sigma^{inclusion}$ (from [141]).

The semi-analytical solution proposed by [142] allows calculation of the change in Coulomb stress for a pre-determined fault orientation, by assuming a reservoir under plane strain conditions with elliptical cross-section. Being a semi-analytical solution, it assures a fast solution time, but has one limitation in its present form, in that the properties of the rock containing the reservoir and the reservoir itself must be identical.

From this model we obtain a distribution of the “fault reactivation factor” (λ) which is the ratio between the change in Coulomb failure stress and the traction due to reservoir depletion:

$$\lambda = \frac{\Delta CFS}{\alpha \Delta P}$$

We will assume α , the Biot’s coefficient, equal to 1, while the pressure depletion will be 10 bar (1 Mpa). The distribution of the fault reactivation factor (λ) for a fault dipping at 30° in a thrust tectonic regime is depicted in **Figure VII.29**.

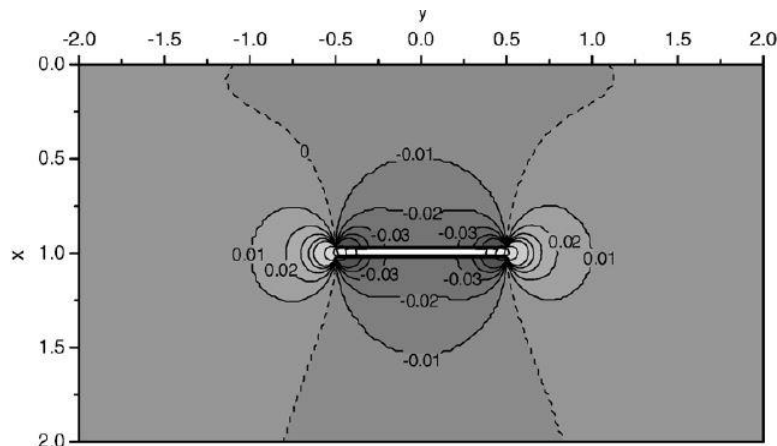


Figure VII.29 Distribution of fault reactivation factor (λ) in a thrust fault regime for a horizontal rectangular reservoir with a fault dip angle of 30° . Distances normalized to reservoir width. To obtain the ΔCFS values must be scaled with $\alpha \Delta p$.

Since the expected pressure change is -1 MPa, the Coulomb stress change is the opposite of the fault reactivation factor seen in the picture. The threshold determining a significant ΔCFS of 0.01 MPa is still debated in the scientific community.

For the Emilia earthquake and for the fault ruptured on the 29th of May evaluating the aftershock decay-time in [99] a threshold value 2 to 5 times lower has been calculated (0.002 to 0.005 MPa).

From the mechanical model results we can conclude that:

- the location of the 20th May 2012 earthquake is expected to stay outside the area of influence.
- the location 29th of May 2012 Earthquake is in a zone where the Coulomb stress change is positive, but smaller ($3 \cdot 10^{-4}$ MPa) than the threshold value and smaller than the stress transfer due to the 20th of May earthquake.

D. Statistical analysis of seismic series and production data

This section presents statistical analyses of seismicity that occurred in the study area prior to the earthquake from May 20th, 2012 (from now on denoted as E20), and its possible correlations with production and injection data of the Mirandola concession.

1. Analyzed data

Seismic

The seismic data has been provided by the Istituto Nazionale di Geofisica e Vulcanologia (INGV). At the beginning of 2005 modifications were made to the seismic network. Therefore in order to ensure homogeneity of seismic information only the data from the period from May 1st, 2005 to May 19th, 2012 is included in this investigation. The studied data consists of 120 events in the magnitude range from 1.3 to 4.1ML. The occurrence time, geographical coordinates of epicenters, hypocentral depth and magnitude parameterize the events. Hypocenters of some of events have been relocated.

In addition to the above-mentioned information, occurrence times, hypocentral locations and magnitudes of seven major shocks, M5+, from May-June 2012 have been used. From now on two of them, the M5.9 event from May 12th, 02:03:52 and the M5.8 event from May 29th, 07:00:03 are denoted as E20 and E29, respectively.

Production

The analysis of production data has only been carried out on the data from the Mirandola concession due to its proximity to E20 location. The analyzed production data consists of monthly production levels of oil and gas, daily volume injected through the well C14 and daily well-head pressure. This data spans the same period as the seismic data, namely May 1st, 2005 to May 19th, 2012.

The small size of the seismic data set requires we make analyses with a time unit of no less than one month. A one-month time unit has therefore also been used for the oil and gas production data. Due to that, the injection data has been converted into monthly averages.

Injected volume in a month is parameterized by

$$\text{Average volume injected} = \frac{\sum_{i=1}^m V_i}{m}$$

where V_i is the total volume injected in day i , and m is the number of days in the month.

The input information on well-head pressure is apparently incomplete. Occasionally pressure information is missing or is set to zero while the volume injected is not zero. Therefore injection pressure in a month is averaged in a different way. The used parameter is:

$$\text{Effective average pressure} = \frac{\sum_{i=1}^m P_i}{m_+}$$

Where P_i is the well-head pressure in day i , and m_+ is the number of days in the month, in which the well-head pressure was non-zero.

2. Seismic data analysis

Catalog completeness

The range of magnitudes of the seismic events that occurred before May 20th 2012 is 1.3 – 4.2. **Figure VII.30** presents a histogram of magnitude. It is clear that the data is incomplete below magnitude 2.0M_L.

Figure VII.31 presents histograms of magnitude for events from selected shorter time periods:

Figure VII.31a: 01/05/2005-31/10/2009, 60 events;

Figure VII.31b: 01/11/2009-19/05/2012, 60 events;

Figure VII.31c: 01/05/2005-31/12/2008, 46 events;

Figure VII.31d: 01/01/2009-31/12/2010, 38 events;

Figure VII.31e: 01/01/2011-19/05/2012, 34 events.

As can be seen, the completeness level does not change. It is the same, and equal to 2.0, regardless of the period of observation. Altogether there are 87 events in the complete part of the catalog.

A sample comprising 120 events acquired in seven years period is rather poor in order that more sophisticated statistical analyses, which include time changes assessments can be carried out. If we only had 75% of such a sample it would preclude any analysis at all. What then are the consequences, which result from including into a statistical analyses the incomplete part of the catalog as well?

The spatial distribution of events from an incomplete part of a catalog is altered artificially. The weak events that occur in favorable locations are recorded while those that occur in less favorable locations are not recorded. Therefore the spatial distribution of events from the whole catalog together with its incomplete part has an artificially increased density at some places and a decreased density at others. As long as a monitoring seismic network remains unchanged in geometry and also stations' sensitivity; the recording capability of this network and its effects i.e. the mentioned alterations of event spatial distribution are constant. Therefore the incompleteness has little influence on time changes of event rate.

The incompleteness can have an effect on the geographical distribution of events and its correlation with other geographical elements of an area under study. However, the locations of INGV stations, lie mostly far from the study area, and the fact that at least 5 stations were used to estimate earthquake locations suggest that the stations' distribution had little influence on the observed incompleteness. Hypocentral depth could be a more important factor. Therefore it can be expected that the incompleteness did not alter significantly the horizontal distribution of sources. Moreover, as long as conclusions do not concern relations between particular parts of the study area, their positive outcomes (e.g. that event epicenters correlate with a fault location) are correct overall.

In this connection, the whole catalog is used here when event rate changes are analyzed, when correlations between the preceding event and major shock locations are assessed and when a time-space clustering of events is studied. It can happen that because the incompleteness compromises spatial distribution of events correlations may be missed but if they are found they are genuine because they cannot be generated by a removal of some data points (incompleteness effect). Similarly, if some events turn out to form a time-space cluster, missing (not recorded) events could enrich this cluster but their absence has no effect on the fact that a group of recorded events is clustered.

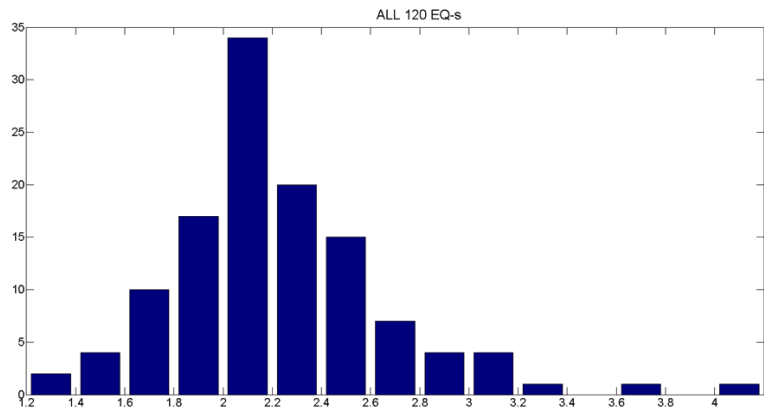


Figure VII.30 Histogram of magnitude for the whole data sample.

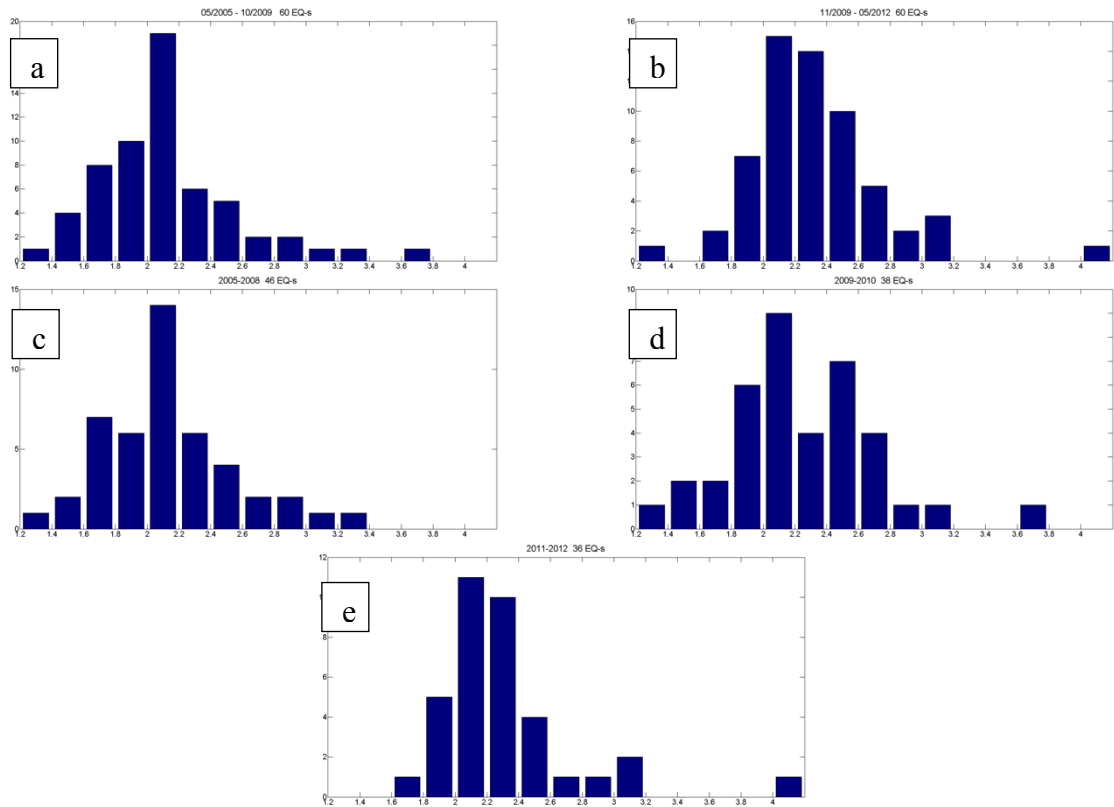


Figure VII.31 Histograms of magnitude for the data from shorter time periods.

Event rate

Earthquakes in the studied catalog are weak. The magnitude range is 1.3 – 4.1. The largest value, 4.1, was achieved only once for the last event before the mainshock E20. Events of magnitude 3+ can produce at best a few aftershocks in the range 1.3 – 3+, which cannot alter long term trends of activity.

If the studied earthquake series is a background seismicity sample without aftershocks then the event occurrences are the outcomes of a Poisson process with a constant event rate. For a Poisson process the time between every two consecutive events (the interevent time) has an exponential distribution. Therefore, to check whether or not the earthquake occurrences in the studied sample fulfilled conditions of a background seismicity occurrence process the null hypothesis:

H0(interevent time distribution is exponential)

is tested by means of the Kolmogorov-Smirnov test. The test is performed for both the whole data catalog, and the data from the complete part of catalog, i.e. for earthquakes of magnitude greater than or equal to 2. The test results are presented in **Table VII.8**. When all the events are taken into account the significance of H0 is low (below 6%) for the whole catalog, as well as for its subsets from shorter time periods. For the complete part of catalog the samples from the first years of observations (the second and fourth row) do not suggest a rejection of H0. However, these two periods had the lowest event rates and it is not clear whether the higher *p*-values indicate that H0 is true or they result from small size of the tested samples. Nevertheless, it is concluded that with the passage of time the occurrence process was beginning to deviate from Poissonianity i.e. it was becoming less similar to a background seismicity occurrence process.

Table VII.8. Results of Kolmogorov-Smirnov test of hypothesis

Time period	All data			Complete part (M≥2.0)		
	Sample size <i>n</i>	Significance of H0, <i>p</i>	Mean event rate [1/day]	Sample size <i>n</i>	Significance of H0, <i>p</i>	Mean event rate [1/day]
05/2005 – 05/2012	120	$1 \cdot 10^{-5}$	0.046	87	$8 \cdot 10^{-4}$	0.034
05/2005 – 10/2009	60	0.034	0.036	37	0.54	0.023
11/2009 – 05/2012	60	$2 \cdot 10^{-4}$	0.064	50	$8 \cdot 10^{-5}$	0.053
05/2005 – 12/2008	46	0.008	0.034	30	0.45	0.022
01/2009 – 12/2010	38	0.051	0.054	27	0.008	0.042
01/2011 – 05/2012	36	0.006	0.077	30	0.012	0.064

The mean rate estimates from **Table VII.8** suggest that the event rate was changeable, generally increasing with time for both the whole data as well as the complete part of the data. The rate changes are more clearly visible in **Figure VII.32**, which presents a graph of cumulative number of events versus time. Based on this graph 13 time periods of different event rate are distinguished, see **Table VII.9**. Event rate variations between the periods seem to be significant.

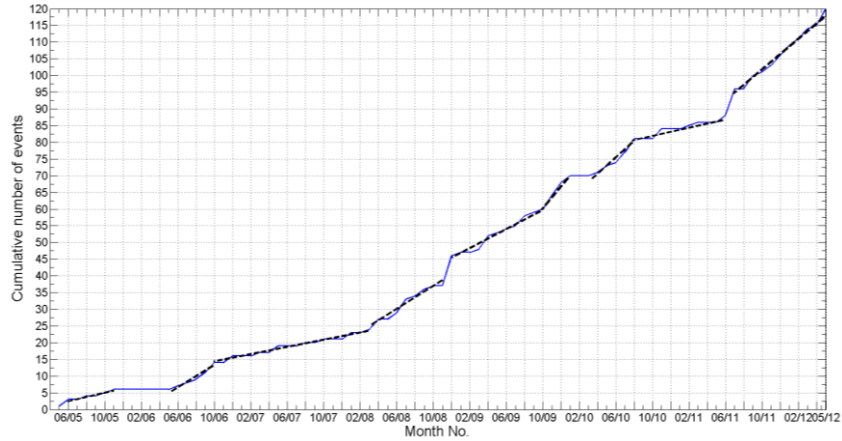


Figure VII.32 Cumulative number of events per month. The straight-line segments identify periods of approximately constant rate.

Table VII.9. Identified periods of different event rates.

ID number	Time period	No. of events / No. of months	Mean event rate [1/month]
1	05/2005 – 11/2005	6 / 7	0.86
2	12/2005 – 05/2006	0 / 6	0.00
3	06/2006 – 10/2006	8 / 5	1.60
4	11/2006 – 03/2008	10 / 17	0.59
5	04/2008 – 11/2008	13 / 8	1.62
6	12/2008	9 / 1	9.00
7	01/2009 – 10/2009	14 / 10	1.40
8	11/2009 – 01/2010	10 / 3	3.33
9	02/2010 – 03/2010	0 / 2	0.00
10	04/2010 – 08/2010	11 / 5	2.20
11	09/2010 – 05/2011	5 / 9	0.55
12	06/2011 – 07/2011	10 / 2	5.00
13	08/2011 – 05/2012	24 / 10	2.40

Magnitude distribution

The Gutenberg-Richter statistical law :

$$\log n(M) = a - bM, \quad M \geq M_c,$$

where $n(M)$ is the number of earthquakes of magnitude M , M_c is the magnitude completeness level, and a , b are constants, characterizes well the magnitude distribution of background seismicity, while it is often violated for induced seismicity. If the Gutenberg-Richter law is obeyed then the magnitude distribution is a left hand side truncated exponential distribution of the cumulative distribution function:

$$F(M) = \begin{cases} 0, & M < M_c \\ 1 - \exp[-\beta(M - M_c)], & M \geq M_c \end{cases}$$

where $\beta = b \cdot \ln(10)$, and b is the Gutenberg-Richter b-value.

In order to test whether or not magnitudes from the complete part of the studied seismic catalog follow the Gutenberg-Richter law the null hypothesis:

H0(magnitude distribution is (GR))

is tested by means of the Kolmogorov-Smirnov test.

The magnitude data is provided with only one digit after the decimal point. Because of that the analyzed sample of magnitudes contains repetitions and the Kolmogorov-Smirnov test cannot be used to test a sample with repeated values. Therefore the magnitudes are randomized within the round-off interval of 0.1, according to the procedure described in [169].

Results of the test applied to the randomized data are presented in **Table VII.10**. The null hypothesis significance is high for the complete data sample as well as for all its subsets.

Since the randomization process changes the sample data subtly so that it is slightly less likely to reject H0, the hypothesis has also been tested by the chi-square test applied to the original magnitude data. Chi-square test results confirm the results of Kolmogorov-Smirnov test. There is no statistical evidence of violation of the Gutenberg-Richter law.

The Gutenberg-Richter b-value is not, however, constant during the period of observation (see **Figure VII.33**). It takes a larger value for the period up to and including 31/03/2008 than for the period from 04/2008 – 06/2011 when on average the event rate increased. In the last time period, 07/2011 – 05/2012, the period of the next increase of event rate, b seems to decrease although due to small size of samples and hence wide error ranges this fact cannot be fully confirmed. Smaller b-values indicate an increased probability of generation of larger magnitudes and greater involvement of pre-existing faulting. It can be concluded from **Figure VII.33** that with respect to magnitude the seismic process under consideration was varying in time and that the potential to generate bigger events was generally increasing.

Such time variations of b-value are not observed for background seismicity.

Table VII.10. Results of Kolmogorov-Smirnov test of hypothesis

Time period	Sample size (No of events $M \geq 2$), n	Significance of H0, p	b-value
05/2005 – 05/2012	87	0.47	1.25
04/2008 – 05/2012	71	0.30	1.17
11/2009 – 05/2012	61	0.57	1.22
06/2011 – 05/2012	28	0.75	1.19

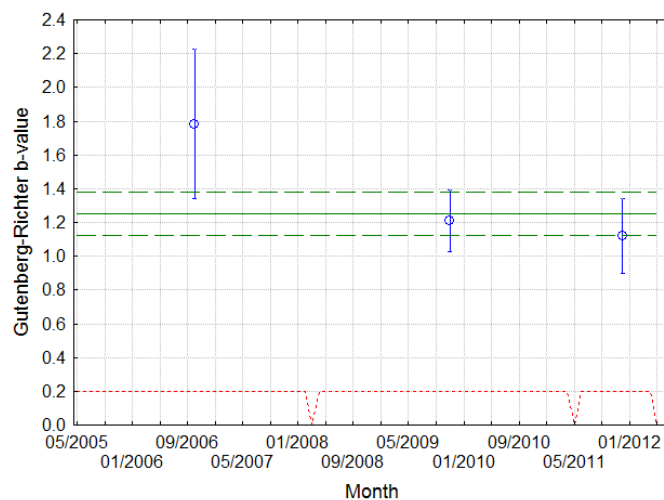


Figure VII.33 b-value estimates. The points are related to the periods 05/2005-03/2008, 04/2008-06/2011 and 07/2011-19/05/2012, respectively. Bars lengths are two standard deviations of the estimates. The green lines represent the b-value for the whole sample (solid) +/- one standard deviation (dashed).

Locations of events

The locations of the epicenters of the studied events, together with the locations of the 7 major shocks and active production/injection wells in Mirandola concession, are shown in **Figure VII.34**. The events are not distributed uniformly in the area under study. Some of them are, to some extent, organized along the line, along which the major shocks are located (solid line in **Figure VII.34**). It is a matter of question as to whether this line should be continued towards the west-south further than the dashed vertical segment, that is towards the western cluster of epicenters or not. However, a spatial connection between the major shocks' epicenters and the epicenters of weaker events located east from the dashed segment is clear .

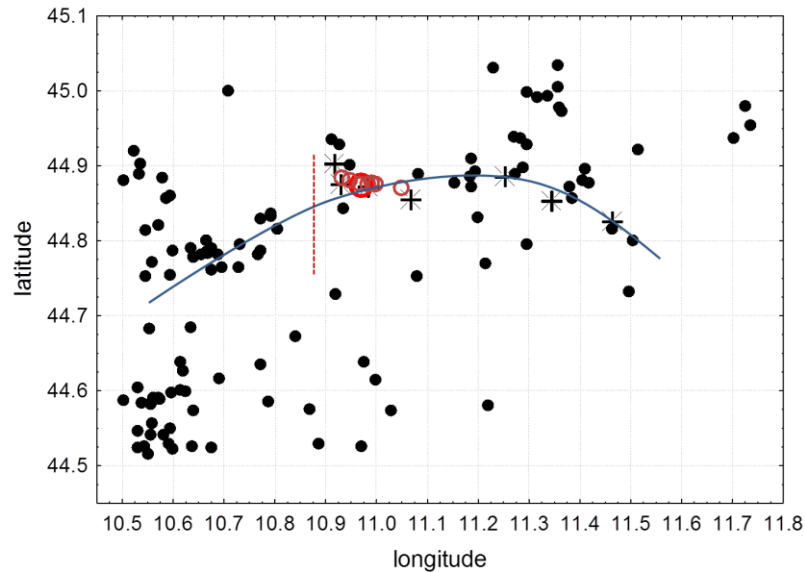


Figure VII.34 Locations of epicenters of events from the period 05/2005-19/05/2012 (black dots), epicenters of major shocks, M5+ (black crosses) and active wells of Mirandola concession (circles). The three crosses to the left of longitude 11.2 are E20 and the next two are from the sequence of seven major shocks,;the crosses on the right of longitude 11.2 are E29 and the next three events from this sequence. The big red circle marks the location of C14 injection well and the smaller brown circles denote the locations of producing wells.

The earthquake productivity in the vicinity of future major shock locations was uneven throughout the analyzed 7 years. This can be observed in **Figure VII.35**. Each part of the figure presents locations of earthquakes that occurred in a successive constant rate period from **Table VII.9**. These locations are superimposed on locations of events from previous periods. Events related to different periods are marked with different colors.

Events began to locate closer to the future major shocks only from period #5 i.e. from 04/2008 and continued to occur there until period #8 (until 01/2010). There were no events in this part of the area in periods #9 - #11 (02/2010 – 05/2011). After then the seismic events reappeared there during the period #12 and #13 (06/2011 – 05/2012), with an increasing rate by the end of period #13, just before E20.

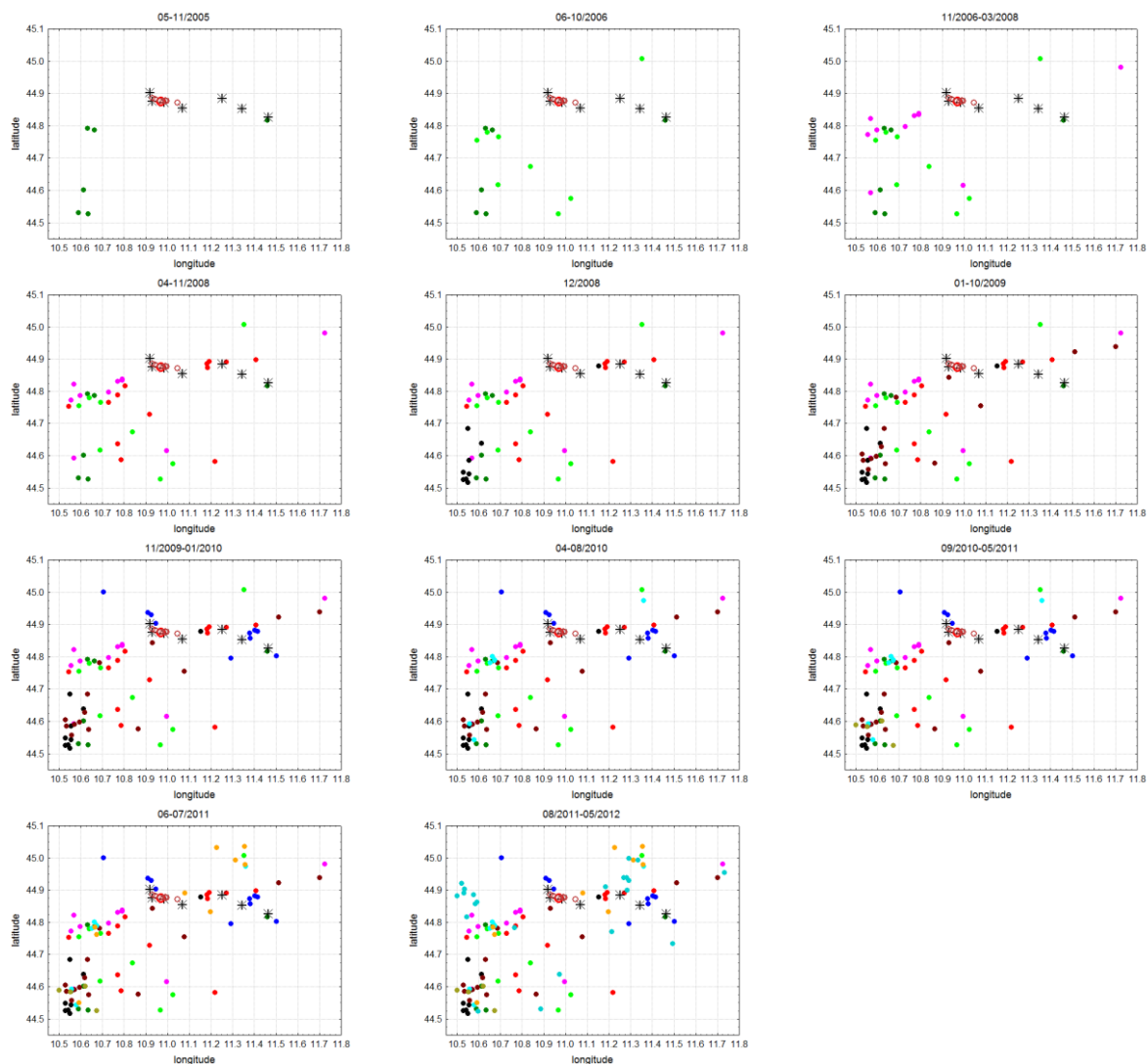


Figure VII.35 Epicenters of events from the constant rate periods defined in Table 2 (color dots). Each part of the figure presents locations of events from a respective time period superimposed on the locations of events from all previous periods. Events from different periods are drawn in different colors. Black crosses are the locations of major shocks (M5+) and circles are the locations of production/injection wells.

The sequence of major shocks splits into two parts:

- The first part starts with E20 and comprises three events and is located more towards the east, and the hypocentral depths of its events are between 4.2 and 5.5km.
- The second part starts with E29 and comprises four events located west of the first part. Foci of these events were generally much deeper than those of the first part events and with one exception (4.2km) they were below 8.5km. Epicenter locations of the major shocks of the second part are close to the locations of production/injection wells.

Although the depth estimates of weaker events are uncertain it is interesting to check possible correlations between the average depths of weaker event groups and the depths of major shocks. For this purpose the weaker studied events are divided into 6 groups according to the locations of their epicenters. The division is presented in **Figure VII.36**. The Z value in the figure legend is the average depth of events in a group and the number in parenthesis is

the standard deviation of the depth. In spite of the fact that depths are strongly dispersed within event groups – the standard deviation is of order of the mean value, a certain logic in the average depth values and their correlation with the major event depths can be found. The depth of events located close to the first part of major shock sequence (blue circles) is on average much shallower than the depth of events located close to the second part of the sequence (black squares). The average depth of the northernmost group of events is the smallest, which agrees with the geometry of the seismogenic zone.

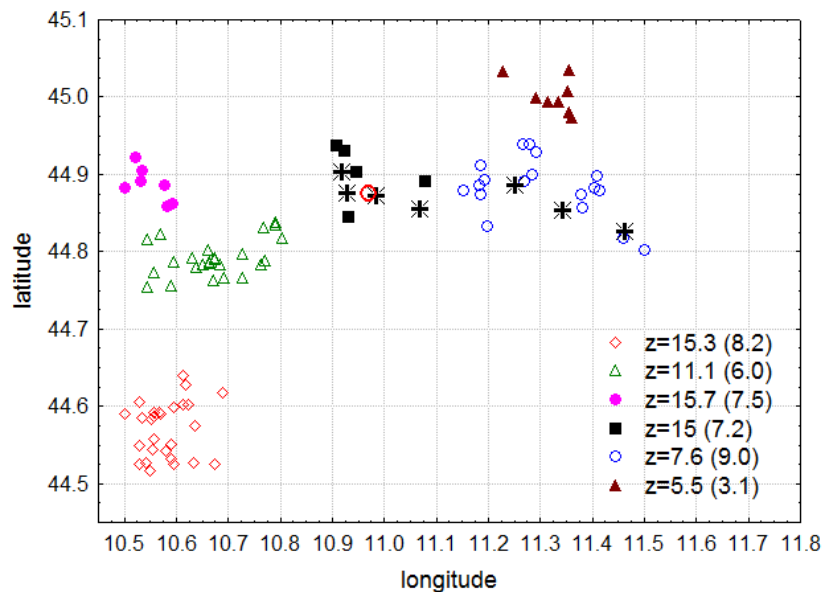


Figure VII.36 Selected groups of events and average hypocentral depths in the groups. See text for further explanations.

Time-space clustering

The weaker events we have studied, are irregularly located close to the locations of major (M5+) shocks; however, there were longer periods without such events, in which, other events, not so well spatially correlated with major shocks occurred.

There are events in the studied series, which are located in clusters at considerable distances from the major shock locations. These suggest that not all events from the studied catalog were related to the major shocks. A time-space hierarchical clustering procedure is applied to extract from the catalog, events which are connected in the time-space with the major shocks.

The procedure consists of two steps. First, occurrence times, latitudes and longitudes of all weaker events and the major shocks are transformed to equivalent dimensions. An equivalent dimension U of an earthquake parameter X is $U=F_X^{-1}(X)$, where $F_X^{-1}(X)$ is the inverse cumulative distribution function of X . The usually unknown distribution functions of earthquake parameters are replaced by their non-parametric, kernel estimates based on the whole available information (all catalog data) as sample data. Parameters transformed to equivalent dimensions scale in the same way, hence are comparable, and the metric of a multidimensional equivalent dimension space is Euclidean. Details on the transformation to the equivalent dimension method are in [170].

In the second step, the Ward's hierarchical clustering method with the Euclidean distance is used to construct a hierarchical tree. Results of the time-space clustering are shown in **Figure VII.37** in the form of a hierarchical tree plot, and a magnified part of the tree is presented in **Figure VII.38**. Seismic events are numbered in ascending order of occurrence

time. Events #121-127 are major shocks. **Figure VII.39** presents the linkage distance of consecutive clustering steps.

The graph in **Figure VII.39** indicates that most of clustering takes place at relatively short linkage distances, less than 2-3. There is no quantitative statistical method to determine at which linkage distance clustering is significant. However, the shape of the graph in **Figure VII.39** and the hierarchical tree plot in **Figure VII.37** suggest that genuinely clustered groups are those linked at a distance below 5. There may be some loose connection between groups linked at a distance of about six but the links at above seven seem to be only formal without signifying any actual connections between event groups. In this way the seismic data splits into three groups separated and distinct in time-space. The group to which all the major shocks belong is very far in time-space from the other two groups.

The seven major shocks form a strongly clustered group together with the five events from 18-19/05/2012 that directly preceded E20 (#116-120). This cluster is denoted as **1a**. Examination of the internal structure of **1a** shows that the major shock sequence splits into two parts. This division of major shocks into two parts is identical with that which has been done in the previous section. It is interesting that the first major shocks group consisting of E20 and the next two shocks is much more strongly linked to four weaker events immediately prior to E20 than to the subsequent four major shocks.

The second strongly clustered group, **1b**, consists of the 5 events, #89, #90, #101, #102 and #115, which occurred on 3/07/2011, 19/07/2011, 30/10/2011, 4/11/2011 and 11/04/2012, respectively. **1a** and **1b** join at the relatively short linkage distance of 1.29.

The next pair of clusters closely related to **1a-1b** pair is:

- **2a** comprising #77 from 26/07/2010, the series of six events: #92-97 from 27/07/2011 (first five events) and 11/09/2011 and #100 and #106 from 27/09/2011 and 27/12/2011, respectively;

- **2b** consisting of four events: #65-68 from 12/2009.

2a and **2b** join at the linkage distance of 1.48, and **1a-1b** group and **2a-2b** group join at 2.51.

The linked group of clusters **1a - 1b - 2a - 2b** has a weak connection, at the linkage distance of 5.73 with the other group of three clusters, namely:

- **3a** consisting of two events: #58, #59 from 25/08 and 22/09/2009, four events: #61-64 from 11/2009 and two events: #69, #70 from 01/2010;

- **3b** consisting of #29 (07/06/2007), three events: #32-34 (23/07/2008, 24/07/2008, 19/08/2008), and #38 (19/12/2008);

- **3c** consisting of #5 (30/10/2005), #8 (27/07/2006), #21 (06/10/2007), #26 (15/04/2008).

3b and **3c** join at the distance 0.77 and **3a** links to them at the distance 1.69. Due to the considerable linkage distance from **3a-c** to **1a,b-2a,b** group their actual connection is uncertain.

Figure VII.40 presents the locations of the clusters described previously.

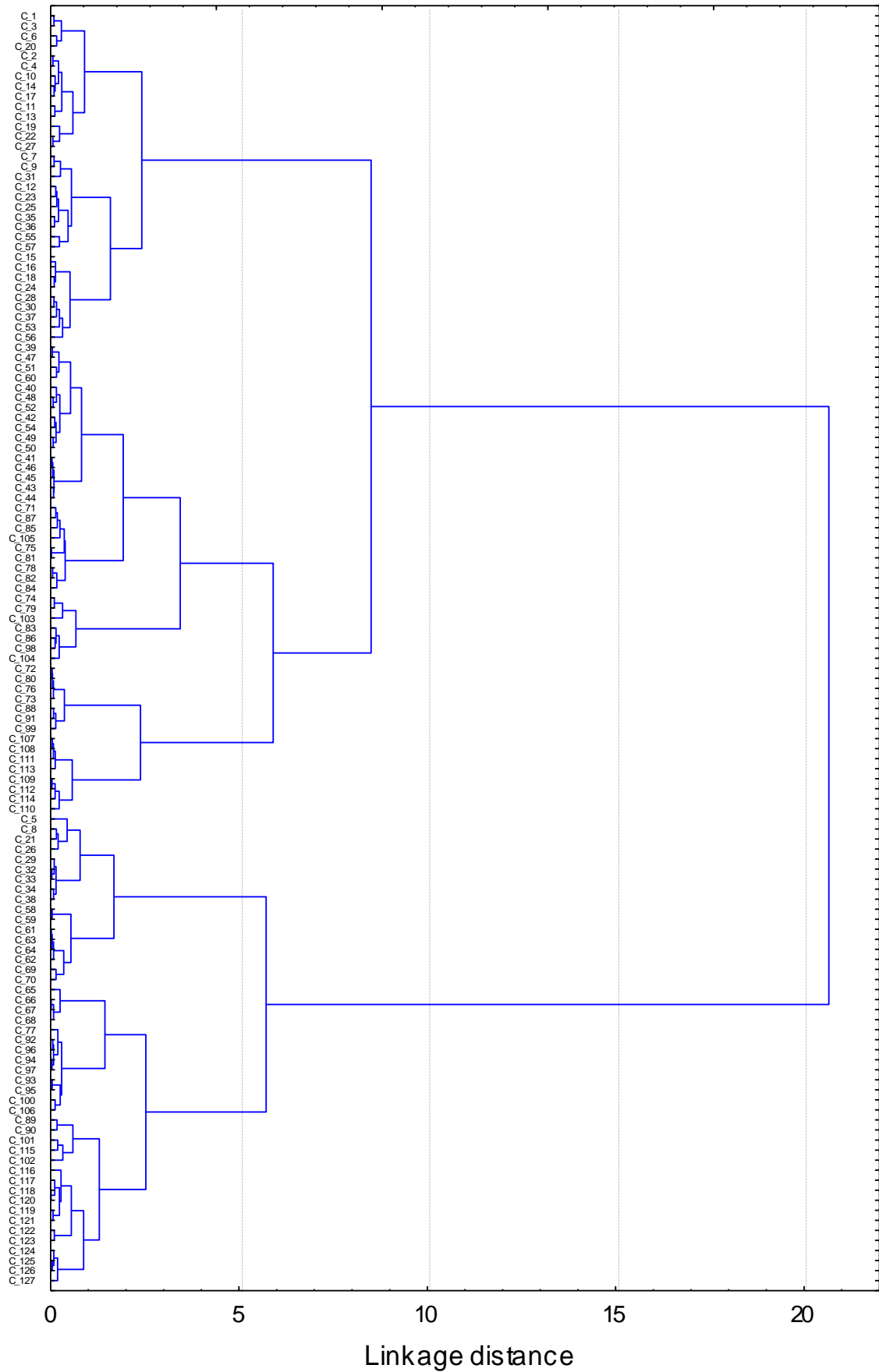


Figure VII.37 Results of time-space clustering of events from 05/2005 – 19/05/2012 and the major shocks. Hierarchical tree plot. The events are numbered according to ascending occurrence time. The major shocks have numbers 121-127.

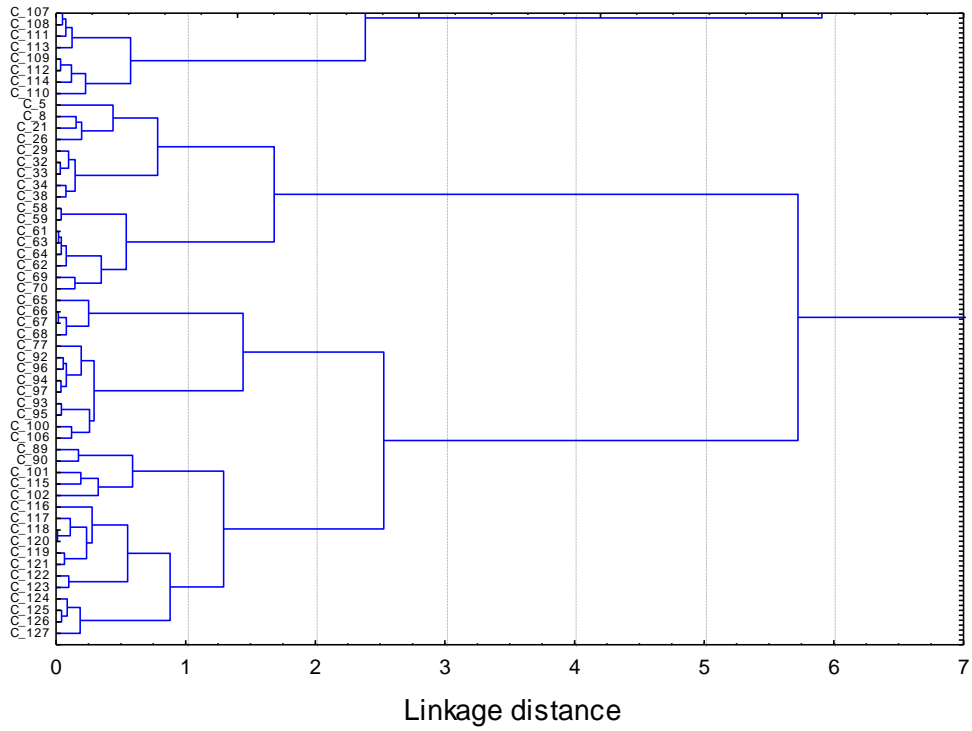


Figure VII.38 Magnified part of the previous figure.

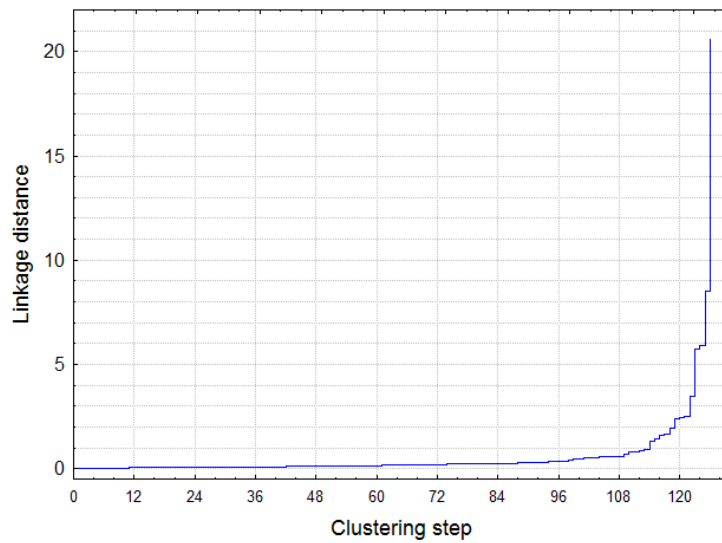


Figure VII.39 Linkage distance of consecutive clustering steps.

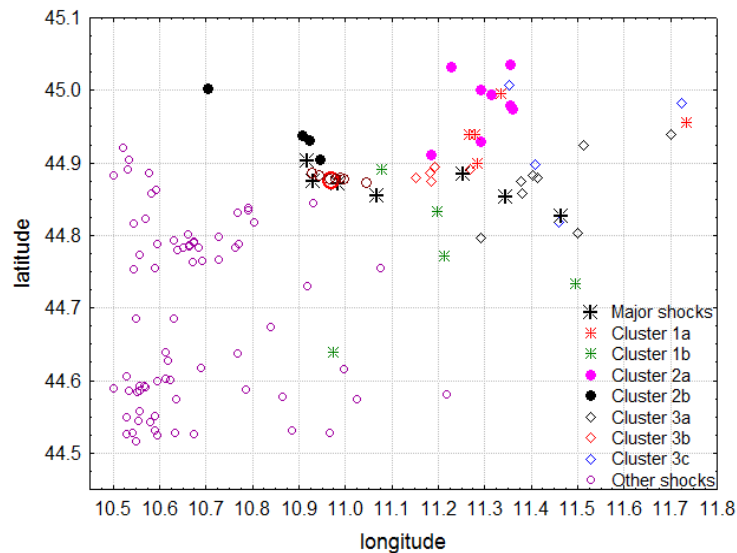


Figure VII.40 Locations of the identified time-space clusters of events. Major shocks (big black crosses) belong to cluster 1a.

Conclusions

We have taken into account

- the non-Poissonian event occurrence process;
- the time-varying magnitude distribution expressed by changes in b-value with time;
- the changeable event rate and the fact that it increased considerably in the last year before the seismic crisis;
- the correlation of locations of a part of the studied events with the locations of major shocks;
- the fact that many weaker events appeared close to the locations of major shocks in the last year before the crisis;
- a certain correlation of the depth weaker events with the depths of major shocks;
- the results of time-space clustering of events indicating a strong connection between 22 events from the studied catalog and seven major shocks. 18 of these events occurred within one year before E-20 major shock and constitute more than half of the events that occurred in that year.

It is therefore concluded that the studied seismic series, at least from the middle of 2008, was in part connected with the subsequent major shock sequence.

ETAS model

As indicated in Chapter 3, the epidemic-type aftershock sequences (ETAS) model is a stochastic point process in which each earthquake has some magnitude-dependent ability to trigger its own Omori law type aftershocks ([171], [172], [173]).

The total occurrence rate can be described, in time, as the superposition of a background uncorrelated seismicity μ_0 and the events triggered by another earthquake:

$$\lambda(t) = \mu_0 + \sum_{i:t_i < t} \lambda_i(t)$$

where $\lambda_i(t)$ is the rate of aftershocks induced by an event occurred at time t_i with magnitude M_i , defined as (for details see [171]):

$$\lambda_i(t) = \frac{\kappa}{(c + t - t_i)^p} e^{\alpha(M_i - M_c)}$$

for $t > t_i$. The parameter κ measures the productivity of the aftershock activity; α defines the relation between triggering capability and magnitude M_i of a triggering event; c measures the incompleteness of the catalog in the earliest part of each cluster; the parameter p controls the temporal decay of triggered events; M_c is the completeness magnitude of the catalogue.

The data used to estimate the ETAS model parameters is shown in **Figure VII.41**. For this process, a time window of 30 days was selected starting from the M4.1 event occurred on 05/19/2012 23:13 from the whole available catalog (May 2005 - July 2013). This time window encloses the period of main activity during the seismic sequence.

The catalog is considered complete for magnitudes ≥ 2.3 .

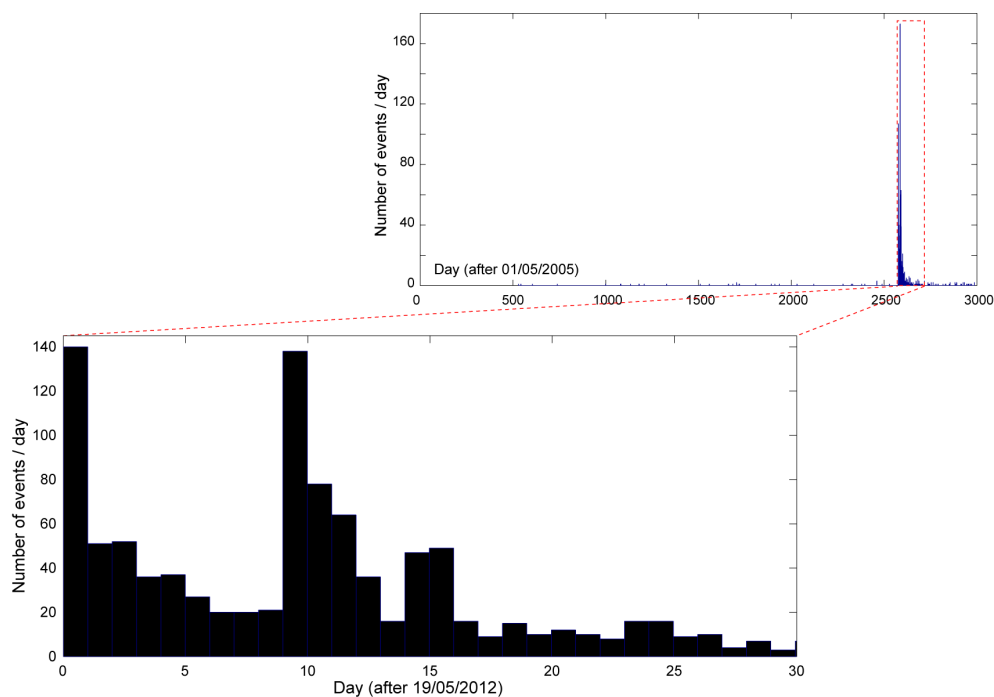


Figure VII.41 Complete catalogue (top) and data used for the estimation of the ETAS model (bottom)

The maximum likelihood estimations of the ETAS model parameters are summarized in the **Table VII.11**. Using the value obtained for the background uncorrelated seismicity; we can estimate that the percentage of background activity for the analyzed period is in the order of 5.2% (the rest of the events can be considered as aftershocks). **Figure VII.42** shows the cumulative number of events against the ordinary time; the black line corresponds with the observed seismicity, and the red line shows the expected values from the ETAS model with

the maximum likelihood parameter values. This figure may be used to check how well the fitted model describes the observed data.

Table VII.11. ETAS model parameter values (2012 Emilia sequence)

Parameter	Value
μ_0	1.84
K	0.05
C	0.05
A	1.38
P	1.24

ETAS Fit and Prediction (r.seisetas)

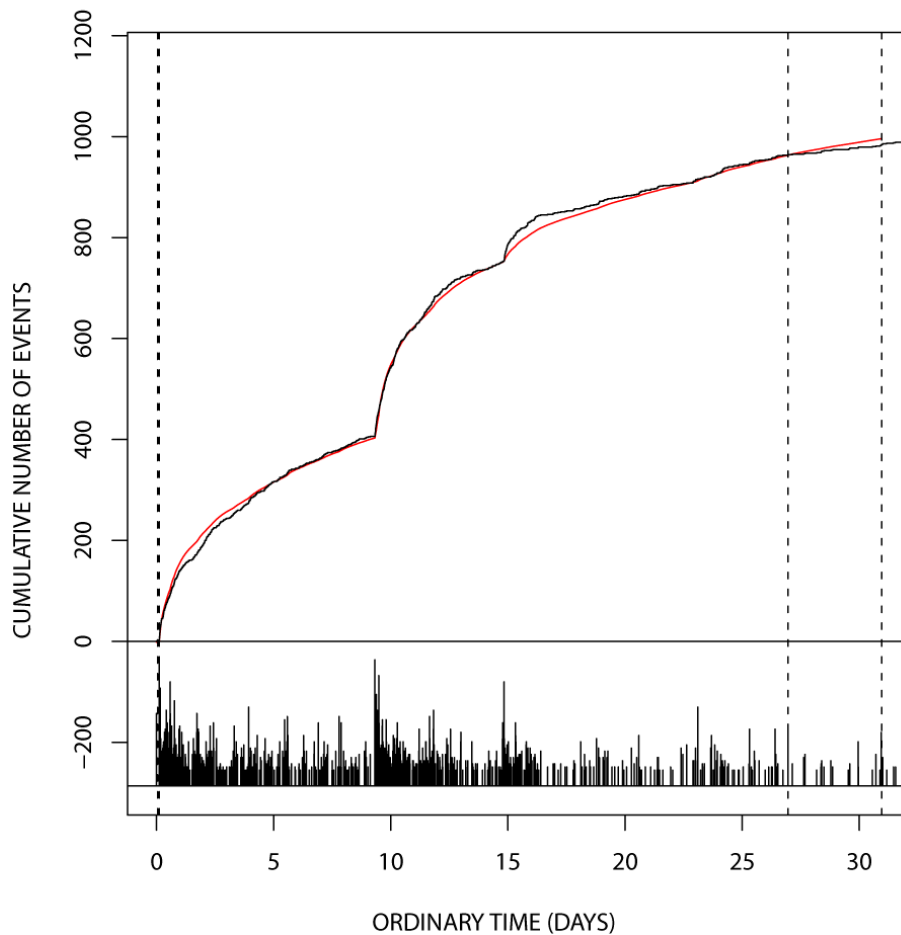


Figure VII.42 Cumulative number of events (observed and modelled by ETAS), against the ordinary time.

In order to explore the possibility of temporal changes in the processes, we use a generalized version of the ETAS model by considering a non-stationary behavior of some model parameters. In particular, we consider the time variations of μ_0 and p as suggested by [174]. Those parameters are thought to be the more directly linked to physical processes responsible for seismicity, and have been used by different authors to track changes in seismic swarms in different environments (e.g., [175]; [174]; [176]). Specifically, time variations in the μ_0 parameter have been interpreted as indicators of seismicity that cannot be

explained without considering complex patterns resulting from both pore pressure variations and earthquake-connected stress field changes (e.g., [175]; [174]); for this reason it has been used to track “fluid signals” in complex seismic swarms. On the other hand, the p values have been found to be positively correlated with crustal temperature, which controls stress release and therefore aftershock decay (e.g., [177]; [178]; [174]).

We have estimated the model parameter values in a moving time window $\tau=5$ days allowing the background seismicity μ_0 and the p parameter to change. The results of the temporal behavior of the μ_0 and p parameters are shown in **Figure VII.43**. The p parameter exhibits a value typically found in tectonic sources (ranging between 1.1 and 1.3), and it can be considered constant since it does not exhibit significant variations in the inferred values in different time periods. Conversely, the background seismicity shows a higher rate at the beginning of the sequence and, afterwards, a systematically decreasing trend. It is worth noting that the most significant higher value is found at the beginning of the sequence (around the first 5 days of activity after the main shock on May 20, 2012). After that, the μ_0 value exhibits lower values and does not display significant variations up to the end of the analyzed period (see **Figure VII.43**, top).

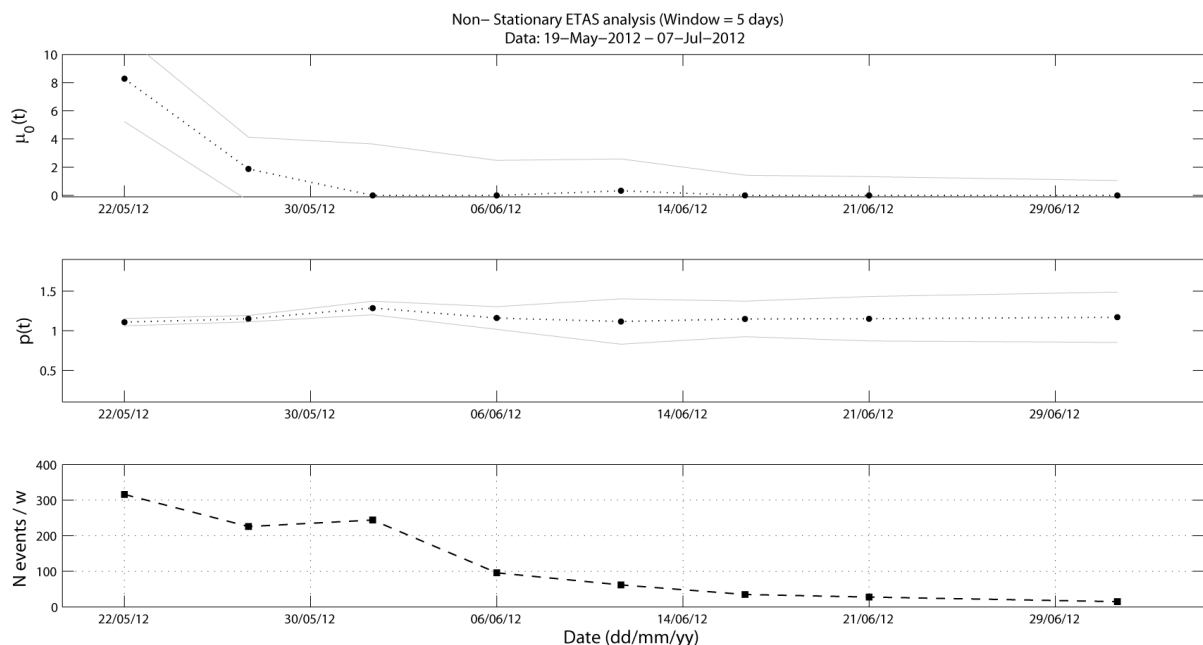


Figure VII.43 Time variations of the background seismicity (μ_0) and the p parameter of the ETAS model.

As discussion of these results, we can point out that considering the interpretations of time variations in the background seismicity found in literature (e.g., [175]; [174]; [176]), the high μ_0 values may indicate the effects a strong fluid impulse. Nevertheless, in this case, the higher μ_0 values are observed just at the beginning of the sequence, where the estimated percentage of background seismicity reaches a maximum of 13.1% of the total number of events. It should be pointed out that this behavior with a higher background rate at the beginning of a seismic sequence triggered by a mainshock has been observed also in other seismic sequences analysed using the non-stationary procedure described here, and in many cases the high μ_0 values during the first days of a seismic sequence is the result of an increase in the completeness magnitude threshold in these periods characterized by intense seismicity. Conversely, it is worth noting that the second main event occurred on May 29, 2012 is not correlated with any significant variation in the background seismicity, as can be seen in **Figure VII.43** (top).

Conclusion:

- The percentage of background activity for the whole analyzed period is in the order of 5.2%; the rest of the activity can be interpreted as aftershock events.
- When allowing time variations in the μ_0 and p model parameters, the p value remains constant, not showing significant variations (from the a value of ~ 1.2), whereas the μ_0 parameter shows a decreasing trend with the higher background rates observed at the very beginning of the sequence (about 13% of the activity during the first week). It is worth noting that summing up the fraction of background seismicity calculated for all the time windows considered in the non-stationary analysis, the total percentage of background activity is 5.1%, equivalent to the value calculated for the whole sequence.
- The high μ_0 values are often interpreted as an evidence of fluids enhancing the occurrence of seismic events. Nevertheless, in this case, the high μ_0 values are detected just at the very beginning of the sequence, where the completeness magnitude of the catalog often exhibits a higher threshold. This effect may result also in an increase of the background seismicity when the ETAS model parameters are estimated. Then, in cases as this one in which high μ_0 values are observed at the beginning of the seismic sequence, the possible interpretation of the higher μ_0 values can range from effective effects from fluids, to “noise” in the calculations of the non-stationary ETAS model parameters, or a combined effect of both. Conversely, the second ‘main’ event occurred on May 29, 2012 is not correlated with any significant variation in the background seismicity.

3. Production data analysis

Figure VII.44 presents the time series of monthly oil and gas production in the Mirandola concession. It can be seen that oil production and gas production were strictly correlated. The Spearman’s rank correlation coefficient between these two time series is 0.9998 and is obviously significant. From 2005 to 2012 the Cavone field produced 0.237 Mtonn of oil, 75 MSm³ of gas and 1.05 Mm³ of water where extracted and reinjected.

Production parameters were not constant throughout the study period. The following constant trend periods of oil (and gas) production can be distinguished in **Figure VII.44** (solid line segments), see **Table VII.12**. The average values are not very instructive when taken over periods in which production parameters were not constant. They are only used to indicate changes between periods. The last month, 05/2012 is not considered, as the production in this month was altered by the seismic crisis.

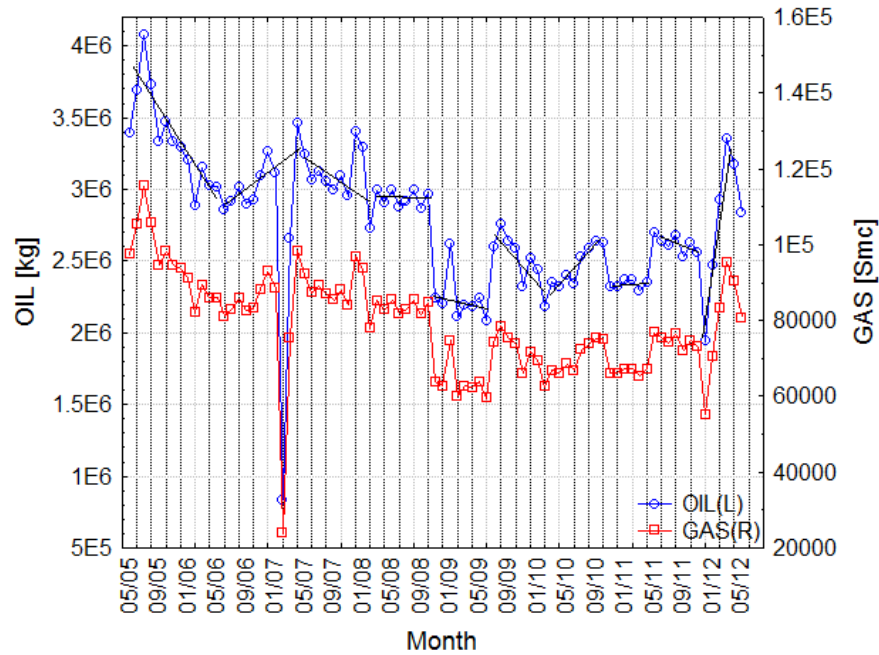


Figure VII.44 Monthly production of oil and gas in the Mirandola concession from 05/2005 to 05/2012.

Table VII.12 Distinguished periods of constant trends in oil and gas production.

ID number	Time period	Description	Average oil output [kg]	Average gas output [Smc]
1	05/2005-05/2006	Fast decreasing from high values	3353348	95376
2	06/2006-04/2007	Increasing	2821188	80264
3	05/2007-02/2008	Decreasing	3094758	88173
4	03/2008-10/2008	Constant at relatively high level	2939377	83736
5	11/2008-06/2009	Jump down. Constant at low level with a slight decrease	2234941	63701
6	07/2009-02/2010	Jump up and decrease	2506812	71439
7	03/2010-10/2010	Increasing	2476943	70585
8	11/2010-04/2011	Jump down and constant at relatively low level.	2335702	66501
9	05/2011-11/2011	Jump up. Constant at higher level with slight decrease.	2620394	74679
10	12/2011-04/2012	Very fast increase.	2775162	79020

Oil and gas production parameters were correlated with injection parameters: the average volume injected and the effective average pressure. The Spearman's rank correlation coefficient between oil production and average volume injected is 0.78 with a significance $2 \cdot 10^{-18}$, the coefficient between oil production and effective average pressure is 0.62 with significance $2 \cdot 10^{-10}$. As anticipated, the injection parameters were highly correlated. The rank correlation coefficient between average volume injected and effective average pressure is 0.85 with significance $2 \cdot 10^{-25}$.

Figure VII.45 and **Figure VII.46** present time series of injection data: average volume injected and effective average pressure. Based on **Figure VII.45** and **Figure VII.46** constant trend periods of injection parameters are identified. The periods are presented in **Table VII.13** and **Table VII.14**.

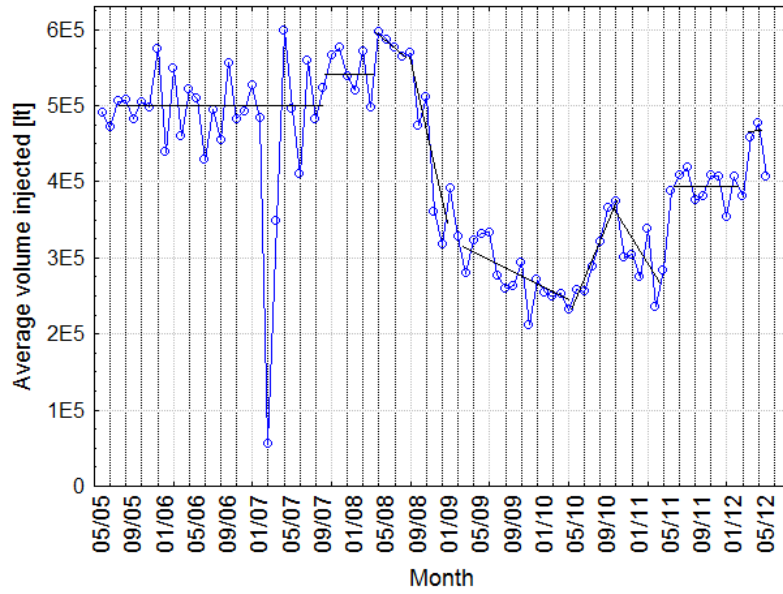


Figure VII.45. Average volume injected through C14 well.

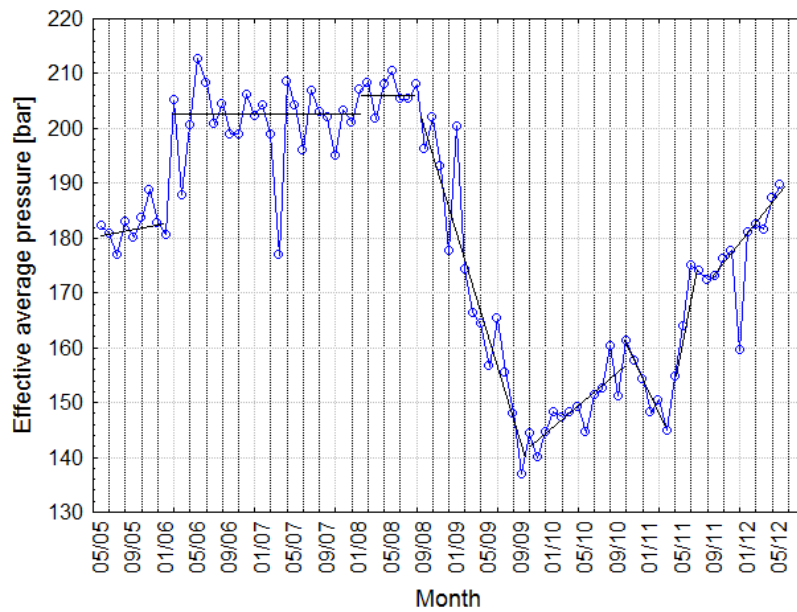


Figure VII.46. Effective average pressure in C14 well.

Table VII.13. Identified periods of constant trends of injected volume.

ID number	Time period	Description	Average volume [lit]
1	05/2005-09/2007	Constant high values	479395
2	10/2007-03/2008	Increased constant	545014
3	04/2008-08/2008	Decreasing from high values	578532
4	09/2008-01/2009	Very fast decrease	410871
5	02/2009-03/2010	Further decrease with lesser rate.	280673
6	04/2010-10/2010	Increase	299205
7	11/2010-04/2011	Decrease	289498
8	05/2011-02/2012	Jump up and constant at moderately high level.	392931
9	03/2012-04/2012	Next jump up to high values.	467769

Table VII.14 .Identified periods of constant trends of effective average pressure.

ID number	Time period	Description	Average pressure ¹⁷ [bar]
1	05/2005-01/2006	Slight increase at moderately high values.	182.1
2	02/2006-01/2008	Increased constant.	201.4
3	02/2008-08/2008	Further slight increase and constant	206.7
4	09/2008-09/2009	Very fast decrease.	172.1
5	10/2009-10/2010	Increasing	149.5
6	11/2010-03/2011	Decreasing	151.1
7	04/2011-07/2011	Very fast increase.	166.9
8	08/2011-05/2012	Further fast increase to relatively high values.	178.1

The time-periods of constant trends, presented in **Table VII.12**, **Table VII.13** and **Table VII.14** are selected qualitatively from **Figure VII.44** to **Figure VII.46**, and hence subjectively. However, they are useful for roughly correlating the periods of different production parameters, which had comparable trends. In three cases at close time points all three parameters changed their trends in a correlated way. In 09/2008 both injected volume and pressure began to decrease very fast (injected water from 14,225 to 11,775 m³/month; well-head pressure from 196 to 137 bar), and oil production dropped down in 11/2008 (from 2.30*10⁶ to 2.08 *10⁶ Kg/month). In 11/2010 volume and pressure began to decrease and oil production jumped down to a relatively low level in the same month (from 2.63 *10⁶ Kg/month in October to 2.30 *10⁶ Kg/month in November).

Finally, in 04-05/2011 all three parameters started to increase and they continued this increase in the same way until the crisis in 05/2012 (oil from 2.29 to 3.33*10⁶ Kg/month; reinjected water from 7,325 to 14,300 m³/month and well-head pressure from 144 to 190 bar).

Conclusions:

There were significant time changes of production and injection in the seven-year period under consideration. Sometimes these changes took the form of rapid jumps of variations with a high rate.

The production and injection parameters are strongly correlated but they are not redundant; they represent different aspects of the technological activity.

There are three time points when all three parameters of production/reinjection concurrently underwent rapid changes. For the first two points, in 09-11/2008 and in 11/2010 they decreased. The third time point, 04-05/2011, saw a rapid growth in production/reinjection.

4. Correlation between seismicity and production

There are three time points at which all production parameters changed their trend directions in a correlated way. The question to be posed is whether these changes correlate with changes of seismicity rate. Imagine that at a certain time point, t_0 the trend of the production parameters changes from increasing (or constant higher) to decreasing (or constant lower). Let for a production parameter the period of increasing trend before t_0 be Δ_1 , and the period of decreasing trend after t_0 be Δ_2 . Let the number of events that occurred in the period $[t_0 - \Delta_1, t_0]$ be n_1 and the number of events that occurred in the period $[t_0, t_0 + \Delta_2]$ be n_2 .

¹⁷ Field original pressure: 296 bar

If the seismicity rate is correlated with the trends in the considered time periods then the actual division of the total number of events in both periods, $N=n_1+n_2$ into n_1 and n_2 should be significantly different from the division which could be attained by random processes. Hence the following null hypothesis is set:

H0(n_2 could be obtained at random from N under probability P)

where $P = \Delta_2 / (\Delta_1 + \Delta_2)$. This hypothesis is tested by means of the binomial test which provides the probability, p that if N events occur in a random way in $[t_0 - \Delta_1, t_0 + \Delta_2]$, the number of events in $[t_0, t_0 + \Delta_2]$ can be less than or equal to n_2 . This probability reads:

$$p = \Pr(n \leq n_2 | N, P) = \sum_{n=0}^{n_2} \binom{N}{n} P^n (1 - P)^{N-n}$$

If p is small, then it is right to conclude that the rate in $[t_0, t_0 + \Delta_2]$ decreased with respect to the rate in $[t_0 - \Delta_1, t_0]$, hence the rate changes correlated with the trend change of the production parameter. The parameter p , is the significance of H0 i.e. the probability of making an error when rejecting H0.

In the opposite case of production parameter change, from a decreasing to an increasing trend, the same null hypothesis H0 is tested but the binomial test is to answer what is the probability of obtaining in $[t_0, t_0 + \Delta_2]$ a number of events greater than or equal to n_2 . This probability reads:

$$p = \Pr(n \geq n_2 | N, P) = 1 - \sum_{n=0}^{n_2-1} \binom{N}{n} P^n (1 - P)^{N-n}$$

The first time point of correlated change of production parameters trends, 09/2008 was the change from a high constant to a low constant level (oil and gas production), from a decreasing trend to a faster decreasing trend (average volume injected) and from a constant level to a very fast decrease (effective average pressure). The results of the binomial test of H0 are assembled in **Table VII.15**. In the case of average volume injected two periods of decreasing trend, Δ_1 , are separately analyzed.

The significance of H0 is in all cases quite high. The test does not indicate a significant decrease of seismicity rate in the analyzed time periods of decreasing trends of production parameters with respect to the seismicity rate in the preceding time periods of increasing trends.

Table VII.15 Binomial test results for the first correlated changes of production parameter trends. See: text for further explanations.

Production parameter	$[t_0 - \Delta_1, t_0]$	$[t_0, t_0 + \Delta_2]$	Δ_1 [month]	Δ_2 [month]	P	n_1	n_2	p
Oil production	03/2008-10/2008	11/2008-06/2009	8	8	0.5	14	17	0.76
Volume injected	04/2008-09/2008	09/2008-02/2009	5.5	5.5	0.5	11	12	0.66
Volume injected	04/2008-09/2008	09/2008-03/2010	5.5	18.5	0.76	11	35	0.49
Effective pressure	02/2008-10/2008	10/2008-09/2009	8.5	11.5	0.57	14	22	0.73

The second time point of correlated change of production parameters trends, 11/2010 was the change from an increasing trend to a jump down and the constant at a low level for oil and gas production and from an increasing to a decreasing trend in both cases of volume injected and injection pressure. Results of the binomial test of H0 are shown in **Table VII.16**.

Also in this second case the significance of H0 is considerably high for all production parameters, although it is lower than in the first case. The test results do not provide convincing arguments that the seismicity rate decreased in the analyzed time periods of decreasing trends of production parameters with respect to the seismicity rate in the preceding time periods of increasing trends.

Table VII.16 Binomial test results for the second correlated changes of production parameter trends. See: text for further explanations.

Production parameter	$[t_0 - \Delta_1, t_0]$	$[t_0, t_0 + \Delta_2]$	Δ_1 [month]	Δ_2 [month]	P	n_1	n_2	p
Oil production	03/2010-10/2010	11/2010-04/2011	8	6	0.43	11	5	0.23
Volume injected	04/2010-10/2010	11/2010-04/2011	7	6	0.46	11	5	0.17
Effective pressure	10/2009-10/2010	11/2010-03/2011	13	5	0.28	22	5	0.20

The third time point of correlated change of production parameters trends, 04-05/2011 is the change from the decreasing trends, which have been already used in connection with the second time point above, to increasing trends that lasted until the seismic crisis in 05/2012. Oil/gas production jumped up and remained constant until 11/2011 after which it again began increasing very fast. Injected volume jumped up in 05/2011 and remained constant until 02/2012 after which it again jumped up to a high level. Effective pressure of injection was increasing very fast from 04-07/2011, and from 08/2011 it continued a fast increase but at a lesser rate. In connection with changes in the rates of increase, two periods of the increasing trend, Δ_2 , are separately analyzed for every parameter. Results of the binomial test of H0 are shown in **Table VII.17**.

The significance of H0 is low in all cases. The largest value is below 8%. In contrast to the two previous cases, the test signifies that the seismicity rate increased in the time period before the crisis, when all production parameters increased together. Additionally, a low significance of H0 when shorter periods of the production parameters increase are used (until 11/2011, 02/2012, 07/2011, respectively) indicates that this rate increase is not explained by the increase of seismicity directly before the crisis (in 04-05/2012).

Table VII.17 Binomial test results for the third correlated changes of production parameter trends. See: text for further explanations.

Production parameter	$[t_0-\Delta_1, t_0]$	$[t_0, t_0 + \Delta_2]$	Δ_1 [month]	Δ_2 [month]	P	n_1	n_2	p
Oil production	11/2010-04/2011	05/2011-11/2011	6	7	0.54	5	17	0.021
Oil production	11/2010-04/2011	05/2011-04/2012	6	12	0.67	5	29	0.013
Volume injected	11/2010-04/2011	05/2011-02/2012	6	10	0.62	5	25	0.012
Volume injected	11/2010-04/2011	05/2011-04/2012	6	12	0.67	5	29	0.013
Effective pressure	11/2010-03/2011	04/2011-07/2011	5	4	0.44	5	10	0.071
Effective pressure	11/2010-03/2011	04/2011-05/2012	5	14	0.74	5	34	0.035

The cluster analysis in Section 2 of this chapter has selected a group of weaker events from before 05/2012 that were clustered in time-space with the seven major shocks (M5+) from 05-06/2012. This clustered group has been denoted as **1a-1b-2a-2b** and comprises 23 events from before 20/05/2012 (see: Section 2). The first time event in this cluster group occurred in 10/12/2009. This was during a period of decreasing trend in oil and gas production (see: Table VII.10). Including this period there were altogether two time periods of decreasing trend and two periods of increasing trend of production until 05/2012, namely:

07/2009 – 02/2010	decreasing 8 months
03/2010 – 10/2010	increasing 8 months
11/2010 – 04/2011	low level 6 months
05/2011 – 04/2012	increasing 12 months.

Altogether there were 14 months of a decrease/low level and 20 months of increases.

Out of 23 events from the group of clusters **1a-1b-2a-2b** that occurred prior to the crisis in 05/2012, 4 occurred in the decreasing trend months shown above and 19 in the increasing trend patterns. The probability of obtaining such a division of 23 events at random is

$$p = \Pr\left(n \geq 19 \mid 23, \frac{20}{34}\right) = 0.0144.$$

Similarly, for injected the volume the pattern was:

02/2009 – 03/2010	decreasing 14 months
04/2010 – 10/2010	increasing 7 months
11/2010 – 04/2011	decreasing 6 months
05/2011 – 04/2012	increasing 12 months

that is 20 months of decreases and 19 months of increases. The division of event occurrences is the same as previously that is 4 in the decreasing trend months and 19 in the increasing trend ones, and the probability of obtaining this division at random is $p=8.7 \cdot 10^{-4}$.

For effective average pressure it was:

10/2009 – 10/2010	increasing 13 months
11/2010 – 03/2011	decreasing 5 months
04/2011 – 05/2012	increasing 14 months

that is 5 months of decreases and 27 months of increases. All 23 events occurred in the periods of increasing trend of effective average pressure. The probability of obtaining this at random is

$$p = \Pr\left(n = 23 \mid 23, \frac{27}{32}\right) = 0.0201.$$

This analysis shows that the weaker events, which were clustered in time-space with the seven major shocks (M5+), had a distinct tendency to occur during periods of increasing trends of production parameters.

The same analysis has been performed using the energy release instead of the rate of seismicity to take into account for the different earthquake energy content. The results are strictly comparable with those presented above.

In summary:

- In 09-11/2008 and in 11/2010 there was a concurrent rapid decrease of all parameters of production and injection. No significant change between the seismic event rate in the period before and in the period after 09-11/2008, neither between the event rate in the period before and the period after 11/2010 has been found.

- In 04-05/2011 there was a concurrent rapid increase of all parameters of production and injection. This increase correlates with an increase of event rate. The binomial test results indicate that the event rate after 04-05/2011 was significantly higher than the event rate before 04-05/2011.

- The binomial test has also shown that the events forming the group strongly clustered in time-space with the major shocks had a significant tendency to occur in the periods of increasing trends of production and injection.

5. Conclusions

- i. The interevent time does not follow the exponential distribution, hence the studied event occurrence process is not Poissonian. The seismicity rate and the b-value of magnitude distribution change in time. It is therefore concluded that the studied seismicity was not background seismicity.
- ii. The event rate considerably increased in the last year before the seismic crisis. The locations of a part of the studied events correlate with the locations of major shocks. There is also a certain correlation of studied events depth with the depths of major shocks. The analysis of time-space clustering of events has indicated a strong connection between 22 events from the studied catalog and seven major shocks. 18 from these events occurred within one year before the E-20 major shock. Altogether there were 34 events in that year and therefore more than 50 percent of the events which occurred in that year were clustered in time-space with the major shocks. It is therefore concluded that the studied seismicity was in part connected with the subsequent major shock sequence.
- iii. ETAS modelling of 31 days history of the seismicity after E20 major shock signifies that these were typical mainshock-aftershock sequences with no signs of non-tectonic influence.
- iv. Out of three concurrent rapid changes of all parameters of production and injection one correlated with a change of event rate. This happened in 04-05/2011 when production and injection trends rapidly changed from decreasing to fast increasing. The change in 04-05/2011 was the last out of the three and the only transition from a decrease to an increase. The binomial test has indicated that the event rate after 04-05/2011 was significantly higher than the event rate before 04-05/2011.
- v. The events strongly clustered in time-space and the major shocks had a significant tendency to occur in the periods of increasing trends of production and injection.
- vi. It is therefore concluded that the seismic process that began before May 20th, 2012 and continued with the sequence of earthquakes in May-June 2012 is statistically correlated with increases in production and injection in the Cavone oil field.

E. Geothermal activity analysis

The relationship between seismic events and operation of geothermal plants has been widely discussed in the recent times. The recently concluded FP7 EC Project GEISER (Geothermal Engineering Integrating Mitigation of Induced Seismicity in Reservoirs) was dedicated to this issue (www.geiser-fp7.eu). The process of high-pressure injection of cold water into hot rock, which is the preferred method to develop a new reservoir if natural fluid circulation is inadequate (Enhanced Geothermal Systems, EGS), dramatically changes the stress field in the immediate vicinity of the injection point. The reduction in effective normal stress unlocks pre-existing faults in rocks that are tectonically near-critically stressed, typically causing seismic events.

The characteristics of induced seismicity depend on regional and local stress history and on the volume of fluid involved. Normal geothermal applications, especially in systems with production and injection, are volume-balanced and differ from exploited systems such as gas and coal. The exploitation of gas and coal causes changes in the mass balance in the underground. Such changes can lead to subsidence and the likelihood for seismicity is higher than in volume balanced systems like geothermal.

Occasionally, seismic events large enough to be felt at the surface have occurred in geothermal fields, creating nuisance for the population and occasionally non-structural damage to nearby buildings.

Therefore, the geothermal plant of Ferrara must be taken into the considerations in order to understand its possible relationship with the Emilia event of 2012.

In Ferrara a geothermal plant has been in operation since 1995 ([179]). The heat exploitation recovers thermal water from 2 wells (Casaglia 2 and 3) with a formation temperature of about 100 °C, and re-injects all of it totally at a temperature of about 70 °C into the injection well Casaglia 1. The data provided by ENI spa (See Appendix D) indicate that in the period 1995 - 2012 a total of 36 million m³ was produced and reinjected, i.e. the volume is balanced. No significant time variations of extracted and injected volumes are indicated, therefore, the likelihood for seismicity is lower than in unbalanced systems.

The monitoring of pressure in 2012 shows that production pressure (13 bar) and injection pressure (6 bar) were kept constant and no significant change in the hydraulic system can be inferred. The injected volume per day was reduced in May to half of the injected volume of the winter operations.

The injection of cold water into hot rock has to be considered as a possible cause geomechanical changes. In fact Hassanzadegan et al [180] investigated temperature induced geomechanical effects in doublets. They concluded that re-injection of water with a temperature drop of 80 K in comparison to the formation temperature can induce a total subsidence in the order of mm after 30 years of operations, with variation due to different rock type but remaining of the same order . These values are very low and the damaging potential is very low.

In the case of Casaglia the temperature difference between production and in injection is less than half of the value indicated by [180] so this possibility can also be ruled out.

Consistent with the above reported conclusions, the map of earthquakes recorded from the Casaglia network (see chapter 4) from March 2010 to September 2013 shows that no events occurred at distances closer than 5 km to the field before the May 2012 sequence. A few $ML < 4.0$ events occurred close to the field after the first main shock (see **Figure IV.25**). Their hypocenters are from 3 km to more than 10 km deeper than the point of injection except one, whose depth was not calculated. Most probably all these events were dynamically triggered by the main May 2012 sequence.

The operation of the Ferrara geothermal plant is extremely unlikely to have produced seismicity for the following reasons. (1) Natural subsidence in the Po Plain is of the order of mm/yr ([181]). (2) The plant is operated with volume balance in the far field. (3) The

reported geothermal seismicities induced by geothermal operation at other locations, such as Landau ([182]), which is volume balanced but non-balanced close to the injection point, have epicenters close to this borehole section. This does not seem to be the case in Ferrara.

VIII. Conclusions

The Technical-Scientific Commission for evaluating the possible relationships between hydrocarbon exploration and increase of seismicity in the Emilia Romagna area hit by the May 2012 earthquakes (ICHESE) was appointed on December 11, 2012 by a decree of Dr. Franco Gabrielli, Head of the Department of Civil Protection of the Presidency of Council of Ministers, following the request of the President of Emilia-Romagna Region. The composition of the Commission has been modified by further decrees.

The Commission was appointed with the following statement of charge:

“The International Committee shall produce a report answering the following questions, on the basis of the technical-scientific knowledge available at the moment:

1. Is it possible that the seismic crisis in Emilia has been triggered by the recent researches at the Rivara site, particularly in the case of invasive research activities, such as deep drilling, fluids injections, etc.?
2. Is it possible that the Emilia seismic crisis has been triggered by activities for the exploitation and utilization of reservoirs carried out in recent times in the close neighbourhood of the seismic sequence of 2012?”

The Commission started its activity on May 2, 2013 and had its first plenary meeting on June 18, 2013. The Commission acquired all the available data on seismic activity, ground deformation, geology, reflection seismology, hydrocarbon exploration, exploitation, gas storage and geothermal activities. In order to carry this out, the Commission conducted interviews with the representatives of INGV (*Istituto Nazionale di Geofisica e Vulcanologia*), OGS (*Istituto Nazionale di Ocenografia e di Geofisica Sperimentale*), Seismological Service of Regione Emilia-Romagna, and the companies performing hydrocarbon exploitation and exploration and natural gas storage activities in the study area and asked for the available data. The Commission also interviewed *Independent Gas Management Srl*, a company which had studied the geological setting of the Rivara area in order to prepare for a gas storage project in deep aquifers.

The first step has been a review of the scientific literature and available reports on the issue. In fact, an extensive scientific literature, developed mainly in the last two decades, reports that in some circumstances technological operations involving extraction and/or injection of fluids in underground rocks can affect the tectonic stress fields producing variations in rock pore-pressures and migration of fluids. Consequently, earthquakes occurring in spatial and temporal proximity to such operations are under suspicion that they may have been affected by anthropogenic factors.

Earthquakes are generally classified into the following categories:

- **Tectonic Earthquakes**, due to naturally existing stress systems, where the tectonic stress has already exceeded the resisting frictional stress and the region was seismogenically ‘ripe’.
- **Anthropogenic Earthquakes**, where human activity has played some part in bringing the system to failure:
 - a. **Induced Earthquakes**, where external anthropogenic activities produce stress changes, which are sufficiently large as to produce a seismic event. The rock-mass may not necessarily have been in a stress-state, which would have led to an earthquake in the reasonably foreseeable future (in a

geological sense!). Earthquakes produced by procedures such as thermal or hydraulic stimulation of a rock, such as Hydraulic Fracturing (Fracking) and Enhanced Geothermal Systems, fall into this category.

b. **Triggered Earthquakes** where a small perturbation generated by human activity has been sufficient to move the system from a quasi-critical state to an unstable state. The event would have eventually occurred anyway although probably at some unknown, later time. That is, these activities have advanced the earthquake clock. In this case the additional perturbing stress is often very small in comparison with the pre-existing stress system. The necessary condition for the occurrence of seismicity is a tectonically pre-stressed fault near the human operations altering the stress field, where ‘near’ can be even tens of km away depending on the duration and type of the stimulus. Under certain circumstances, such stress changes can eventually cause the loaded fault to fail. Importantly, since technological operations act only to activate the tectonic stress release process, the magnitudes of such earthquakes can be high, and within the same range as those of natural earthquakes, depending on the amount of elastic strain accumulated on the fault due to tectonic loading.

Several authoritative reports describe well-studied cases where extraction and/or injection of fluids in hydrocarbon or geothermal fields has been *associated* with the occurrence of earthquakes, of magnitudes even higher than 5. It is difficult, sometimes not possible, to use the word *proven* in these circumstances. The reported cases are only a small fraction of all of the existing cases of extraction and injection of fluids and are mostly related to the additional load imposed by very large reservoirs and to the injection of large volumes of fluid (usually waste water) into surrounding rocks and not into in the same reservoir during enhanced recovery or pressure maintenance. However, some cases do exist, where earthquakes have been associated with waste-water disposal within the same reservoir where oil and gas have been extracted.

The main lessons learnt from the reported cases are:

- Extraction and/or injection of fluids in hydrocarbon fields can, in certain circumstances, induce or trigger seismic activity;
- Most of the documented cases of seismicity that have been associated with hydrocarbon exploitation are related to extraction from very large reservoirs or water injection in situations where the pressure of fluid is unbalanced.
- The number of documented cases of seismicity of medium to high magnitude, that have been associated with water injection in the reservoir from which extraction has taken place, is a small fraction of cases;
- The induced and, specifically, the triggered seismic response to extraction/injection is complex and variable among cases and its correlation with technological parameters is far from being fully known;
- The magnitude of triggered earthquakes depends more on the dimensions of the fault and its strength, rather than the characteristics of the injection.

- Recent research on stress diffusion suggests that the activated fault may also be few tens of km away from the injection/extraction location, some kilometres deeper than the reservoir and several years after activities commenced.
- The greater focal depths for some extraction-related earthquakes have been interpreted to be a direct reflection of the fact that extraction or injection of large volumes of fluids has the potential to induce crustal-scale deformation and seismicity.
- Many cases of earthquake activity have been recorded during the exploitation of geothermal energy. Most of them are related to projects for the development of Enhanced Geothermal Systems, where induced fractures must be produced in impermeable igneous rocks to develop permeable pathways. Several cases are also related to traditional exploitation of geothermal energy. The induced earthquakes are generally of medium to low magnitude and no more than a few km away from the extraction or injection wells.
- Exhaustive examination of all the available literature shows that the discrimination between natural and triggered/induced earthquakes is a difficult problem and does not presently have a reliable, ready-to-use solution.

This being the state of knowledge, the Commission investigated the possibility of a connection between the actions of extraction/injection/storage of fluids and the seismic activity in the Emilia area hit by the seismic sequence of May to June 2012.

The seismic sequence covered an elliptical area of about 30 km x 10 km extending in an E-W direction over the Cavone-Mirandola anticline. On the basis of the seismo-tectonic structure, the Commission defined an area of interest of about 4000 km² encompassing the location of the 2012 seismicity. The area includes three hydrocarbon exploitation licences, Mirandola (including the Cavone field), Spilamberto and Recovato, as well as the gas storage reservoir of Minerbio and the geothermal field of Casaglia (Ferrara).

The Rivara project for the development of a natural gas storage reservoir within an aquifer is also in the area under consideration. The first question posed to the Commission is related to this project. After a critical review of the available information provided by the Company, and in the light of the official statement by the Ministry of Economic Development (MISE) that no mining activity related to the Rivara storage project has been authorized and that they have no evidence of mining activities carried out in the past 30 years, the Commission believes that the answer to the first question is NO.

In order to answer the second question, the Commission considered the available information on seismic activity and on the operations carried out in the exploitation and storage fields in the area and for the following reasons, decided to focus its attention on the nearest fields to the 2012 seismic activity, which are:

The Mirandola hydrocarbon exploitation licence and

The Casaglia geothermal field

The Cavone fields, belonging to the Mirandola licence, are about 20 km west of the main shock of May 20, and close to the events exceeding 5 ML of May 29 and June 3. Two other large shocks, exceeding 5 ML, which occurred on May 20, were displaced towards the

Casaglia geothermal field, which is about 20 km North-East of the May 20 main shock epicentre.

Although extraction activity has been continuous at Cavone, Recovato and Spilamberto up to and including the onset of the sequence of earthquake in May 2012, the Cavone 14 well was the only site carrying out continuous waste-water injection before and during the 2012 seismicity. Moreover, whereas the Cavone reservoir is located within Mesozoic carbonate formations and may be connected hydraulically to underlying thrust faults, the other reservoirs are in Plio-Pleistocene formations above some impervious units; consequently the connection with seismogenic structures is highly unlikely.

In order to have a homogeneous picture of the characteristics of seismic activity of the geological information and on the operations of extraction and injection of fluids, the Commission decided to re-process the most significant available data. It was then decided:

- To re-evaluate the main available reflection seismology and well-logging data to check the tectonic model of the area and to build a 3D velocity model to be used for the re-location of seismic activity. The use of a 3D model is required by the strong asymmetry of the shallow geological structures along on N-S direction;
- To recalculate the classical parameters (geographical coordinates, depth, focal mechanism) of the seismic activity with epicentres in the considered area recorded by the INGV seismic network starting from 2005 when the INGV instrumental catalogue reached the present configuration.
- To estimate the Coulomb stress transfer due to the May 20 major events in order to evaluate whether they have contributed to bring the fault of the May 29/June 3 events closer to failure.
- To perform a statistical analysis of the seismic activity in the considered area since 2005, including May 2012, in order to detect possible deviations from the typical trends of natural seismicity and possible correlations with variations in extraction/injection activity.
- To check the available physical model of the reservoir, in particular the evidence for strong variations in permeability.

The production in the Cavone field started in 1980 from a 400-700 m thick anticlinal reservoir located at a minimum depth of 2500 m in Mesozoic carbonate rocks. The field is divided into 5 fault segmented but connected blocks, which extend in an E-W direction and a separate compartment, the San Giacomo reservoir, which was inactive from December 2010 to April 2011 and then became reactivated in April 2011. These structures cover a total surface area of about 15 km². The original recoverable reserves were estimated at 3.0 Mm³ from a total resource of 15 Mm³; the residual reserves in 2012 are about 0.16 Mm³ after recovery of 3.06 Mm³.

Since 1993, the produced waste-water from the Cavone wells has been re-injected through the Cavone-14 well to a depth of approximately 3350 m into the same thick reservoir from which it has been extracted; from 2005 the re-injected water includes that from the San Giacomo reservoir. The fluid pressure in the reservoir seems to be maintained from the nearby aquifer and also thanks to the contribution of the injected water. The total volume of the injected water to date is equal to 2.6 Mm³ (0.07 Mm³ from San Giacomo – 2.5 % of the total volume). The injected water was at a maximum of 200,000 m³/year in 2004, at a minimum of 100,000 m³/year in 2010 and increased to 130,000 m³/year in 2011.

Since 2005 the monthly average effective injection pressure at the wellhead increased from the initial value of about 18 MPa to 21 MPa in 2008, and then decreased to about 13.8 MPa in the period 2009-2010. Its value then started to grow again up to about 19 MPa in May 2012. This volume of injected water was allowed to avoid large variations of the fluid volume in the reservoir. The volume difference during the life of the reservoir has been about -21%. The presence of several highly impervious layers in the stratigraphic sequence probably prevents a direct hydraulic contact between the Cavone reservoir and the seismogenic thrust zone. This does not preclude some connection through the thrust slices but the high permeability makes it difficult to sustain differential pressure. In fact, the changes in salinity during the lifetime of the production well do indicate some influxes of saltier water.

Considering the activity in the Cavone and Casaglia fields, the geological-structural characteristics and the seismic history in the area, the Commission deems very unlikely that the Emilia seismic sequence has been induced.

Consequently the Commission focused on the possibility that the main shocks of May 20 and 29 and the following sequence were triggered, i.e. that human activity may have contributed to the tectonic stress already existing on the fault system.

The Commission considered the possibility that the trigger was due to the variation in load due to extraction and /or injection.

The Coulomb stress change due to reservoir depletion is negative and would therefore inhibit the onset of the 20 May event, and while the location of the 29 May earthquakes are in a zone where the Coulomb stress change is positive, it is smaller than the tectonic transfer value reported in literature, although recent research suggests that triggering may occur over a wide range of stress changes, depending on the fault system and the nature of the triggering process.

Recent literature reports that fluctuations in injection of fluids may also lead to positive stress changes due to long-range variations in pore pressure. However in the studied case it has not been possible to assess this effect with available data.

The area struck by the May 20-29 2012 earthquakes is an elliptic region about 30 km long and about 10 km wide, which follows the crest of the buried Cavone-Mirandola anticline. The geological structures responsible for the seismic activity have been identified as thrust faults delimitating the outer margin of the Northern Apennines.

In current geological literature, the compressional regime, which is active in the region, has been associated either with Africa-Europe convergence, or to the flexural-hinge retreat of the south-western margin of Adria, undergoing passive sinking beneath the Apennines. The kinematic framework deduced from the geological and geophysical regional information fits the present-day seismicity pattern of Northern Italy, as well as the geodetic measurements available for the region.

Consideration of the historical seismicity of the region indicates that it is very likely that the stress field of some faults within the fault system were in 2012 already close to the conditions necessary to generate an earthquake with a magnitude approaching 6 ML.

The Moment Magnitude of the main shock of May 20, 2012 was estimated at between 5.63 and 6.11 and it occurred at a depth of 5.3 (± 1.0) km and at a distance of 20 km from the Mirandola site. The main shock of May 29 (Mw 5.44-5.96) was located close to Mirandola, at a depth of 9.2(± 0.9) km. Earthquakes triggered at these distances from the extraction/re-

injection site are less common, but some cases have been reported in the literature. The time-depth conversion of the interpreted seismic profiles shows that the fault is located at a depth between 4,000 and 4,500 metres and in agreement with instrumental determination. Therefore it could be the source of the 20 May. The May 29 earthquakes are located on a different structure. The analysis of seismic profiles shows that this structure may lie between 10,000 and 11,500 metres in fairly agreement with instrumental determination.

The prevalent focal mechanism is reverse faulting and is consistent in style with the seismo-tectonic thrust/fold system, which accommodates motion at the WNW-ESE outer margin of the Northern Apennines, buried under the Po Plain. Earthquakes occurred on different segments of this system, for a distance of 30 km along its length. This fault system had been identified as an active structure prior to the 2012 Emilia earthquakes, but was only roughly mapped, even if it was included in the Italian Database of Individual Seismogenic Sources

Low to medium magnitude seismic activity, mostly in the range 1.5 to 3 M_L , but reaching the value of 4 M_L a few hours prior to the mainshock occurred in the study period before May 2012. Some of these were located in the area of the first main event some 20 km away from the injection well. Some characteristics of the seismic activity (non-Poissonian event occurrence process, time variation of the magnitude distribution) point to a pattern, which is different to that of typical background activity. The result of space-time clustering analysis indicates that, at least from the middle of 2008, some parts of the pre-May 20th seismicity were connected with the subsequent major shock sequence.

A detailed analysis of the production and injection data at Mirandola for the period 2005-2012 shows a fluctuating pattern. Simultaneous changes from increasing trend to decreasing trend of monthly extracted and injected volumes of fluid and of the well-head pressures occurred twice. These occurred between 09/2008 and 11/2008 and in 11/2010 and these variations were not correlated with changes in the seismicity. A rapid trend change from decreasing to increasing of all the production parameters occurred in April-May 2011, and is statistically correlated with an increase both in number and energy of earthquakes. The order of magnitude of the variations of the production parameters in the period from April/May 2011 to May 2012 is some MPa for the effective well-head pressure, hundreds of cubic meters/month for oil volume and for the reinjected water. For comparison the variations of volumes for some other cases of waste-water disposal within the reservoir, such as Huangjiachang and Rongchang in China, are about tenfold higher.

These observations indicate that the last pre-May 20 seismic activity and the May 20 main event are statistically correlated with an increase of extraction and injection activity at Cavone.

The next step is to understand whether the post May 20 activity, in particular the events of May 29, may have been activated by a non tectonic contribution.

ETAS modelling of 31 days of history of the subsequent seismicity after the May 20 mainshock signifies that these were typical mainshock/aftershock sequences with no indication of non-tectonic influences.

Generally an earthquake produces static and dynamic stress variations in the surrounding rocks. The static stress variation produced by high magnitude earthquakes can bring nearby faults closer to failure. The estimate of the static stress variation for the Emilia 2012 sequence, considering all the uncertainties in the parameters describing source and receiver

faults, indicates that the main shock of May 20 produced a positive stress transfer to the fault generating the May 29 earthquakes (at 80% significance level). The dynamic stress transfer is linked to the propagation of time-varying loads from seismic waves, which can be sufficient to produce earthquakes from a fault which is already ripe. Analysis of the dynamic stress, due to the seismic waves and produced by consecutive events is available in the literature. It has been calculated that the dynamic stress is greater than the static stress and sufficient to trigger the May 29 activity.

In the Ferrara geothermal system, the geothermal fluid is produced by the wells “Casaglia 2” (open hole from 890m to 1950m) and “Casaglia 3” (open hole from 890m to 1950m). After extraction, geothermal fluid is circulated through a heat exchanger and it is then filtered and reinjected into well “Casaglia 1” (open hole from 1119m to 1950m), at a distance of 1 km from the two production wells. The reservoir from which the hot fluid is produced is a confined aquifer in the fractured Mesozoic carbonates within a very large structural high. Since the start of extraction in 1990, the temperature of the produced fluid and the pressure of production and reinjection have not shown significant variations, therefore it is possible to assume the reservoir boundaries to be far away from the wells. Due to the completion scheme of the wells, the re-injection and the production of the fluid takes place in the same unit, which can be identified as the geothermal reservoir.

Considering that:

- (a) The heat exploitation recovers thermal water with a formation temperature of 100° C and re-injects all of it totally at a temperature of 70° C
- (b) Temperature induced geomechanical effects have been observed when the temperature drop between injection and extraction is at least of 80°
- (c) In the period 1995-2012 a total of 36 million m³ was produced and re-injected at constant pressure,

The operation of the Ferrara geothermal plant is extremely unlikely to have produced seismicity for the following three reasons:

- 1) The temperature drop between extraction and re-injection is 30° and the observed subsidence does not seem to be influenced by the activity of the geothermal field being comparable to the regional subsidence in the Po Plain (<2.5 mm/year).
- 2) The plant is operated with volume balance in the far field, i.e. the volume is balanced overall but may be locally unbalanced close to the injection
- 3) The reported seismicity cases induced by geothermal activities operated with volume balance in the far field have epicenters close to the borehole section of the injection well. This seems not to be the case for Ferrara where seismicity has been minimal.

It is very unlikely that the operations performed in the Casaglia geothermal field have had any effects on seismic activity of the Emilia sequence.

The low and negative static stress change generated by the depletion of the reservoir, may argue in favour of a tectonic origin of the whole earthquake sequence. The small, positive coseismic stress transferred from the May 20 events to the May 29 faults may explain the

second phase of seismicity. However, there are statistical correlations between the increase of seismic activity before the May 20 2012 event and the increase of production parameters since April/May 2011. This means that it cannot be ruled out that the combined anthropogenic actions of extraction and injection of fluids in a tectonically active region may have contributed, adding a minute additional load, to the activation of a pre-stressed fault system, already close to the conditions required to produce a significant earthquake.

The Commission believes that it is highly unlikely that the activities of hydrocarbon exploitation at Mirandola and the geothermal activity at Casaglia have produced sufficient stress change to generate an **'induced'** seismic event. While it cannot constitute proof, the current state of knowledge and all the processed and interpreted information does not allow the ruling out of the possibility that the actions involved in hydrocarbon exploitation in the Mirandola field may have contributed to **'trigger'** the Emilia seismic activity.

Therefore in order to build a physical model that supports the statistical analysis it would be necessary to have an image as complete as possible of the dynamics of fluids in the reservoir and in the surrounding rocks .

Predicting earthquakes is a holy grail, which has been sought for many generations, and while progress has been made in forecasting, we are not currently able to reliably predict: 'the where', "the when" and "the how-big" of an earthquake. A **triggered** earthquake is a special case of a tectonic earthquake where small effects of operational activities have advanced the earthquake clock and so the difficulties are even greater. **Induced seismicity**, in contrast, can be more easily mitigated as the anthropogenic influence is significant and changes to operational methodologies can make significant improvements to likelihoods of further events. Traffic-light systems, where they have been developed, have to date concerned **induced seismicity**.

The study does not indicate that there is evidence which can associate the Emilia 2012 seismic activity to the operation activities in Spilamberto, Recovato, Minerbio and Casaglia fields, whereas it cannot be ruled out that the activities carried out in the Mirandola License area have had a triggering effect.

In any case, the whole Apennine orogen under the Po Plain is seismically active and therefore it is essential that production activity should be accompanied by appropriate actions, which will help to manage the seismic risk associated with these activities.

To this end the Commission makes the following recommendations.

Triggered and induced seismicity is a rapidly developing area of study but the present state of knowledge, and in particular a lack of experience in Italy, does not currently allow the identification of protocols of actions which can be immediately used for practical purposes for seismic risk management. The first need is the development of know-how through acquisition of detailed data, some of which must be provided by operators, and research which can improve the knowledge of the relationships between technological operations and triggered seismicity. Examples of seismicity in close proximity to hydrocarbon fields could usefully be studied, perhaps using the methodologies, which have been applied here by the Commission. Examples are Caviaga (1951), Correggio (1987 -2000) and there may be others. The seismicity and operational parameters should be closely inspected, and it is essential to have more than one case in order to be able to derive useful tools such as a traffic-light system.

New hydrocarbon/geothermal exploration activities must be preceded by preliminary desk study and field-based screening evaluation based on an extensive and detailed 3-D geophysical and geological study, allowing the determination of the main fault systems which can be suspected to be active and their seismogenic characteristics (fault length, occurrence rate, etc.). The return periods of major (5+ML) events should be carefully considered as this can give some indication of the state of 'ripeness' of major fault systems in the area.

Existing and new hydrocarbon/geothermal activities must be accompanied by high technology monitoring networks aimed at following the time evolution of the three fundamental aspects: microseismic activity, ground deformation and pore pressure. These should be put into operation as soon as practicable when licensing is being considered, so that as long as possible periods of prior ambient seismicity can be gathered. Microseismic monitoring can give indications of fault activity and source mechanisms which are useful in characterizing seismogenic zones.

Seismic monitoring should be carried out with a dedicated local network capable of detecting, locating and characterizing all earthquakes with magnitudes of at least 0.5 M_L .

Ground deformation, mostly with Earth observation satellite: interferometric (INSAR) and GPS technology, should be carried out allowing a resolution of some mm/year with the aim of identifying subsidence trends.

Fluid pore pressure must be measured directly at the bottom of the wells and in the surrounding rocks on a daily basis.

On the basis of the experience gained from other areas in the world and the geological and seismotectonic characteristics of the area under study, an operational traffic light system should eventually be generated with a relative threshold system.

It is advised that all the seismic data should be continuously statistically analyzed for deviations from typical background seismicity with discrimination techniques such as, changes in inter-event time, changes in b-value of magnitude distribution, temporal and spatial clustering, non-Poissonian behaviour, ETAS methodologies and incorporation of new developing techniques should be encouraged as they become available.

It is necessary that all the relevant data provided by operators are made available to the authorities responsible for the control.

It is critically important to implement an Outreach and Communication Program to local residents/administrative authorities so that they can gain confidence that operations are being managed optimally.

IX. Conclusioni

La Commissione tecnico-scientifica incaricata di valutare le possibili relazioni tra attività di esplorazione per idrocarburi ed aumento dell'attività sismica nell'area colpita dal terremoto dell'Emilia-Romagna del mese di maggio 2012 (ICHESE) è stata istituita l'11 dicembre 2012 con decreto del Dott. Franco Gabrielli, Capo del Dipartimento della Protezione Civile della Presidenza del Consiglio dei Ministri su richiesta del Presidente della Regione Emilia. La composizione della Commissione è stata modificata con successivi decreti.

La Commissione ha avuto il seguente incarico:

“La Commissione Internazionale dovrà produrre un rapporto che, sulla base delle conoscenze tecnico-scientifiche al momento disponibili, risponda ai seguenti quesiti:

1. E' possibile che la crisi emiliana sia stata innescata dalle ricerche nel sito di Rivara, effettuate in tempi recenti, in particolare nel caso siano state effettuate delle indagini conoscitive invasive, quali perforazioni profonde, immissioni di fluidi, ecc.?
2. E' possibile che la crisi emiliana sia stata innescata da attività di sfruttamento o di utilizzo di reservoir, in tempi recenti e nelle immediate vicinanze della sequenza sismica del 2012?

La Commissione ha iniziato i suoi lavori il 2 maggio 2013 e si è riunita per la prima volta in forma plenaria il 18 giugno 2013. La Commissione ha acquisito dati sulla attività sismica e deformazioni del suolo, sulla geologia e sismica a riflessione e sulle operazioni di esplorazione, e sfruttamento di idrocarburi, stoccaggio di gas e attività geotermica, tra l'altro attraverso riunioni con rappresentanti dell'INGV (*Istituto Nazionale di Geofisica e Vulcanologia*), dell'OGS (*Istituto Nazionale di Oceanografia e Geofisica Sperimentale*), del Servizio Sismologico della Regione Emilia Romagna e delle Ditte che svolgono attività di esplorazione e sfruttamento idrocarburi nell'area. La Commissione ha incontrato altresì la società *Independent Gas Management Srl* che ha studiato le caratteristiche geologiche dell'area di Rivara per preparare un progetto di stoccaggio in acquifero.

Il lavoro della Commissione è iniziato con una revisione della letteratura scientifica e dei rapporti disponibili. Esiste infatti una vasta letteratura scientifica, sviluppata soprattutto negli ultimi venti anni, che mostra come in alcuni casi azioni tecnologiche intraprese dall'uomo, comportanti iniezione o estrazione di fluidi dal sottosuolo, possano avere una influenza sui campi di sforzi tettonici principalmente attraverso variazioni nella pressione di poro nelle rocce e migrazione di fluidi. Pertanto sull'attività sismica che si verifica in prossimità spaziale con i siti e temporale con le operazioni sorge il sospetto che le operazioni antropiche possano aver avuto una influenza.

Nella letteratura scientifica viene spesso adottata una distinzione dei terremoti nelle seguenti categorie:

- **Terremoti tettonici**, che sono prodotti dai sistemi di sforzo naturali, dove lo sforzo tettonico ha superato lo sforzo di attrito esistente e la regione era “matura” da un punto di vista sismico.
- **Terremoti antropogenici**, nei quali l'attività umana ha avuto un qualche ruolo nel portare il sistema al punto di rottura:
 - a) **Terremoti indotti**, nei quali uno sforzo esterno, prodotto dalle attività antropiche, è sufficientemente grande da produrre un evento sismico in una

regione che non era necessariamente sottoposta a un campo di sforzi tale da poter generare un terremoto in un futuro ragionevolmente prossimo (in senso geologico). Cadono in questa categoria i terremoti prodotti da procedimenti di stimolazione termica o idraulica di una roccia, quali la Fratturazione Idraulica (*Fracking*) e gli *Enhanced Geothermal Fields*.

b) **Terremoti innescati**, per i quali una piccola perturbazione generata dall'attività umana è sufficiente a spostare il sistema da uno stato quasi-critico ad uno stato instabile. L'evento sismico sarebbe comunque avvenuto prima o poi, ma probabilmente in tempi successivi e non precisabili. In altre parole, il terremoto è stato anticipato. In questo caso lo sforzo perturbante "aggiunto" è spesso molto piccolo in confronto allo sforzo tettonico pre-esistente. La condizione necessaria perché questo meccanismo si attivi è la presenza di una faglia già carica per uno sforzo tettonico, vicina ad un sito dove avvengono azioni antropiche che alterano lo stato di sforzo, dove vicina può voler dire anche decine di chilometri di distanza a seconda della durata e della natura dell'azione perturbante. In alcuni casi queste alterazioni possono provocare l'attivazione della faglia già carica. È importante ricordare che, poiché in questo caso le operazioni tecnologiche attivano solamente il processo di rilascio dello sforzo tettonico, la magnitudo dei terremoti innescati può essere grande, dello stesso ordine di quella dei terremoti tettonici, e dipenderà dall'entità della deformazione elastica accumulata sulla faglia a causa del carico tettonico.

Numerosi rapporti scientificamente autorevoli descrivono casi ben studiati nei quali l'estrazione e/o l'iniezione di fluidi in campi petroliferi o geotermici è stata *associata* al verificarsi di terremoti, a volte anche di magnitudo maggiore di 5. È difficile, a volte impossibile, utilizzare il termine *provata* per questi casi. I casi riportati sono solo una piccola percentuale di tutti i casi esistenti di estrazione ed iniezione di fluidi, e si riferiscono in gran parte all'aumento di pressione di carico legato a serbatoi molto grandi e a iniezioni di grandi volumi di fluido (in genere acqua di processo) nella roccia circostante, non nello stesso serbatoio in cui avviene l'estrazione, durante operazioni per recupero avanzato di idrocarburi o per tenere costante la pressione. Esistono comunque alcuni casi in cui l'attività sismica è stata associata a re-iniezione di acqua di processo nello stesso serbatoio dal quale è stato estratto olio o gas.

Le principali conclusioni che si possono trarre dai casi riportati sono:

- Estrazioni e/o iniezioni legate allo sfruttamento di campi petroliferi possono produrre, in alcuni casi, una sismicità indotta o innescata;
- La maggior parte dei casi documentati in cui una attività sismica è stata associata a operazioni di sfruttamento di idrocarburi è relativa a processi estrattivi da serbatoi molto grandi o a iniezione di acqua in situazioni in cui la pressione del fluido non è bilanciata;
- Il numero di casi documentati di sismicità di magnitudo medio-alta associabile a iniezione di acqua nello stesso serbatoio da cui ha avuto luogo l'estrazione di idrocarburi è una piccola percentuale del numero totale;

- La sismicità indotta e, ancor più, quella innescata da operazioni di estrazione ed iniezione sono fenomeni complessi e variabili da caso a caso, e la correlazione con i parametri di processo è ben lontana dall'essere compresa appieno;
- La magnitudo dei terremoti innescati dipende più dalle dimensioni della faglia e dalla resistenza della roccia che dalle caratteristiche della iniezione;
- Ricerche recenti sulla diffusione dello sforzo suggeriscono che la faglia attivata potrebbe trovarsi anche a qualche decina di chilometri di distanza e a qualche kilometro più in profondità del punto di iniezione o estrazione, e che l'attivazione possa avvenire anche diversi anni dopo l'inizio dell'attività antropica;
- La maggiore profondità focale di alcuni terremoti rispetto all'attività di estrazione associata è stata interpretata come una evidenza diretta del fatto che l'estrazione o l'iniezione di grandi volumi di fluidi può indurre deformazioni e sismicità a scala crostale;
- Esistono numerosi casi di sismicità indotta da operazioni di sfruttamento dell'energia geotermica. La maggior parte di essi è legata allo sviluppo di *Enhanced Geothermal Systems*, nei quali vengono provocate fratture in rocce ignee impermeabili per produrre delle zone permeabili. Esistono anche diversi casi di terremoti associati all'utilizzazione tradizionale dell'energia geotermica. I terremoti prodotti sono di magnitudo medio-bassa e a distanze non più grandi di alcuni kilometri dai pozzi di estrazione o iniezione.
- L'esame di tutta la letteratura esistente mostra che la discriminazione tra la sismicità indotta o innescata e quella naturale è un problema difficile, e attualmente non sono disponibili soluzioni affidabili da poter essere utilizzate in pratica.

Partendo da questo stato delle conoscenze, la Commissione ha cercato di stabilire l'eventuale nesso esistente tra le operazioni di iniezioni/estrazione e stoccaggio di fluidi e l'attività sismica nell'area dell'Emilia Romagna colpita dalla crisi sismica del maggio-giugno 2012.

L'area colpita dalla sequenza sismica in questione ha forma di una ellisse lunga circa 30 km e larga circa 10 km, che si estende in direzione est-ovest sopra l'anticlinale di Cavone-Mirandola. La Commissione ha definito, su basi sismo-tettoniche, una area di interesse di circa 4000 km² che include la zona dell'attività sismica del 2012. Nell'area sono presenti tre concessioni di sfruttamento per idrocarburi, Mirandola (con incluso il campo di Cavone), Spilamberto e Recovato, nonché il campo geotermico di Casaglia (Ferrara) e il giacimento di stoccaggio di gas naturale di Minerbio situato al margine sud-est dell'area.

Nella zona è inoltre inclusa l'area del progetto Rivara per un sito di stoccaggio di gas naturale in acquifero, cui si riferisce il primo quesito posto alla Commissione. Dopo aver analizzato la documentazione fornita dalla Compagnia *Independent Gas management* e preso visione della dichiarazione del Ministero dello Sviluppo Economico (MISE), il quale ha certificato che non era stata concessa alcuna autorizzazione per attività minerarie e che non risulta sia stata effettuata alcuna attività di esplorazione mineraria negli ultimi 30 anni, la Commissione ritiene che la risposta al primo quesito sia NO.

Per la risposta al secondo quesito, dopo aver considerato le informazioni disponibili sia sull'attività sismica che sulle operazioni relative allo sfruttamento e allo stoccaggio nelle concessioni nell'area, la Commissione ha deciso, per le ragioni di seguito esposte, di concentrare la sua attenzione sui campi più vicini all'attività sismica del 2012, e cioè:

La concessione di coltivazione di Mirandola e
Il campo geotermico di Casaglia.

Il giacimento di idrocarburi di Cavone, è situato nella concessione di Mirandola, si trova circa 20 km a ovest della scossa principale del 20 maggio 2012, è molto vicino agli epicentri degli eventi di magnitudo maggiore di 5 del 29 Maggio e del 3 Giugno. Gli epicentri di altre due scosse di magnitudo superiore a 5, verificatesi il 20 maggio, sono spostati verso il campo geotermico di Casaglia, che si trova 15-20 km a nord-est dell'epicentro della scossa principale del 20 maggio.

Sebbene l'attività estrattiva sia proceduta con continuità fino ai giorni del terremoto sia a Cavone che a Spilamberto e Recovato, il pozzo Cavone-14 era l'unico attivo nel re-iniettare l'acqua di processo prima e durante la sequenza sismica del 2012. Inoltre, mentre il serbatoio di Cavone è situato nelle rocce carbonatiche Mesozoiche e potrebbe essere connesso idraulicamente con le faglie di sovrascorrimento sottostanti, gli altri serbatoi sono situati in formazioni Plio - Pleistoceniche al disopra di livelli di rocce altamente impermeabili. Ciò rende altamente improbabile un contatto diretto con le faglie sismogeniche.

Allo scopo di avere un quadro quanto più omogeneo possibile sulle caratteristiche dell'attività sismica, sulle conoscenze geologiche e sulle operazioni di iniezione ed estrazione di fluidi, la Commissione ha ritenuto opportuno procedere ad una rielaborazione dei dati esistenti più rilevanti. In particolare a:

- Rianalizzare i profili di sismica a riflessione e le informazioni fornite dai log dei pozzi di perforazione per verificare il modello tettonico dell'area e costruire un modello 3D di velocità delle onde sismiche da usare per la ri-localizzazione dell'attività sismica. L'utilizzazione di un modello 3D è opportuna data la forte asimmetria in direzione nord-sud delle strutture geologiche superficiali.
- Ricalcolare i parametri classici (coordinate geografiche, profondità, meccanismi focali) dell'attività sismica, con epicentro nella zona in esame, registrata dalla rete sismica INGV a partire dal 2005 quando il catalogo strumentale INGV ha raggiunto la configurazione attuale.
- Stimare il trasferimento di sforzo di Coulomb prodotto dalle scosse principali del 20 maggio allo scopo di verificare se esse possano aver contribuito a portare più vicino al punto di rottura la faglia degli eventi dal 29 maggio al 3 giugno.
- Effettuare un'analisi statistica dell'attività sismica nell'area di interesse a partire dal 2005, inclusa la sequenza del maggio 2012, cercando possibili deviazioni dall'andamento tipico della sismicità naturale e possibili correlazioni con le variazioni dell'attività di estrazione/iniezione.
- Studiare il modello fisico di serbatoio disponibile, in particolare verificando se vi erano evidenze di forti variazioni di permeabilità.

La produzione nel campo di Cavone è iniziata nel 1980, attingendo da un serbatoio di 400-700 m di spessore il cui tetto si trova ad una profondità minima di 2.500 m, situato nei carbonati mesozoici in una struttura anticlinale. Il campo è diviso in 5 blocchi segmentati da faglie, ma connessi tra di loro, che si estendono in direzione est-ovest, e da un compartimento separato, il serbatoio di San Giacomo, che è stato inattivo dal dicembre 2010 all'aprile 2011, ed è stato riattivato in quest'ultima data. Queste strutture, in totale, coprono un'area di circa 15 km². Le riserve recuperabili furono originariamente stimate in circa 3 Mm³ da un volume

totale di 15 Mm³; nel 2012, dopo aver estratto 3,06 Mm³, è presente una riserva residua di circa 0.16 Mm³.

Dal 1993 l'acqua estratta insieme agli idrocarburi viene re-iniettata attraverso il pozzo Cavone-14 a circa 3350 m di profondità nello stesso serbatoio dal quale avviene l'estrazione; dal 2005 nello stesso pozzo viene anche re-iniettata l'acqua estratta dal serbatoio di San Giacomo. La pressione di fluido nel serbatoio sembra essere sostenuta dalla falda acquifera confinante, con il contributo dell'acqua re-iniettata. Il volume complessivo di acqua re-iniettata è ad oggi pari a 2,6 Mm³ (di questi 0,07 Mm³, pari a circa il 2,5% del volume totale, vengono da San Giacomo). Il volume iniettato ha raggiunto un massimo di circa 200.000 m³ annui nel 2004, un minimo di circa 100.000 m³ nel 2010 per poi risalire a circa 130.000 m³ annui nel 2011. La pressione effettiva media mensile di re-iniezione a bocca pozzo è aumentata da 18 MPa nel 2005 a 21 MPa nel 2008, per poi diminuire a 13.8 MPa nel periodo 2009-2010 e infine aumentare di nuovo a 19 MPa nel maggio 2012. Il volume di acqua re-iniettata ha permesso di non avere grandi variazioni del volume di fluido nel serbatoio. La differenza di volume durante tutto il periodo di sfruttamento del serbatoio è di circa -21%. La presenza di diverse formazioni altamente impermeabili nella sequenza stratigrafica probabilmente impedisce una diretta connessione idraulica tra il serbatoio di Cavone e la zona sismogenica. Ciò non precluderebbe una connessione attraverso le faglie di sovrascorrimento che limitano le falde sovrascorse, ma l'alta permeabilità rende difficile la persistenza di pressioni differenziali. Di fatto le variazioni di salinità riscontrate durante tutto il periodo della produzione, testimoniano l'arrivo di flussi di acqua più salata dall'esterno.

Considerando l'attività nei campi di Cavone e Casaglia, le caratteristiche geologico-strutturali e la storia sismica della zona, la Commissione ritiene che sia molto improbabile che la sequenza sismica dell'Emilia possa essere stata indotta (cioè provocata completamente dalle attività antropiche).

Di conseguenza la Commissione ha concentrato la sua attenzione sulla possibilità che le scosse principali del 20 e del 29 maggio e la sequenza sismica connessa fossero state innescate, cioè che l'attività umana possa aver fornito un contributo allo sforzo tettonico che già agiva sul sistema di faglie.

La Commissione ha considerato la possibilità che l'innescò possa essere dovuto a variazioni di carico conseguenti alle operazioni di estrazione e /o iniezione di fluidi.

La variazione dello sforzo di Coulomb dovuta allo svuotamento del serbatoio ha valori negativi nella zona della scossa del 20 maggio e quindi avrebbe avuto l'effetto di inibirla, mentre le scosse del 29 maggio sono ubicate in una zona dove la variazione di sforzo di Coulomb è positiva ed è minore dei valori spesso assunti in letteratura come necessari per attivare una faglia. Tuttavia ricerche recenti suggeriscono che terremoti possano essere innescati per valori molto diversi delle variazioni di sforzo, a seconda delle caratteristiche del sistema di faglie e della natura del processo di innescò.

Ricerche recenti indicano inoltre che fluttuazioni nelle iniezioni di fluidi potrebbero indurre variazioni di sforzo positive dovute a variazioni a largo raggio della pressione di poro. Tuttavia nel caso in esame non è possibile valutare questo effetto con i dati disponibili.

L'area colpita dalla sequenza sismica del maggio 2012 è una regione ellittica lunga circa 30 km e larga circa 10 km che segue la cresta dell'anticlinale sepolta di Cavone-Mirandola. Le strutture geologiche identificate come responsabili dell'attività sismica sono le faglie di sovrascorrimento che delimitano il margine esterno dell'Appennino settentrionale.

Secondo la letteratura geologica corrente, il regime tettonico compressivo attivo nella regione è stata associato alla convergenza Europa-Africa oppure all'arretramento flessurale del margine sud-occidentale del blocco di Adria in sprofondamento passivo al di sotto degli Appennini. Il quadro cinematico deducibile dalle informazioni geofisiche, geologiche e geodetiche si accorda bene con le caratteristiche della sismicità attuale dell'Italia settentrionale.

In base alla sismicità storica della zona si può ritenere molto probabile che il campo di sforzi su alcuni segmenti del sistema di faglie nel 2012 fosse ormai prossimo alle condizioni necessarie per generare un terremoto di magnitudo locale (M_L) intorno a 6.

La scossa del 20 maggio 2012 caratterizzata da una magnitudo momento (M_w) stimata tra 5.63 e 6.11, è avvenuta a una profondità di 5.3 (± 1.0) km e a una distanza di circa 20 km dalla concessione di Mirandola, mentre quella del 29 (M_w 5.44-5.96) è avvenuta ad una profondità di 9.2 (± 0.9) km e in prossimità della concessione. Segnalazioni di terremoti innescati a distanze di questo ordine dal sito di estrazione e/o re-iniezione non sono frequenti ma esistono alcuni casi riportati in letteratura. La conversione tempo-profondità dei profili sismici interpretati mostrano che la faglia si trova tra 4000 e 4500 metri di profondità e, in accordo con i dati strumentali, essa potrebbe essere la sorgente del terremoto del 20 maggio. I terremoti del 29 maggio sono invece su una diversa struttura, per i quali la interpretazione dei profili sismici mostra che questa struttura giace ad una profondità compresa tra 10.000 e 11.500 metri, in discreto accordo con le determinazioni strumentali.

I meccanismi focali dei terremoti della sequenza sono prevalentemente di faglia inversa, e concordano con lo stile tettonico di sovrascorrimento dovuto al movimento in direzione ONO-ESE del margine esterno dell' Appennino settentrionale, al di sotto della pianura padana. L'attivazione di diversi segmenti di questo sistema ha prodotto la sequenza sismica del 2012. Questo sistema di faglie era stato identificato come struttura attiva prima del terremoto del maggio 2012, ed è riportato, seppure in modo non dettagliato, nel Database italiano delle Sorgenti Sismogeniche Individuali (INGV).

Un'attività sismica di intensità medio-bassa (per lo più tra 1.5 e 3 M_L , ma che ha raggiunto i 4 M_L poche ore prima della scossa principale del 20 maggio) si è verificata nel periodo studiato prima del maggio 2012. Alcuni di questi eventi sono ubicati vicino all'epicentro della scossa principale del 20 maggio, a circa 20 km di distanza dal pozzo di re-iniezione. L'analisi di alcune caratteristiche dell'attività sismica (andamento non poissoniano della distribuzione degli eventi nel tempo, variazione della distribuzione della magnitudo) hanno evidenziato un comportamento diverso rispetto a quello generalmente presentato dalla sismicità di fondo. Il risultato dell'analisi di *clustering* spazio-temporale è che almeno a partire dalla metà del 2008, una parte dell'attività sismica è connessa alla sequenza sismica del maggio 2012.

Un'analisi dettagliata dei dati di produzione ed iniezione relativi alla concessione di Mirandola per il periodo temporale 2005-2012 mostra un andamento fluttuante. In particolare per due volte i volumi di fluido estratto e iniettato e la pressione a bocca pozzo sono variati simultaneamente passando da un andamento crescente nel tempo a un andamento decrescente. Ciò si è verificato tra il 09/2008 e l' 11/2008 e nel novembre 2010. Queste variazioni non sono correlate a variazioni nell'attività sismica. Nell'aprile-maggio 2011 c'è stato una repentina variazione di tendenza, da decrescente a crescente, di tutti i parametri di produzione, che risulta correlata statisticamente con un aumento della sismicità, sia in numero di eventi che in energia. L'ordine di grandezza delle variazioni dei parametri di produzione nel periodo da Aprile/Maggio 2011 a Maggio 2012 è di qualche MPa per la pressione effettiva a bocca pozzo, di centinaia di m^3 /mese per i volumi di olio e di acqua re-iniettata. Per confronto si ricorda che le variazioni dei volumi di acqua di processo re-iniettata dei serbatoi sono circa dieci volte più grandi nei casi riportati in letteratura, quali quelli di Huangjiachang e Rongchang in Cina.

Queste valutazioni indicano che l'attività sismica immediatamente precedente il 20 maggio e l'evento principale del 20 maggio sono statisticamente correlati con l'aumento dell'attività di estrazione e re-iniezione di Cavone.

Il problema successivo è stato di capire se per le scosse successive al 20 maggio, in particolare gli eventi del 29, sia possibile ipotizzare un contributo non tettonico.

L'analisi con il metodo ETAS di 31 giorni di attività sismica successiva alla scossa principale del 20 maggio indica che si tratta di una tipica sequenza *mainshock-aftershocks* e non vi sono indicazioni di un contributo non tettonico.

Generalmente un terremoto produce nelle rocce circostanti una variazione di sforzo di due tipi: statico e dinamico. La variazione di sforzo statico associato a terremoti di elevata magnitudo può attivare faglie adiacenti generando quindi nuovi terremoti. La stima del trasferimento di sforzo statico per la sequenza emiliana del 2012, considerando le incertezze in gioco sui parametri che descrivono le faglie sorgenti e riceventi, indica che la scossa del 20 maggio ha prodotto un trasferimento di sforzo positivo sulla faglia che ha generato i terremoti del 29 maggio (con un livello di significatività dell'80%). La variazione di sforzo dinamico è legata ad effetti transienti provocati dal passaggio delle onde sismiche che possono attivare una faglia già matura. Per la sequenza emiliana, la stima della variazione di sforzo dinamico dovuto al passaggio delle onde sismiche e prodotto da eventi consecutivi nella sequenza è disponibile nella letteratura. E' stato calcolato che lo sforzo dinamico è maggiore di quello statico ed è sufficiente a innescare l'attività sismica del 29 maggio.

Per quanto riguarda il sistema geotermico di Ferrara, il fluido geotermico viene prodotto dai pozzi "Casaglia 2" (open-hole dagli 890 ai 1950 metri) e "Casaglia 3" (open-hole dagli 890 ai 1950 metri). Dopo l'estrazione, il fluido geotermico circola in uno scambiatore di calore, viene filtrato e re-iniettato nel pozzo "Casaglia 1" (open hole da 1119 metri a 1950 metri) ad una distanza di 1 km dai pozzi produttori. Il serbatoio da cui il fluido viene estratto è un acquifero confinato in calcari Mesozoici fratturati facenti parte di un alto strutturale molto esteso. Dall'inizio della produzione nel 1990 ad oggi, la temperatura del fluido prodotto e le pressioni di produzione/re-iniezione non hanno presentato variazioni significative; è possibile quindi assumere che i confini del serbatoio siano a distanze molto maggiori dai pozzi rispetto alla distanza tra i pozzi stessi. Lo schema di funzionamento dei pozzi mostra che la re-iniezione e la produzione avvengono nelle stesse rocce, che possono essere identificate con il serbatoio geotermico.

Considerando che:

(a) l'acqua viene estratta ad una temperatura di circa 100°C e re-iniettata completamente a circa 70°C;

(b) effetti geo-meccanici dovuti alle variazioni termiche sono stati osservati in altri casi quando la differenza tra le temperature di iniezione ed estrazione è di almeno 80°

(c) dal 1995 al 2012 sono stati estratti ed iniettati in totale 36 Mm³ di acqua a pressione costante

La possibilità che l'attività sismica sia stata in qualche modo provocata dall'impianto geotermico risulta estremamente improbabile almeno per 3 motivi:

1) la differenza di temperatura tra iniezione ed estrazione è di 30° e la subsidenza osservata non sembra essere influenzata dal campo geotermico essendo confrontabile con quella regionale della Pianura Padana, (< 2,5 mm/anno).

2) l'impianto funziona con un bilanciamento di volume in campo lontano, cioè il volume è bilanciato complessivamente, ma può non esserlo solo in vicinanza del punto di iniezione;

3) l'attività sismica registrata in casi di questo tipo è generalmente localizzata in prossimità della sezione del pozzo di iniezione. Questo non sembra essere il caso di Ferrara dove la sismicità è stata minima.

In conclusione, è molto improbabile che le operazioni effettuate nel campo geotermico di Casaglia possano avere influenzato l'attività sismica del 2012.

I valori bassi e negativi della variazione di sforzo generato dal graduale svuotamento del giacimento di Cavone porterebbero argomenti a favore di una origine tettonica dell'intera sequenza sismica. Il piccolo, ma positivo, valore dello sforzo co-sismico trasferito dal terremoto del 20 maggio sulla faglia che ha generato gli eventi del 29 maggio può spiegare la seconda fase di sismicità. Comunque, esiste una correlazione statistica tra l'aumento della sismicità prima del 20 maggio 2012 e l'aumento dei parametri di produzione da aprile/maggio 2011. Quindi non può essere escluso che le azioni combinate di estrazione ed iniezione di fluidi in una regione tettonicamente attiva possano aver contribuito, aggiungendo un piccolissimo carico, alla attivazione di un sistema di faglie che aveva già accumulato un sensibile carico tettonico e che stava per raggiungere le condizioni necessarie a produrre un terremoto.

La Commissione ritiene altamente improbabile che le attività di sfruttamento di idrocarburi a Mirandola e di fluidi geotermici a Casaglia possano aver prodotto una variazione di sforzo sufficiente a generare un evento sismico “**indotto**”. L'attuale stato delle conoscenze e l'interpretazione di tutte le informazioni raccolte ed elaborate non permettono di escludere, ma neanche di provare, la possibilità che le azioni inerenti lo sfruttamento di idrocarburi nella concessione di Mirandola possano aver contribuito a “**innescare**” l'attività sismica del 2012 in Emilia.

Pertanto sarebbe necessario avere almeno un quadro più completo possibile della dinamica dei fluidi nel serbatoio e nelle rocce circostanti al fine di costruire un modello fisico di supporto all'analisi statistica.

La predizione dei terremoti è come la ricerca del Santo Graal alla quale si sono dedicate generazioni di studiosi, e mentre si sono fatti significativi progressi nel campo della previsione probabilistica, al momento non è possibile predire in modo deterministico e affidabile quando e dove ci sarà un terremoto e quale sarà la sua intensità. Un terremoto **innescato** è un particolare tipo di terremoto tettonico, nel quale piccoli effetti prodotti da attività umane hanno anticipato il momento in cui il terremoto sarebbe avvenuto e pertanto è ancora più difficile da trattare. Più semplice è il caso della sismicità **indotta**, in quanto le azioni umane hanno una influenza significativa; pertanto possono essere studiate variazioni nelle metodologie operative utilizzabili per abbassare significativamente la probabilità di questi eventi. Sistemi di monitoraggio con livelli crescenti di allarme (i cosiddetti sistemi a semaforo) sono in effetti stati sviluppati e applicati solo per casi di sismicità indotta.

Lo studio effettuato non ha trovato evidenze che possano associare la sequenza sismica del maggio 2012 in Emilia alle attività operative svolte nei campi di Spilamberto, Recovato, Minerbio e Casaglia, mentre non può essere escluso che le attività effettuate nella Concessione di Mirandola abbiano avuto potuto contribuire a innescare la sequenza.

Va comunque considerato che tutto l'orogene appenninico sottostante la pianura padana è sismicamente attivo ed è quindi essenziale che alle attività produttive vengano associate azioni appropriate che contribuiscano a gestire il rischio sismico inerente queste attività.

A tal fine la Commissione ha formulato le seguenti raccomandazioni.

La sismicità indotta e innescata dalle attività umane è un campo di studio in rapido sviluppo, ma lo stato attuale delle conoscenze, e in particolare la mancanza di esperienza in Italia, non permette la elaborazione di protocolli di azione che possano essere di uso

immediato per la gestione del rischio sismico. Ha quindi carattere prioritario lo sviluppo delle conoscenze attraverso l'acquisizione di dati dettagliati, alcuni dei quali devono essere forniti dagli operatori, e attraverso una ricerca che possa migliorare la conoscenza delle relazioni tra operazioni tecnologiche e sismicità innescata. Potrebbero essere studiati casi di sismicità nelle immediate vicinanze di campi di sfruttamento di idrocarburi, quali ad esempio quello di Caviago (1951) e di Correggio (1987-2000) e probabilmente anche altri, eventualmente utilizzando le metodologie applicate in questo rapporto dalla Commissione. Sarebbe necessario analizzare in dettaglio sia la sismicità che i parametri di produzione, ed è essenziale avere informazioni su più di un caso per poter sviluppare strumenti utili alla gestione del rischio, quale ad esempio i "sistemi a semaforo".

Nuove attività di esplorazione per idrocarburi o fluidi geotermici devono essere precedute da uno studio teorico preliminare e di acquisizione di dati su terreno basati su dettagliati rilievi 3D geofisici e geologici. Ciò deve essere volto alla determinazione dei principali sistemi di faglie con indizi di attività e delle loro caratteristiche sismogeniche (lunghezza della faglia, variazione dell'attività sismica nel tempo, ecc.). I periodi di ritorno dei terremoti principali ($>5 M_L$) devono essere considerati attentamente per avere indicazioni sul grado di "maturità" dei principali sistemi di faglia.

Le attività di sfruttamento di idrocarburi e dell'energia geotermica, sia in atto che di nuova programmazione, devono essere accompagnate da reti di monitoraggio ad alta tecnologia finalizzate a seguire l'evoluzione nel tempo dei tre aspetti fondamentali: l'attività microsismica, le deformazioni del suolo e la pressione di poro. Queste reti dovrebbero essere messe in funzione al più presto, già quando si attende la concessione, in modo da raccogliere informazioni sulla sismicità ambientale precedente all'attività per il più lungo tempo possibile. Il monitoraggio micro-sismico può fornire indicazioni sulla attività delle faglie e sui meccanismi di sorgente che possono essere utili alla caratterizzazione delle zone sismogeniche.

Il monitoraggio sismico dovrebbe essere effettuato con una rete locale dedicata capace di rilevare e caratterizzare tutti i terremoti di magnitudo almeno $0,5 M_L$.

Le deformazioni del suolo devono essere rilevate principalmente con metodi satellitari. Dovrebbero essere utilizzate tecnologie interferometriche (INSAR) e GPS che permettono di identificare processi di subsidenza con una risoluzione di alcuni millimetri all'anno.

La pressione dei fluidi nei serbatoi e nei pori delle rocce deve essere misurata al fondo dei pozzi e nelle rocce circostanti con frequenza giornaliera.

Infine, utilizzando l'esperienza di altri casi simili nel mondo e le caratteristiche geologiche e sismotettoniche dell'area in studio, deve essere generato un sistema operativo "a semaforo", e devono essere stabilite le soglie tra i diversi livelli di allarme.

È consigliabile che tutti i dati sismici vengano continuamente analizzati con metodologie statistiche per evidenziare variazioni dagli andamenti tipici della sismicità di fondo, quali variazioni dell'intervallo di tempo tra eventi, variazioni nel valore di b della distribuzione della magnitudo, clustering spaziali o/e temporali, comportamenti non-poissoniani. L'utilizzo di metodologie ETAS e di eventuali altre nuove metodologie va incoraggiato.

È necessario che i dati rilevanti per il conseguimento di quanto sin qui indicato e in possesso delle compagnie siano da esse messi a disposizione degli enti responsabili per il controllo.

Infine, l'implementazione di un Programma di Interazione e Comunicazione con la popolazione e gli amministratori locali ha una importanza critica perché venga acquisita fiducia nella gestione ottimale delle operazioni.

Acknowledgment

This report required an immense amount of work for retrieving all the available literature, the available seismological and production data and their processing. This was possible only with the efficient help of a research staff of support. Eng. Simona Esposito of AMRA Scarl took the burden of scientific coordination of the whole activity of the ICHESE Commission. Researchers supporting the activity of specific areas of expertise are Prof. Paolo Capuano and Dr. Alexander Garcia-Aristizabal from AMRA Scarl, Eng. Liliana Panei, Dr. Ilaria Antococchi, Dr. Serena Pannone and Dr. Raffaella Mastrella from MISE, Dr. Lucari Urpi from GFZ and Prof. Beata Orlecka-Sikora from Polish Academy of Sciences. Dr. Daniela Di Bucci from DPC si also aknowledged for the very efficient contribution to the secretary and coordination activities.

References

- 1 McGarr, A., Simpson, D. (1997). A broad look at induced and triggered seismicity. In: *Rockbursts and Seismicity in Mines* (Gibowicz, S.J., Lasocki, S., eds.), Balkema, Rotterdam, pp. 385-396.
- 2 McGarr, A., Simpson, D., Seeber, L. (2002). Case histories of induced and triggered seismicity. In: *International Handbook of Earthquake and Engineering Seismology part A* (Lee, W.H.K., Kanamori, H., Jennings, P.C., Kisslinger, C., eds.), Academic Press, London, pp. 647-661.
- 3 Dahm, T., Hainzl, S., Becker, D., Bisschoff, M., Cesca, S., Dost, B., Fritschen, R., Kuhn, D., Lasocki, S., Klose, C. D., Meier, T., Ohrnberger, M., Rivalta, E., Shapiro, S., Wegler, U. (2010). How to discriminate induced, triggered and natural seismicity. *Proceedings of the Workshop Induced seismicity: November 15 - 17, 2010, Hotel Hilton, Luxembourg, Grand-Duchy of Luxembourg, (Cahiers du Centre Européen de Géodynamique et de Séismologie,30), Centre Européen de Géodynamique et de Séismologie, 69-76.*
- 4 Ellsworth W.L. (2013). Injection-Induced Earthquakes. *Science* 341, doi: 10.1126/science.1225942
- 5 Davis, S. D., and Frohlich C. (1993). Did (or will) fluid injection cause earthquakes? Criteria for a rational assessment. *Seismol. Res. Lett.*, **64**: 207–224.
- 6 Green C. A., Styles P., Baptie. B. J. (2012). Preese Hall Shale gas fracturing Review & recommendations For Induced seismic mitigation. *Report to UK Department of Energy and Climate Change*, 26pp.
- 7 Keranen K.M., Savage H.M, Abers G.A., Cochran E.S. (2013). Potentially induced earthquakes in Oklahoma, USA: Links between wastewater injection and the 2011 Mw 5.7 earthquake sequence. *Geology*, **41**: 699-702.
- 8 Turuntaev S. (2012) Personal communication.
- 9 Brodsky E.E., Lajoie L.J. (2013). Anthropogenic Seismicity Rates and Operational Parameters at the Salton Sea Geothermal Field. *Science* 341, 543, doi: 10.1126/science.1239213
- 10 van der Elst N. J., Savage H. M., Keranen K. M., Abers G.A. (2013). Enhanced Remote Earthquake Triggering at Fluid-Injection Sites in the Midwestern United States. *Science*, **341**: 164-167.
- 11 Committee on Induced Seismicity Potential in Energy Technologies: Hitzman M.W. (Chair), Clarke D.D, Detournay E., Dieterich J.H., Dillon D.K., Green S.J, Habiger R.M., McGuire R.K., Mitchell J.K. Shemeta J.E., Smith J.L (Bill) (2013). Induced Seismicity Potential in Energy Technologies. National Academy of Sciences. *The National Academies Press Washington, D.C.*, pp. 248.
- 12 Suckale J. (2009). Induced seismicity in hydrocarbon fields. *Advances in Geophysics*, **51**: 55-106.
- 13 Frohlich C., Hayward C., Stump B. and Potter E. (2011). The Dallas–Fort Worth Earthquake Sequence: October 2008 through May 2009. *Bulletin of the Seismological Society of America*,

- 14 Evans K. F., Zappone A., Kraft T., Deichmann N. and Moia F. (2012). A survey of the induced seismic response to fluid injection in geothermal and CO₂ reservoirs in Europe. *Geothermics*, **41**: 30-54.
- 15 Gruenthal G. (2013). Induced seismicity related to geothermal projects versus natural tectonic earthquakes and other types of induced seismic events in Central Europe. *Geothermics* 10.1016
- 16 Davies R., Foulgera G., Bindleya A., Styles P. (2013). Induced seismicity and hydraulic fracturing for the recovery of hydrocarbons. *Marine and Petroleum Geology*, **45**: 171–185.
- 17 Nicol, A., Carne R., Gerstenberger M., Christophersen A. (2011). Induced seismicity and its implications for CO₂ storage risk. *Energy Procedia*, **4**: 3699-3706.
- 18 Zoback M. (2012). Managing the seismic risk posed by wastewater disposal. *Earth*, **57**: 38–43.
- 19 Segall, P. and Yerkes R.F. (1990). Stress and fluid pressure changes associated with oil field operations: a critical assessment of effects in the focal region of the 1983 Coalinga earthquakes, In The Coalinga, California Earthquake of May 2, 1983. *U.S. Geological Survey Professional Paper, U.S. Geological Survey, 1990*.
- 20 Segall, P. (1985). Stress and subsidence resulting from subsurface fluid withdrawal in the epicentral region of the 1983 Coalinga earthquake. *Journal of Geophysical Research*, **90**: 6801–6816.
- 21 McGarr A. (1991). On a possible connection between three major earthquakes in California and oil production. *Bull Seismol Soc Am*, **81**: 948-970.
- 22 Stein R. and Yeats R. S. (1989). Hidden Earthquakes. *Sci. Am.*, **260**: pp. 48-57.
- 23 Caloi P., De Panfis M., Di Filippo D., Marcelli L., Spadea M. C. (1956). Terremoti della Val Padana del 15-16 maggio 1951. *Annali Geofisica*, **9**: 63-1956.
- 24 Ottemöller, L., Nielsen H. H., Atakan K., Braunmiller J. and Havskov J. (2005). The 7 May 2001 induced seismic event in the Ekofisk oil field, North Sea. *Journal of Geophysical Research*, **110**, B10301.
- 25 Suckale J. (2009). Induced seismicity in hydrocarbon fields. *Advances in Geophysics*, **51**: 55-106.
- 26 Adushkin V. V., Rodionov V. N., Turuntaev S., and Yudin A. E. (2000). Seismicity in the oil field. *Oil Field Review*, **12**: 2–17.
- 27 Yerkes, R.F., and Castle, R.O. (1970). Surface deformation associated with oil and gas field operations in the United States. *Land subsidence: International Association of the Science of Hydrology, UNESCO Publication*, **89**: 55-66.
- 28 Chanpura R., (2001). Fault reactivation as a result of reservoir depletion. PhD Thesis Georgia Institute of Technology, USA.
- 29 Segall, P. (1989). Earthquakes triggered by fluid extraction. *Geology* **17**: 942-946.
- 30 Van Eck, T., Goutbeek F., Haak H. and Dost B. (2006). Seismic hazard due to small magnitude, shallow-source, induced earthquakes in The Netherlands. *Environmental Geology*, **87**: 105–

- 31 Dost (2013). *AAPG Induced Seismicity Workshop*, London.
- 32 Wassing (2013). *AAPG Induced Seismicity Workshop*, London
- 33 Majer E.L., Baria, R., Stark, M., Oates, S., Bommer, J., Smith, B., and Asamuma, H. (2007). Induced seismicity associated with Enhanced Geothermal Systems. *Geothermics*, **36**: 185-222.
- 34 Haring M., Ulich S., Ladner F., and B. Dyer (2008). Characterisation of the Basel 1 enhanced geothermal system. *Geothermics*, **37**: 469-495.
- 35 McGarr, A. (1976). Seismic Moments and Volume Changes. *Journal of Geophysical Research*, **81**: 1487–1494.
- 36 Healy, J. H., Rubey W. W., Griggs D. T., and Raleigh C. B. (1968). The Denver earthquakes. *Science*, **161**: 1301–1310.
- 37 Horton, S. (2012). Disposal of hydrofracking waste fluid by injection into subsurface aquifers triggers earthquake swarm in central Arkansas with potential for damaging earthquake. *Seism. Res. Lett.*, **83**: 250-260.
- 38 Frohlich C., Hayward C., Stump B. and Potter E. (2011). The Dallas–Fort Worth Earthquake Sequence: October 2008 through May 2009. *Bulletin of the Seismological Society of America*, **101**: 327-340.
- 39 Cochran E.S., Sumy D.F., Keranen K.M., Abers G.A. and Savage H.M. (2012). Coulomb stress modeling of the 2011 M5.7 Oklahoma earthquake sequence. *American Geophysical Union 2012 Fall Meeting, San Francisco, California, 3–7 December 2012*, S53I–05.
- 40 McGarr (2013 pers comm)
- 41 Zoback, M.D., and Harjes, H-P, 1997. Injection-induced earthquakes and crustal stress at 9km depth at the KTB deep drilling site, Germany. *J. Geophys. Res.*, **102(B8)**: 18477-18491
- 42 de Pater C.J., Baisch S. (2011). Geomechanical Study of Bowland Shale Seismicity – Synthesis Report commissioned by Cuadrilla Resources Ltd. <http://www.cuadrillaresources.com/news/media-and-image-library/downloads/>
- 43 Holland, A. A. (2013). Earthquakes Triggered by Hydraulic Fracturing in South-Central Oklahoma. *Bull. Seismol. Soc. Am.*, **103**: 1784-1792.
- 44 Seeber, L., Armbruster J., and Kim W. Y. (2004). A fluid-injection-triggered earthquake sequence in Ashtabula, Ohio: Implications for seismogenesis in stable continental regions. *Bull. Seismol. Soc. Am.*, **94**: 76–87.
- 45 Nicholson C. and Wesson R. L. (1990). Earthquake Hazard associated with Deep Well Injection, *USGS Report 1951*, 74pp.
- 46 Kim W.Y. (2013). Induced seismicity associated with fluid injection into a deep well in Youngstown, Ohio. *Journal of Geophysical Research: Solid Earth*. **118**: 3506–3518.

-
- 47 Ake J., Mahrer K., O'Connell D., and Block L. (2005). Deep-Injection and Closely Monitored Induced Seismicity at Paradox Valley, Colorado. *Bulletin of the Seismological Society of America*, **95**: 64–683.
- 48 Meremonte, M.E., Lahr J. C., Frankel A. D., Dewey J. W., Crone A. J., Overturf D. E., Carver D. L., and Bice W. T. (2002). Investigation of an Earthquake Swarm near Trinidad, Colorado, August-October 2001, *USGS Open-File Report 02-0073*. <http://pubs.usgs.gov/of/2002/ofr-02-0073/ofr-02-0073.html>
- 49 Nicholson, C., Roeloffs E. and Wesson R. L. (1988). The northeastern Ohio earthquake of 31 January 1986: was it induced?. *Bull. Seism. Soc. Am.* **78**: 188-217.
- 50 Herrmann, R. B., Park, S. K., and Wang C. Y. (1981). The Denver earthquakes of 1967-1968. *Bull. Seism. Soc. Am.*, **71**: 731-745.
- 51 Hsieh, P. A., and J. S. Bredehoeft (1981). A reservoir analysis of the Denver earthquakes—a case study of induced seismicity, *J. Geophys. Res.* **86**, 903–920.
- 52 Frohlich C., Ellsworth W., Brown W. A., Brunt M., Luetgert J. H., MacDonald T., and Walter S. (2014). The 17 May 2012 M4.8 earthquake near Timpson, east Texas: an event possibly triggered by fluid injection. *J. Geophys. Res. Solid Earth*, (in press), doi:10.1002/2013JB010755
- 53 Rubinstein et al., manuscript in preparation;
- 54 Lei X., Yu G., Ma S., Xueze W., Wang Q. (2008). Earthquakes induced by water injection at 3km depth within the Rongchang gas field, Chongqing, China. *Journal of Geophysical Research*. 113
- 55 Lei X., Mas., Chen W., Pang C., Zeng J. , Jang B. (2013). A detailed view of the injection-induced seismicity in a natural gas reservoir in Zigong, southwest Sichuan Basin, China. *Journal of Geophysical Research: Solid Earth*, **118**: 1-16.
- 56 Hsieh, P. A., and J. S. Bredehoeft (1981). A reservoir analysis of the Denver earthquakes—a case study of induced seismicity, *J. Geophys. Res.* **86**, 903–920.
- 57 Committee on Induced Seismicity Potential in Energy Technologies: Hitzman M.W. (Chair), Clarke D.D, Detournay E., Dieterich J.H., Dillon D.K., Green S.J, Habiger R.M., McGuire R.K., Mitchell J.K. Shemeta J.E., Smith J.L (Bill) (2013). Induced Seismicity Potential in Energy Technologies. National Academy of Sciences. *The National Academies Press Washington, D.C.*, pp. 248.
- 58 Hainzl S., Kraft T., Wassermann J., Igel H. and Schmedes E. (2006). Evidence for rainfall triggered earthquake activity. *Geophys. Res. Lett.*, **33**, L19303, doi: 10.1029/2006GL027642
- 59 Shapiro, S. A., and Dinske C. (2009). Scaling of seismicity induced by nonlinear fluid-rock interaction. *J. Geophys. Res.*, **114**.
- 60 Scholz C. (1990). Earthquakes as Chaos. *Nature*, **348**: 197-198

-
- 61 Segall, P. (1992). Induced stresses due to fluid extraction from axisymmetric reservoirs. *Pure and Applied Geophysics*, **139**: 535–560.
- 62 Altmann, J., Müller T., Müller B., Tingay M. and Heidbach O. (2010). Poroelastic Contribution to The Reservoir Stress Path. *International Journal of Rock Mechanics and Mining Sciences*, **47**: 1104–1113.
- 63 Nicol, A., Carne R., Gerstenberger M., Christophersen A. (2011). Induced seismicity and its implications for CO2 storage risk. *Energy Procedia*, **4**: 3699-3706.
- 64 IEA 9/2013
- 65 Ogata Y. (1998). Space-time point process models for earthquake occurrences. *Ann Inst Statist Math*, **50**: 379–402.
- 66 Dieterich J. (1994). A constitutive law for rate of earthquake production and its application to earthquake clustering. *J. Geophys. Res.*, **99**: 2601– 2618.
- 67 Lasocki, S. (2008). Some unique statistical properties of the seismic process in mines. *Proc. 1st Southern Hemisphere International Rock Mechanics Symposium SHIRMS 2008, Perth, 16-19 September 2008*, (Potvin, Y., Carter, J., Dyskin, A., Jeffrey, R., eds.), Australian Centre for Geomechanics, pp. 667-678
- 68 Węglarczyk, S., Lasocki, S. (2009). Studies of short and long memory in mining-induced seismic processes. *Acta Geophys.* **57**: 696-715.
- 69 Lasocki S., Orlecka-Sikora B. (2013) Key-note lecture. Nonstationarity, memory, interactions in mining-induced seismic process – a chance of predictability. Scientific Seminar of Observation and Monitoring of Geological and Geotechnical Risks, Precursory signs and prediction: between Myth and Scientific Reality. *INERIS, Nancy, France, 21.03.2013*
- 70 Lasocki S., Dahle A., Dahm T., Dost B., Grasso J-R., Kraft T. and other Members of W10 “Infrastructure for Georesources, EPOS” (2013b). Science Plan. Conclusions from the discussion held during WG10:Infrastructure for Georesources Meeting in Kraków, Poland, 17-19.02.2013. *EPOS PP 2nd Regional Conference Bergen Norway, 25-26 February 2013*.
- 71 Urban P., Lasocki S., Blascheck P., do Nascimento A.F., Kwiatek G., Turuntaev S.B. (2013). The complexity of size distribution of seismic sources induced by different technologies. *Joint Assembly IAHS-IAPSO-IASPEI Gothenburg, Sweden, 22-26 July 2013*.
- 72 Lasocki S. (2013a). From hazard assessment to hazard management. The case of mining-induced seismicity. *Key-note lecture. Soc. Expl. Geophys. D&P Forum ‘Integrated Geophysics for Unconventional Resources’, Kraków, Poland 7-11 July 2013*
- 73 Lasocki S. (2013b). Induced seismicity. *EPOS workshop ‘A Roadmap for Earth Science in Europe: The next generation of Geophysical Research Infrastructures’. ‘Ettore Majorana’ Foundation and Centre for Scientific Culture Erice, Sicily, Italy 26/08 – 4/09/2013*

-
- 74 Bachmann C. E., Wiemer S., Woessner J. and Hainzl S. (2011). Statistical analysis of the induced Basel 2006 earthquake sequence: introducing a probability-based monitoring approach for Enhanced Geothermal Systems. *Geophysical Journal International*, **186**: 793–807.
- 75 Gruenthal G. (2013). Induced seismicity related to geothermal projects versus natural tectonic earthquakes and other types of induced seismic events in Central Europe. *Geothermics* 10.1016
- 76 Murphy S., O'Brien G.S., McCloskey J., Bean C.J., Nalbant S. (2013). Modelling fluid induced seismicity on a nearby active fault. *Geophys. J. Int.*, doi: 10.1093/gji/ggt174
- 77 Malagnini R., Herrmann R., Munafò I., Buttinelli M., Anselmi M., Akinci A., and Boschi E. (2012). The 2012 Ferrara seismic sequence: Regional crustal structure, earthquake sources and seismic hazard. *Geophys. Res. Lett.*, **39**: L19302, doi:10.1029/2012GRL053214.
- 78 Di Manna P., Guerrieri L., Piccardi L., Vittori E., Castaldini D., Berlusconi A., Bonadeo L., Comerci V., Ferrario F., Gambillara R., Livio F., Lucarini M., Michetti A. M. (2012). Ground effects induced by the 2012 seismic sequence in Emilia: implications for seismic hazard assessment in the Po Plain. *Annals Of Geophysics*, **55**: 4, doi: 10.4401/ag-6143.
- 79 Scognamiglio L., Margheriti L., Mele F. M., Tinti E., Bono A., De Gori P., Lauciani V., Lucente F. P., Mandiello A. G., Marocci C., Mazza S., Pintore S., Quintiliani M. (2012). The 2012 PianuraPadanaEmilianaseismic sequence: locations, moment tensors and magnitudes. *Annals Of Geophysics*, **55**; doi: 10.4401/ag-6159.
- 80 Chioccarelli E., De Luca F., Iervolino I. (2012). Preliminary study of Emilia (May 20th 2012) earthquake ground motion records V2.1, available at <http://www.reluis.it>.
- 81 Chioccarelli E., De Luca F., Iervolino I. (2012), Preliminary study of Emilia (May 29th 2012) earthquake ground motion records V1.0, available at <http://www.reluis.it>.
- 82 Wald D.J., Worden C.B., Quitoriano V., Pankow K.L. (2006). ShakeMap Manual, technical manual, users guide, and software guide, available at <http://pubs.usgs.gov/tm/2005/12A01/pdf/508TM12-A1.pdf>.
- 83 Rovida A., Camassi R., Gasperini P., Stucchi M. (2011). CPTI11, versione 2011 del Catalogo Parametrico dei Terremoti Italiani, Milano/Bologna; <http://emidius.mi.ingv.it/CPTI> (last access July 2012).
- 84 Camassi R., Castelli V., Molin D., Bernardini F., Caracciolo C.H., Ercolani E., Postpischl L. (2011). Materiali per un catalogo dei terremoti italiani: eventi sconosciuti, rivalutati o riscoperti. *Quaderni di Geofisica*, 96, 50+387 pp.; available online: <http://istituto.ingv.it/1-ingv/produzionescientifica/quaderni-di-geofisica>.

-
- 85 Castelli V., Bernardini F., Camassi R., Caracciolo C. H., Ercolani E., Postpischl L. (2012). Looking for missing earthquake traces in the Ferrara-Modena plain: an update on historical seismicity. *Annals of Geophysics*, **55**: 4, 2012; doi: 10.4401/ag-6110.
- 86 Zollo A., De Matteis R., Capuano P., Ferulano F., Iannaccone G., (1995). Constraints on the shallow crustal model of the Northern Apennines (Italy) from the analysis of microearthquake seismic records. *Geophys. J.Int.*, 120, 646– 662.
- 87 Selvaggi G., Ferulano F., Di Bona M., Frepoli A., Azzara R., Basili A., Chiarabba C., Ciaccio M.G., Di Luccio F., Lucente F.P., Margheriti L., Nostro C. (2001). The October 15, 1996, Reggio Emilia seismic sequence: active compression tectonics in the Po Plain Italy. *Geophys. J.Int.*, 144, 1-13.
- 88 Scognamiglio L., Margheriti L., Mele F. M., Tinti E., Bono A., De Gori P., Lauciani V., Lucente F. P., Mandiello A. G., Marocci C., Mazza S., Pintore S., Quintiliani M., (2012). The 2012 PianuraPadanaEmilianaseismic sequence: locations, moment tensors and magnitudes. *Annals Of Geophysics*, 55; doi: 10.4401/ag-6159.
- 89 Chiarabba, C., personal communication
- 90 Ventura, G. and di Giovanbattista R. (2012). Fluid pressure, stress field and propagation style of coalescing thrust from the analysis of the 20 May 2012 ML 5.9 Emilia earthquake (Northern Apennines, Italy). *Terra Nova*, **25**: 72-79, doi: 10.1111/ter.12007.
- 91 Meletti C., Galadini F., Valensise G., Stucchi M., Basili R., Barba S., Vannucci G., Boschi E. (2008). A seismic source zone model for the seismic hazard assessment of the Italian territory. *Tectonophysics*, **450**: 85-108
- 92 Basili, R., Valensise G., Vannoli P., Burrato P., Fracassi U., Mariano S., Tiberti M. M., and Boschi E. (2008). The database of individual seismogenic sources (DISS), version 3: Summarizing 20 years of research on Italy's earthquake geology. *Tectonophysics*, 453, 20–43, doi:10.1016/j.tecto.2007.04.014.
- 93 Tizzani P., Castaldo R., Solaro G., Pepe S., Bonano M., Casu F., Manunta M., Manzo M., Pepe A., Samsonov S., Lanari R., Sansosti E. (2013). New insights into the 2012 Emilia (Italy) seismic sequence through advanced numerical modeling of ground deformation InSAR measurements, *Geophysical Research Letters*, 40, 1–7, doi:10.1002/GRL.50290
- 94 Fantoni, R., Franciosi, R. (2010). Mesozoic extension and Cenozoic compression in Po Plain and Adriatic foreland. *Rend. Fis. Acc. Lincei*, 21, suppl. 1, 197–209.
- 95 Ganas A., Roumelioti Z., Chousianitis K. (2012). Static stress transfer from the May 20, 2012, M 6.1 Emilia-Romagna (northern Italy) earthquake using a co-seismic slip distribution model. *Annals Of Geophysics*, **55**; doi: 10.4401/ag-6176.

-
- 96 Tramelli A., Convertito V., Piochi M., Troise C., De Natale G., Pino N. A. (2013) The 2012 Emilia (Italy) quasi-consecutive friggeremainshoks: implications for seismic hazard (in preparation)
- 97 Convertito V., Catalli F., Emolo, A. (2013) Combining stress transfer and source directivity: the case of the 2012 Emilia seismic sequence. *SCIENTIFIC REPORTS* DOI:10.1038/srep03114.
- 98 Marzocchi W., Murru M., Lomabrdi A.M, Falcone G., Console R. (2012). Daily earthquake forecasts during the May-June 2012 Emilia earthquake sequence (northern Italy). *Annals Of Geophysics*, **55**
- 99 Marzocchi, W. (personal communication).
- 100 Boccaletti M., Corti G., Martelli L. (2011). Recent and active tectonics of the external zones of the Northern Apennines (Italy). *Int.J. Earth Sc.(Geol. Rondshau)*, **100**: 1331-1348.
- 101 Viti M., Mantovani E., Babbucci, D., Tamburelli C., 2011. Plate kinematics and geodynamics in the Central Mediterranean. *J.Geodyn.* 51, 190–204.
- 102 Cesca S., Braun T., Maccaferri F., Passarelli L., Rivalta E., Dahm T. (2013). Source modelling of the M5-6 Emilia-Romagna, Italy, earthquakes (2012 May 20-29). *Geophys. J. Int.*, **193**: 1658-1672.
- 103 Malinverno A., Ryan W.B.F. (1986). Extension in the Tyrrhenian Sea and shortening in the Apennines as a result of arc migration driven by sinking of the lithosphere. *Tectonics*, **5**: 227-245.
- 104 Royden L., Patacca E., Scandone P. (1987). Segmentation and configuration of subducted lithosphere in Italy: an important control on thrust-belt and foredeep-basin evolution. *Geology*, **15**: 714-717.
- 105 Patacca E., Scandone, P. (1989). Post-Tortonian mountain building in the Apennines. The role of the passive sinking of a relic lithospheric slab. In: *BORIANI A., BONAFEDE M., PICCARDO G.B., VAI G.B. (Eds.) "The lithosphere in Italy. Advances in Earth Science Research"*. It. Nat. Comm. Int. Lith. Progr., Mid-term Conf. (Rome, 5-6 May 1987). *Atti Conv. Lincei*, 80, 157-176.
- 106 Anderson H., Jackson J. (1987). Active tectonics of the Adriatic Region. *Geophys.J. R. Astron. Soc.*, **91**: 937-983.
- 107 Westaway R. (1990). Present-day kinematics of the plate boundary zone between Africa and Europe, from the Azores to the Aegean. *Earth and Planet. Sci. Lett.*, **96**: 392-406.
- 108 Ward S.N. (1994). Constraints on the seismotectonics of the central Mediterranean from Very Long Baseline Interferometry. *Geophys. J. Int.*, **117**: 441-452.

-
- 109 Meletti C., Patacca E., Scandone P. (2000). Construction of a seismotectonic model: the case of Italy. *Pageoph*, **157**: 11-35.
- 110 Cinque A., Patacca E., Scandone P., Tozzi M. (1993). Quaternary kinematic evolution of the Southern Apennines. Relationships between surface geological features and deep lithospheric structures. *Spec. Issue on the Workshop: "Modes of crustal deformation: from the brittle upper crust through detachments to the ductile lower crust"*, (Erice, 18-24 November 1991), *Ann. Geofis.*, **36**: 249-260.
- 111 CNR-P.F.GEODINAMICA (1991). Synthetic structural-kinematic Map of Italy. Time of main alpidic deformations and of related sedimentary metamorphic and magmatic processes. Scale 1:2.000.000. In: "Structural Model of Italy 1:500.000 and Gravity Map". Quad. Ric. Sci., 3(114), S.EL.CA., Firenze.
- 112 Rosenbaum G., Lister G.S., Dubioz C. (2002). Relative motions of Africa, Iberia and Europe during Alpine orogeny. *Tectonophysics*, **359**: 117-129.
- 113 Devoti R., Esposito A., Pietrantonio G., Pisani A.R., Riguzzi F. (2011). Evidence of large scale deformation patterns from GPS data in the Italian subduction boundary. *Earth and Planetary Science Letters*, **311**: 230-241
- 114 Pierdominici S., Heidbach O. (2012). Stress field of Italy – Mean stress orientation at different depths and wave-length of stress pattern. *Tectonophysics*, 532-535, 301-311.
- 115 Montone P., Mariucci M.T. (1999). Active stress along the NE external margin of the Apennines: the Ferrara arc, northern Italy. *Geodynamics*, **28**: 251-265
- 116 Selvaggi G., Ferulano F., Di Bona M., Frepoli A., Azzara R., Basili A., Chiarabba C., Ciaccio M.G., Di Luccio F., Lucente F.P., Margheriti L., Nostro C. (2001). The October 15, 1996, Reggio Emilia seismic sequence: active compression tectonics in the Po Plain Italy. *Geophys. J. Int.*, **144**: 1-13.
- 117 Ciaccio M.G., Chiarabba C. (2002). Tomographic models and seismotectonics of the Reggio Emilia region, Italy. *Tectonophysics*, **344**: 261-276.
- 118 Moody J.D., Hill M.J. (1956). Wrench-fault tectonics. *Bull. Geol. Soc. Amer.*, 67, 1207-1246.
- 119 Zollo A., De Matteis R., Capuano P., Ferulano F., Iannaccone G., (1995). Constraints on the shallow crustal model of the Northern Apennines (Italy) from the analysis of microearthquake seismic records. *Geophys. J. Int.*, **120**: 646– 662.
- 120 Carminati E., Scrocca D., Doglioni C. (2010). Compaction-induced stress variations with depth in an active anticline: Northern Apennines, Italy. *J. Geophys. Res.*, **115**: B02401, doi:10.1029/2009JB006395.

-
- 121 Serpelloni E., Anzidei M., Baldi P., Casula G., Galvani A. (2005). Crustal velocity and strain-rate fields in Italy and surrounding regions: new results from the analysis of permanent and non-permanent GPS networks. *Geophys. J. Int.*, **161**: 861-880.
- 122 Devoti R., Pietrantonio G., Pisani A.R., Riguzzi F., Serpelloni E. (2010). Present day kinematics of Italy. *Journal of the Virtual Explorer*, 36 Paper 2, 1-14.
- 123 Cenni N., Mantovani E., Baldi P., Viti M. (2012). Present kinematics of Central and Northern Italy from continuous GPS measurements. *Journal of Geodynamics*, **58**: 62-72.
- 124 Slejko D., Peruzza L., Rebez A. (1998). Seismic hazard maps of Italy. *Annali di Geofisica*, **41**: 183-214.
- 125 Romeo R., Pugliese A. (2000). Seismicity, seismotectonics and seismic hazard of Italy. *Engineering Geology*, **55**: 241-266.
- 126 Scandone P., Patacca E., Meletti C., Bellatalla M., Perilli N., Santini U. (1992). Struttura geologica, evoluzione cinematica e schema sismotettonico della penisola italiana. *Atti del Convegno Annuale del Gruppo Nazionale per la Difesa dai Terremoti (Pisa, 25-27 giugno 1990)*, 1, Ed. Ambiente - Bologna 1992, 119-135.
- 127 Meletti C., Valensise G. (2004). Zonazione sismogenetica ZS9 – App. 2 al Rapporto Conclusivo. In: *GRUPPO DI LAVORO “Redazione della mappa di pericolosità sismica prevista dall’Ordinanza PCM 3274 del 20 marzo 2003”*. Rapporto Conclusivo per il Dipartimento della Protezione Civile, INGV, Milano-Roma, aprile 2004, 65pp. + 5 appendici.
- 128 Meletti C., Galadini F., Valensise G., Stucchi M., Basili R., Barba S., Vannucci G., Boschi E. (2008). A seismic source zone model for the seismic hazard assessment of the Italian territory. *Tectonophysics*, **450**: 85-108.
- 129 CNR-P.F.GEODINAMICA (1990). Structural Model of Italy 1:500.000 and Gravity Map, Sheet n. 1. Quad. Ric. Sci., 3(114), S.EL.CA., Firenze.
- 130 Annual Report (2013) - Executive Summary of DGRME Annual Report 2013, available at: <http://unmig.sviluppoeconomico.gov.it/unmig/stat/ra2013eng.pdf> .
- 131 Annual Report (2013)- GSE Annual Report of GSE activities, available at: <http://www.gse.it/it/Dati%20e%20Bilanci/Rapporti%20delle%20attivit%C3%A0/Pages/default.aspx>
- 132 Kohen K.M., Finney S., Gibbart P.L. (2012). International Chronostratigraphic Chart. *International Commission on Stratigraphy*, August 2012. www.stratigraphy.org.

-
- 133 Masetti D., Fantoni R., Romano R., Sartorio D., Trevisani E. (2012). Tectonostratigraphic evolution of the Jurassic extensional basins in the eastern southern Alps and Adriatic foreland based on an integrated study of surface and subsurface data. *AAPG Bulletin*, **96**: 206-2089
- 134 Sahabi M., Aslanian D., Olivet J.L. (2004). Un nouveau point de départ pour l'histoire de l'Atlantique central. *Comptes Rendus Geoscience*, **336**: 1041-1052.
- 135 Chabou M.C., Bertrand H., Sebai S. (2010). Geochemistry of the Central Atlantic Magmatic Province (CAMP). South western Algeria. *African Earth Sciences*. doi: 10.1016/j.jafrearsci.2010.02.009.
- 136 Bosellini A., Mattavelli L., Masetti D., Sarti M. (1981). La piattaforma di Bagnolo (sottosuolo padano) e il suo significato paleotettonico. *Annali Università Ferrara, Sez. IX Sc. Geol. Paleontol.*, **7**: 103-109.
- 137 Ghielmi M., Minervini M., Nini C., Rogledi S., Rossi M. (2013). Late Miocene-Middle Pleistocene sequences in the Po Plain-Northern Adriatic Sea (Italy). The stratigraphic record of modification phases affecting a complex foreland basin. *Marine and Petroleum Geology*, **42**: 50-81.
- 138 Rossi M., Rogledi S., Barbacini G., Casadei D., Iaccarino S., Papani G. (2002). Tectonostratigraphic architecture of Messinian piggyback basins of Northern Apennines: the Emilia Folds in the Reggio-Modena area and comparison with the Lombardia and Romagna sectors. *Boll. Soc. Geol. Ital.*, **Vol. spec. 1**: 437-447.
- 139 Nardon S., Marzorati D., Bernasconi A., Cornini S., Gonfalini M., Mosconi S., Romano A., Terdich P. (1990). Cavone oil field (Italy): an example of the application of integrated methodologies to reservoir characterization. *Mem. Soc. Geol. Ital.*, **45**: 791-805.
- 140 Pieri M., Groppi G. (1981). Surface geological structure of the Po Plain, Italy. *CNR Publ. 414 Progetto Finalizzato Geodinamica*, 13 p.
- 141 Segall P., Fitzgerald S. D. (1998). A note on induced stress changes in hydrocarbon and geothermal reservoirs. *Tectonophysics*, **289**: 117-128.
- 142 Soltanzadeh H., Hawkes C. D. (2008). Semi-analytical models for stress change and fault reactivation induced by reservoir production and injection. *Journal of Petroleum Science and Engineering*, **60**: p 71-85.
- 143 Lasocki, S. (2008). Some unique statistical properties of the seismic process in mines. *Proc. 1st Southern Hemisphere International Rock Mechanics Symposium SHIRMS 2008, Perth, 16-19 September 2008*, (Potvin, Y., Carter, J., Dyskin, A., Jeffrey, R., eds.), Australian Centre for Geomechanics, pp. 667-678

-
- 144 Lasocki S., Orlecka-Sikora B. (2013) Key-note lecture. Nonstationarity, memory, interactions in mining-induced seismic process – a chance of predictability. Scientific Seminar of Observation and Monitoring of Geological and Geotechnical Risks, Precursory signs and prediction: between Myth and Scientific Reality. *INERIS, Nancy, France, 21.03.2013*
- 145 Hassanzadegan, G. Blöcher, G. Zimmermann, H. Milsch, I. Moeck (2011). Induced Stress in a Geothermal Doublet System. *PROCEEDINGS, Thirty-Sixth Workshop on Geothermal Reservoir Engineering Stanford University, Stanford, California, January 31 - February 2, 2011 SGP-TR-191*
- 146 Costa M. (2003). The buried Apenninic arcs of the Po Plain and northern Adriatic Sea (Italy): a new model. *Boll. Soc. Geol. Ital.*, **122**: 3-23.
- 147 Massoli D., Koyi H.A., Barchi M.R. (2006). Structural evolution of a fold and thrust belt generated by multiple décollements: analogue models and natural examples from the Northern Apennines (Italy). *J. of Struct. Geol.*, **28**: 185-199.
- 148 Toscani G., Burrato P., Di Buccu D., Seno L., Valensise G.,(2009). Plio-Quaternary tectonic evolution of the Northern Apenninic thrust fronts (Bologna-Ferrara section, Italy): seismotectonic implications. *Ital. J. Geosci (Boll. Soc. Geol. Ital.)*, **128**: 605-613.
- 149 Lomax A.J., Virieux P., Volant & Berge C. (2000). Probabilistic earthquake location in 3D and layered models: introduction of a Metropolis-Gibbs method and comparison with linear locations, in *Advances in Seismic Event Location*, pp. 101–134, eds Thurber, C.H. & Rabinowitz, N., Kluwer, Amsterdam.
- 150 Podvin P. and Lecomte I. (1991). Finite difference computations of traveltimes in very contrasted velocity models: a massively parallel approach and its associated tools. *Geophys. J. Int.*, **105**, 271–284.
- 151 Lomax A., Zollo A., Capuano P. and Virieux J. (2001). Precise, absolute earthquake location under Somma–Vesuvius volcano using a new three-dimensional velocity model. *Geophys. J. Int.*, **146**: 313–331.
- 152 Stein R.S., King G.C.P. and Lin J. (1992). Change in failure stress on the southern San Andreas fault system caused by the 1992 magnitude = 7.4 Landers earthquake. *Science*, **258**: 1328–1332.
- 153 Stein R.S., Barka A.A. and Dieterich J.H. (1997). Progressive failure on the North Anatolian fault since 1939 by earthquake stress triggering. *Geophys. J. Int.* **128**: 594–604.
- 154 Harris R.A. and Simpson R.W. (1992). Changes in static stress on southern California faults after the 1992 Landers earthquake. *Nature* **360**: 251–254.

-
- 155 Hodgkinson K.M., Stein R.S. and King G.C.P. (1996). The 1954 Rainbow Mountain-Fairview Peak-Dixie Valley earthquakes: A triggered normal faulting sequence. *J. Geophys. Res.*, **101**: 25459–25471.
- 156 Nostro C., Cocco M. and Belardinelli M.E. (1997). Static stress changes in extensional regimes: An application to southern Apennines (Italy). *Bull. Seismol. Soc. Am.*, **87**: 234–248.
- 157 Toda S., Stein R.S., Reasenber P.A., Dieterich J.H. and Yoshida A. (1998). Stress transferred by the 1995 Mw = 6.9 Kobe, Japan, shock: Effect on aftershocks and future earthquake probabilities. *J. Geophys. Res.* **103**: 24543–24566.
- 158 Cocco M., Nostro C. and Ekström G. (2000). Static stress changes and fault interaction during the 1997 Umbria-Marche earthquake sequence. *Journal of Seismology* **4**: 501–516.
- 159 Harris R.A. (1998). Introduction to special section: Stress triggers, stress shadows, and implications for seismic hazard. *J. Geophys. Res.* **103**: 24347–24358.
- 160 Cesca, S., Braun, T., Maccaferri F., Passarelli L., Rivalta E., Daham, T. (2013). Source modelling of the M5–6 Emilia-Romagna, Italy, earthquakes (2012 May 20–29). *Geophys. J. Int.* 193(3): 1658-1672.
- 161 Lin J. and Stein R.S. (2004). Stress triggering in thrust and subduction earthquakes, and stress interaction between the southern San Andreas and nearby thrust and strike-slip faults. *Journal of Geophysical Research*, **109**: B02303, doi:10.1029/2003JB002607.
- 162 Toda S., Stein R. S., Richards-Dinger K. and Bozkurt S. (2005). Forecasting the evolution of seismicity in southern California: Animations built on earthquake stress transfer. *Journal of Geophysical Research*, **110**: B05S16, doi:10.1029/2004JB003415.
- 163 Toda S., Stein R.S., Sevilgen V., and Lin J. (2011). Coulomb 3.3 Graphic-rich deformation and stress-change software for earthquake, tectonic, and volcano research and teaching—user guide: *U.S. Geological Survey Open-File Report 2011-1060*, 63 p., available at <http://pubs.usgs.gov/of/2011/1060/>.
- 164 Tramelli A., Convertito V., Piochi M., Troise C., De Natale G., Pino N. A. (2013). The 2012 Emilia (Italy) quasi-consecutive triggered mainshocks: implications for seismic hazard. *Submitted paper (Nat. Geo), and EGU 2013 conference*.
- 165 Ganas, A., Roumelioti Z., and Chousianitis K. (2012). Static stress transfer from the May 20, 2012, M 6.1 Emilia-Romagna (northern Italy) earthquake using a co-seismic slip distribution model. *Annals of Geophysics*, **55**, 4, 2012; doi: 10.4401/ag-6176.
- 166 Del Pezzo G., MerrymanBoncori J. P., Tolomei C., Salvi S., Atzori S., Antonioli A., Trasatti E., Novali F., Serpelloni E., Candela L. and Giuliani R. (2013). Coseismic deformation and source

-
- modeling of the May 2012 Emilia (northern Italy) earthquakes. *Seismological Research Letters*, **84**:645-655.
- 167 Saraò A. and Peruzza L. (2012). Fault-plane solutions from moment-tensor inversion and preliminary Coulomb stress analysis for the Emilia Plain. *Annals of Geophysics*, 55, 4, 2012
- 168 Chiarabba, C., personal communication.
- 169 Lasocki S., Papadimitriou, E. E. (2006). Magnitude distribution complexity revealed in seismicity from Greece. *J. Geophys. Res.*, **111**, B11309, doi:10.1029/2005JB003794
- 170 Lasocki S. (2013). Transformation to equivalent dimensions – A new methodology to study earthquake clustering. *Geophys J Int.* (under review)
- 171 Ogata Y. (1988). Statistical models for earthquake occurrences and residual analysis for point processes. *J. Am. Stat. Assoc.*, 83 , 9–27.
- 172 Ogata, Y., Matsu'ura R. S., and Katsura K. (1993). Fast likelihood computation of epidemic type aftershock-sequence model. *Geophys. Res. Lett.*, 20 , 2143–2146
- 173 Ogata Y. (1998). Space-time point process models for earthquake occurrences. *Ann Inst Statist Math*, **50**: 379–402.
- 174 Lombardi, A. M., Marzocchi W., and Selva J.(2006). Exploring the evolution of a volcanic seismic swarm: The case of the 2000 Izu islands swarm. *Geophys. Res. Lett.*, 33.
- 175 Hainzl S. and Ogata, Y. (2005). Detecting fluid signals in seismicity data through statistical earthquake modeling. *J. Geophys. Res.*, 110.
- 176 Garcia-Aristizabal A. (2010). Analysis of eruptive and seismic sequences to improve the short- and long-term eruption forecasting, *PhD Thesis in Geophysics, Università di Bologna, Italy, 2010. (Chapter 3: Volcano-Tectonic Swarms: Non-stationary ETAS modeling). Url: <http://amsdottorato.cib.unibo.it/2621/>*
- 177 Mogi, K. (1967). Earthquakes and fractures. *Tectonophysics*, 5 , 35–55, 1967.
- 178 Kisslinger, C. and Jones, L. (1991). Properties of aftershock sequences in southern California, *J. Geophys. Res.*, 96, 11,947–11,958.
- 179 Carella R. (1999). Italian geothermal district heating systems. *GHC Bulletin*, December 1999
- 180 Hassanzadegan A., Blöcher G., Zimmermann G., Milsch H., Moeck I. (2011). Induced Stress in a Geothermal Doublet System. *PROCEEDINGS, Thirty-Sixth Workshop on Geothermal Reservoir Engineering Stanford University, Stanford, California, January 31 - February 2, 2011 SGP-TR-191*

-
- 181 Carminati E., Doglioni C. and Scrocca D. (2005). Chapter 4: Magnitude and causes of long-term subsidence of the Po Plain and Venetian region. *Flooding and Environmental Challenges for Venice and its Lagoon: State of Knowledge*, ed. C. A. Fletcher and T. Spencer with J. Da Mosto and P. Campostrini. Published by Cambridge University Press, © Cambridge University Press 2005, p21-28.
- 182 Groos J. C., Fritschen R., Ritter J. R. R. (2013). Untersuchung induzierter Erdbeben hinsichtlich ihrer Spürbarkeit und eventueller Schadenswirkung anhand der DIN 4150, Bauingenieur, Band 88, September 2013, p 374-384.